# UNIVERSITY OF SOUTHAMPTON


# MODELING AND SIMULATION OF MAGNETIC COMPONENTS IN ELECTRIC CIRCUITS


## PETER REID WILSON


## SUBMITTED FOR THE DEGREE OF PHD


## DEPARTMENT OF

## ELECTRONICS AND COMPUTER SCIENCE

## NOVEMBER 2001

**UNIVERSITY OF SOUTHAMPTON**

# <u>ABSTRACT</u>

**FACULTY OF ENGINEERING**

**DEPARTMENT OF ELECTRONICS AND COMPUTER SCIENCE**

<u>Doctor of Philosophy</u>

**MODELING AND SIMULATION OF MAGNETIC**

**COMPONENTS IN ELECTRIC CIRCUITS**

**by Peter Reid Wilson**

This thesis demonstrates how by using a variety of model constructions and parameter extraction techniques, a range of magnetic component models can be developed for a wide range of application areas, with different levels of accuracy appropriate for the simulation required. Novel parameter extraction and model optimization methods are developed, including the innovative use of Genetic Algorithms and Metrics, to ensure the accuracy of the material models used. Multiple domain modeling, including the magnetic, thermal and magnetic aspects are applied in integrated simulations to ensure correct and complete dynamic behaviour under a range of environmental conditions.

Improvements to the original Jiles-Atherton theory to more accurately model loop closure and dynamic thermal behaviour are proposed, developed and tested against measured results. Magnetic Component modeling techniques are reviewed and applied in practical examples to evaluate the effectiveness of lumped models, 1D and 2D Finite Element Analysis models and coupling Finite Element Analysis with Circuit Simulation. An original approach, linking SPICE with a Finite Element Analysis solver is presented and evaluated.

Practical test cases illustrate the effectiveness of the models used in a variety of contexts. A Passive Fault Current Limiter (FCL) was investigated using a saturable inductor with a magnet offset, and the comparison between measured and simulated results allows accurate prediction of the behaviour of the device. A series of broadband hybrid transformers for ADSL were built, tested, modeled and simulated. Results show clearly how the Total Harmonic Distortion (THD), Inter Modulation Distortion (IMD) and Insertion Loss (IL) can be accurately predicted using simulation.

A new implementation of ADSL transformers using a planar magnetic structure is presented, with results presented that compare favourably with current wire wound techniques. The inclusion of transformer models in complete ADSL hybrid simulations demonstrate the effectiveness of the models in the context of a complete electrical system in predicting the overall circuit performance.

# List of Contents

# List of Figures

# List of Tables

# Acknowledgements

I would like to express my appreciation for the people who have contributed to the production of this thesis in a variety of ways.

Firstly I would like to express my gratitude to Dr Neil Ross for supervising this project. His guidance has been instrumental in ensuring that the scope of the project has been kept within reasonable bounds. I also thank Professor Alan Evans for agreeing to be the internal examiner for this thesis. His comments have helped greatly with the development of the structure of the thesis. I have always appreciated the opportunity to study on this course and for this my thanks go to Professor Andrew Brown for allowing me to study in his group.

Finally, and most importantly, I wish to express my sincere thanks to my family and friends. Without the support and understanding of my wife, Caroline, this work could not have taken place. It is also important to keep perspective, and in this regard my children, Nathan and Heather, have been instrumental. I also owe a debt of gratitude to my parents for providing me with the education to get this far. Sincere thanks also go to Alan Abernethy and my father for agreeing to proof read the manuscripts.

# Declaration

I declare that the work in this thesis is entirely my own unless otherwise stated.

Peter Reid Wilson, November 2001

# List of Abbreviations

| | |
|---|---|
| A.C. | Alternating Current |
| ADSL | Asymmetric Digital Subscriber Line – A form of High Speed Digital Communication |
| AHDL | Analogue Hardware Description Language |
| CAD | Computer Aided Design |
| D.C. | Direct Current |
| EMC | Electro-Magnetic Compatibility |
| E.M.F. | Electro Motive Force |
| FDM | Frequency Division Multiplexing |
| FFT | Fast Fourier Transform |
| HDL | Hardware Description Language |
| HDSL | High-speed Digital Subscriber Line – A form of High Speed Digital Communication |
| Hysteresis | Non-linear behaviour of magnetic materials |
| IEEE | Institution of Electrical and Electronics Engineers |
| IL | Insertion Loss |
| IMD | Inter Modulation Distortion |
| ISDN | Integrated Subscriber Digital Network |
| Major Loop | Large Hysteresis Loop |
| Minor Loop | Small Hysteresis Loop |
| QAM | Quadrature Amplitude Modulation |
| SMPS | Switch Mode Power Supply |
| THD | Total Harmonic Distortion |
| VDSL | Very high-speed Digital Subscriber Line – A form of High Speed Digital Communication |
| VHDL | Very high-speed ASIC Hardware Description Language IEEE Standard 1076-1993 |
| VHDL-AMS | VHDL plus Analogue and mixed signal extensions from IEEE Standard 1076.1-1999 |
| xDSL | Generic Label for Digital Subscriber Line Technologies such as ADSL or VDSL |

*Chapter 1*

# 1   Introduction

## 1.1   *Project Motivation and Goals*

Over the last ten years there has been a significant increase in the use of computer simulation in the design of electronic circuits. Simulation has been used to replace prototyping to some extent, partially for a wide variety of printed circuit boards (PCB) and completely in the case of application specific integrated circuits (ASIC), primarily in order to reduce the development time for designs and hence the costs of the design cycle.  It has also been recognized that the use of simulation enables tests to be undertaken on a design that would be impossible practically, prohibitively expensive or dangerous thereby providing potentially much greater insight into the design's performance and reliability.

This use of simulation for design performance prediction and optimization can be termed "Virtual Prototyping" – a prototype on the computer that can be modified and experimented in a similar fashion to a breadboard. Unfortunately, the use of simulation may not be completely accurate, as the accuracy of the results depends entirely on the models used for the individual components, and also the circuit as a whole (e.g. circuit parasitics). This is no different to the case of breadboard parasitics, which may be significantly different to the final production design. If the simulation results are to be relied on to any extent for performance prediction, it is crucial that the models used  are accurate, appropriate for the results required, and used in the manner for which they were designed. It is therefore imperative that prior to attempting to model or simulate an electronic system, the simulation requirements for the system and individual models are thoroughly understood, especially the accuracy and range of operation.

In this project, the modeling of magnetic components in electric circuits has been undertaken from the perspective of three different application areas, xDSL broadband transformer hybrids, Passive Fault Current Limiters (FCL) and Switch Mode Power Supplies (SMPS). Each of these application areas require different aspects of the magnetic component model to be considered in detail, and widely differing system simulations to be undertaken. As a result, the model requirements for each application will be different. In this project, therefore, the application model requirements have been analyzed, and modeling carried out to support the final system simulations and performance calculations. Existing work is built upon and extended in the areas of magnetic material modeling and characterization, model optimization, model implementation and system simulation using mixed signal simulation. By using appropriate models and techniques, each application has been modeled and simulated with the simulation results compared with measured test results at all stages to demonstrate the accuracy of the methods used. The overall primary goal of this project is

to provide a set of models, techniques and software tools that can be used to efficiently and accurately simulate a wide variety of magnetic components in a range of target applications. The resulting simulations should provide key performance indicators and replicate the behaviour of the target applications in a reasonable time. The specific objectives of this project are discussed in the remainder of this chapter.

## *1.2  Definition of systems to be simulated*

### 1.2.1  Identification of Target Application Areas

The target application areas that were chosen for this project are as follows:

- Passive Fault Current Limiters (FCL)
- ADSL/VDSL broadband hybrid transformers
- Switch Mode Power Supplies (SMPS)

These applications have been deliberately chosen to provide different modeling and simulation challenges in this project, which will be discussed in detail in the next section of this thesis. The wide use of magnetic components in SMPS design made the choice of this application an easy one, with significant areas of work still to be addressed. SMPS designers require models that are accurate and efficient to simulate, without extensive analysis or characterization. Specific modeling issues, such as thermal interactions and parasitics, provide opportunities for significant improvements to previous work. Passive Fault Current Limiters using inductors with some form of magnetic offset (either using windings or permanent magnets) provide different modeling challenges in an area that has been less widely investigated from a simulation perspective. While there are large common research areas with SMPS transformers, enabling similar modeling techniques to be applied, the requirements of the application simulation and model structure are quite different. The potential for original work in this unusual area was identified as high and therefore ideal for further research. The final application requires a quite different set of simulation and modeling criteria. Broadband hybrids (including signal transformers) are high speed, digital, low power and low distortion systems. Where the SMPS and FCL transformers need good modeling of hysteresis losses, the Broadband components operate at low powers and high speeds. The accurate modeling of very low levels of distortion across a wide bandwidth is required, with detailed knowledge of the parasitics and their interactions with the hybrid circuit behaviour. Most existing work in this area has used simple linear models, with limited investigation of the effects of material hysteresis (albeit small) on distortion, signal to noise ratios and inter-modulation. In this project, high power non-linear modeling techniques have been applied to small signal models effectively to provide greater insight into the non-linear behaviour of the small signal transformers.

### 1.2.2   Key Issues to be addressed in Application Simulations

The issues to be addressed in the individual application simulations have been discussed generally in the previous section. In this section, these are pulled together into sets of specific requirements to be addressed given in table 1.1.

| Application | Simulation Requirements |
|---|---|
| SMPS Transformer | Detailed modeling of Core Hysteresis<br><br>Detailed modeling of Core Structure (magnetic domain models)<br><br>Dynamic Thermal Behaviour of Magnetic Material<br><br>Accurate Modeling of the Relationship between Magnetic Hysteresis and Electrical Waveforms<br><br>Device Characterization from Physical Data<br><br>Accurate Modeling of Frequency Effects in Core and Windings (Eddy Currents) – up to 1MHz<br><br>Characterization and modeling of Leakage Inductance and Losses<br><br>Efficient Model for Fast Simulation Times<br><br>Accurate with arbitrary waveforms |
| Fault Current Limiter | Detailed modeling of Core Hysteresis<br><br>Detailed modeling of Core Structure (magnetic domain models)<br><br>Dynamic Thermal Behaviour of Magnetic Material<br><br>Permanent Magnet Modeling in Core<br><br>Accurate Modeling of the Relationship between Magnetic Hysteresis and Electrical Waveforms<br><br>Accurate Impedance Modeling<br><br>Device Characterization from Physical Data<br><br>Accurate Modeling of Frequency Effects in Core (Eddy Currents) – up to 1kHz<br><br>Accurate for sinusoidal waveforms (50Hz Line) |
| Broadband Transformer | Accurate Model of Hysteresis Minor Loops<br><br>Accurate Distortion Measurements<br><br>Accurate Model across a wide frequency Range (core and winding – eddy currents)<br><br>Accurate for arbitrary waveforms<br><br>Accurate loss and signal to noise ratio behaviour<br><br>Hybrid Transformer, Filter and Line Modeling<br><br>Accurate Parasitic and Impedance Characterization |

**Table 1.1: Application Model and Simulation Requirements**

Using the requirements listed in table 1.1, it is possible to establish the areas of research to provide the tools, methods and models to support the necessary simulations.

## 1.3    Application specific modeling and simulation techniques

In order to provide appropriate models to simulate the target applications, techniques are required in each case to develop the models. In this section, each application is considered in turn, and the required techniques listed and briefly described.

### 1.3.1    Techniques Required for SMPS component modeling

In the simulation of Switch Mode Power Supplies (SMPS), the design engineer requires different types of model for different simulations. Initial 'what if' simulations may require a simple linear model, with only a magnetizing inductance and a turns ratio (for transformers). As the simulation requirements become more detailed the need for a non-linear model increases. It may be necessary to estimate efficiencies more accurately, incorporate thermal behaviour into the simulation, view the effect of core saturation on electrical waveforms and measure the effects of component parasitics such as leakage inductance, winding loss and winding capacitance. If the design requires some form of integrated magnetics, or complex physical structure, then the designer will require a model which is not restricted to a simple electrical model, but also includes a magnetic domain structure. The specific techniques required to support these requirements are now discussed.

#### 1.3.1.1    Magnetic Domain Modeling

For anything other than the most simple magnetic structure, it becomes much easier to model magnetic components using a mixed domain approach. For complex magnetic and winding structures, this becomes a necessity. The requirement to achieve this from a modeling standpoint is a set of building block models, including windings, core models and loss components that can be built into a complete electrical-magnetic component model.

#### 1.3.1.2    Magnetic Material Modeling

If non-linear hysteresis behaviour is required, then non-linear magnetic material models are essential. The development of models for use in a variety of simulators is needed, with supporting characterization tools and methods to ensure the accuracy of the resulting models.

#### 1.3.1.3    Simulator Support

For practical use, a variety of modeling approaches needs to be considered. To demonstrate this practically, the de facto standard simulator SPICE was used as the primary modeling approach, but also the emerging Hardware Description Language (HDL) VHDL-AMS, and Saber's MAST modeling language.

### 1.3.1.4  Dynamic Thermal Effects

The inclusion of dynamic thermal behaviour of the model behaviour is essential if accurate simulations are to be achieved in a wide variety of operating conditions. Thermal models, links to the magnetic domain and parameter characterization methods need to be developed.

### 1.3.1.5  Model Characterization and Optimization

The provision of the model building blocks is not enough to ensure accurate simulation results. It is necessary to characterize the models using either analytical or experimental data, and optimization methods are needed to ensure that the resulting model behaviour matches the original data.

### 1.3.1.6  Frequency Dependent Effects

As the switching frequencies of SMPS circuits has increased, it has become important for the models to support the resulting change in behaviour. Eddy currents induced in the magnetic core and windings can fundamentally alter the device behaviour and must be included.

### 1.3.1.7  Model Performance and Metrics

While it has been usual practise to check model accuracy using a simple least squares error approach, sometimes it is necessary to ensure that specific aspects of the model are modeled extremely accurately. For example, the hysteresis loop shape may not need to be modeled accurately to a high degree, but the loop loss may need to be very accurate to ensure correct efficiency estimation. By using specific performance metrics as goal functions in the modeling process can provide models that are tailored to the application specific requirements.

## 1.3.2   Techniques required for Fault Current Limiting

The operation of the passive Fault Current Limiter (FCL) depends on the hysteresis behaviour of the core material. A permanent magnet or offset winding is used to bias the core into saturation, giving a nominally low inductance in series with the load. If the current deviates enough, the core is forced out of saturation and the inductance will markedly increase, providing the current limiting effect. Two such devices are required in series to provide current limiting for positive and negative excursions. It is most important in modeling such devices that the hysteresis model is accurate. The specific techniques required include the same ones as the SMPS devices, but with the following additional requirements.

### 1.3.2.1  Permanent Magnet Modeling

In the Passive Fault Current Limiter described in this thesis, a permanent magnet was used to provide the bias magnetic field. Accurate modeling of the magnet behaviour including hysteresis and magnetic recoil is required to ensure predictions of the device performance are valid.

### 1.3.3 Techniques required for Broadband Hybrid Transformers

The Broadband Hybrid Transformers were specifically chosen as an example because of the markedly differing requirements when compared to the 'power' devices previously described. The critical factors in obtaining good performance in a hybrid transformer are wide bandwidth, low losses and low distortion. To predict these factors in simulation requires accurate calculation of parasitics, good modeling over a wide frequency range (10s of MHz) and accurate modeling of material behaviour for small loops. The use of linear and non-linear models is required to allow both frequency response and time domain analysis of the hybrid and associated filter combinations. Specific model requirements include:

#### 1.3.3.1 Frequency Dependent Parasitics

The modeling of parasitic variation with frequency, primarily leakage inductance, has been less well described in the literature than the variation of winding loss with frequency. This will affect the performance over a wide bandwidth and needs addressing.

#### 1.3.3.2 Integrated Simulations

It is necessary to integrate the magnetic component model, with filters and line models to estimate the Trans Hybrid Loss (THL). Methods need to be created to allow the THL to be calculated automatically without the need for extensive, time-consuming post processing.

### 1.4 Project Scope

### 1.4.1 Introduction

The scope of this project is to develop the ideas for modeling magnetic materials and windings into a form that can be used efficiently to model magnetic components accurately in electrical circuits. This requires the development of theory and modeling techniques for magnetic materials, parameter extraction and characterization, the construction of practical simulation models for magnetic components and the testing of the resulting models in practical examples.

There are aspects of magnetic material modeling that have not been adequately covered from a simulation perspective, particularly the area of parameter extraction and material characterization, which offers various research opportunities. It is not the purpose of this thesis, however, to develop fundamental magnetic material theory. There has also been significant effort applied in the modeling of magnetic component windings, particularly for Power Supply transformers, so this area does not offer much scope in the way of original study.

There are gaps in the knowledge, especially when the high frequency behaviour of parasitics is considered. The dependence with frequency of leakage inductance is one specific area covered in this thesis that is not discussed in the literature a great deal. Challenging the assumptions made

when using Finite Element Analysis (FEA) to extract parameters such as the leakage inductance is important in understanding the validity of parameters extracted using FEA, and this is discussed in detail. The technique is extended to evaluate the performance of a direct FEA-Circuit simulation coupling.

When considering the overall component model, in the context of a power switching circuit such as a power supply, the overall environmental conditions are often ignored. In this thesis, the thermal behaviour of the magnetic component is integrated into a single model with the electromagnetic behaviour. This allows a true analysis of the circuit performance including the decrease in performance as the temperature goes up, even to the extent of the magnetic component failing if the Curie temperature is reached for the material.

With the development of magnetic component models, several examples were chosen to specifically test different aspects of the models. Figure 1.1 summarises the problem neatly, i.e. how is it possible to accurately simulate a system that contains a mixture of analogue electronics, digital electronics, magnetic components and real world interfaces using conventional methods ?
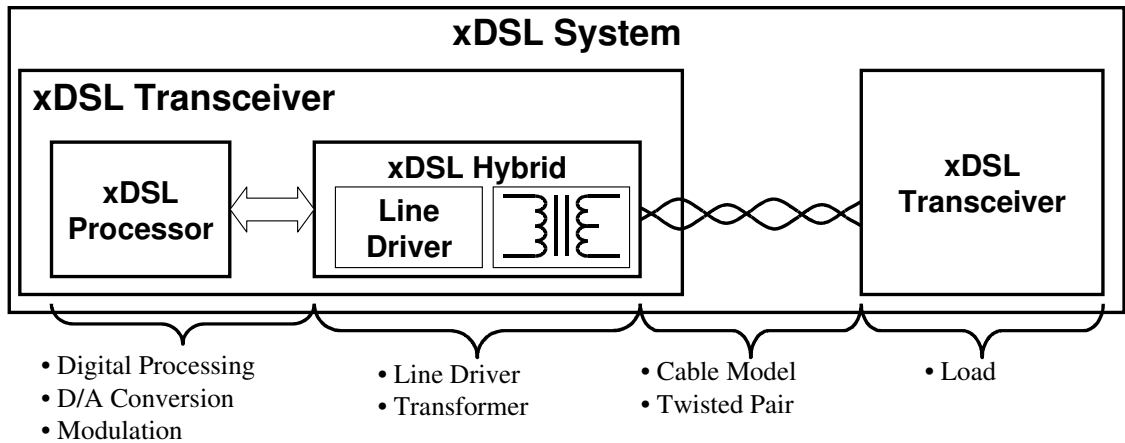


**Figure 1.1 : Example system to be simulated**

The goal of the project is to be able to simulate systems such as these, and establish key performance criteria including any effects due to the magnetic component.

### 1.4.2   Structure of the Project

The project was split into three main phases as shown in figure 1.2.
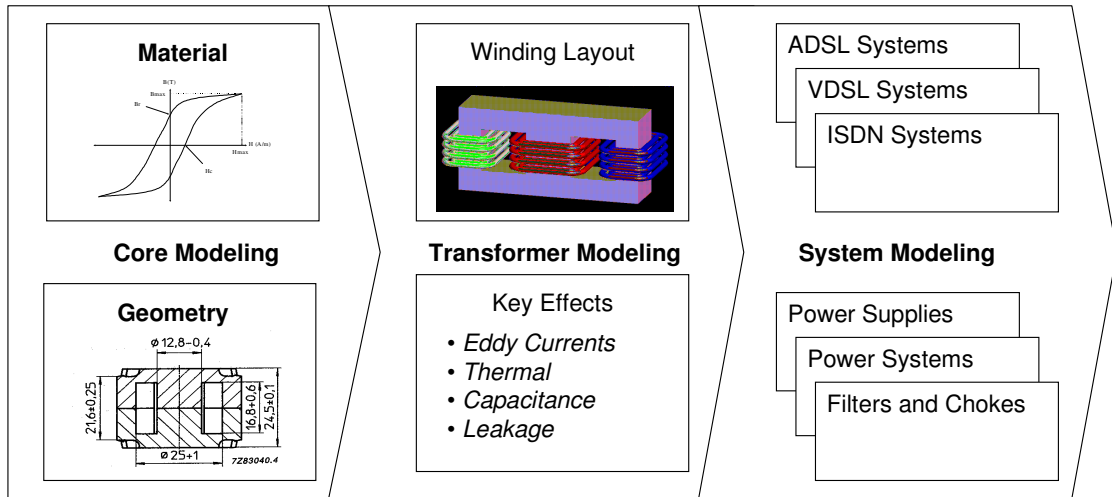
**Figure 1.2 : Project Structure**

The first phase of the project was to establish methods for modeling the core material accurately. This required extensive literature review and the development of models to be used in the target simulators (discussed later in this thesis). Further to this, the techniques for parameter extraction and characterization were considered to be vital in ensuring the accuracy of the final simulations. The second phase was to build in the windings into the models. It was necessary to consider high frequency effects in some detail. Although most of the theory is well known and understood, it was necessary to develop and implement aspects of the component behaviour such as leakage inductance modeling for high frequencies and thermal behaviour. The third and final phase of the project was to apply the models generated to solving real engineering problems. This concentrated on two main areas, power and high-speed digital communications.

### 1.4.3  Specific Project Hypotheses

As a basis for the research in this project, several specific hypotheses were made as follows:

- Existing magnetic material models have inadequacies that need to be addressed including minor loops, loop tip closure and dynamic thermal behaviour.

- Parameter extraction methods are weak and new techniques require to be developed.

- Characterized model parameters are generally poor and new techniques are required for optimization and assessing performance.

- Magnetic component modeling approaches for high frequency circuits are limited and inaccurate.

- Limited use is made of mixed domain modeling techniques to provide more insight into the behaviour of magnetic components in their target applications.

8

- Simplistic modeling approaches used for high-speed digital communications do not take into account magnetic component parasitics or non-linear behaviour.

- The application of new modeling technology such as VHDL-AMS will allow detailed integrated modeling of systems including mixed technology aspects such as magnetic and thermal behaviour.

These hypotheses are all tested in this thesis, with conclusions drawn as to their validity or otherwise.

## 1.5   Thesis Structure

In this section, the thesis structure is explained chapter by chapter with the main point of each chapter and its original contribution defined. The thesis can be divided into 3 main sections. Chapters 1-3 contain much of the background theory and literature review and leads into chapters 4-9 looking at specific aspects of implementation and modeling. The final phase of the project, looking at practical examples is covered in chapters 10-11, with discussion of the results, conclusions and further work in the final chapter 12. Each chapter is now considered in turn, with its main contribution highlighted along with any significant original content.

### 1.5.1   Chapter 1 : Introduction

In the first chapter of the thesis, the overall project scope and goals are defined. The techniques that are required to be investigated are highlighted and the overall structure of the project outlined.

### 1.5.2   Chapter 2 : Review of Modeling and Simulation Theory

This chapter reviews the fundamentals of modeling and simulation for electric circuits. The aspects of mixed-technology time domain modeling are reviewed and contrasted with electromagnetic device modeling techniques, such as Finite Element Analysis. The key issues to be considered when modeling multiple-domain systems are highlighted at this stage.

### 1.5.3   Chapter 3 : Review of Magnetic Material Modeling

The purpose of this chapter is twofold. The first aim is to review the fundamental requirements for modeling magnetic materials accurately. The second aim is to review the modeling methods available in the literature, and to provide a comparative study of those models to establish the most appropriate model that will be fit for purpose in this project. Potential model limitations in existing approaches are defined at this stage.

### 1.5.4   Chapter 4 : Implementation and Characterization of Magnetic Material Models

This chapter demonstrates how to implement magnetic material models for circuit simulation. Extensions to existing models are proposed, implemented and tested  demonstrating significant improvements to those models. Novel methods of characterizing the behaviour of the models using metrics are proposed. Parameter extraction and characterization techniques are also developed including a new genetic algorithm approach for model optimization. A comparative study of standard simulated annealing and the new genetic algorithm is carried out, including statistical analysis to demonstrate the strengths and weaknesses of the approaches. This chapter contains a significant amount of original work.

### 1.5.5   Chapter 5 : Modeling Windings

The area of modeling windings has been very well covered in the literature, especially in the area of power electronics, therefore this chapter mainly reviews the techniques available for modeling windings in magnetic components. Weaknesses or deficiencies in the existing approaches are highlighted, so that they can be addressed later in the thesis.

### 1.5.6   Chapter 6 : Modeling Magnetic Components

This chapter draws together the individual threads and techniques into a coherent strand to model magnetic components as a whole. Different types and level of model are discussed and explained, with insight into how they can be implemented using various target simulators.

### 1.5.7   Chapter 7 : Modeling a Simple transformer

In this chapter an example is used to demonstrate how the techniques developed so far can be used to model a simple transformer. The modeling of leakage inductance is concentrated on with theoretical calculations used to predict the model parameters, which are tested using various two-dimensional Finite Element Analysis (FEA) approximations. Existing one-dimensional modeling approaches are also tested to compare the accuracy, model creation time and simplicity of resulting model. A new model for leakage inductance is proposed for use in circuit simulations that is easy to characterize, accurate and fast to simulate.

### 1.5.8   Chapter 8 : Coupled SPICE-Finite Element Analysis Simulation

Following on from the use of Finite Element Analysis (FEA) to extract model parameters previously described, a coupled SPICE-FEA simulation approach was created to evaluate the possibility of using this integrated physical model and circuit simulation together. The interface between SPICE and FEA is proposed and its implementation described. The results of a simple inductor and switch mode power supply simulations are presented to show the effectiveness of this approach.  This chapter contains a significant amount of original work.

### 1.5.9  Chapter 9 : Dynamic Electric-Magnetic-Thermal Modeling

This chapter extends the electromagnetic models to include dynamic thermal effects. A modification to the Jiles-Atherton model is proposed to directly obtain the power loss from the magnetic material model and is linked to a thermal model to provide self-heating and dynamic thermal behaviour for the magnetic component. Parameter characterization over a wide temperature range is presented, with comparisons between measured and simulated results demonstrating the accuracy of the approach. This chapter contains a significant amount of original work.

### 1.5.10  Chapter 10 : Modeling a Passive Fault Current Limiter

In choosing the examples, it would have been very easy to use switch mode power supplies exclusively, however that would have limited new interest, so one of the examples chosen was a Passive Fault Current Limiter (FCL). This type of component relies on the non-linear magnetic material behaviour entirely for its operation and is therefore a good candidate for testing out modeling approaches. In this chapter a Passive FCL component is modeled and compared with measured results. Although the concept in itself is not original, the modeling approach has significant original content.

### 1.5.11  Chapter 11 : Modeling Broadband Hybrid Transformers

In this chapter, a high-speed digital communication system hybrid was modeled and simulated. Similarly to the Fault Current Limiter, this device requires a different set of modeling techniques to the conventional power supply components and is therefore ideal to extend the validity range of the models. Different model types are tested and discussed, and the relationship between the transformers in the hybrid and the circuit are examined using simulation. Key performance indicators such as Trans Hybrid Loss, Insertion Loss and Total Harmonic Distortion are used to measure the performance. The simulations of these devices clearly highlight the benefits of applying simulation to solving real design problems in this area. In this chapter the original content is mainly on the application of techniques to solve a range of new problems, however testing of the potential applicability of planar components and integrated hybrids was also carried out.

### 1.5.12  Chapter 12 : Discussion and Conclusions

In this chapter, the results obtained are discussed and compared. The accuracy of models, efficiency and speed of simulation are discussed. Simulations issues such as convergence and portability of models are discussed in some detail.

Conclusions are drawn and a statement about the original hypotheses made. The main results achieved are highlighted, along with the papers published as a result of this work and the contribution the work has made to the sponsoring company.

Areas that were not covered in this thesis, but that could provide the basis of future work are highlighted.

# 2 Review of Modeling and Simulation Theory

## *2.1 Modeling Theory*

### 2.1.1 Introduction to Modeling and Simulation

Before embarking on a detailed description of modeling, it is important to understand the relationship between modeling and simulation. In essence, the simulator is a black box process, with the models as its ammunition. The purpose of the simulator in the context of analogue electronic system design is to solve non-linear ordinary differential equations that describe the behaviour of the system. The model is the method by which the equations are described. Generally, each system is described using a circuit diagram or list of models, called a netlist. The netlist can often be generated from the circuit diagram by CAD software automatically. Each symbol in the circuit diagram, for example resistors or capacitors, is represented by an underlying set of equations in the final problem to be solved by the simulator. The simulator interprets the list of individual models, and constructs a matrix of equations for the complete system. This matrix is then solved by the simulator.

### 2.1.2 Continuous and Discrete Time Simulation

The details of the simulation process will be discussed later in the chapter, but there is an important aspect of the model definition to be considered first. Electronic circuits fall into two main areas, analogue and digital. While it is true that ultimately all electronics systems can be described as analogue circuits, for example a *digital* logic inverter can also be described using individual *analogue* transistors, it is useful to consider methods for simulating using an analogue or digital approach.

Analogue simulation using digital computers is based on approximating the continuous time behaviour of the electronics circuit, solving non-linear differential equations using techniques such as Newton-Raphson, and using a Predictor-Corrector method to estimate time-steps between approximation points. The individual connections in the circuit are solved using network analysis techniques such as KVL or KCL with the complete circuit stored in a large matrix.

Digital simulation with digital computers relies on an event-based approach. Rather than solve differential equations, events are scheduled at certain points in time, with discrete changes in level. Resolution of multiple events and connections is achieved using logical methods.

If the two approaches are compared, it is clear that in the analogue simulation approach, although the time axis is discretized, if the time-steps are small enough it is effectively continuous. At each

time-step, the analogue simulation requires the complete system to be solved. This can be time-consuming and the simulation time increases with the square of the size of the system. With the digital simulation method, in contrast, variables only need to change if an event occurs, in general leading to much faster simulations. Using logical variable resolution rather than numerical techniques as in the analogue case is also generally faster and simpler to implement.

Developments in simulation technology combine the two techniques into a form of *mixed-signal* simulation that can take advantage of the relatively high accuracy of the analogue simulation and the high speed of the digital simulation.

The models developed in this thesis are largely analogue but there are occasions where mixed-signal modeling is useful, especially if the system contains digital elements. For the remainder of this thesis, models are assumed to be analogue unless specifically stated.

### 2.1.3   Definition of a Model

*2.1.3.1   General Definition*

In circuit simulation, a model *represents* a physical element such as a resistor or capacitor. The model consists of a core set of equations, the connection points to other elements in the circuit and parameters that characterize the exact behaviour of the physical element. This is illustrated in figure 2.1.



Connection points

Model Behaviour
v = iR
P=vi
etc...

**p**                                                                     **n**

Parameters : e.g. R=1000
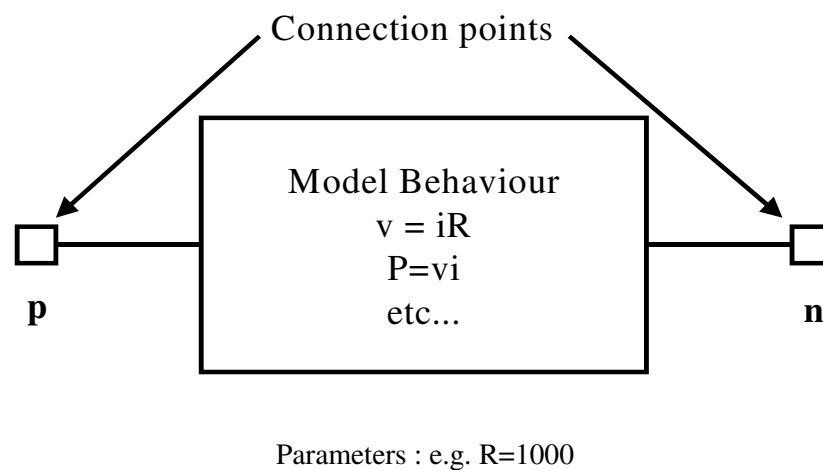
**Figure 2.1 : General Model Concept**

*2.1.3.2   Variable Classes*

In analogue and mixed-signal models there are four basic ways of representing variables. *Parameters* are numbers that are defined once at the beginning of a simulation and do not subsequently change. An example of this is the value of a resistor, e.g. 100 Ω. Analogue variables consist of *procedural* and *simultaneous* values. Procedural variables can be thought of as analogous to variables in a sequential programming language such as C. The values of the

14

variables are calculated sequentially in the order the equations appear at each time step and iteration. Simultaneous variables, on the other hand, are solved concurrently using matrix solution methods. The final type of variable is *event-based* and this is used for the digital part of the mixed-signal model, such as digital logic or Z-domain.

### 2.1.3.3 Representing Model Behaviour

Generally, analogue models are described using non-linear ordinary differential equations, and these provide the simultaneous equations fundamental to the matrix to be solved by the simulator. Parameters and Sequential variables may use sequential assignments, including if-then-else type expressions, but ultimately they must feed values into the appropriate simultaneous equations to be solved. Event-based equations are not included in the analogue solver directly, but use a discrete logic solver called an event wheel. Logic methods are used to handle events, changes, scheduling and conflict resolution. Mixed -signal simulation requires the transfer of information between the boundary elements of the analogue and digital systems respectively.

### 2.1.3.4 Connections types

There are two general types of connection used in analogue simulation, *signal flow* and *conserved energy*. Signal flow is the classical control system definition, where the signal has a single value only. An example is shown in figure 2.2(a), with a simple gain block. The model has an input pin *in*, and an output pin *out*. In this type of model, there is no concept of loading or impedance, so the output will always be the input times the gain. In contrast, the conserved energy connections have two values. This apparent contradiction is best explained using a simple example of an electrical resistor, shown in figure 2.2(b). At the connection pin p, there is both a potential difference between the pin and ground (voltage), and a current through the pin. This becomes important when models are connected together in a circuit, as the conserved energy case will be dependent on impedances and loading.



(a)                                     (b)
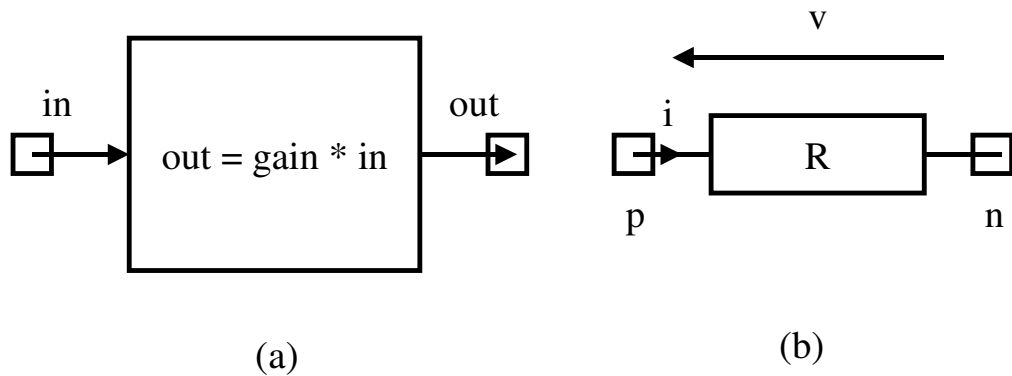
**Figure 2.2 : Signal Flow and Conserved Energy Model Examples**

### 2.1.3.5   Through and Across Variables

In conserved energy systems, the variables at each connection can be divided into *through* or *across* variables. It is useful to explain this concept using practical examples, in this case the resistor. The voltage across the resistor is defined as the potential difference between the pins p and n. Therefore the voltage (v) is defined as an *across* variable as it is literally *across* the component pins. The current passes *through* the pins and is therefore defined as a *through* variable.

### 2.1.3.6   Generic versus Component Models

A model can be defined in two terms, one of which is a *generic* model that is the general behaviour of a physical type of part, e.g. an opamp or mosfet model. The other type is the *component* or characterized model. This is where the model parameters of a generic model are characterized such that the model behaviour matches that of a specific physical part. Using the example of an opamp, the generic model may be the Boyle *et al* [221] macromodel with the component model defined with parameters for the specific part e.g. UA741.

### 2.1.3.7   Summary of Model Definition

The fundamental concepts of what constitutes a model have been defined, but it is helpful to demonstrate with practical examples. Sections 2.1.4-2.1.6 show how these concepts are applied to the three main technologies used in this thesis, electrical, magnetic and thermal. Section 2.1.7 explores mixed-technology modeling and shows how to link the domains together in models. It is important to recognise at this stage that the choice of simulator affects fundamentally how the different technologies are defined. All SPICE based simulators are purely electrical, there is therefore no concept of other technologies inherent in the models. If other domains are modeled in SPICE, the units are *analogous* to voltage and current. Hardware Description Languages (HDLs) such as Saber's MAST modeling language or the IEEE 1076.1 (VHDL-AMS) modeling language allow the specification of different technologies directly in the model and can therefore be considered true multiple-domain modeling languages.

## 2.1.4   Electrical System Modeling

Electrical connections or nets have the units of voltage (V) for potential difference and current (A) for through current flow.  KCL is used by circuit simulators to solve for these variables at junctions in schematics using standard matrix techniques described specifically later in this thesis. All the connection points in SPICE simulators are considered electrical and therefore all nets will have an associated voltage and current. HDL based modeling languages (e.g. MAST or VHDL-AMS) require the explicit definition of connection points as electrical. Thus, using a resistor as an

example with the MAST modeling language, its connection points p & n need to be explicitly defined as electrical, implicitly defining the voltage and current variables for the pins in question.

Defining the variables of electrical models is in terms of the connection points and internal variables (through and across). The resistor example has a current *ir* through the device from pins *p* to *n*, and this is defined using the HDL construct (2.1).

$$i(p\text{->}n) \mathrel{+}= ir \tag{2.1}$$

This means "The current flowing through from pin *p* to pin *n* is equal to the variable *ir*". The voltage across the resistor is similarly defined using the construct (2.2)

$$v(p) - v(n) = vr \tag{2.2}$$

This means "The variable *vr* is equal to the voltage at pin *p* minus the voltage at pin *n*". The variables *vr* and *ir* are defined using the definitions (2.3) and (2.4) respectively.

$$var\ i\ ir \tag{2.3}$$

$$val\ v\ vr \tag{2.4}$$

These mean, *ir* is a simultaneous equation variable (var), with units of *i* (current) in the electrical domain and *vr* is a procedural variable (val), with units of *v* (voltage) in the electrical domain.

## 2.1.5   Thermal System Modeling

Thermal modeling uses the same basic construction as electrical with some basic differences. The through variable is defined as Heat Flow (W) and the across variable is temperature (ºC or K). This makes sense from a physical point of view, as the heat flows through the physical elements, and this causes a temperature difference between points.

Modeling thermal networks in electrical simulators is then a case of assigning thermal connections to analogous electrical connections, where the voltage represents the temperature and the current represents the heat flow.

Using HDLs with explicit thermal declarations allows the direct specification of thermal connection pins using the construct of the form in (2.5)

$$thermal\_c\ j\_th \tag{2.5}$$

which means, the pin *j_th* is a thermal pin, with a through variable type of heat flow (W) and an across variable of type ºC.  Taking a thermal resistor as an example, it has a heat flow *pth* through the device from pins *p* to *m*, and this is defined using the HDL construct (2.6)

$$p(p\text{->}m) \mathrel{+}= pth \tag{2.6}$$

This means "The heat flow flowing through from pin *p* to pin *m* is equal to the variable *pth* (W)". The temperature difference across the thermal resistor is similarly defined using the construct (2.7)

$$tc(p) - tc(m) = tempj \qquad (2.7)$$

This means "The variable *tempj* is equal to the temperature at pin *p* minus the temperature at pin *m*". The variables *pth* and *tempj* are defined using the definitions (2.8) and (2.9) respectively:

$$var\ p\ pth \qquad (2.8)$$

$$val\ tc\ tempj \qquad (2.9)$$

These mean, *pth* is a simultaneous equation variable (var), with units of p (W) in the thermal domain and *tempj* is a procedural variable (val), with units of tc (ºC) in the thermal domain.

## 2.1.6   Magnetic System Modeling

Magnetic modeling again uses the same basic construction as electrical with some differences. The through variable is defined as Flux (Wb) and the across variable is MMF (Magneto Motive Force) (A). This makes sense from a physical point of view, as the flux flows through the magnetic elements, and this causes a magnetic field difference between points.

Modeling magnetic networks in electrical simulators is then a case of assigning magnetic connections to analogous electrical connections, where the voltage represents the mmf and the current represents the flux.

Using HDLs with explicit magnetic declarations allows the direct specification of magnetic connection pins using the construct of the form in (2.10).

$$magnetic\ p \qquad (2.10)$$

Which means, the pin *p* is a magnetic pin, with a through variable type of flux (Wb) and an across variable of type MMF (A).  Taking a linear core as an example, it has a flux *f* through the device from its pins *p* to *m*, and this is defined using the HDL construct (2.11).

$$f(p\text{->}m) += f \qquad (2.11)$$

This means "The flux flowing through from pin *p* to pin *m* is equal to the variable *f* (Wb)". The MMF across the core is similarly defined using the construct (2.12).

$$mmf(p) - mmf(m) = mmf \qquad (2.12)$$

This means "The variable *mmf* is equal to the mmf at pin *p* minus the mmf at pin *m*". The variables *f* and *mmf* are defined using the definitions (2.13) and (2.14) respectively.

$$var\ f\ f \qquad (2.13)$$

$$val\ mmf\ mmf \quad\quad\quad (2.13)$$

These mean, *f* is a simultaneous equation variable (var), of type flux (Wb) in the magnetic domain and *mmf* is a procedural variable (val), of type mmf (A) in the magnetic domain.

### 2.1.7 Mixed System Modeling – Electromagnetic

The power of multiple domain modeling becomes apparent when different technologies require to be simulated in the same circuit. A good example of this is simulating a magnetic component in the context of an electrical circuit. If we consider a winding, it has electrical connections to the circuit with voltages and currents, but there are also the magnetic variables, flux and magnetic field in the magnetic domain. As has been stated previously, if a purely electrical simulator is used, then all the variables will be electrical anyway, but analogies are used to infer the correct type. If HDLs are applied, then the correct units can be explicitly stated in the models. The example of a winding has four connections as shown in figure 2.3.
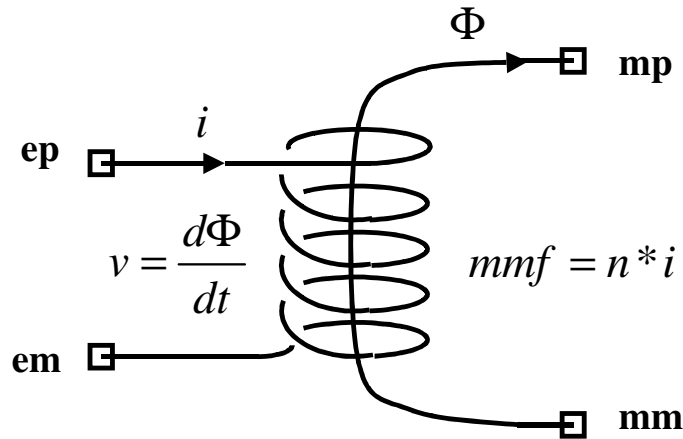


**Figure 2.3 : Winding Model**

The connections ep and em are electrical (voltage & current) with the connections mp and mm magnetic (flux & mmf). The nature of the relationship between the domains is defined in figure 2.3. Cherry [15], Laithwaite [16] and Carpenter [17] describe the relationship between the electrical and magnetic domains specifically. Note that the transfer from electrical to magnetic is straightforward, with the MMF proportional to the current in the winding, but that the magnetic to electrical transfer has the voltage proportional to the *derivative* of the flux. This has important implications with regard to operating points and offsets in the domains, and a magnetic offset will not be recognized directly in the electrical domain. One possible approach therefore is to use the derivative of the flux as the through variable, but this precludes the setting of D.C. flux conditions in the model. This is a severe limitation and important in accurate modeling of power transformers especially.

Using the basic definitions of current, voltage, flux and mmf previously described, the equations for the mixed technology model can be implemented using these variables. In this case, the winding is represented by the two main equations (2.15) and (2.16) using an HDL (MAST).

$$i: v = d\_by\_dt(f*n) \tag{2.15}$$

Which means, "solve for the current $i$ such that the voltage across pins $ep$ and $em$ is equal to the derivative of the flux ($f$) multiplied by the number of turns ($n$)".

$$f: mmf = i*n \tag{2.16}$$

which means "solve for the flux $f$ such that the MMF is equal to the current in the winding ($i$) multiplied by the number of turns ($n$)".

## 2.2   Component Modeling Techniques

### 2.2.1   Introduction

There are different methods of creating component models of real devices ranging from highly abstract models using simple, approximate equations to complex structural models including detailed physical effects. The approaches fall into two main categories *behavioural* and *structural*. Behavioural modeling can take the form of direct implementation of model equations using Hardware Description Languages or so-called macro-modeling using building blocks (gain, derivative, combinations etc) to provide the correct behaviour. Structural modeling involves building as close a representation of the actual physical device as possible. Actually, the models are all essentially behavioural and it is purely a question of how abstract the model is, that defines the model type fundamentally.

### 2.2.2   Behavioural Modeling using Hardware Decription Languages

Implementing behavioural models directly using languages such as MAST or VHDL-AMS is rapidly becoming the technique of choice in a wide variety of design situations. It is already prevalent in high density ASIC design (VHDL & Verilog are used in this case for digital designs), but the same techniques are becoming widely used in general electronic design. The advantages of this type of approach are that a direct implementation of the equations in a model allows direct control of the accuracy and features in the model, with an efficient and fast simulation. In this case, accuracy does not necessarily get sacrificed at the expense of faster simulations as that depends entirely on the accuracy of the behavioural model equations.

### 2.2.3   Behavioural Modeling using Macro-Modeling

Macro-Modeling has historically been used with SPICE derivative simulators for one simple reason. The original SPICE simulator contained a fixed number of pre-compiled primitive models,

requiring any new model to be built up from these basic primitives. The technique has been successfully applied in a wide variety of cases through necessity, and modern spice simulators such as Pspice allow limited equation based entry for 'Psuedo' behavioural modeling. The approach can provide similar improvements in simulation speed depending on the equations, but may give slightly less efficient and robust models than a Hardware Description Language. This is because the underlying macro-model may not have the same stability as a tuned direct equation model, and extra components are required to give convergence (such as the ubiquitous large resistances to ground in SPICE). HDLs also generally provide convergence aids, which help non-linear circuits particularly.

### 2.2.4   Structural/Component Level Modeling

It is often the case, that despite the behavioural model being accurate and fast, a full physical model of the device is required. This is where structural modeling becomes necessary. An example of this would be an operational amplifier, where after a behavioural simulation demonstrates the basic performance is acceptable, the design using transistors needs testing to ensure that the individual transistor parameters (length, width, technology) will meet the designer's requirements. This type of simulation can be much slower than behavioural methods and in general judicious choice of which type of model to use in different circumstances is required for optimum efficiency.

### *2.3   Circuit Simulation Techniques*

Circuit simulation is a method whereby electric circuits are modeled using behavioural blocks representing individual components, such as resistors and capacitors, and the resulting equations are solved to determine the function of the circuit. Vlach and Singhal [9] and Kielkowski [10] are good textbooks for explaining circuit simulation. However, it is important to review the key concepts involved as they are common to almost every commercial simulator available on the market today.

### 2.3.1   Solving linear equations using Gaussian Elimination

The first step in the simulation of an electric circuit is to construct a set of equations that describe the elements in the circuit and their connections using either Kirchoff's Voltage Law (KVL) or Current Law (KCL). Taking the circuit example shown in figure 2.4 the nodal equations for the circuit can be obtained using KCL, summing the currents at nodes n1, n2 and n3.
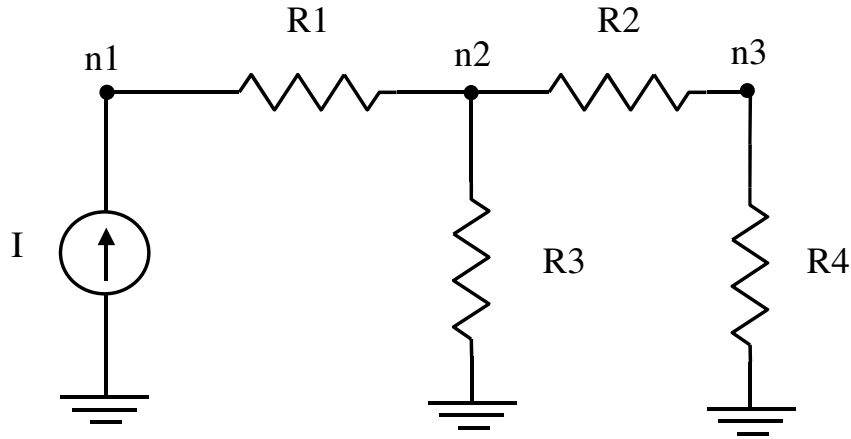
**Figure 2.4 : Simple Linear Network[1]**

The method of equation formulation is basically the same regardless of whether the system contains linear or non-linear elements. The resulting equations can then be rewritten in a matrix form as shown in equation 2.17 and then solved using standard methods for solving simultaneous equations such as Gaussian Elimination (described in good numerical analysis textbooks, such as [11]).

$$\begin{bmatrix} \dfrac{1}{R_1} & -\dfrac{1}{R_1} & 0 \\ \dfrac{1}{R_1} & -\dfrac{1}{R_1}-\dfrac{1}{R_2}-\dfrac{1}{R_3} & \dfrac{1}{R_2} \\ 0 & \dfrac{1}{R_2} & -\dfrac{1}{R_2}-\dfrac{1}{R_4} \end{bmatrix} \begin{bmatrix} V(n1) \\ V(n2) \\ V(n3) \end{bmatrix} = \begin{bmatrix} I \\ 0 \\ 0 \end{bmatrix}$$

(2.17)

If we apply forward elimination to this network using a current source of 1A and resistor values of R1=R2=5Ω and R3=R4=10Ω, we obtain the set of matrix equations given in equation 2.18.

$$\begin{bmatrix} -2 & 2 & 0 \\ 0 & 3 & -2 \\ 0 & 0 & -5/3 \end{bmatrix} \begin{bmatrix} V(n1) \\ V(n2) \\ V(n3) \end{bmatrix} = \begin{bmatrix} 10 \\ -10 \\ 20/3 \end{bmatrix}$$

(2.18)

Solving this set of equations is now trivial using back substitution with n3 = 4V, n2 = 6V and n1=11V. This in fact is effectively how simulators such as SPICE calculate operating point solutions for circuits although in practice a more efficient approach of the Gaussian Elimination Method known as LU decomposition [11] is applied.

---

[1] This example is a general circuit based on a specific case given in Vlach and Singhal [9].

### 2.3.2 Circuit Elements and Netlists

The manual construction of system equations by hand is not useful for anything other than trivial circuits, so a more practical automated approach is required. In simulation programs each circuit element, such as a resistor, is represented by a set of equations, which can be written in a matrix form referred to as a template. The templates for the complete circuit are then constructed into a single matrix that can be solved as described previously. The method of describing how the templates are connected, numbered and any parameters defined is called a netlist. The general form of a SPICE netlist entry is given in figure 2.5 and the complete SPICE netlist for the example circuit previously shown in figure 2.4 is given in figure 2.6.

<Element><Identifier> <Pin1> <Pin2> .. <PinN> <Parameters>

**Figure 2.5 : General Form of Netlist Entry**

```
I1    n1    0     1
R1    n1    n2    5
R2    n2    n3    5
R3    n2    0     10
R4    n3    0     10
```

**Figure 2.6 : SPICE Netlist  for example circuit with realistic values**

In practical software the netlist is usually generated automatically from a schematic diagram of the circuit, although small netlists are frequently created manually.

### 2.3.3 Solving Non-linear Equations

It is of course not realistic to restrict the model equations to a linear form and so a method for solving non-linear equations must be used. Common non-linear solution techniques are the Newton-Raphson and Katz-Nelson methods. The Newton-Raphson method [10] is commonly used in commercial simulators such as SPICE and applies an iterative technique to approach the exact solution for a non-linear equation. The basic Newton-Raphson formula is given in equation 2.19 where $F(X)=0$ is the equation to be solved and $F'(X)$ is its derivative. $X_n$ is the value of $X$ during the current iteration and $X_{n+1}$ is the value of $X$ at the next iteration.

$$X_{n+1} = X_n + \frac{F(X_n)}{F'(X_n)} \tag{2.19}$$

This method requires the formula to be iterated until the value for F(X) approaches zero. It is necessary to specify the value of target error, and when F(X) falls below this value convergence is achieved. It is important to notice that if the derivative F'(Xn), or slope, of the function F(Xn) tends to zero, then equation 2.19 will go to infinity and therefore not converge to a useful solution. To illustrate how the method operates in practice a non-linear example is shown in figure 2.7.
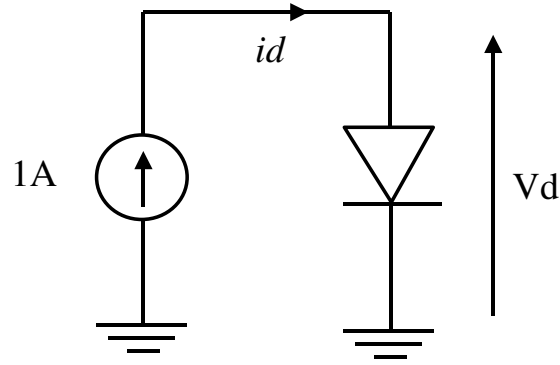
**Figure 2.7 : Non-Linear Diode Circuit Example**

The equation for the non-linear diode model used is given by equation 2.20.

$$i_d = (e^{40V_d} - 1) * 10^{-12} \qquad (2.20)$$

Using equation 2.20, the complete circuit equation can be rewritten in the form shown in equation 2.21, where all the terms are brought onto one side (this becomes *F(Xn)* in equation 2.19) and differentiated to provide the slope for the Newton-Raphson equation *F'(Xn)* as shown in equation 2.22.

$$F(V_d) = (e^{40.V_d} - 1) * 10^{-12} - i_d \qquad (2.21)$$

$$F'(V_d) = 40.e^{40.V_d} * 10^{-12} \qquad (2.22)$$

Figure 2.8 shows how the values of Diode Voltage *Vd (Xn)* converge onto a solution value of 0.6908V within 20 iterations from an initial starting point of 1V.
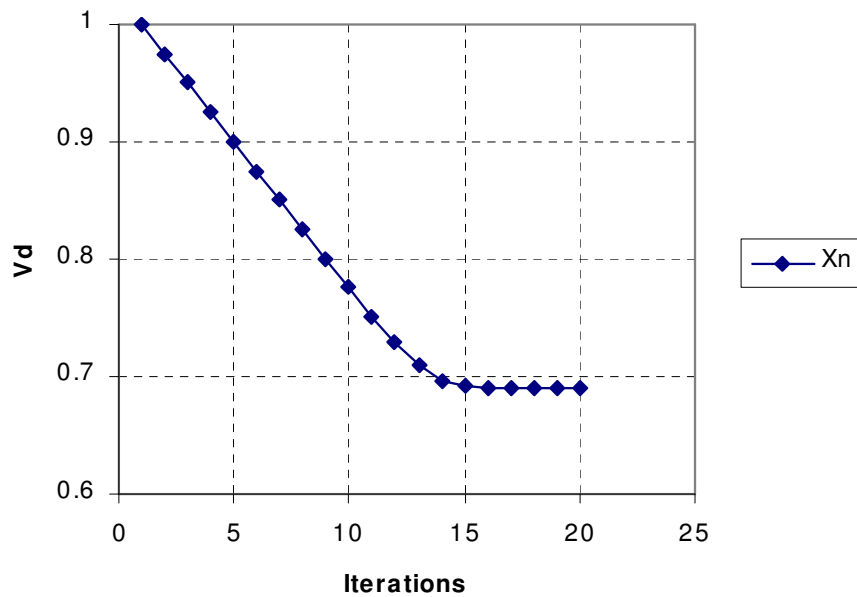


**Figure 2.8 : Graph of the Diode Voltage, *Vd (Xn),* showing convergence to 0.69V**

24

Note that in this example there is rapid convergence with reasonable stability. It is important to ensure however that a reasonable initial condition value is chosen so that convergence occurs to the anticipated correct solution as the solution found may not necessarily be unique.

### 2.3.4   Integration Methods

#### 2.3.4.1   Introduction

In order to establish the time domain response of a network, the differential equations for the system variables need to be numerically integrated. The methods for numerical integration consist of two main types, the Linear Multi-Step (LMS)[2] and Runga-Kutta methods. The LMS techniques contain methods such as forward and backward Euler, and variations on the trapezoidal method. In the descriptions of all the methods, the following basic notation is used. The variable to be found is $x$ with respect to time ($t$) and so the equation to be integrated is:

$$x' = f(x,t) \tag{2.23}$$

Which can be rewritten as:

$$x = x(a) + \int_a^b f(x,t)dt \tag{2.24}$$

The value of $x$ at the current time, $t_n$, is the current solution and is denoted by $x_n$. The initial condition is defined by

$$x_0 = x(a) \tag{2.25}$$

The solution at a time after a small step forward, $t_{n+1}$, is denoted by $x_{n+1}$, and the resulting time difference between the current and next solutions is called the timestep ($h$) and is given by 2.26.

$$h = t_{n+1} - t_n \tag{2.26}$$

#### 2.3.4.2   Forward Euler Integration

The forward Euler method uses the knowledge of the current point ($x_n$), the timestep ($h$) and the derivative ($x'$) and approximates the slope between the current and next point ($x_{n+1}$) using:

$$x_n' = \frac{x_{n+1} - x_n}{h} \tag{2.27}$$

---

[2] Vlach and Singhal [9] provide examples of these methods of intgeration applied to circuit simulation and Hosking, Joe, Joyce and Turner [11] from a general numerical analysis perspective. The latter gives psuedo code listings that are helpful in coding routines. C Code can also be found in "Numerical Recipes in C" [83].

Rearranging 2.27 provides an expression for the next value of $x$ as given by:

$$x_{n+1} = x_n + x_n' h \qquad (2.28)$$

This is the simplest, and probably least accurate method for calculating the integral of $x'$.

### 2.3.4.3  Backward Euler Integration

The Backward Euler method is similar to the forward Euler approach apart from using the next point $x_{n+1}$ as the point for calculating the derivative:

$$x_{n+1}' = f(x,t) \qquad (2.29)$$

And similarly again to the Forward Euler, the next value, $x_{n+1}$, is estimated using:

$$x_{n+1} = x_n + h x_{n+1}' \qquad (2.30)$$

This procedure is then iterated until $x_{n+1}$ converges onto a solution.

### 2.3.4.4  Trapezoidal Integration

Trapezoidal Integration uses a combination of the derivatives at the current and next simulation points to calculate the integral. The average value is taken as shown by:

$$x_{n+1} = x_n + \frac{h}{2}\left(x_{n+1}' + x_n'\right) \qquad (2.31)$$

### 2.3.4.5  Runga-Kutta Integration

One problem with the previously described LMS methods, is the poor accuracy that can result unless a very small timestep ($h$) is used. This can be a severe penalty in time domain simulation, and so alternative techniques are used such as the Runga-Kutta method [83]. The basis of this technique is to take a trial step and use the information to provide a more accurate estimate of the average slope over the complete time step. The Runga-Kutta method may use different orders, which define the number of trial steps to be taken. If the second order Runga-Kutta is used to illustrate the method, the equations can be easily derived. The first step is to calculate an intermediate point , $k_1$:

$$k_1 = h f(x_n, t_n) \qquad (2.32)$$

And use this point to calculate a second intermediate point, $k_2$:

$$k_2 = h f(x_n + k_1, t_n + h) \qquad (2.33)$$

The next value is then obtained by using the intermediate points in:

$$x_{n+1} = x_n + \frac{1}{2}(k_1 + k_2)$$ (2.34)

Hosking, Joe, Joyce and Turner [11] have compared the methods of integration, and show that even a second order Runga-Kutta integration of a simple equation can be over 25 times more accurate that the corresponding Backward Euler approach. The fourth order Runga-Kutta method has generally been used in this thesis for any numerical integration

### 2.3.5 Time Domain Simulation

With the methods previously described in this section, it is possible to carry out time-domain or transient analysis simulations. The flowchart in figure 2.9 shows how this can be carried out. It is worth noting that the timestep, $h$, is usually allowed to be variable in practical simulators. This is important in non-linear and switching systems in particular to obtain efficient use of the available computing power where the timestep can be decreased to improve accuracy on fast switching waveforms and then increased where the waveform becomes relatively slowly changing.

### 2.3.6 Small Signal AC Analysis

Small signal AC analysis is used to provide a frequency response of the linearized behaviour of a system. The matrix solution techniques are the same as for a steady state (DC) operating point analysis, with the difference being that all the variables are complex. The conventional way of carrying out such an analysis is to sweep the frequency of the sources, while keeping the applied voltage magnitude normalized to 1V and the phase to 0. An important assumption is that the actual voltage is considered very small, with regard to any non-linearities in the system, and therefore the linearized model is valid for this purely linear analysis. This also implies that the choice of operating point is crucial in determining the correct behaviour.
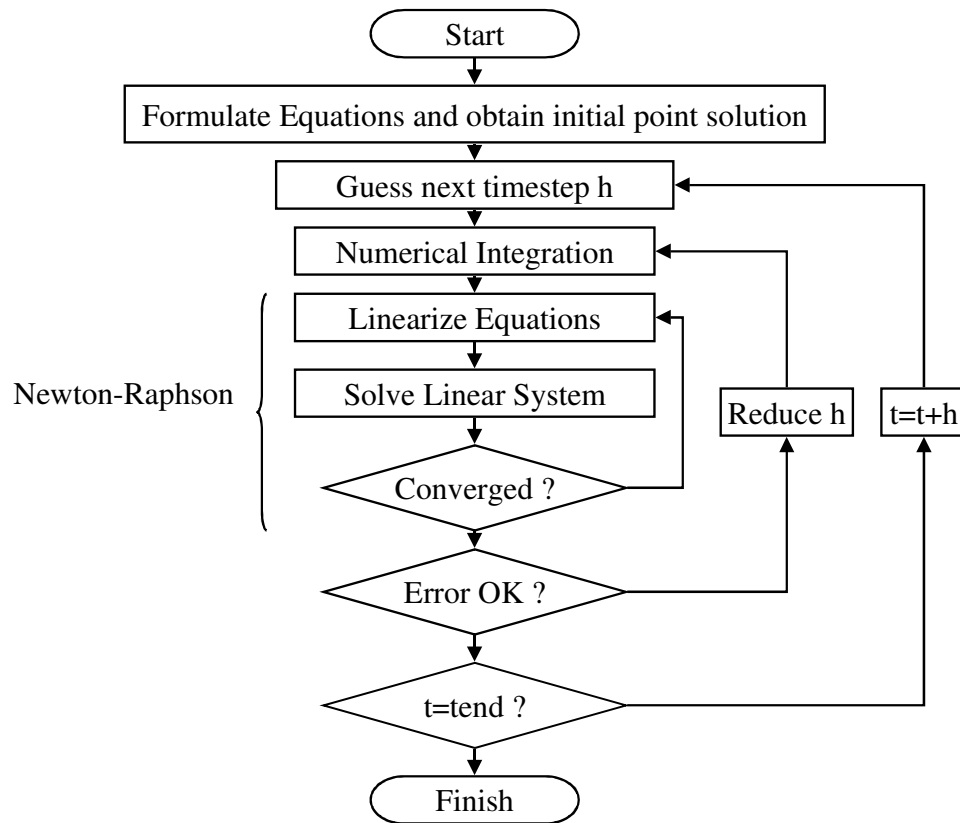
**Figure 2.9 : Time Domain Analysis Flowchart**

## 2.4   Electro-Magnetic Device Modeling

### 2.4.1   Introduction

So far the simulation methods outlined have been applicable to circuits and networks of lumped elements, but there are a range of techniques which are based on sub-dividing the geometry of the component into small elements and solving for the fields directly. These methods range from the Tubes and Slices approach, which is related to magnetic circuit models, to two- and three-dimensional field solutions using Finite Element and Finite Difference methods.

### 2.4.2   Finite Element Analysis

#### 2.4.2.1   Introduction

Finite element analysis (FEA)[3] has been used in mechanical modeling and structural analysis for many years, but comparatively recently in the field analysis application area. Silvester and Ferrari [5] provide an excellent practical overview of the method, its application in electrical engineering problems and example coding structures. Lowther and Silvester [12] give practical insight into the

---

[3] Also known as the Finite Element Method (FEM)

design and construction of CAD software and more theoretical texts, Hoole and Hoole [13] and Binns, Lawrenson & Trowbridge [6], are also useful in understanding the mechanisms behind the method. In this project commercially available Finite Element Analysis Software was used, but an understanding of the approach is useful in ensuring accuracy and validity of the results.

The basis of the Finite Element Analysis technique is to initially divide the geometric description into a set of smaller geometric elements such as triangles. The set of elements is called a Finite Element Mesh. Problems in electrical engineering field analysis require that Laplace's equation for the field in the problem region to be solved to calculate the field distribution as illustrated by Silvester and Ferrari [5]. Using the field distribution, the stored energy must be minimized, to meet the requirement of minimum potential energy in the system. Ferrari and Silvester [5] show how this can be coded, and give examples of finite element analysis software in Fortran.

### 2.4.2.2 Boundary Conditions

There are two basic types of boundary used in Finite Element Analysis, the Dirichlet and the Neumann boundaries. The Dirichlet Boundary specifies a fixed value of potential for the element in question. An example of this type of boundary would be to apply a voltage of 10V to one plate of a capacitor, and -10V to the other plate. The Neumann boundary is where the derivative of the field value is 0 and this is used to define symmetrical boundary conditions. Hoole and Hoole [13] provide a good explanation of the different boundary condition mathematical representations and examples. The judicious use of boundary conditions and symmetry can reduce the complexity and simulation time of a problem significantly.

### 2.4.2.3 Post-Processing and Analysis

After the Finite Element Analysis has been completed, the flux lines or equipotentials can be plotted. Using the calculated energy value, it is also possible to derive component parameters such as Inductance or Capacitance from the results.

### 2.4.3 Tubes and Slices

The tubes and slices approach described by Hammond and Sykulski [14] for the modeling of magnetic devices is a method of dividing the geometric region into slices of constant potential and tubes of constant flow. The approach can be used for electrical, electrostatic and electromagnetic problems with a similar geometric construction, but with different variables for the tubes and slices.

### 2.4.4 Finite Difference

An alternative to the Finite Element Method is the Finite Difference Method. As the similarity in the name implies, the method also involves subdividing the problem region into smaller sections, but there are some major differences in the approach. The Finite Difference method for meshing is

to apply a uniform mesh of lines parallel to the coordinate system used. Using the mesh previously generated, each node in the mesh can then be described using its immediate neighbours. This can then be constructed into a matrix to represent the equations for all the nodes in the geometry, and solved using standard Gaussian Elimination.

*Chapter 3*

# 3   Review of Magnetic Material Modeling

## *3.1   Introduction to Magnetism in Soft Ferrite Materials*

In this project the magnetic materials used are generally soft ferrites and so other materials such as Iron or Steel Alloys are not discussed in this introduction. The use of the terms 'hard' and 'soft' when applied to magnetic materials do not refer to their physical hardness but to their coercivity (although there is a correlation and is in fact where the term comes from originally). Soft magnetic materials have coercivity less than 1 kA/m and hard magnetic materials greater than 10kA/m as discussed by Philips [2] and Boll [8]. Ferrites are chemically inert ceramic materials which have the general structure $XFe_2O_4$ where X is one of the transition metals given in table 3.1.

| Metal | Symbol |
|---|---|
| Manganese | Mn |
| Zinc | Zn |
| Nickel | Ni |
| Cobalt | Co |
| Copper | Cu |
| Iron | Fe |
| Magnesium | Ma |

**Table 3.1 Divalent Transition Metals used in Soft Ferrites**

Combinations of powders of these metals are then mixed according to specific proportions, milled to ensure the required grain size and then pressed into shape. Sintering, heating to between 1150ºC and 1300ºC, hardens the material physically and ensures the desired magnetic properties. The sintered core may still require further finishing to ensure accurate dimensions or smooth surfaces for mating core halves and if so the material is finely ground. This grinding is also used to accurately implement centre core air gaps.

The sintered and finished material contains thousands of small crystals or grains of the ferrite material [2], usually 10s of μm across.  Figure 3.1 shows a Scanning Electron Microscope Image of a soft ferrite material magnified 2,500 times illustrating the shape and size of the grains in the material. Each grain has one or more magnetic regions called domains that are already randomly magnetically oriented due to the material's intrinsic magnetization after heating. These domains come into progressive alignment with the application of an external magnetic field as shown in figure 3.2. Explanations of the physical mechanisms behind these processes are given in Cullity [3] and Tebble & Craik [7].
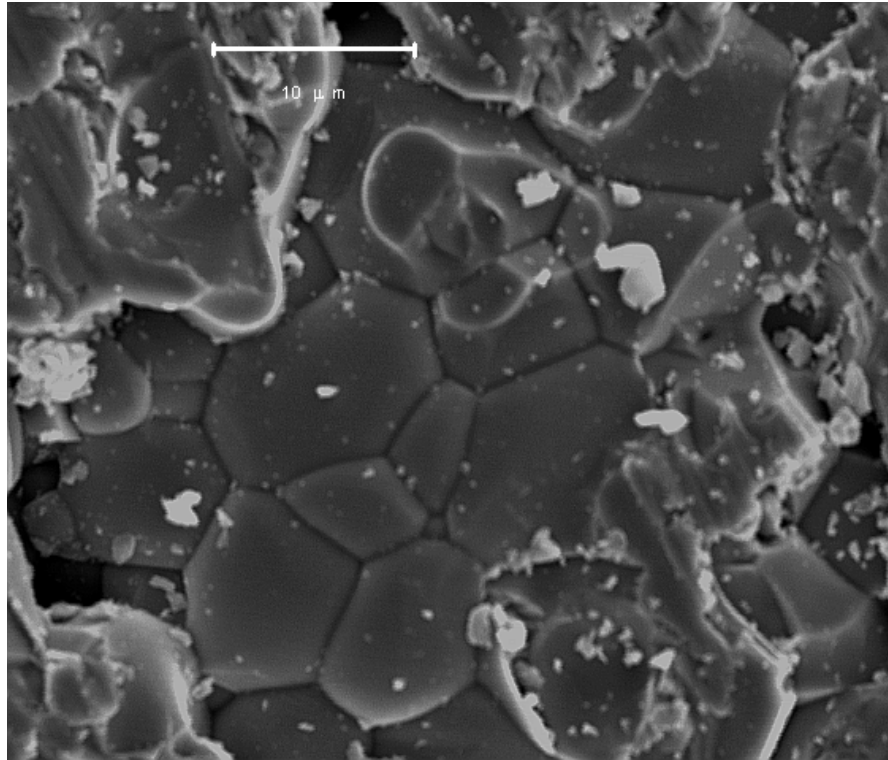
**Figure 3.1 Scanning Electron Microscope (SEM) Image of Philips 3F3 soft ferrite material with a magnification of 2,500 showing ferrite grains. [4]**
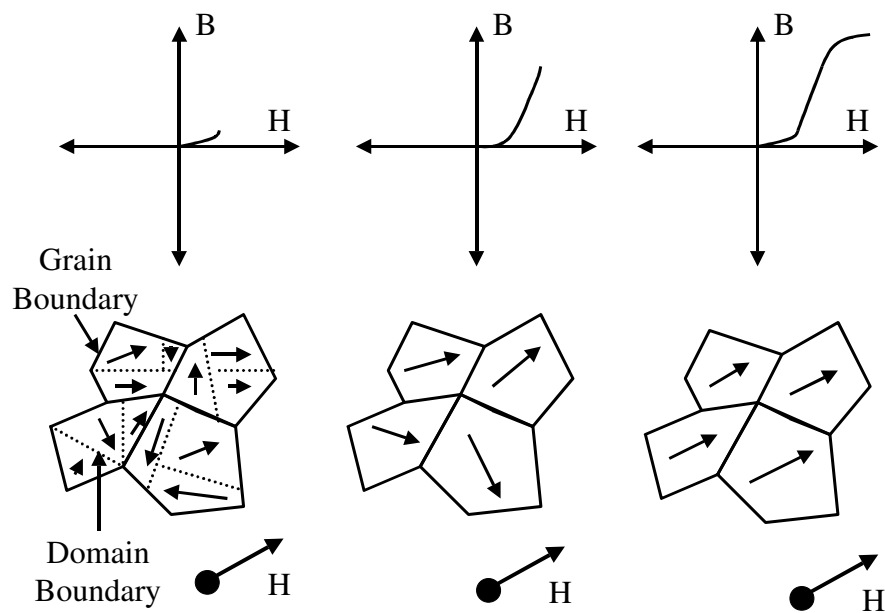


**Figure 3.2: Progressive alignment of magnetic domains and grains, and the resulting magnetization curves for applied field strength H**

---

[4] The Scanning Electron Microscope used was a JEOL JSM-6400 & the photomicrograph was taken by the author at the Southampton University Electron Microscopy Centre.

Techniques for domain observation are described by Cullity [3], Tebble & Craik [7] and Jiles [47], and include the use of transmission electron microscopy to observe the change of domain shape under changing applied magnetic fields. The energy lost during the transition of domains from one magnetic state to another gives rise to the effect of hysteresis in soft magnetic materials. Globus, Duplex and Guyot [84] postulate a method for predicting the macroscopic effects such as the initial magnetization curve from the grain sizes in the material.

## 3.2  Magnetic Material Definitions, Metrics and Model Requirements

### 3.2.1  Introduction

In order to assist in the definition of appropriate magnetic models it is important to define the model requirements. It is quite normal to classify the differences between materials simply using the overall major loop characteristics, but it is also important to consider specific metrics, such as remanence or coercive force. The behaviour of smaller loops, called minor loops, is significant for wide-band transformers. The accurate characterization of the energy loss is critical for energy conservation and power calculations especially with arbitrary applied fields. With the use of specific metrics clear distinctions can be drawn between materials and their equivalent models under any applied field conditions. In this section, the important aspects of the behaviour of magnetic material hysteresis are defined. Metrics are also specified for the measurement of, and comparison between, different materials and material models.

### 3.2.2  Hysteresis Loop Definitions

In order to understand the different requirements of magnetic models it is useful to distinguish between different types of hysteresis behaviour in magnetic materials. The basic types of magnetization curves are shown in figure 3.3.
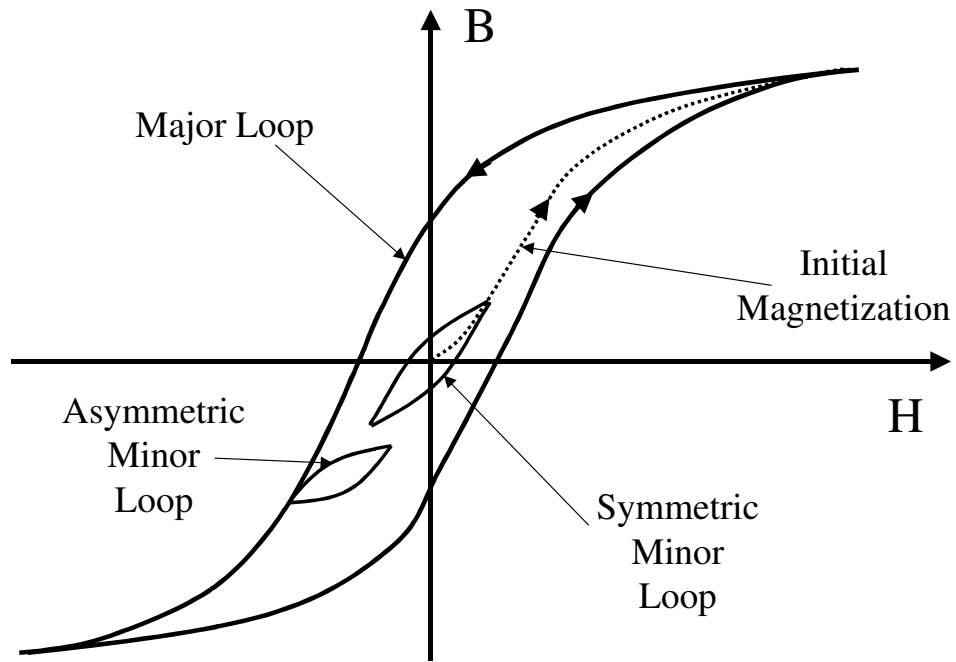
**Figure 3.3: Types of Magnetization Curve and Hysteresis Loop**

The Major Loop is the magnetization curve when the applied field (H) is high enough to force the material into saturation and the BH loop closes at the tips. The Initial Magnetization curve is the transition of the flux density (B) from the initial condition of zero flux to the tip of the major loop. Any loop inside the Major Loop is defined as a Minor Loop, and these may be Asymmetric or Symmetric about the origin as shown in figure 3.3. It is obvious that for accurate simulation of an arbitrary applied field, the initial conditions of flux or magnetization in the model must be correct. The anhysteretic curve is that which the magnetization would relax to for any specific value of applied field (H). This is effectively the minimum state of energy and is shown in figure 3.4.
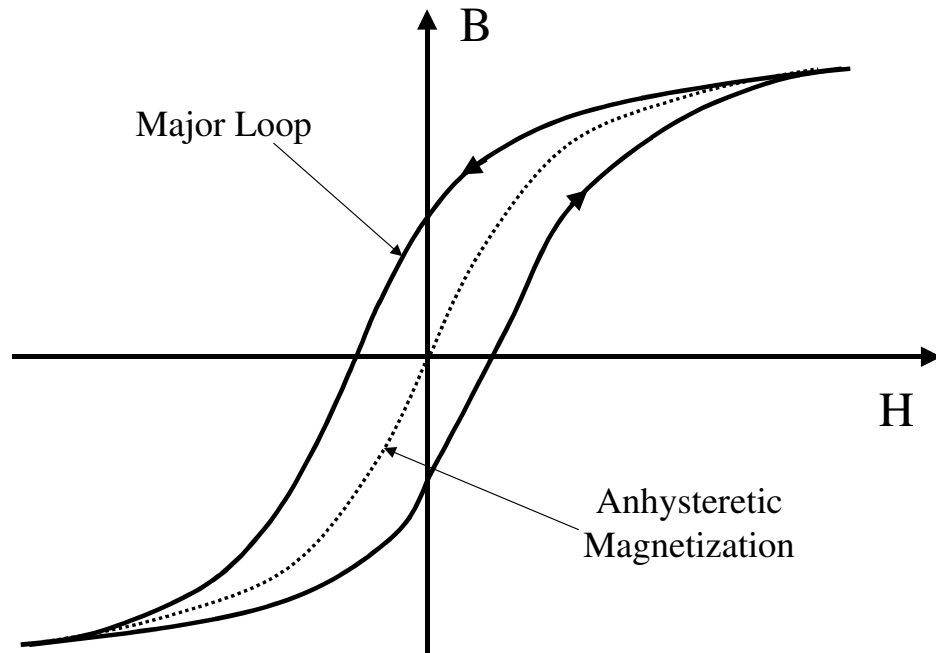
**Figure 3.4: Anhysteretic Magnetization Curve**

When considering the minor loop behaviour of magnetic materials, it is necessary for a model to be capable of exhibiting non-congruency. This means that the minor loop shape changes depending on the initial flux level.

### 3.2.3 Hysteresis Loop Metrics

It is possible to compare the performance of magnetic materials and their models using numerical methods such as the least squares approach, as used by Schmidt and Guldner [40] or Philips, Dupre and Melkebeek [56]. However, it is more useful to compare standard measured characteristics and use them as metrics which define the performance of the material and allow better classification of the materials. Manly [57] defines some of these appropriate metrics and uses them to compare different types of model. Jiles and Thoelke [24] determine specific model parameters using a direct solution of the model equations, and Wilson and Ross [89] have applied the use of metrics for improved general optimization of magnetic material model parameters. Figure 3.5 shows a basic set of the metrics for a major hysteresis loop. The definitions of the metrics are given in Table 3.2.
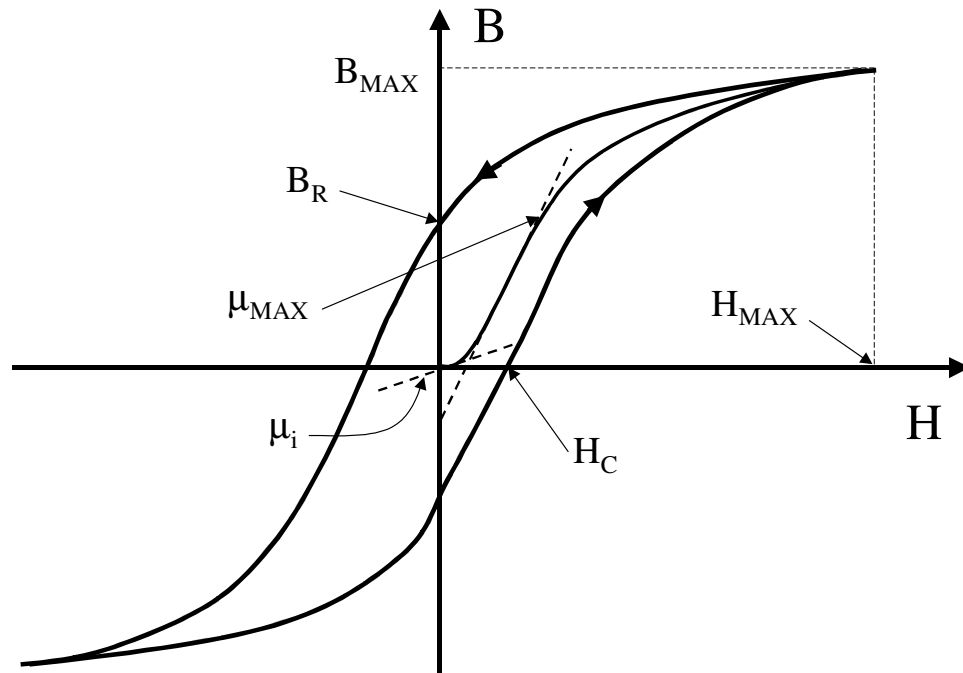
**Figure 3.5: Major BH Loop showing basic set of metrics**

| Metric Symbol | Metric Definition |
|:---:|:---:|
| $B_R$ | Remanence - B Axis Crossing Point |
| $H_C$ | Coercive Force - H axis crossing point |
| $B_{MAX}$ | Maximum Flux Density |
| $H_{MAX}$ | Maximum Applied Field |
| $\mu_{MAX}$ | Maximum Permeability |
| $\mu_i$ | Initial Permeability |

**Table 3.2 Definition of Magnetic Material Metrics**

While these metrics are straightforward to measure directly from a BH Curve, there are other metrics which are also of use including the area of the BH Loop. This defines the energy lost per cycle and in conjunction with the frequency can be used to estimate the power lost by the material. This can be characterized using the Steinmetz expression [92] for each material, which is a simple expression using the peak flux density and frequency to estimate the average power loss. Examples of the estimated power loss for a range of materials can be found in Snelling [27] or typical Manufacturer's Data [2]. Snelling also explains how the Steinmetz equation can be characterized for specific materials. The maximum permeability $\mu_{MAX}$ can refer to the maximum initial permeability (as shown), the maximum incremental permeability (when a small A.C. signal is

applied on top of a D.C. offset signal and the permeability measured), or the maximum effective permeability (measured at the extremities of the BH loops).

### 3.2.4  Energy Considerations

When considering the behaviour of a magnetic material it is important to ensure that the laws of energy conservation are maintained in any model used for circuit simulation. This is particularly important where efficiency is to be calculated, multiple domain simulations are applied and thermal losses are to be extracted. The loss of energy inside a hysteresis loop also has implications for minor loops and their relaxation to a steady state condition. This issue is discussed specifically later in this chapter. If a major hysteresis loop of the form shown in figure 3.5 is considered, the overall energy in the material consists of a stored energy, which is recovered and an energy lost. This is illustrated in figure 3.6 (a) & (b), which shows the transfer of energy in the hysteresis loop through one positive half cycle of the applied field.
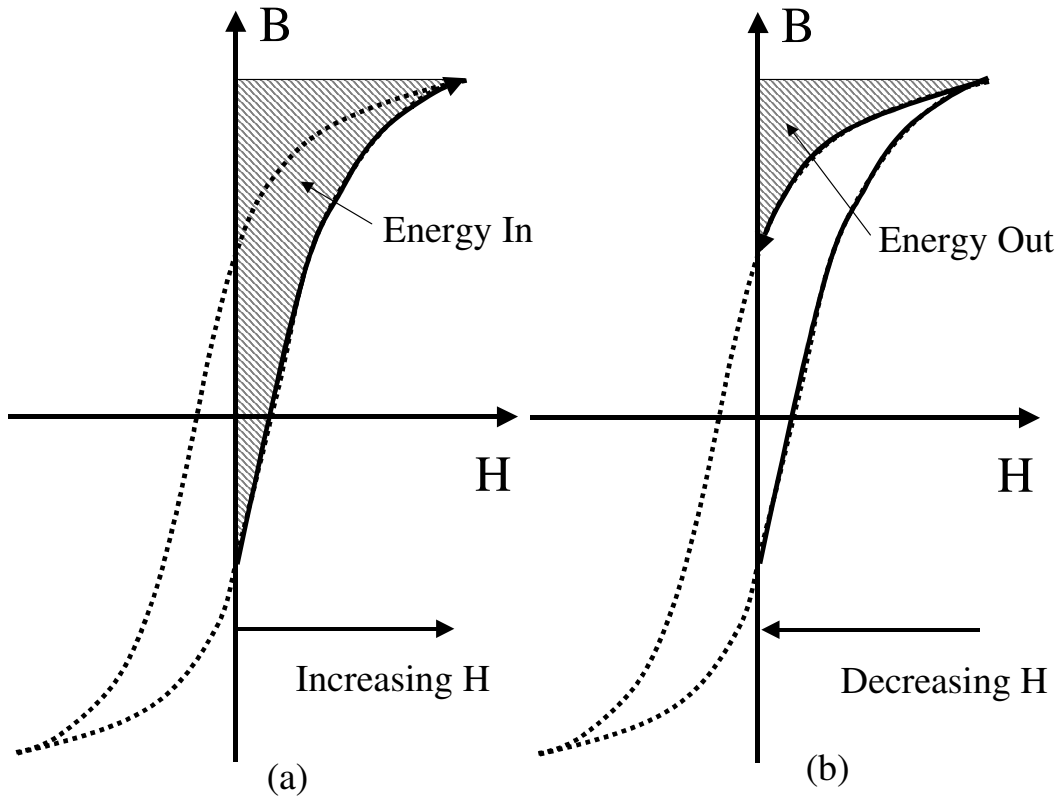


**Figure 3.6: (a) Energy In due to increasing Applied Field (H) (b) Energy Out due to decreasing Applied field (H)**

The 'energy out' is clearly less than that of the 'energy in' the magnetic material and the resulting energy lost is obtained from the area inside the hysteresis loop. The energy lost can be obtained mathematically by using equation 3.1, which is the integration of H with respect to dB over the volume of the material.

$$E = \int_{Volume} H \, dB \qquad (3.1)$$

The area inside the BH Loop, and hence the energy loss, is obtained by integrating H.dB over a complete cycle. This method is appropriate for steady state calculations of energy, but is not adequate for the instantaneous calculation of the energy loss required for simulation in the time domain. An alternative method is therefore discussed later in this thesis which separates the stored and lost energy components of the BH curve and allows the direct extraction of the instantaneous energy loss.

### 3.2.5 Relaxation of Minor Loops

As has been discussed previously in this section there are smaller hysteresis loops called minor loops which may occur symmetrically about the origin, in an implied steady state condition, or asymmetrically from an initial offset flux density (such as a major loop). In the asymmetric case, the minor loop will move to the condition of least energy, and as energy is lost inside the loop will relax to its steady state condition. This is termed the accommodation property of the material, and is discussed by Torre and Vajda [222]. The steady state condition is conventionally assumed to be, but not always, the anhysteretic BH Curve as shown in figure 3.4. This aspect of the material behaviour is a good test of a model, particularly its characterization of the energy loss for an arbitrary applied field or flux. An illustration of the relaxation of a set of minor loops to the effective steady state condition is given in figure 3.7.
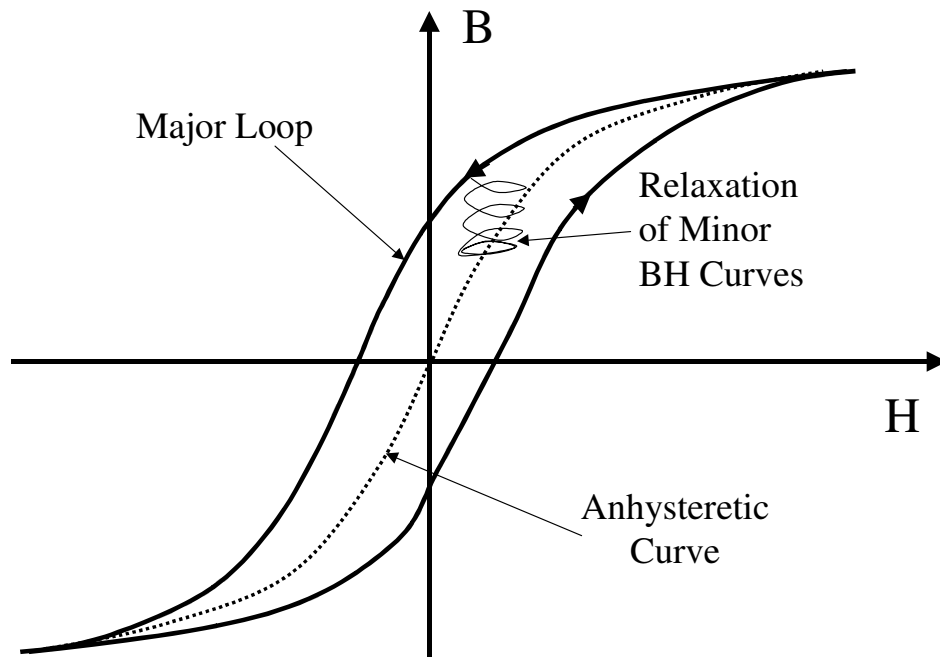


**Figure 3.7: Minor Loop Relaxation Curves**

### 3.2.6 First Order Reversal Curves

Major and Minor Loops have been generally defined, but there is a specific set of minor loops which have been applied to the problem of model parameter extraction (discussed by Doong & Mayergoyz [74] and Mayergoyz and Friedman [76]). These loops are called the first order reversal curves. This set of curves is obtained by applying the field strength necessary to create a Major BH Loop and then reversing the field strength at some point during the cycle and returning to the opposite maximum field strength. If this is repeated across the applied field strength range a set of curves result which are called the first order reversal curves as shown in figure 3.8.
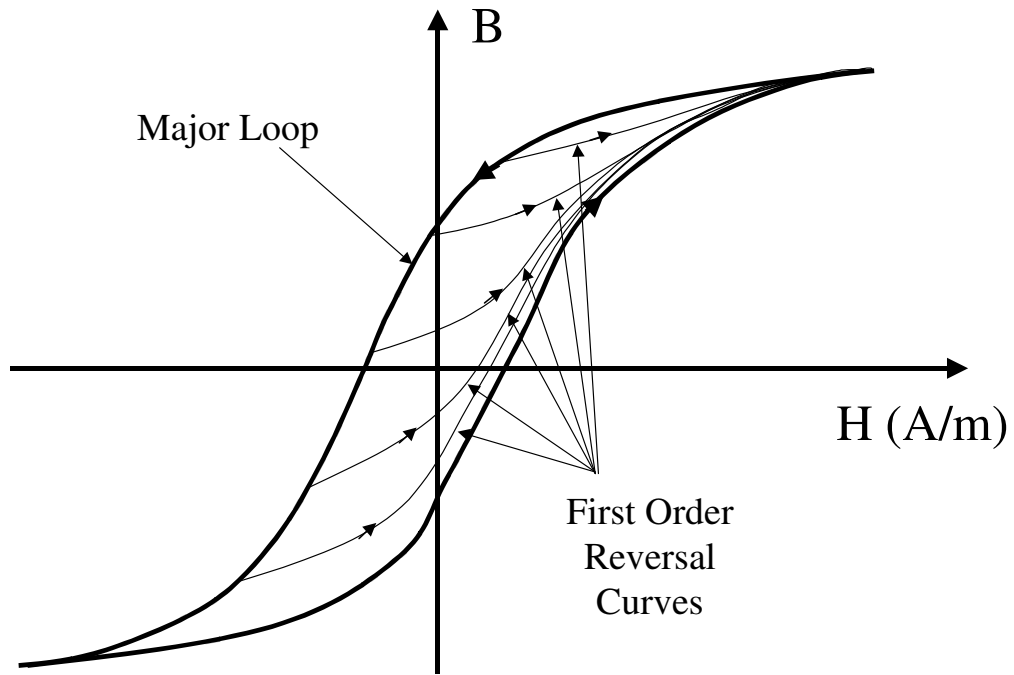


**Figure 3.8: First Order Reversal Curves**

### 3.2.7 Temperature Dependence of Hysteresis Loops

As explained by Jiles [47 pp258-260] the magnetization behaviour of a magnetic material is dependent on its thermo-dynamic characteristics. This dependence on the temperature is apparent in both changes in the effective permeability [2] and the effective energy lost, as described by Steinmetz [92]. In general, for soft ferrites the saturation flux density decreases with temperature, as does the area of the BH curve and the resulting hysteresis losses. If the material temperature rises beyond its Curie Temperature, then the material is unable to align magnetically, and thermal demagnetization occurs. The effect of temperature on the magnetic components, while running in the power electronic circuit, has not really been considered for simulation except in static temperature conditions such as Jesse [36], Hsu & Ngo [103] and Tenant, Rousseau and Zegadi [104]. Due to the dependence on temperature of the magnetic material characteristics it is

necessary to include dynamic thermal variations into the behaviour of the magnetic model, to ensure that the component is accurately modeled when placed in the electrical circuit simulation. Previous work by Hefner and Blackburn [81] and Mantooth and Christen [37] has used the energy generated in electrical circuits as the stimulus to a thermal network and this technique has been extended to the magnetic-thermal boundary. The modeling of the dynamic thermal behaviour of magnetic materials using this type of approach will be discussed later in this thesis.

### 3.2.8 Frequency Dependence of Hysteresis Loops and Eddy Currents

As the frequency of the applied field or flux to a magnetic material increases, changes in the behaviour will result primarily due to Eddy Currents. Konrad [34] provides a good review of the range of analyses that have been carried out in this area, Carpenter [32] examines the problem from a numerical perspective while Zhu, Hui and Ramsden [42] separate the frequency dependence into a lumped model. This can be directly characterized when the applied signal is sinusoidal, but in most applications non-sinusoidal signals such as pulses, or arbitrary waveforms are used resulting in unpredictable behaviour. A more well defined approach is to consider the rate-dependence of magnetic materials as proposed by Hodgdon [22],[49],[53].

### 3.2.9 Summary of Magnetic Material Model Requirements

The general model requirements, which must be considered when a model is being chosen or developed, are summarised below:

- Accurate Major Loop Modeling
- Accurate Symmetric Minor Loop Modeling
- Accurate Asymmetric Minor Loop Modeling
- Minor Loop Relaxation
- Correct Energy Loss and Transfer Across Domains
- Thermal Dependence
- Rate Dependence (Effective Frequency Range)
- Reasonable Parameter Extraction
- Practical Implementation in a circuit simulation environment

### *3.3   Magnetic Material Models of Hysteresis*

### 3.3.1   Introduction

As has been previously discussed, there is a set of significant models which have been used to characterize the behaviour of magnetic materials. In this section, the most important models from a historical and practical point of view are reviewed and described in some detail. The strengths and weaknesses of the variety of approaches are discussed, summarised and conclusions made about the most appropriate model for circuit simulation.

### 3.3.2 Rayleigh Loop Model

The Raleigh model [96] uses a parabolic approach to modeling the hysteresis loop and a practical explanation of this approach is given in Snelling [27]. The model assumes that the permeability is a linear function of the initial permeability and the maximum applied field strength (H) as shown in equation 3.2.

$$\mu_a = \mu_i + v\,\hat{H} \tag{3.2}$$

Where $\mu_a$ is the amplitude permeability, $\mu_i$ is the initial permeability, $v$ is a hysteresis coefficient and $\hat{H}$ is the maximum value of $H$. If this equation is multiplied by $\mu_0\,\hat{H}$, the equivalent maximum flux density is obtained as given by equation 3.3.

$$\hat{B} = \mu_0(\mu_i\,\hat{H} + v\,\hat{H}^2) \tag{3.3}$$

Using this equation for the maximum values of $B$ and $H$, the instantaneous values $B$ and $H$ are estimated using the parabolic relation given by equation 3.4.

$$B = \mu_0\{(\mu_i + v\,\hat{H})H \pm \frac{v}{2}(H^2 - \hat{H}^2)\} \tag{3.4}$$

The resulting hysteresis loop is shown in figure 3.9.
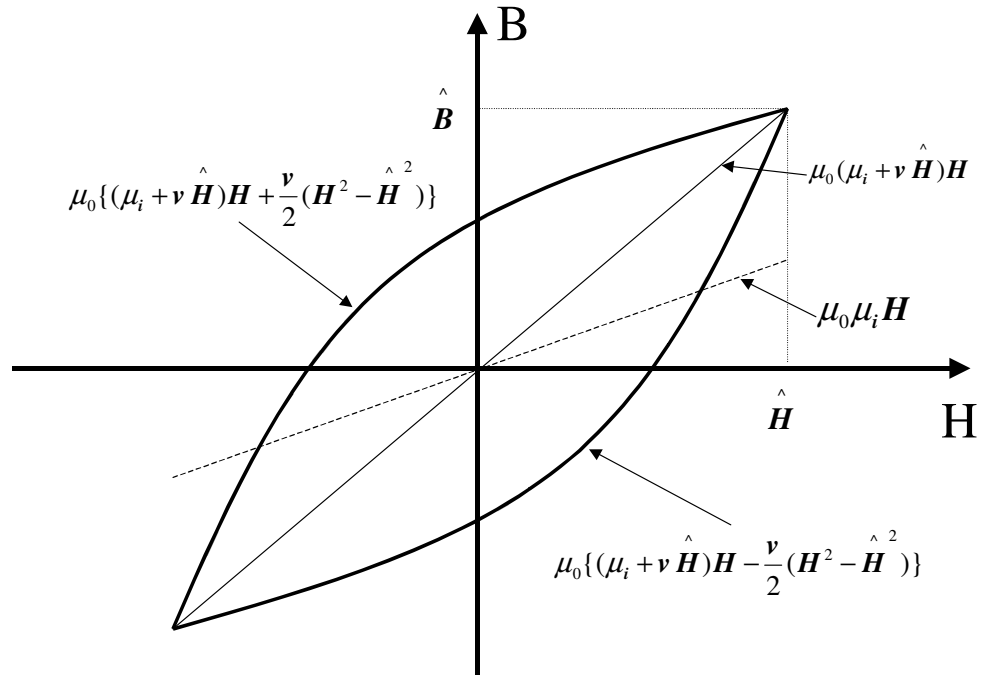


**Figure 3.9: Rayleigh Hysteresis Loop**

### 3.3.3  Jiles-Atherton Model

Jiles and Atherton [100],[20] & [21] have developed a theory of ferromagnetic hysteresis (1983-1986) which separates the hysteresis function into the reversible, or anhysteretic, and the irreversible, or loss, magnetizations. The magnetization is the lumped change in magnetic state when an external magnetic field is applied to the magnetic material and gives rise to an equivalent magnetic flux. Jiles and Atherton explain how the behaviour of individual magnetic particles and domains can be treated as a bulk material and an effective lumped expression derived for the magnetization. The total lumped magnetization as derived by Jiles and Atherton is given in equation 3.5 and illustrated in figure 3.10.

$$M_{TOTAL} = M_{IRREVERSIBLE} + M_{REVERSIBLE} \tag{3.5}$$
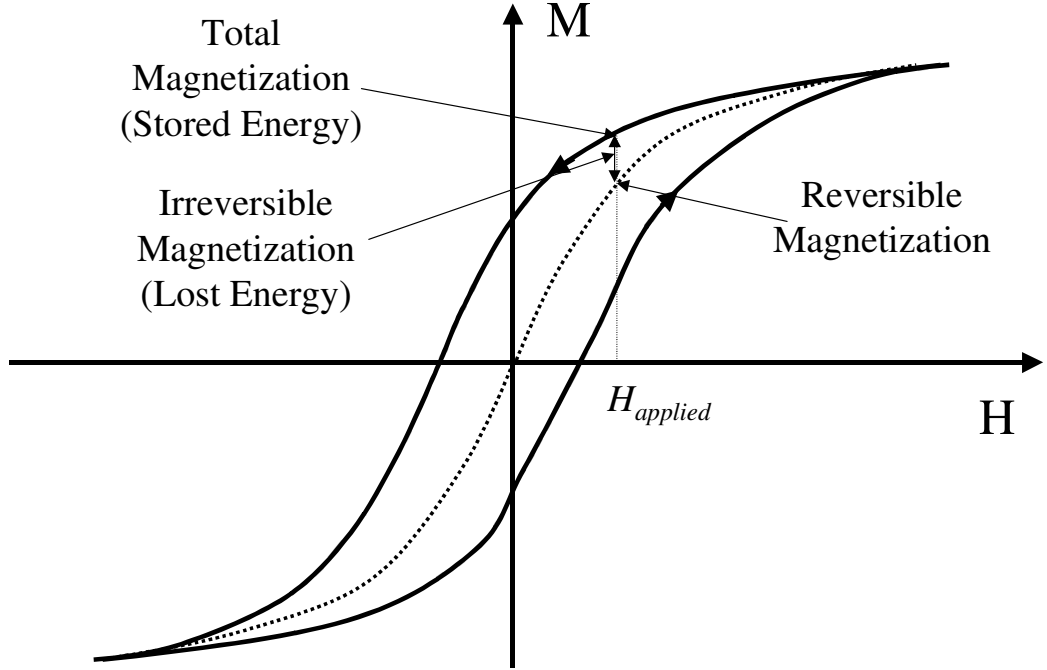


**Figure 3.10: Jiles & Atherton Reversible and Irreversible Magnetization**

The normalised anhysteretic function, Man, is approximated by the Langevin function as given by equation 3.6 where He is the effective applied magnetic field and A is the parameter modifying the curvature of the function. The function must be scaled by the saturation magnetization Ms to obtain the actual reversible magnetization.

$$Man = \frac{1}{\tanh(He/A)} - \frac{A}{He} \tag{3.6}$$

Variations on this basic function exist in commercial simulators, and a recent implementation in VHDL-AMS by Kazmierski and Baranowski [111]. The rate of change of the irreversible magnetization , $M_{irr}$, is obtained using equation 3.7, which is a lumped model of the losses caused by domain wall movement and distortion. $M$ is the total magnetization, $\delta$ is the direction of the applied field strength $H$ (+1 for positive, -1 for negative slope), $\mu$ is the permeability and $k$ is the model parameter that defines the hysteresis of the loop. The parameter $A$ defines inter-domain coupling and is effectively a proportion of the magnetization.

$$\frac{M_{irr}}{dH} = \frac{(M_{an} - M)}{\dfrac{\delta k}{\mu} - \alpha(M_{an} - M)} \tag{3.7}$$

The total magnetization rate of change is calculated using equation 3.8, where $c$ is the parameter dictating the relative proportion of reversible and irreversible magnetizations.

$$\frac{dM}{dH} = \frac{1}{1+c}\frac{Man - M}{\dfrac{\delta k}{\mu} - (Man - M)} + \frac{c}{1+c}\frac{dMan}{dH} \tag{3.8}$$

 This model has been implemented in a variety of commercial simulators, such as PSPICE and SABER, and is the de facto standard model for most non-linear core modelling using circuit simulators.

One of the difficulties with the Jiles-Atherton model is the extraction of model parameters. This was addressed by Jiles, Thoelke & Devine [24] who formulated methods of extracting the parameters from standard measurements and Lewis, Gao, Jiles & Welch [39] who have improved the numerical approach for calculating the magnetic parameters. Prigozy [50] has varied the parameters in the model and studied the effect on the resulting hysteresis loops, and this provides an aid to understanding the behaviour of the model. The model provides a good representation of the behaviour of major loops for materials that have a sigmoid shaped hysteresis characteristic, but there are limitations in the original model.

The original Jiles-Atherton model lacks frequency dependence, which is crucial in accurately applying the model to practical simulations, and this has not been addressed in the literature. The commercial simulator, SABER, has implemented a rudimentary method of frequency dependence using a simple filter to modify the applied field strength [105].

The model also lacks dynamic temperature effects, but this is addressed and described later in this thesis.

When the material is heavily saturated the major loop exhibits a form of early closure. The original Jiles-Atherton model does model this in a fashion that can readily be characterised without

adversely affecting the other regions of the model behaviour. Modifications to the Jiles-Atherton model are therefore presented that demonstrate how this aspect of the physical behaviour can be implemented practically.

The final deficiency of the model has been its inability to accurately model minor loops. Carpenter [51] has attempted to address this with a modification based on the turning points of the loops and Jiles [52] has used a similar technique to modify the original theory. Attempts to provide a method of optimizing the model parameters to fit major or minor loops have concentrated largely on the major loop alone either using direct numerical techniques as described by Jiles, Thoelke & Devine [24] and Lewis, Gao, Jiles & Welch [39], or using a least squares approach to fit the model and experimental data such as Schmidt and Guldner [40] or Lederer, Igarashi, Kost & Honma [88]. Later in this thesis a more subtle technique is described using multiple loop with weighting optimization (Wilson and Ross [90]) allowing the specification of the size of the loop to be optimized appropriate for the application.

The main strengths of the model are that it can be easily implemented in most circuit simulators, has reasonable convergence and is reasonably accurate across a variety of materials and operating conditions. Despite the deficiencies of the model, it is thus useful and widely used in circuit simulation.

### 3.3.4   Preisach Model

Friedrich Preisach proposed a diagrammatic approach to expressing the hysteresis of a magnetic material in 1935 [19]. Unfortunately, this method was effectively ignored until comparatively recently, when computing power made this method more useful. It is now widely used, especially in Finite Element Analysis applications [74],[76] & [80], and the model has also been implemented in the commercial circuit simulator SABER [101].

The original Preisach method assumes that the magnetic material consists of an infinite set of magnetic dipoles with the idealised hysteresis function given in figure 3.11. The hysteresis function has saturation values of $\Delta B_{sat}$ , which is a value of flux density within the range 0 to the saturation flux density of the material as a whole. The hysteresis function also has a value of applied field which causes the dipole to switch from one saturated state to the other, which is a statistical function around a nominal value of $H_{sat}$. The points defined by x & y are two examples of the positive and negative transitions after the variation has been applied and must satisfy the basic conditions defined by 3.9.

$$x < +Hsat$$
$$y > -Hsat$$
$$x > y$$

(3.9)
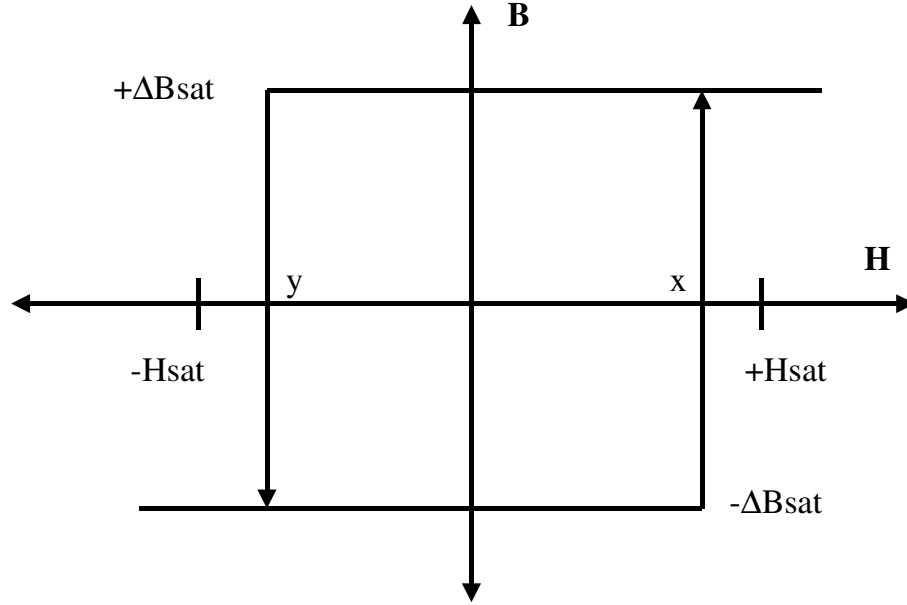
**Figure 3.11: Simple Magnetic Dipole**

Using a set of these simple dipoles, and the relationship defined in equation 3.9, a chart can be drawn of the set of all dipoles with the x axis provided by increasing applied field H+ and the y axis provided by a decreasing applied field H-. Figure 3.12 shows the triangle area within which the dipoles are positioned. As the field H increases along the H+ axis, all the dipoles with x<H are saturated, but if the field decreases the dipoles with y>H are reversed into negative saturation. Any dipoles outside the triangle have value zero. The instantaneous value of the overall flux density is obtained by integrating over the whole plane, with the total value normalized to 1 as shown in equation 3.10. The function F(x,y) is a statistical function which describes the values of x & y for a dipole.

$$\int_{-\infty}^{\infty}\int_{-\infty}^{\infty} F(x, y).dx.dy = 1$$

(3.10)
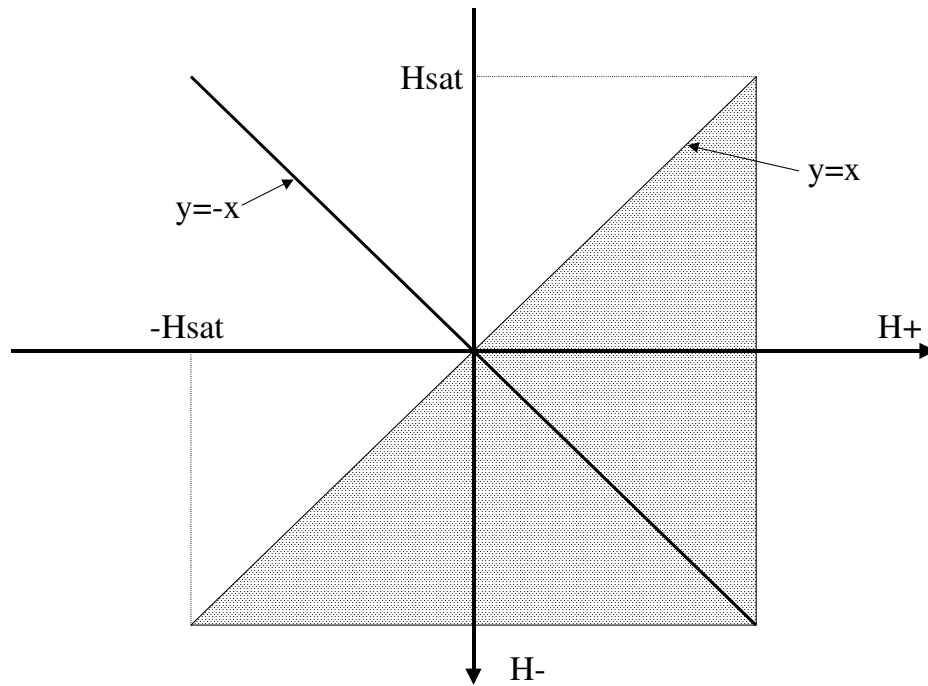
**Figure 3.12: Preisach Triangle**

In the initial demagnetized state, the dipoles in the triangle must be either +ve or -ve and for the resulting magnetization to be zero there must be the same number of both. This is easily represented on the Preisach diagram by distributing the dipoles equally within the triangle using the line of symmetry y=-x as shown in figure 3.13.
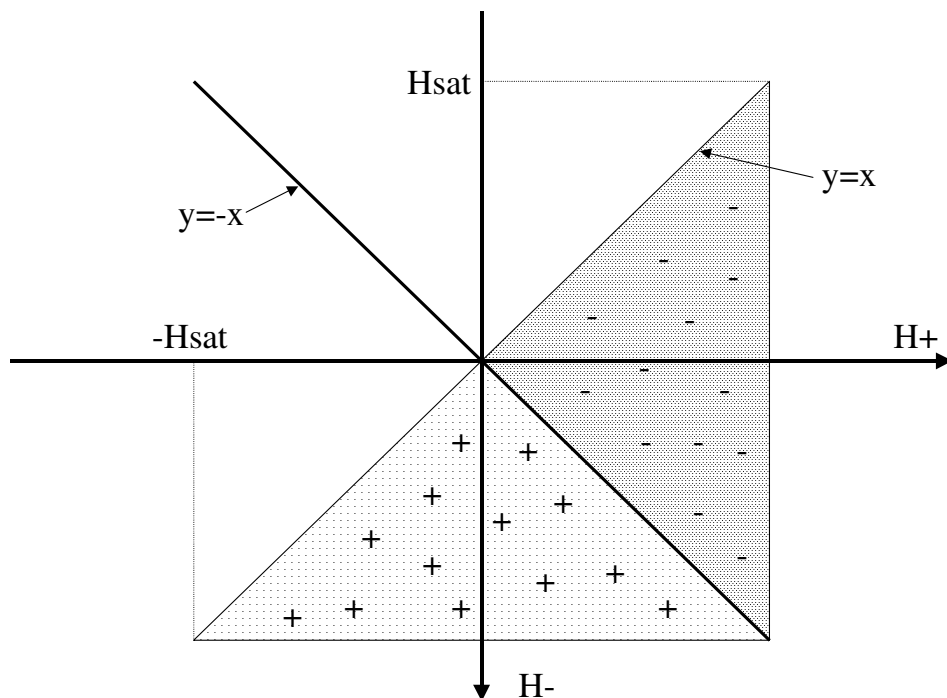


**Figure 3.13 : Preisach Diagram Initial Condition**

The calculation of the net magnetisation is the integration of the region of positive dipoles minus the integration of the region of negative dipoles which is given in equation 3.11.

$$B = B_{sat} \iint\limits_{M+} F(x, y).dx.dy - B_{sat} \iint\limits_{M-} F(x, y).dx.dy \qquad (3.11)$$

As the material is magnetized and demagnetized repeatedly, the boundary between the M+ and M- regions can become increasingly complex, so it is useful to show the transition from the initial condition to a state of magnetization following a series of field direction changes and this is shown in figure 3.14(a)-(d).



(a) Initial Condition H=H_0

(b) Preisach Diagram after increased field $H=H_0+H_1$

(c) Preisach Diagram after decreased field $H=H-H_2$

(d) Preisach Diagram after increased field $H=H+H_3$
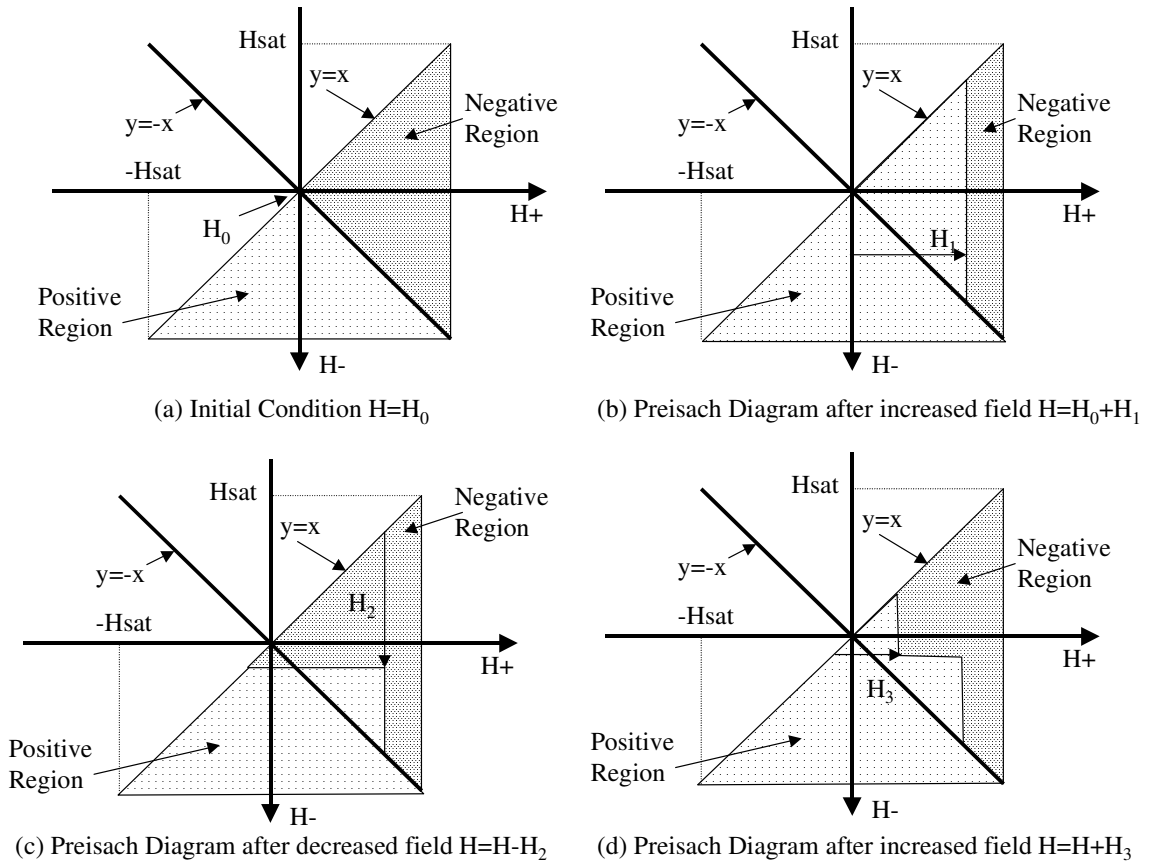
**Figure 3.14: Changes in the Preisach Triangle due to changes in applied field direction**

The Preisach distribution function F(x,y) can be implemented using an Everett integral [106] or Gaussian function and applied in software using a look-up table of values. One of the drawbacks of the approach is the low efficiency of the double integration required to calculate the magnetization. Vajda & Torre [77] , Doong & Mayergoyz [74] and Mayergoyz & Friedman [76] present a simplified method of calculating the integrals that can be implemented in software. A variation on this is proposed by Zhu and Hui [69] who apply a transmission line model instead of the conventional statistical function to simplify the calculations. Oti, Vajda & Torre [108] and Vajda & Torre [109],[79] also provide a method for extracting the parameters to characterize the

Preisach function in the model while Rouve, Waeckerle and Kedous-Lebouc [110] compare characterizations of the Preisach function, in this case for steels.

Mitchler, Dahlberg, Wesseling and Roshko [70] have extended the model to accurately show the behaviour of AC and thermal demagnetization and Park & Hahn [71] suggest that convergence can be improved, and the smoothness of the functions increased if the magnetization M is described as a function of B rather than H.

The original, sometimes referred to as the 'classic', Preisach approach does not distinguish between the reversible and irreversible components of magnetization. This has implications for the energy calculations in the model but has been addressed by Atherton, Szpunar & Szpunar [73] who proposed the splitting of the model into the reversible and irreversible parts, using the Langevin function and the Preisach technique respectively. This has also been addressed by Torre, Oti & Kadar [75] and Torre [43] has also detailed how the energy can be calculated from the model.

### 3.3.5  Chan-Vladirimescu Model

The Chan, Vladirimescu, Gao, Libmann and Valainis model [23] for describing hysteresis uses polynomial techniques developed by Nitzan and El-Sharbiny [59]. The model requires only 3 parameters, all of which are standard measurements found on manufacturers data sheets, which gives the model an advantage over other models which have essentially arbitrary parameters. The Major Loop is described using two expressions 3.12 & 3.13 for the upper and lower loops respectively.

$$B_+^{'}(H) = Bs \frac{H + H_c}{\left| H + H_c \right| + Hc(\frac{B_s}{B_r} - 1)} \qquad (3.12)$$

$$B_-^{'}(H) = Bs \frac{H - H_c}{\left| H - H_c \right| + Hc(\frac{B_s}{B_r} - 1)} \qquad (3.13)$$

Where $B_s$ is the saturation flux density, $B_r$ is the Remanence and $H_c$ is the Coercive Force. The initial magnetization curve is calculated by averaging these two functions as given by equation 3.14.

$$B_{mag}^{'}(H) = \frac{B_+^{'}(H) + B_-^{'}(H)}{2} \qquad (3.14)$$

Minor Loops in this model are defined by using the same expressions as for the major loop, but shifting them by some amount $B_d$ either up or down for lower and upper trajectories respectively.

48

The Chan and Vladrimescu *et al* [23] paper gives a description of how the minor loops are constructed with different entry points from the major loop or magnetization curve.

Frequency dependence in the model is obtained by modifying the parameter Hc with respect to the frequency using 3.15. As the frequency increases the loop widens. The three parameters $f_1$, $f_2$ and $f_3$ are obtained by using the power loss curves on datasheets (usually derived from the Steinmetz equation).

$$H_c^{'} = H_c \left( f_1 + f_2 f^{f_3} \right)$$

(3.15)

Chan and Vladrimescu also discuss modelling of the AC resistance by making the winding resistance dependent on the radius of the wire and the frequency. The expression for winding resistance used is given in 3.16.

$$R_w^{'} = R_w \frac{r^2}{r^2 - \left( r - \frac{504}{\sqrt{\sigma \mu_r f}} \right)^2}$$

(3.16)

where $r$ is the radius of the wire, $f$ is the frequency, $\sigma$ is the wire conductivity (Siemens), $\mu_r$ is the relative permeability of the wire and $R_w$ is the D.C. winding resistance. Modeling of windings will be specifically covered in more detail later in this thesis.

Finally, the model does include rudimentary temperature dependence by applying a linear variation of the three basic parameters with the temperature. The form of the dependence is given in 3.17.

$$B_S^{'} = B_S \left( 1 + (T - T_{nom}) * T_{BS} \right)$$

(3.17)

Where $B_s$ is the saturation flux density, $T$ is the ambient temperature, $T_{nom}$ is the default nominal temperature for the parameters and $TBS$ is the temperature coefficient for $B_s$. Similar expressions are used for the other model parameters $B_r$ and $H_c$.

### 3.3.6   Hodgdon Model

The Hodgdon model [22],[49],[53] is a generally similar approach to the Jiles-Atherton, with more arbirtrary functions for the magnetization, except that rate dependence is built into the model. Diebolt [54] has demonstrated how this model can be implemented in a circuit simulator to effectively model the frequency dependence of material characteristics. The basic differential equation governing the behaviour of the Hodgdon model is given by equation 3.18.

$$\dot{H} = \alpha * |\dot{B}| * [f(B) - H] + \dot{B} * g(B, \dot{B})$$

(3.18)

This equation links the time rate of change of $H$ to the time rate of change of $B$. $\alpha$ is a constant parameter and $f$ & $g$ are functions. If this equation is divided by $\dot{B}$ then the equation can be written in a more convenient form as in 3.19.

$$\frac{dH}{dB} = \alpha * s(\dot{B}) * \left[ f(B) - H \right] + g(B, \dot{B}) \tag{3.19}$$

where: $s(\dot{B}) = \begin{vmatrix} 1 & : & \dot{B} > 0; \\ -1 & : & \dot{B} < 0; \end{vmatrix}$

3.20 & 3.21 define the simplest functions for f and g respectively, although Hodgdon also defines more complex trigonometric functions for increased accuracy.

$$f = \begin{cases} D_1(B + B^*) - D_2 B^* & : & B < -B^*; \\ D_2 B & : & |B| \leq B^*; \\ D_1(B - B^*) + D_2 B^* & : & B > B^*; \end{cases} \tag{3.20}$$

$$g = \begin{cases} (1 + D_3)D_2 & : & |B| \leq B^*; \\ D_1 & : & |B| > B^*; \end{cases} \tag{3.21}$$

where D1-D4 and B* are model parameters.

Hodgdon also addresses the issue of loop closure at saturation and supports minor loops. Anisotropy is discussed, but is not demonstrated with any practical simulations or measurements. Diebolt [54] has implemented this model in a circuit simulator using an Analogue Hardware Description Language and also discusses how the instantaneous power can be calculated in the model, although his logic is slightly flawed in that the power, using his method, is only valid at the completion of each BH cycle. This issue is discussed in detail later in this thesis.

### 3.3.7   Comparative Studies of Models

There have been some useful studies comparing a range of magnetic material models starting with Manly [57], although this precedes the Jiles-Atherton model and the majority of recent Preisach modeling. Takach and Lauritzen [55] have completed a thorough examination of the current range of models and their relative merits, and there is a detailed study of the relative performance of the Jiles-Atherton and Preisach approaches by Philips, Dupre and Melkebeek [56]. Most recently, Liourzou, Phelps and Atherton [102] have reviewed the main macroscopic models including Stoner-Wohlfarth, Globus, Jiles-Atherton and Preisach and conclude that the Jiles-Atherton is the most appropriate for Soft Ferrites.

### 3.4    Magnetic Material Model Summary

The models reviewed were assessed with regard to the previously defined model requirements to enable a decision to be made on the most appropriate model for development and application in this project. A summary of this review is given in table 3.3 with a rating for each model feature of 1 star * for a poor implementation to 5 stars ***** for excellent.

| Model Feature | Jiles-Atherton | Preisach | Hodgdon | Chan et al |
|---|---|---|---|---|
| Accurate Major Loop | ***** | **** | **** | **** |
| Accurate Symmetric Minor Loop | *** | *** | *** | *** |
| Accurate Asymmetric Minor Loop | *** | ** | *** | ** |
| Minor Loop Relaxation | ** | * | *** | *** |
| Correct Energy Loss | **** | *** | *** | *** |
| Transfer Across Domains | ***** | *** | **** | *** |
| Thermal Dependence | *** | * | * | *** |
| Rate Dependence | * | * | ***** | * |
| Parameter Extraction | ***** | ** | ** | ***** |
| Practical Implementation | ***** | *** | *** | *** |

**Table 3.3: Summary of Models and Requirements**

Reviewing the summary of the models in Table 3.3, the Jiles-Atherton model emerges as the most suitable for development from a circuit simulation perspective. The weakness of the model will be addressed in this thesis. The Preisach model suffers in this case from a poor implementation of non-congruency, thermal and rate dependence and is difficult to implement easily in a standard circuit simulator. The main focus of the Preisach model is in Finite Element Analysis where a static model is applicable, and where the computation times are slow in any event. The Hodgdon and Chan *et al* models both have specific strengths as described previously, particularly with regard to rate dependence (Hodgdon) and parameter extraction (Chan *et al*), but in many aspects, the Jiles-Atherton model is still superior. The decision was therefore taken to primarily use the Jiles-Atherton modeling approach in this thesis.

*Chapter 4*

# 4 Implementation and Characterization of Magnetic Material Models

## 4.1 Introduction

The modeling of magnetic components for simulation in electric circuits requires an accurate model for the non-linear behaviour of the core material used. It is important that the parameters extracted for the hysteresis model are optimized across a range of operating conditions which may occur during circuit simulation. In this chapter of the thesis the following key issues will be addressed:

- testing methods for magnetic materials
- accurate and efficient application of simulation models in circuit simulation
- model parameter extraction and characterization
- model parameter optimization methods and procedures
- validation of models with measured results

## 4.2 Methods of Testing Magnetic Materials

### 4.2.1 Introduction

In order to test the behaviour of magnetic materials for accurate model characterization, a flexible method of signal stimulus was required. Initial tests were carried out using standard signal generators, but it quickly became evident that a more sophisticated approach was also required. Jiles and Atherton [20]-[21], and Jiles, Devine and Thoelke [24] have concentrated on major BH loops. These are relatively easy to characterize, simply requiring a constant peak amplitude sinusoidal, triangular or square wave stimulus. Another common characterization approach is to use a decreasing amplitude waveform. This has been used by a wide range of researchers including Jiles et al [24] and Hodgdon [22],[53].

More recently a more sophisticated method of stimulus has been applied by Schmidt and Güldner [40] who use a PC controlled GPIB Instrument to generate the signals applied to the device under test. This method is extremely useful as the test routines can be tailored to the test generator, but is also limited to the abilities of that generator. It can also be difficult and expensive if the test equipment does not have a GPIB interface and if this has to be purchased (as would have been required in this project).

The use of a Digital Signal Processor (DSP) was seen as a useful general low-cost purpose alternative for generating the required arbitrary waveforms for testing magnetic materials with a minimal financial cost and maximum flexibility. This can be used in combination with standard sinusoidal and pulse generators. A significant advantage of the DSP is its ability to be programmed with complex stimulus waveforms and multiple amplitude sequences. These are especially useful when analysing minor loop and arbitrary waveform behaviour.

The aim of this section of the work was to establish the dynamic behaviour of a variety of magnetic materials under a set of defined stimulus conditions:

- Major loops
- Minor loops
- Anhysteretic behaviour
- First order reversal curves
- Multiple loops
- Arbitrary applied magnetic field waveforms

It is also important to establish the behaviour under varying ambient and operating conditions including different stimulus frequencies and ambient temperatures

## 4.2.2   DSP Test Configuration

The Texas Instruments low cost floating point C31x series DSP [183] was used in conjunction with the analogue evaluation module [184], and an interface board constructed to provide a voltage to current conversion function to allow direct current driving of the magnetic component under test. Digital Storage Oscilloscopes were used to capture the current and voltage waveforms across the device windings and both devices controlled electronically from a PC. By controlling the current applied to the device under test, the magnetic field applied to the material is directly controlled. This control of the applied magnetic field gives much more reliable results when the magnetic field and flux density are derived from the device electrical waveforms. The test configuration is shown in figure 4.1 and the current driver circuit diagram in figure 4.2.
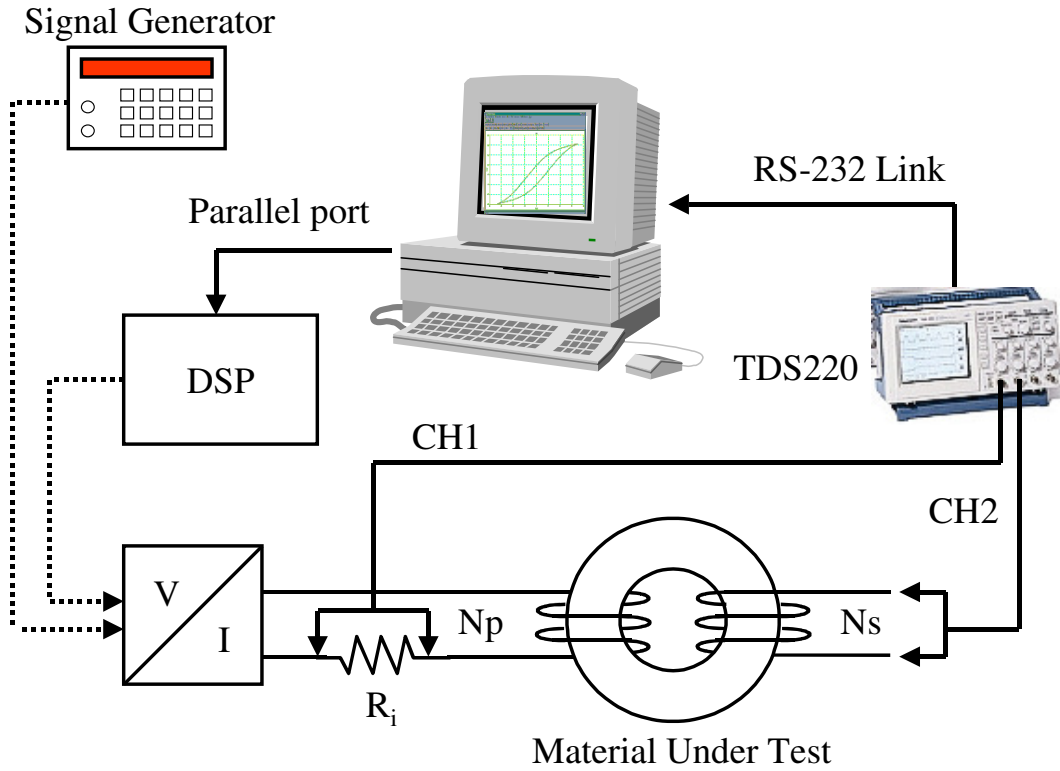
**Figure 4.1: Magnetic Material Test Bench Configuration**
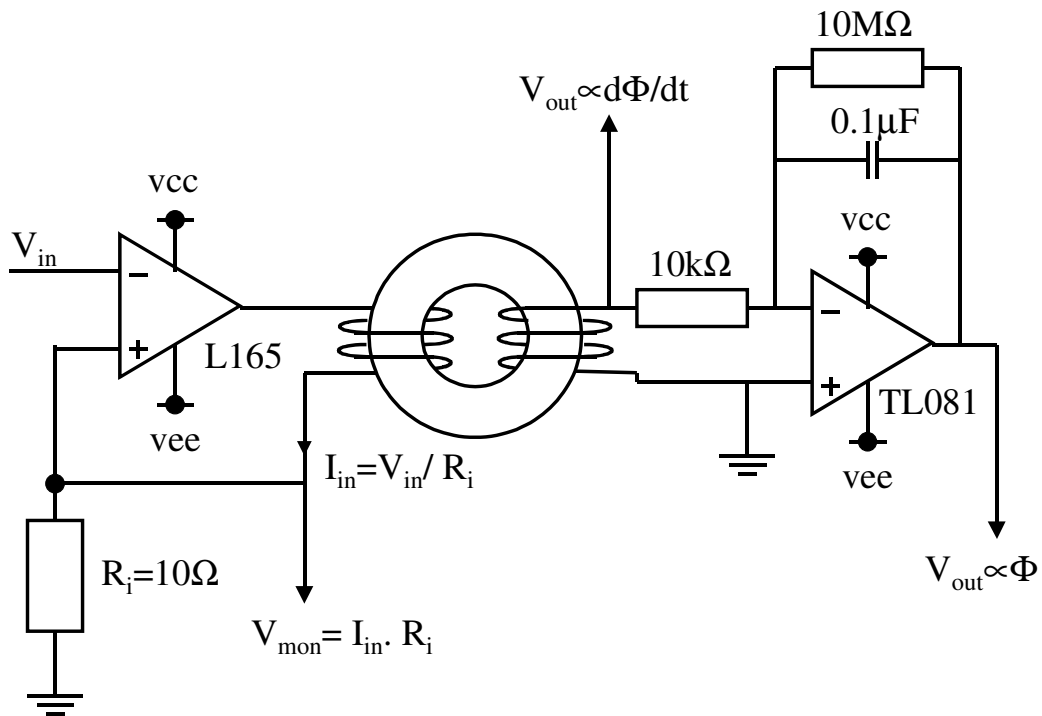


**Figure 4.2: Voltage to Current Driving Circuit Schematic**

### 4.2.3  Magnetic Materials Tested

The following magnetic materials were selected for test because of their common use in SMPS and Communications applications.

- Philips 3F3
- Philips 3E5
- Siemens N30

The materials were tested by applying a current to a primary winding and the resulting voltage measured on a secondary winding. From the measured voltages and currents, the magnetic field strength and flux density were derived.

### 4.2.4  Calculation of Magnetic Field and Flux Density

Software was written to calculate the magnetic field strength and flux density numerically from the measured current and voltage waveforms on the primary and secondary windings of the device under test respectively. The voltage across the primary current sense resistor ($R_i$) shown in figure 4.2 is measured using Channel 1 of the oscilloscope, and the voltage across the secondary winding of the device under test is measured using Channel 2 of the scope. The magnetic field strength is then obtained directly from the Channel 1 measurement data using equation (4.1).

$$H = \frac{N_p * v(CH1)}{L_m * R_i}$$

(4.1)

Where $N_p$ is the number of turns on the primary winding, $L_m$ is the effective magnetic path length (estimated from a data sheet), $R_i$ is the current sense resistance value in Ohms and $v(CH1)$ is the voltage on the primary winding.

The flux density ($B$) is derived from the voltage on the secondary winding using expression (4.2). The integration was carried out numerically in software using trapezoidal integration of the voltage on the secondary winding ($v(CH2)$).

$$B = \frac{1}{N_s A_e} \int v(CH2)dt$$

(4.2)

Where $N_s$ is the number of turns on the secondary winding, $A_e$ is the effective area of the magnetic flux path and the secondary winding voltage is $v(CH2)$.

### 4.2.5  BH Curve Analysis Software

In order to automate the process of BH Curve Capture and Analysis, a software interface was developed (VirtualScope) for this purpose, the graphical user interface of which is shown in figure

4.3. This software takes either BH data or the Channel 1 & 2 test data and can calculate the BH Curves from this.
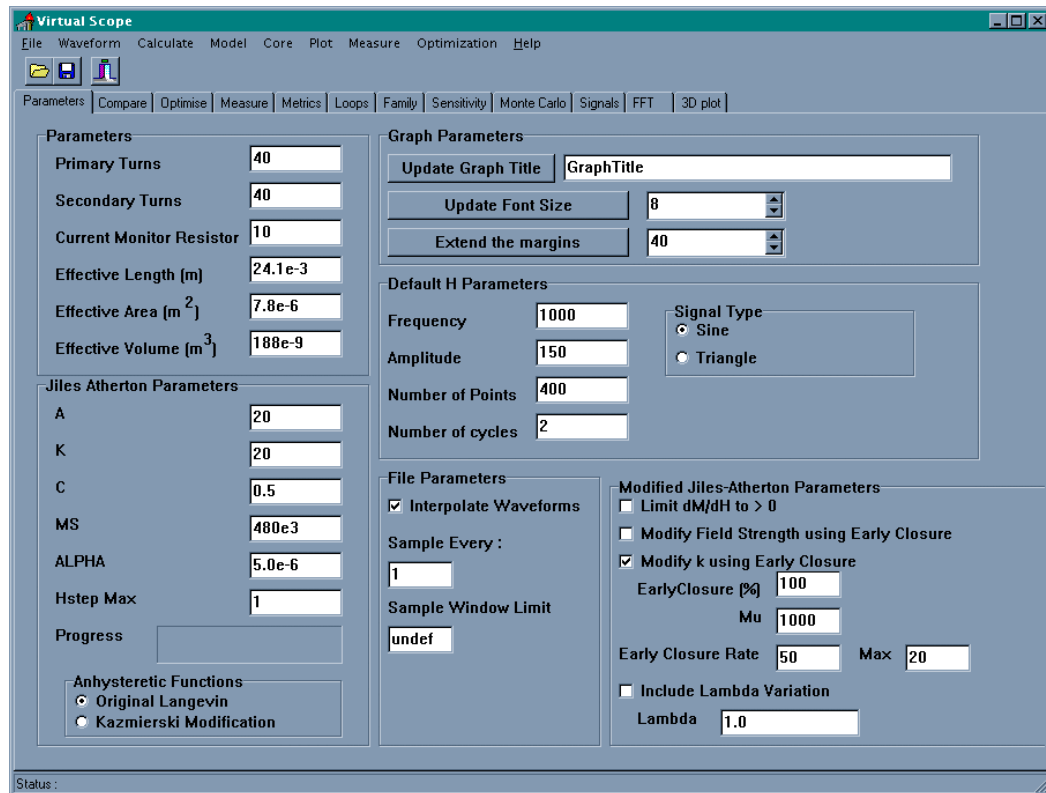


**Figure 4.3: Virtual Scope User Interface**

The software has the following functionality relevant for the measurement of BH Curve Data :-

- Specification of core and winding parameters
- Data point interpolation and smoothing
- Measured and model curve comparison
- B(H), B(t), H(t) curve plotting
- Family of curve plotting
- FFT calculation of signals
- BH data output
- Jiles Atherton magnetic core model generation

## *4.3   Example Magnetic Material Test Results*

### 4.3.1   Introduction

In this section, a cross section of measured results obtained using the testing methods previously described is presented. More results are presented later when dealing with specific implementation issues.

### 4.3.2  Philips 3F3 BH Major Loop Measurements

The Philips 3F3 material is commonly used in power electronics applications such as Switch Mode Power Supplies. Sets of BH Measurements were taken with a sinusoidal current applied with a frequency of 1kHz and amplitude set to apply a magnetic field strength of 35 A/m, 70 A/m and 135 A/m respectively. The resulting family of BH Loops is given in figure 4.4 and shows a minor, medium and major loop.
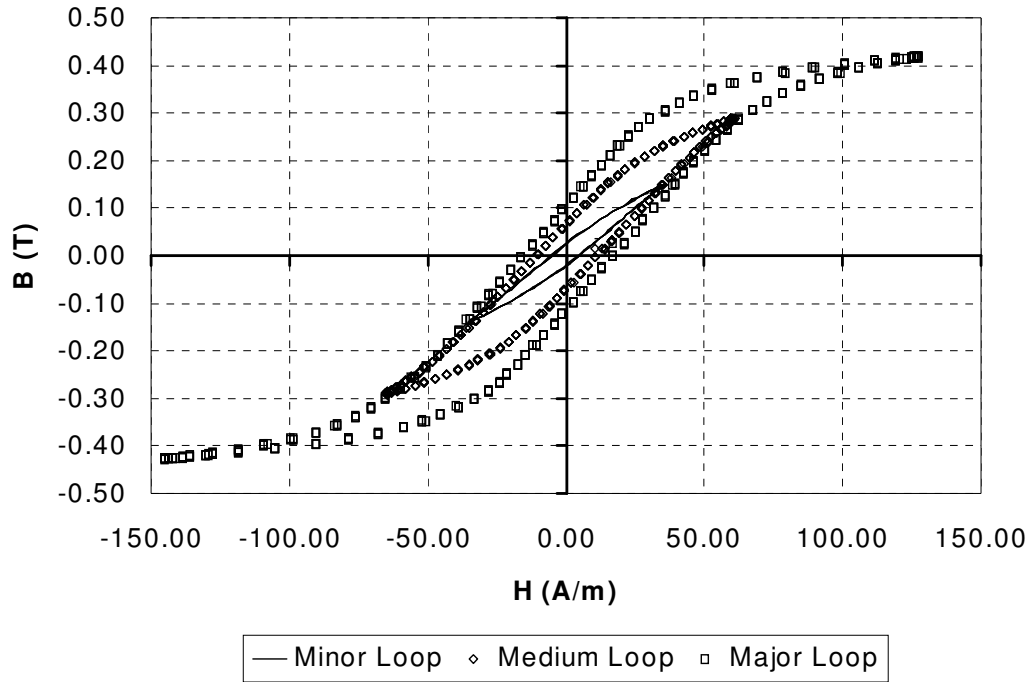


**Figure 4.4: Philips 3F3 Family of Measured BH Curves**

It is clear that as the magnetic field strength is reduced the loop shape changes. The area of the loop reduces, the saturation decreases and the overall slope decreases. As the minor loop is reduced in amplitude, the slope tends towards the initial permeability $(\mu_i)$.

### 4.3.3  First Order Reversal Curves

The use of first order reversal curves for model characterization is potentially useful for a number of reasons. The first reason is that the resulting loops are essentially varying sized asymmetric minor loops, which give a good indication of both major and minor loop dynamic behaviour. The second reason is that the model must be continuous during the transition across the BH Loop, and the first order reversal curves show this across a range of initial values for B and H.

The first order reversal curves can be measured by applying an offset to an applied sinusoidal signal, and controlling the minimum and maximum applied field strength. An example of the measured family of first order reversal curves for Philips 3F3 is shown in figure 4.5.
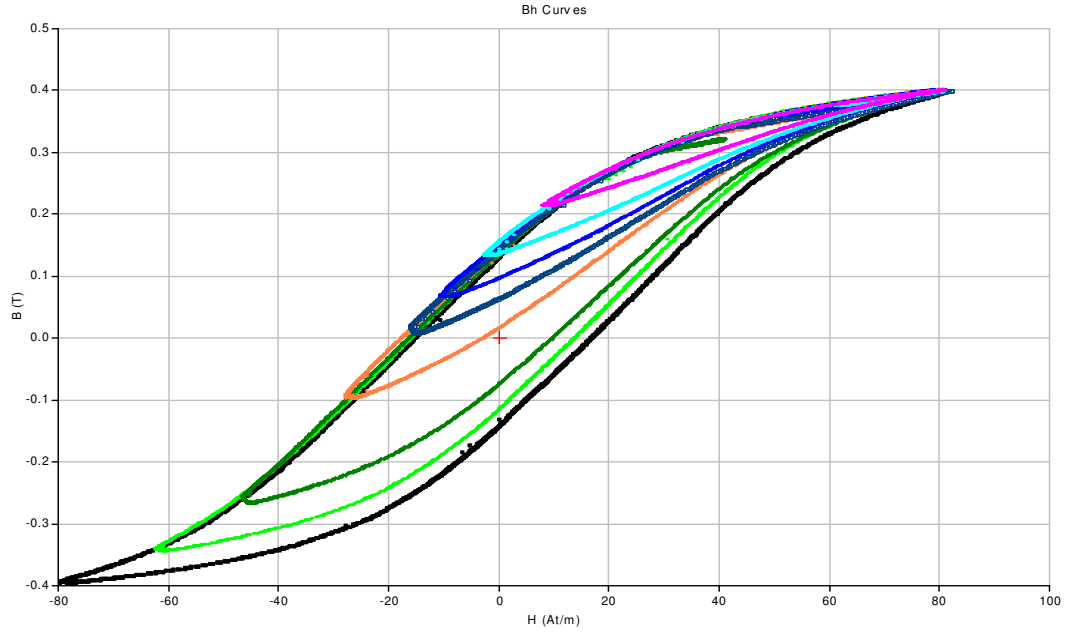
**Figure 4.5: First Order Reversal Curves**

## *4.4  Implementation of Magnetic Material Models*

### 4.4.1  Introduction

The choice of a non-linear core model has been discussed previously in this thesis. For ease of implementation in conjunction with good coverage of required model characteristics the Jiles-Atherton model was chosen as the primary model to be applied.

### 4.4.2  Original Jiles-Atherton Model implemented in PSPICE

The original Jiles-Atherton model of magnetic hysteresis has been described in detail in chapter 2 of this thesis. The structure of the model is shown in figure 4.6 and is shown implemented as a PSPICE macromodel in figure 4.7. The model can be implemented using the Magnetic Field Strength (*H*) and Flux Density (*B*) or the MMF and Flux. In the PSPICE example shown in figure 4.7, the MMF/Flux version is used, and the magnetic path length and area are passed as parameters to the model.

There is a form of the Jiles-Atherton model implemented in the standard PSPICE library, but does not use the same equations as the original model. Experience has shown that this model is less useful than a true magnetic domain model as it cannot be built into physically representative magnetic structures. The internal Pspice model is designed to be used in transformer and inductor components alone. The built-in model has also exhibited convergence difficulties which reduces its general usefulness further.
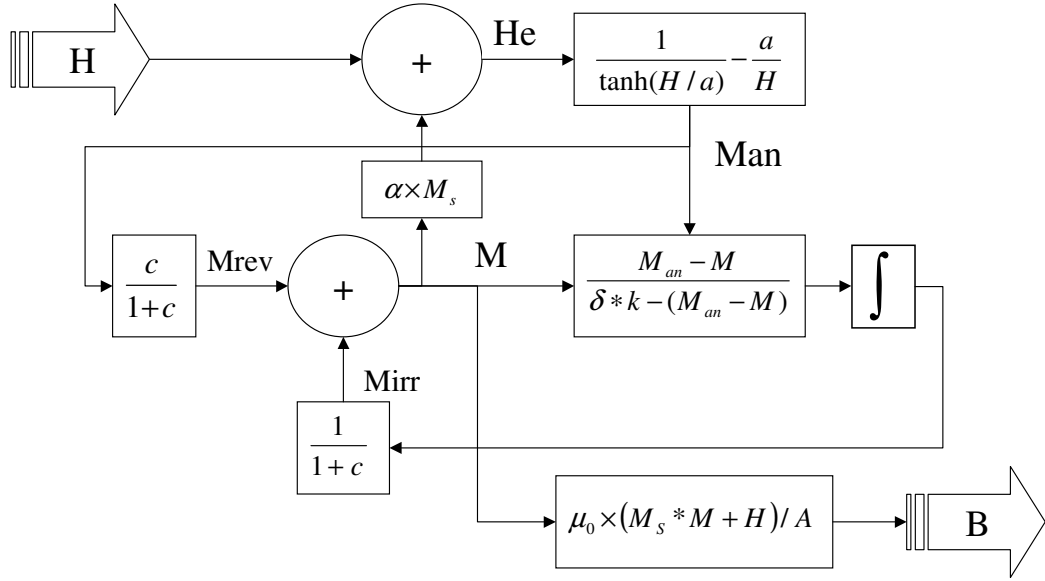
**Figure 4.6: Original Jiles Atherton Model Structure**

```
.SUBCKT COREJA    1    2    PARAMS:    AREA=10E-6 LEN=10E-3
+ MS=680K A=0.22 K=4 C=0.10 ALPHA=0.U RS=1M
* CONVERT MMF TO HE
E1 3    0    VALUE={V(1,2)/LEN+ALPHA*MS*V(12)}
R1 3    0    1MEG
* ANHYSTERETIC MAGNETIZATION
E2 4    0    VALUE={IF(ABS(V(3))>1E-3,1/TANH(V(3)/A)-
A/V(3),0.333*V(3)/A)}
R2 4    0    1MEG
* 1DH/DT
E3 5    0    1    2    1
C1 5    6    1M    (IC=0)
RD 6    7    {RS}
V1 7    0    0V
* DELTA*K
E4 8    0    VALUE={K*SGN(I(V1))}
R3 8    9    1K
C2 9    0    1PF
* INTEGRATE MAGNETIZATION
E5 10   0    VALUE={V(4,12)/(V(9)-ALPHA*MS*V(4,12)+1M)/LEN}
D1 10   11   DMOD
R4 11   0    1K
E6 12   0    VALUE={SDT(1000*I(V1)*V(11)/(1+C))+C*V(4)/(1+C)}
R5 12   0    1K
E7 13   0    VALUE={AREA*1.258E-6*(MS*(V(12)+V(1,2)/LEN)}
R6 13   0    1MEG
G1 1    2    13   0    1
* Calculate B and H for post-processing
E21 B 0      VALUE={V(13)/AREA}
E22 H 0      VALUE={V(1,2)/LEN}
.MODEL       DMOD  D(N=0.01)
.ENDS
```

**Figure 4.7: Original Jiles-Atherton PSPICE model listing**

Testing of the original Jiles-Atherton model in PSPICE provides BH curves that can be used for characterization of measured data. An example of the BH Curves which can be generated using PSPICE is shown in figure 4.8.

One modification to the original Jiles-Atherton model made was that the magnetization could not fall when the applied field was rising, or rise when the applied field was falling. This removes the anomalous situation inherent in certain cases with the original Jiles-Atherton model, where a rise in the applied magnetic field strength (H) causes a fall in the magnetization (or vice versa). This non-physical behaviour usually manifests itself only at the BH loop tips for certain parameter sets and stimulus conditions.
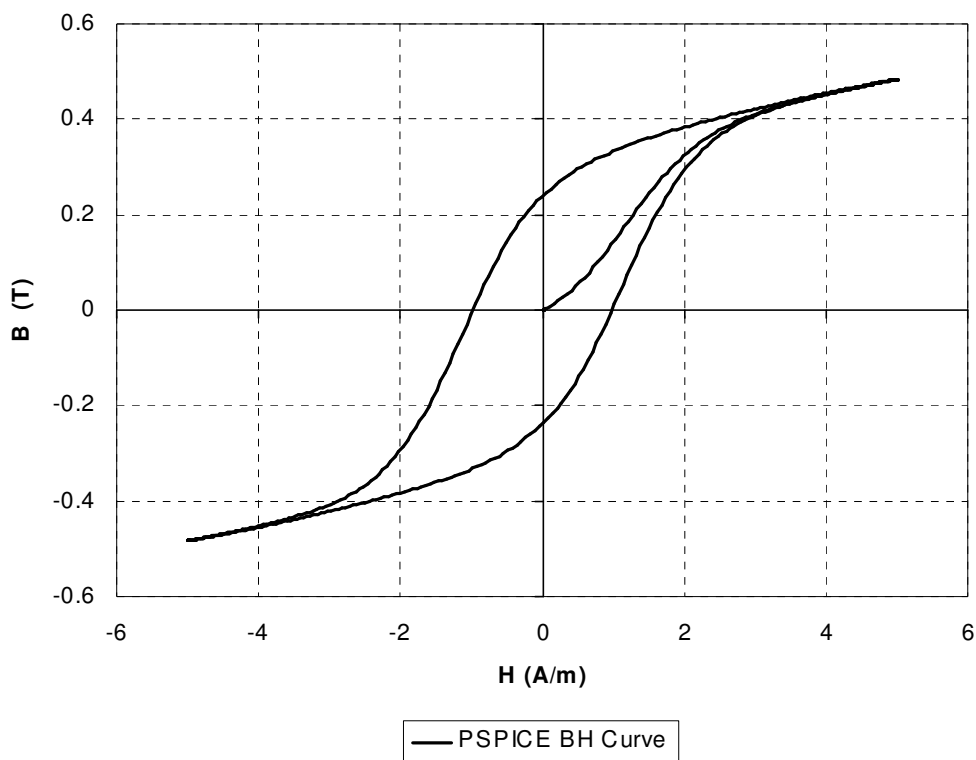


**Figure 4.8: PSPICE BH Curve showing a major loop**

### 4.4.3   Inclusion in PSPICE Circuit Simulation Model

The simulation model for a Jiles-Atherton or other core model is linked with winding models (previously described in this thesis) to create a complete magnetic component model. An example of this is given in figure 4.9, which shows a winding model connected to a non-linear core model to create an electro-magnetic model of an inductor.
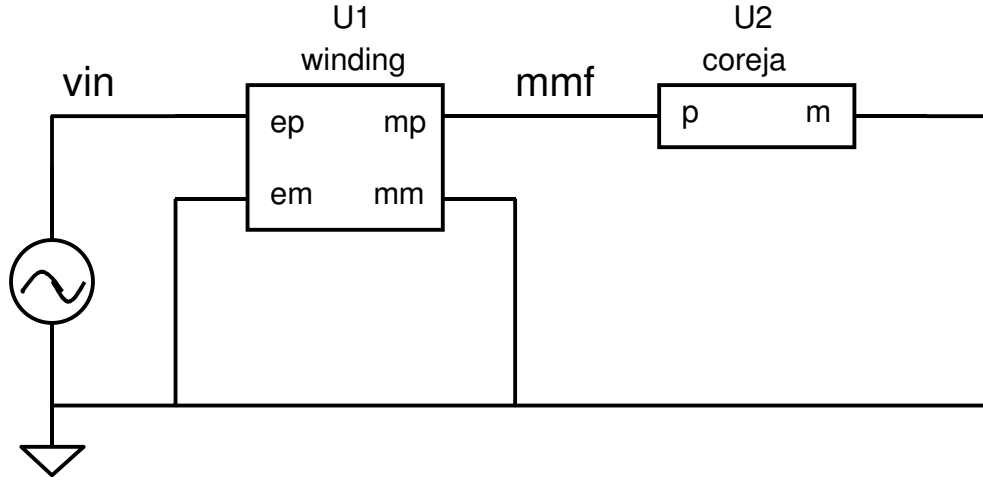
**Figure 4.9: Electro-Magnetic Model of a non-linear inductor using PSPICE**

This approach can be used to build up complex magnetic core and winding structures with individual non-linear core sections representing lumped magnetic sections, linear core sections for leakage paths and air gaps, and winding models for each winding structure. This approach becomes very powerful for expressing the physical layout of magnetic components directly in the model. This aspect of magnetic component modeling will be explored in greater detail later in this thesis.

### 4.4.4   Problem of δK Convergence and Proposed Solution

A significant numerical issue with the Jiles-Atherton approach is the use of the sign of the applied magnetic field, $\delta$, in the equation for the irreversible (or hysteresis) part of the magnetization defined by equation 4.3. The variable $\delta$ is defined by equation 4.4.

$$\frac{dM_{irr}}{dH} = \frac{M_{an} - M}{\delta k - (M_{an} - M)} \tag{4.3}$$

$$\delta = \begin{vmatrix} +1 & \dfrac{dH}{dt} > 0 \\ -1 & \dfrac{dH}{dt} < 0 \end{vmatrix} \tag{4.4}$$

It is clear from equation 4.4 that $\delta$ is discontinuous at zero, and this may cause a problem when the applied (or effective) field strength changes direction. This is a common problem when simulating with the Jiles-Atherton core model, and the symptom of this problem occurring is very small time steps at the BH Curve Loop tips leading to non-convergence of the simulation.

A solution to this problem is to redefine the function for $\delta$ implementing a continuous function through zero. This could be implemented by defining a piece-wise linear function through the origin as shown in figure 4.10.
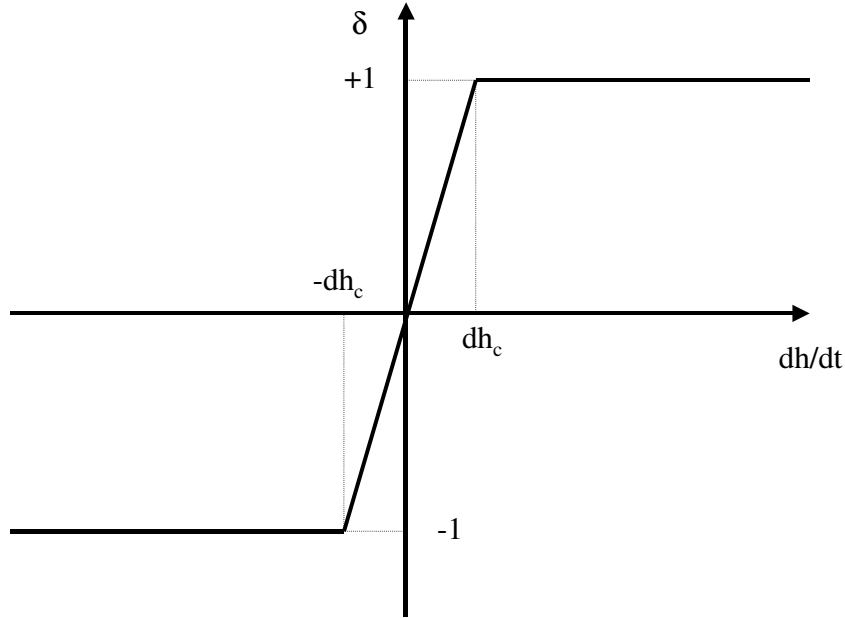


**Figure 4.10: Piece-Wise Linear Function for Jiles-Atherton variable - $\delta$**

This function will simulate, and improves the convergence of the model to an extent, but several problems still remain with this approach. The first problem is that the model is not continuous in the first derivative. As has been explained earlier in this thesis, the non-linear solution method generally used in simulation software is based on the Newton-Raphson method, which requires the use of the first derivative to estimate the next solution point. If this is not continuous, then problems with convergence may occur. The second potential problem is the zero slope of the function for $\delta$ outside the zero crossover region. This may lead to a more subtle problem with the model, in that again due to the use by the Newton-Raphson algorithm of the first derivative to estimate the crossing point, if the slope is zero then the algorithm will be potentially unable to find a convergent crossing of the x axis and non-convergence will occur. This can be addressed by adding a very small slope to the function for $\delta$ outside the crossover region so that the Newton-Raphson algorithm can always find a tangent pointing towards the x axis.

A numerically more robust approach is to 'soften' the crossover by using a continuous function, which is also continuous in the first derivative. An example of this is the **coth** function, which is used in the Jiles-Atherton model to define the anhysteretic behaviour of the core model. Evaluation of this approach has proved effective in cases where the classical Jiles-Atherton model has great difficulty in converging.

### 4.4.5  Modification to Jiles-Atherton model to improve loop closure modeling

As magnetic materials proceed into the region of full saturation, the tips of the BH loop are observed to close as shown clearly in figure 4.11 for Philips 3F3. This behaviour is exhibited by the Jiles-Atherton model, but is not controlled by a specific parameter. This gives the problem that in optimizing the model parameters to achieve best fit, in order to fit the loop closure a modification may reduce the accuracy of another feature of the model.
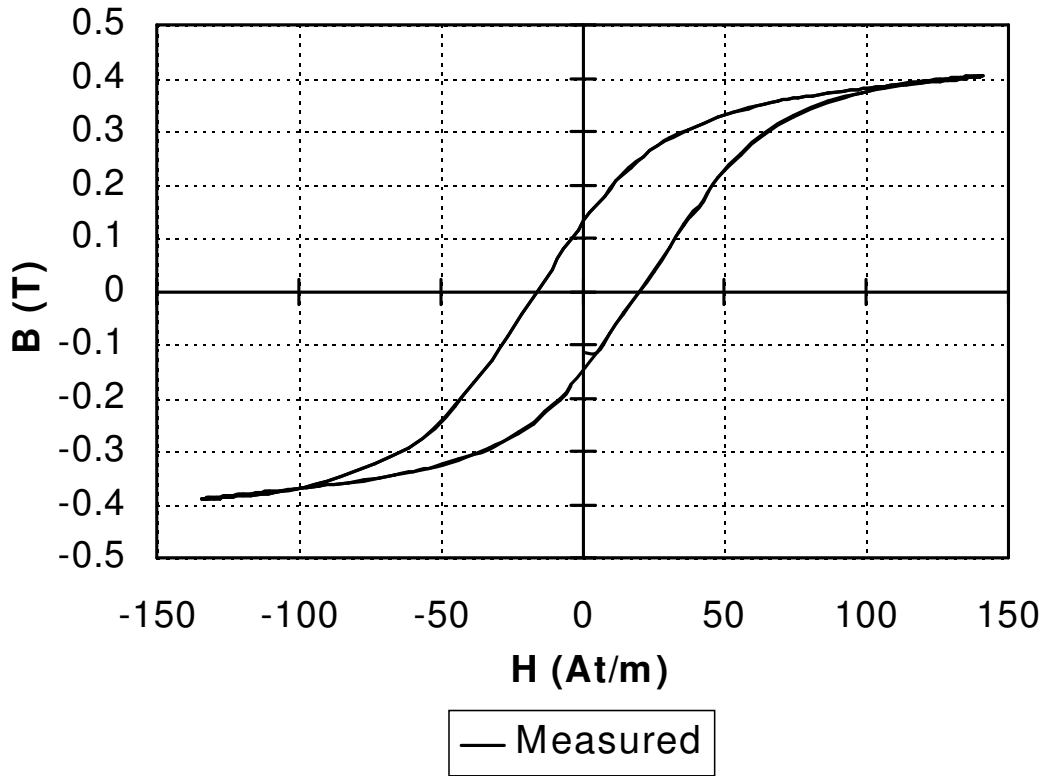


**Figure 4.11: Measured BH curve showing closure at loop tips**

The model was therefore modified with two extra parameters. The first parameter ($H_{ec}$) modifies the applied field such that the field strength level was limited by the value of $H$ at the early closure value. A hard limit function on the applied field was added, modifying this to allow a small slope (*ecrate*) after limit to avoid complete loop closure and to reduce the discontinuity at the transition to the early closure region.  With the limit in place, the model now correctly modeled the early closure, but the slope of the function after closure was too flat. A function was therefore added to the final equation for the Flux Density ($B$) to allow the slope to be varied to give a more realistic hysteresis loop. The structure of the modified model is shown in Fig. 4.12.
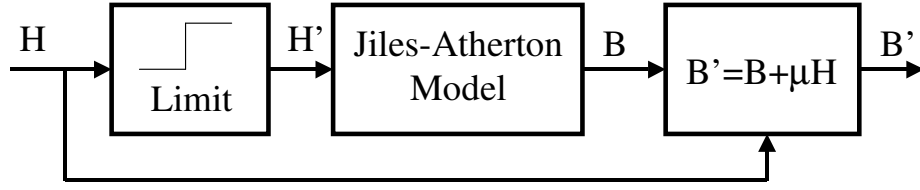
**Figure 4.12: Modified Jiles-Atherton model with field strength limit and Flux slope modifications**

The difficulty with simply changing the slope from a practical, simulation point of view is that a discontinuity is introduced to the first derivative of the effective field strength. The function was therefore modified to have a softer limit by changing the linear change to an exponential change of the form given in (4.5) when the applied field $H$ is greater than the early closure field $H_{ec}$.

$$H' = \begin{cases} H & |H| \leq |H_{ec}| \\ H_{ec} + H_0\left[1 - e^{-ecrate \cdot |H - H_{ec}|}\right] & H > H_{ec} \\ -H_{ec} - H_0\left[1 - e^{-ecrate \cdot |-H_{ec} - H|}\right] & H < -H_{ec} \end{cases} \tag{4.5}$$

While (4.5) is not continuous in the first derivative generally, if (4.6) is used to define the value of $H_0$ then the function becomes continuous through the early closure transitions.

$$H_0 = \frac{1}{ecrate} \tag{4.6}$$

This approach, while being quite effective, has the disadvantage of not being justified on physical grounds. Jiles & Atherton [20] state that there is no fundamental reason why the parameters should be fixed. They can therefore be made functions of the applied field or the flux density to obtain a better fit with measured data. Jiles & Atherton [20] also explain that the parameter which defines the loss, $k$, can be made a function of the applied field or the flux density and propose a linear function. It was found during this project, however, that a Gaussian function of the form shown in (4.7) gave excellent results and this was therefore used in this thesis. This function has the added advantage of no discontinuity around zero when the applied field changes polarity which improves simulation convergence.

$$k = k_0 * e^{-\frac{H^2}{2\sigma^2}} \tag{4.7}$$

Where $k_0$ is the default value of the parameter $k$, $H$ is the applied field and $\sigma$ is the standard deviation of the gaussian function.

### 4.4.6 Comparison of Measured and Simulated Results

In order to assess the effectiveness of modeling different loop shapes using the modified Jiles-Atherton models, measurements were taken at 35 A/m, 70 A/m and 140 A/m respectively using the Philips 3F3 material. The model parameters were optimized using the original and modified Jiles-Atherton model and comparisons made between the resulting BH Curves.

#### 4.4.6.1  Jiles-Atherton Model Parameter Optimization

An optimization engine was written and built into the Virtual Scope software to allow optimization of the BH hysteresis loop using a Least Squares Error between the measured and simulated BH Curves. The optimization engine has univariate search, simulated annealing and a genetic algorithm method implemented, but the univariate method was applied in this section (The alternative optimization methods will be discussed later in this chapter). The optimizer allows the specification of the breadth and depth parameters in a univariate search method, so different types of optimization approach could be implemented. With a breadth type search the parameters are varied, but each parameter has a low number of iterations before moving onto the next parameter. The breadth type search allows local minima to be generally avoided by searching widely across the solution area. The depth first search allows each parameter to be tuned in turn to the best advantage and is useful where optimization is nearly converged. The optimizer also allows the specification of which parameters are to be allowed to vary, therefore allowing control to be anywhere from completely manual (varying one parameter at a time) to automatic (varying every parameter). The optimizer also allows variable step sizes to ensure that different parameter sensitivities are catered for in the software.

The optimizer was run on the experimental data for 3F3 with the original and the modified Jiles-Atherton model. The number of outer iterations (breadth) was set to 20 and the number of inner iterations (depth) was set to 5. The Least Squares Error calculation was started after the initial magnetization of the model had taken place and a 4th Order Runga-Kutta Integration method was used to calculate the Jiles-Atherton model in software.

#### 4.4.6.2  Minor Loop (35 A/m) Optimization Results

The 35A/m field strength measured data was optimized using the defined parameters and with the original Jiles-Atherton Model obtained a Least Squares Error of 0.018. This corresponds to an RMS error of 3.8mT over the range of the BH Curve. When the Modified Jiles-Atherton model was used for the optimization, with the same parameters a Least Squares Error of 0.015 was reached (RMS error of 3.4mT). The resulting measured and simulated BH Curves are shown in Fig. 4.13.
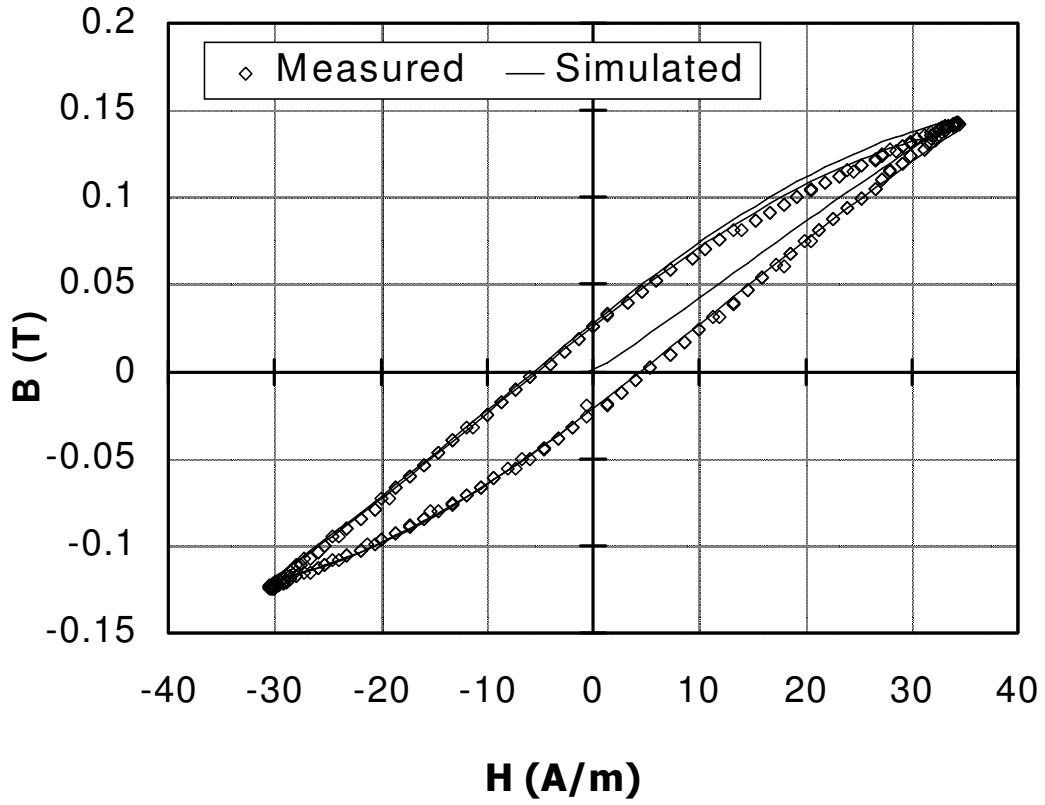
**Figure 4.13: Minor Loop (35 A/m) Optimization Results**

### 4.4.6.3 Medium Field Strength (70A/m) Optimization Results

With the field strength of 70A/m, the same optimization experiment was carried out giving the Least Squares Error for the standard Jiles-Atherton model of 0.062 (RMS error of 7.04mT) and with the modified model 0.026 (RMS Error of 4.56mT). The resulting measured and simulated BH Curves are shown in Fig. 4.14. There is some discrepancy for the first half cycle as the model goes through the initial magnetization sequence, but subsequent cycles show a good correlation.
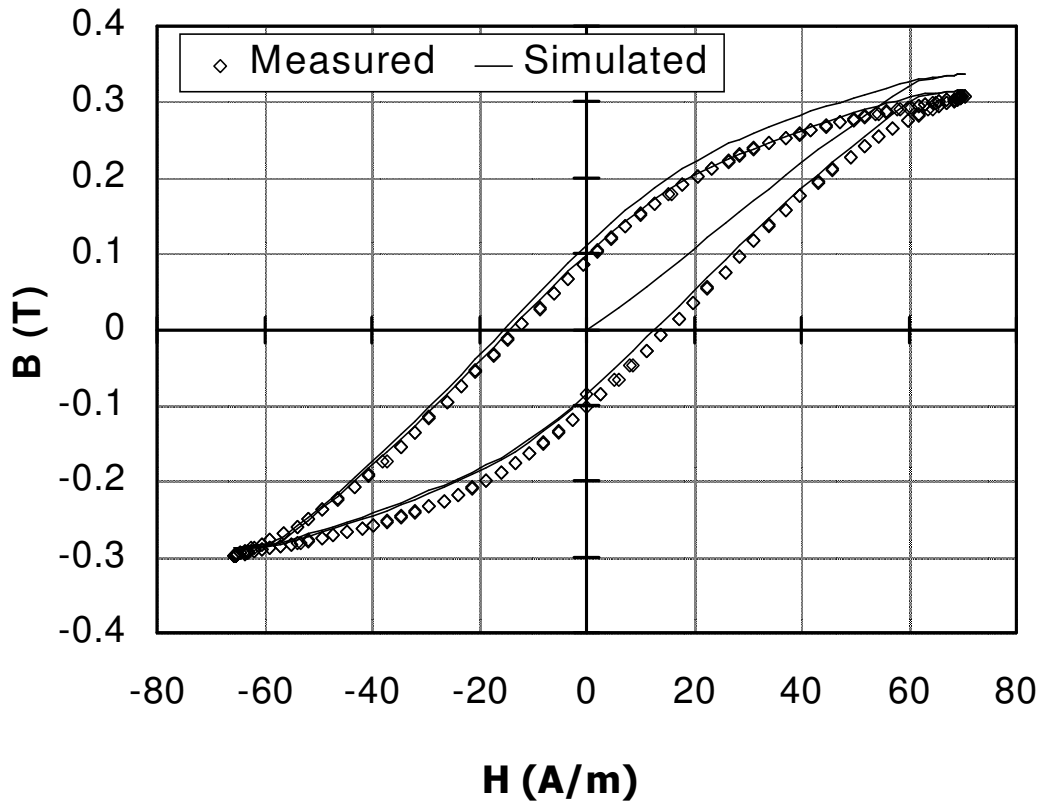
**Figure 4.14: Medium Field Strength (70A/m) Optimization Results**

### 4.4.6.4 *Major Loop (140 A/m) Optimization Results*

The 140A/m field strength measured data was optimized using the defined parameters and with the original Jiles-Atherton Model obtained a Least Squares Error of 0.381. This corresponds to an RMS error of 17.4mT over the range of the BH Curve. When the Modified Jiles-Atherton model was used for the optimization, with the same parameters a Least Squares Error of 0.246 was reached (RMS error of 14.0mT). The resulting measured and simulated BH Curves are shown in Fig. 4.15.
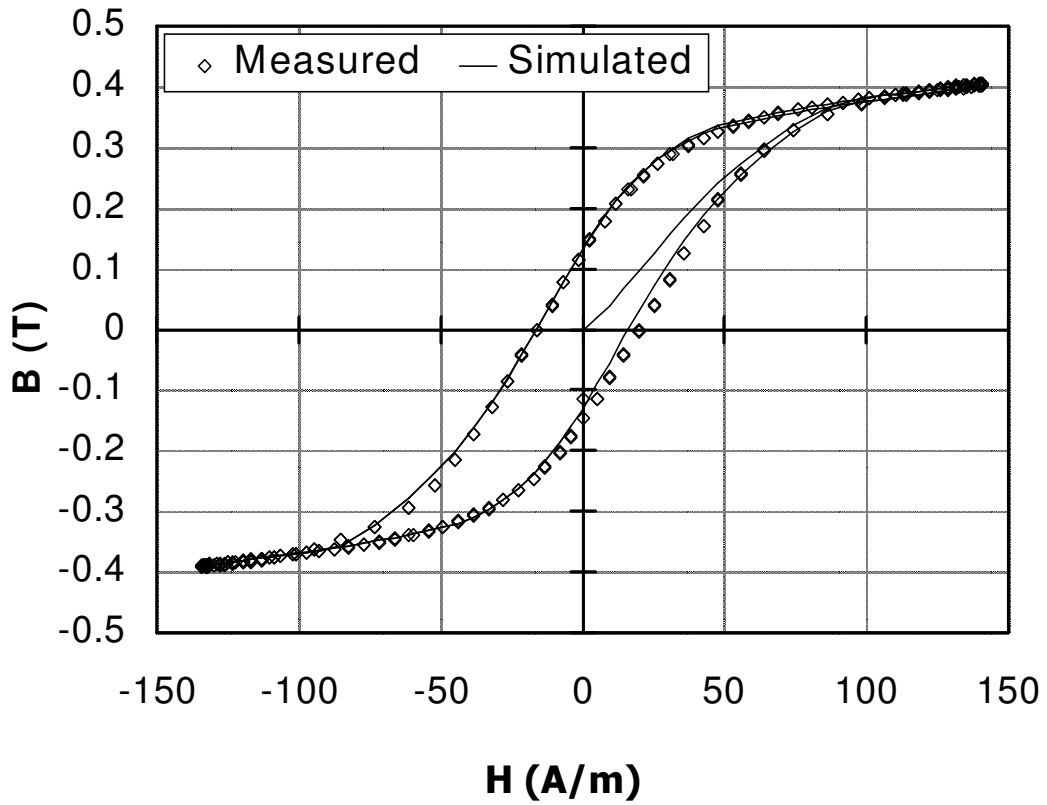
**Figure 4.15: Major Loop (140 A/m) Optimization Results**

### 4.4.7 Comparison of original and modified Jiles-Atherton model

The original and modified Jiles-Atherton models were compared with the measured major BH Curve (140 A/m) to establish the difference obtained by applying the modifications to the model. The resulting curves are shown in figure 4.16. It can clearly be seen that the loop tips are more accurately modeled using the modified modeling approach.
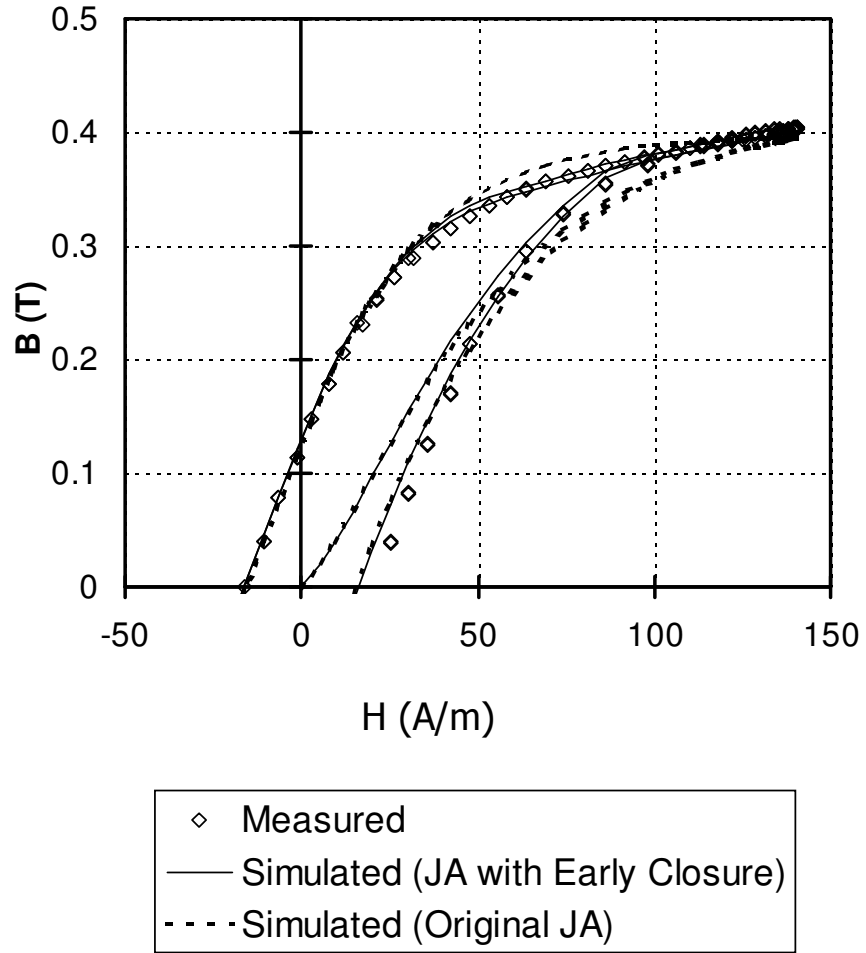
**Figure 4.16: Measured, original and modified Jiles-Atherton BH curves**

## *4.5    Parameter Extraction and Characterization*

### 4.5.1    Measurement of Basic BH Curve Metrics

The core material's basic magnetic characteristics can be defined in terms of the fundamental points on the Hysteresis Curve which are the Maximum Field Strength ($H_{max}$) and Flux Density ($B_{max}$), the Remanence ($B_r$) and the Coercive Force ($H_c$) all of which are shown in Fig. 4.17.
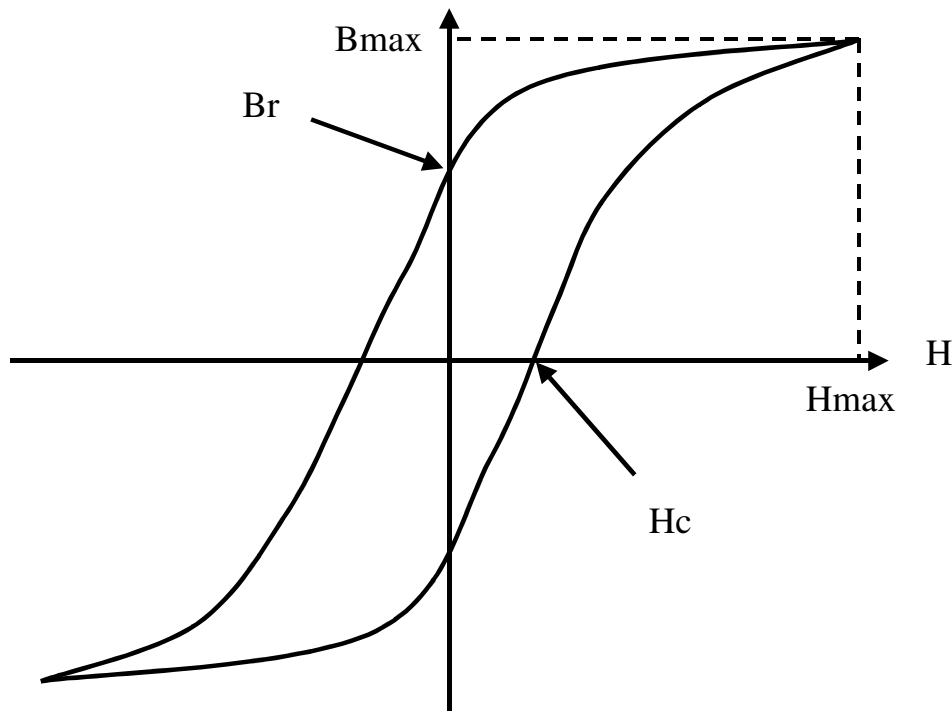
**Figure 4.17: Basic Magnetic Material metrics**

Although these metrics are useful, they do not provide a complete set for optimization. One such situation has been previously discussed, where the material has saturated to such an extent at high field strengths that the hysteresis loop 'closes up' prior to the maximum applied field strength being reached. This 'early closure' of the loops requires a new parameter to be defined, which is the applied field at which early closure takes place ($H_{ec}$). The measurement of where the loop has effectively closed requires the specification of a tolerance (e.g. closure to within 1%).

The permeability of the material is also a significant parameter. There are two key metrics which can be extracted from the BH data; the initial permeability and the maximum incremental permeability at $H_c$ on the BH loop.

The area enclosed by the BH loop defines the energy loss of the material and a measurement of this is crucial if temperature effects are to be included dynamically in the model. The shape of the loop is also important, as can be seen from the variation in shape of the waveforms in Figures 4.12 to 4.14. As the field strength increases, the slope of the hystersis loop as a whole changes, and the shape changes from an almost elliptical minor loop to the sigmoid shape of saturation.

For electrical circuit simulation it is important to ensure that the magnetic component parameters chosen result in the correct electrical behaviour at the terminals of the device. The metrics can be used to ensure that the model parameters are optimized so that the electrical behaviour is accurately represented by the magnetic component. This may be achieved by including specific electrical metrics such as the response of the magnetic component to a voltage applied to the

component terminals as well as the purely magnetic metrics. This can be applied in the optimization approach by using the voltage and current waveforms as the goal rather than the BH curve. For example, in the least squares error approach, it is usual to compare the desired and simulated BH waveforms, but it is equally valid to compare the desired and simulated voltage and current waveforms.

A set of metrics was implemented in the Virtual Scope software, as shown in figure 4.20, to allow the direct comparison of measured and simulated curves using both a least squares error and metric based method. The optimization 'goodness' function also has the option of selecting between these two options. It becomes quite difficult to visualize the difference between multiple parameters, such as metrics, and so a new visualisation scheme was devised using a polar diagram shown in figure 4.18. The measured metrics are all normalized to 1 and spaced equally around the unit circle (e.g. for four metrics the results are spaced 90° apart). The metrics of the simulated results are then plotted on the same graph, equally spaced as before, with the magnitude normalized with respect to the measured value of the metric. It can be clearly seen which metrics of the simulated waveforms after optimization are above or below the measured values and by how much relative to each other.  The unit circle indicated is intended as a visual aid that becomes more useful for a larger number of metrics.
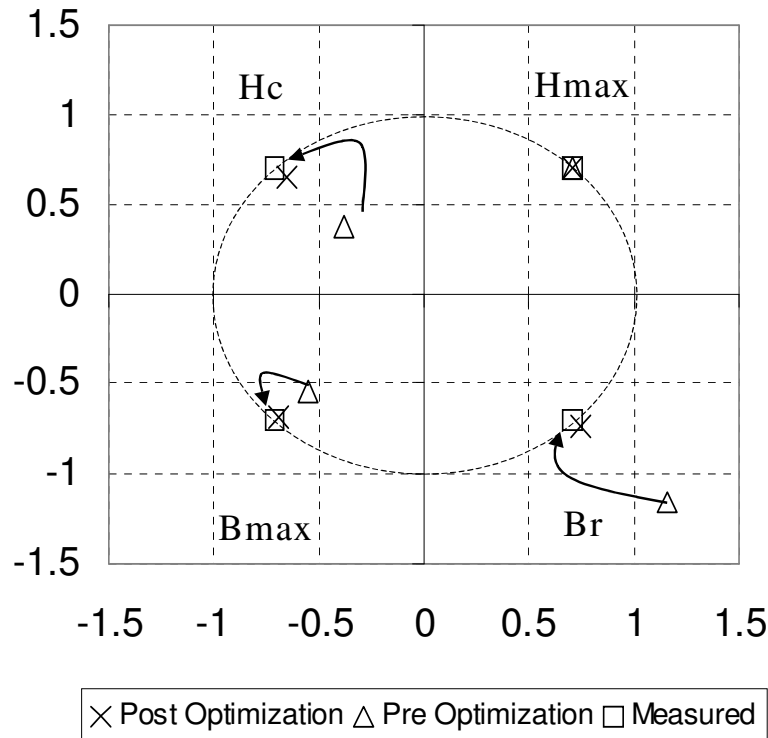


Figure 4.18: Polar Diagram showing Optimized and Measured Metrics

### 4.5.2 Comparison of Metric based and Least Squares Error Functions

Although the Least Squares Error function is generally the best method for optimizing curves of this kind, it is often essential to ensure that a particular facet of the BH Loop characteristic is modeled extremely accurately. This leads to the use of the metrics method to ensure that specific features of the behaviour are optimized directly.

To implement this in software required a simple modification to the error calculation so that instead of calculating the error using Least Squares, the error is the normalized deviation from the defined metrics, with appropriate weighting factors for each metric as defined in equation 4.7.

$$Error = \sum_{Metrics} W_m \cdot (\frac{M_s - M_m}{M_m})^2 \qquad (4.7)$$

Where $M_s$ is the Metric of the simulated curve , $M_m$ is the metric of the measured curve and $W_m$ is the individual weighting for the metric.

The advantage of this method is that the optimization of the material characteristic can be tailored for the end application. For example, a communications pulse transformer may need excellent modeling of the minor loop slope, whereas a power transformer may need more emphasis on the area of the BH loop for energy calculations. The error function for different applications can be easily defined using the weighting factors in equation (4.7). For example, in the characterization of the 3F3 material thus far in this thesis, the method used has been a least squares approach. If the metrics previously defined are applied for an optimization run of a major loop with a Least Squared Error of 0.098T (RMS error of 8.85mT) then although the error is quite small for the whole curve, the normalized error for the remanence is 7.2% and the normalized error for the coercive force is 7.69%.

When the optimization is repeated, but this time using the goal function defined by the remanence, coercive force and maximum B and H, the Least Squared Error increases to 0.195T (RMS Error of 12.49mT) but the normalized error for the remanence reduced to 0.4% and the coercive force reduced to 0%. The normalized errors on the maximum $B$ reduced from 0.9% to 0.17%. The parameters and calculated errors for optimized models based on 3F3 data are shown in Table 4.1.

| Parameter | Least Squares | Metric |
|---|---|---|
| Least Squares Error (mT) | 9.8 | 195 |
| Metric Error (mT) | 11 | 0.001 |
| a  [A/m] | 49.766 | 49.766 |
| k  [A/m] | 24.28 | 21 |
| c | 0.605 | 0.321 |
| α | 10µ | 5µ |
| Ms  [A/m] | 468k | 467.4k |
| ΔBr/ Br | -7.30% | 0.40% |
| ΔBmax/ Bmax | 1.00% | -0.20% |
| ΔHc/ Hc | -7.70% | 0.00% |
| ΔHmax/ Hmax | 0.00% | 0.00% |

**Table 4.1 : Comparison of Metrics and Least Squares Optimized Parameters and Metrics**

The BH Curves for the metric and least squares optimized parameters are shown in Fig. 4.19. It can be seen that although the resulting curves are similar, the metric optimized BH curves have improved accuracy at the key crossing points $B_r$ and $H_c$.
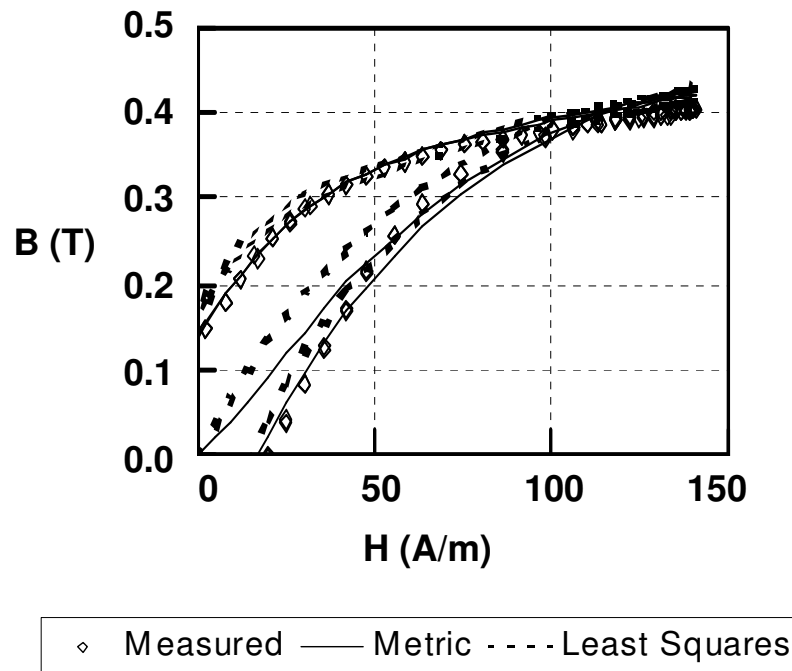


**Figure 4.19: Measured, Least Squares and Metric Based Simulated BH Curves**

### 4.5.3   Implementation of Metric and Parameter Extraction Software

The measured and simulated metrics were implemented into the Virtual Scope using 2 screens. The first screen is shown in figure 4.20 and shows the metrics and the normalized polar plot. Figure 4.21 shows how the weighting function defined by equation 4.7 is implemented in Virtual

Scope. Each metric can be specified or taken from the measured data. The metrics can be weighted and selected, and the overall weighted error calculated.
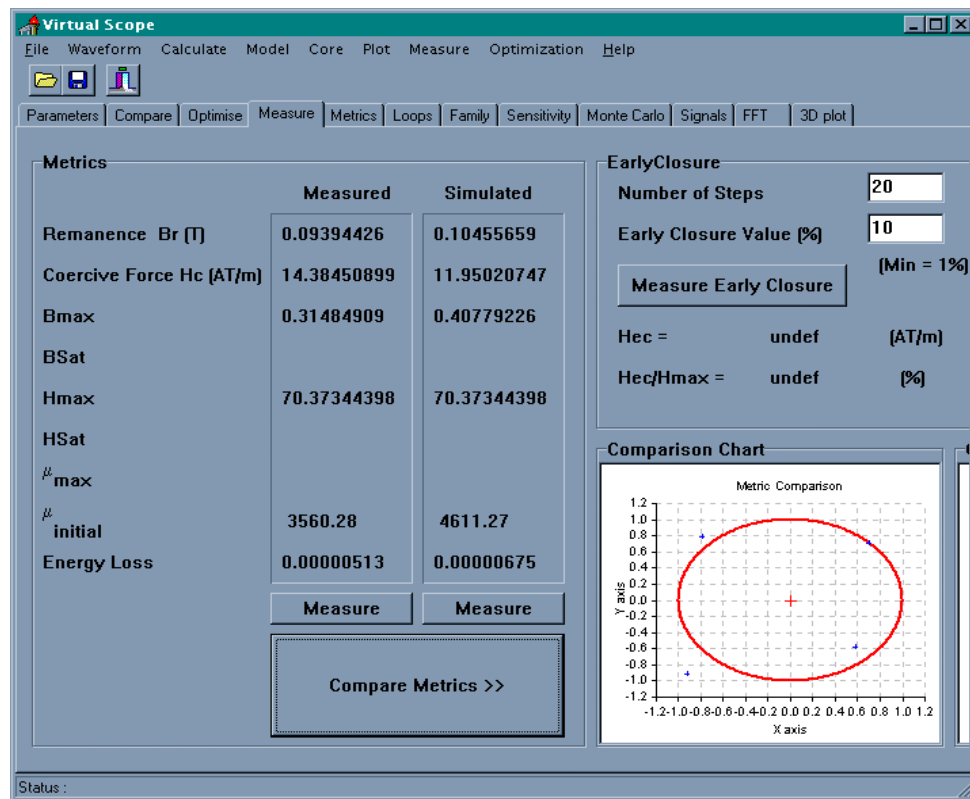


**Figure 4.20: Measured and Simulated Metrics Virtual Scope Screen**

**Virtual Scope**

File  Waveform  Calculate  Model  Core  Plot  Measure  Optimization  Help

Parameters | Compare | Optimise | Measure | Metrics | Loops | Family | Sensitivity | Monte Carlo | Signals | FFT | 3D plot |

**Metric Calculation**

| Metric | Enable | Measure | Specify | Weighting | [(Mi-Mm)/(Mm)]*Wi |
|---|---|---|---|---|---|
| Remanence Br (T) | ☑ | ☑ | | 1 | 0.11296409 |
| Maximum B (T) | ☑ | ☑ | | 1 | 0.29519909 |
| Coercive Force Hc (At/m) | ☑ | ☑ | | 1 | -0.16923077 |
| Maximum H (At/m) | ☑ | ☑ | | 1 | 0.00000000 |
| Initial Permeability $\mu i$ | ☐ | ☐ | | 1 | |
| Maximum Permeability $\mu max$ | ☐ | ☐ | | 1 | |
| Energy Loss | ☑ | ☑ | | 1 | 0.31543886 |
| Saturation Flux Density Bsat (T) | ☐ | ☐ | | 1 | |
| Saturation Field Strength Hsat (At/m) | ☐ | ☐ | | 1 | |

| Calculated Weighted Metric Error | $E = \Sigma \left[ ((Mi-Mm)/Mm)*Wi \right]^2$ | 0.22804412 |

Status :

**Figure 4.21: Metric Weighting Function Implementation in Virtual Scope**

### 4.6  Optimization of Magnetic Material Models

### 4.6.1  Introduction

Optimization methods applied to fit the Jiles-Atherton hysteresis loops to measured data have been investigated by Schmidt and Güldner [40] and Lederer, Igarashi, Kost and Honma [88] using the well known simulated annealing approach. Genetic algorithms provide an alternative approach to optimization that may have some advantages, especially when considering the more complex problem of fitting several loops simultaneously.  The use of genetic, or evolutionary, algorithms to solve difficult engineering problems is a relatively recent innovation. Holland [86] and Goldberg [66] are two of the pioneers of this technique and the last ten years have seen a plethora of applications for genetic algorithms from systems design to topology analysis [87]. The fundamental difference between genetic algorithms and conventional optimization techniques, such as simulated annealing [65], is that in certain problems the computational effort involved in a standard exhaustive search method would be prohibitive. The random nature of genetic algorithms may not find the absolute best solution, but it has a greater chance of finding a good solution, quickly, for difficult problems. This randomness also works well for problems with chaotic or ill-defined behaviour difficult to classify and those problems with local maxima or minima that would perhaps trap a conventional search algorithm.

The optimization of magnetic materials is a problem which has aspects suited to the application of genetic algorithms. Even though the Jiles-Atherton model of hysteresis is well understood mathematically, the parameters are inter-linked in such a way that the set of possible combinations of parameters may be large. Significant changes in the shape of the hysteresis loop may result from small parameter variations. These two aspects give a relatively high risk of local maxima or minima being found or instabilities in a conventional algorithm. Other approaches for modeling magnetic materials such as the Preisach model have no direct link between behaviour and material physical properties so are natural potential targets for the genetic algorithm approach. The background theory to specific optimization methods has been described previously in this thesis.

### 4.6.2 Magnetic Material Model Optimization procedure

The overall structure of the analysis software developed is shown in Fig. 4.22. The software derives the measured field strength ($H$) and flux density ($B$) from the oscilloscope data, with the test configuration able to be customized. The Jiles-Atherton model can be calculated using the derived field strength from the measured data or an ideal internally generated test waveform (sinusoidal or triangle) and then compared with the original test results. Metrics can be applied to both the measured and simulated results to assess the relative performance of the model. An optimization loop allows the model parameters to be modified using iteration to achieve optimum model performance. The optimization method is a steepest descent type of approach, simulated annealing or genetic algorithm.
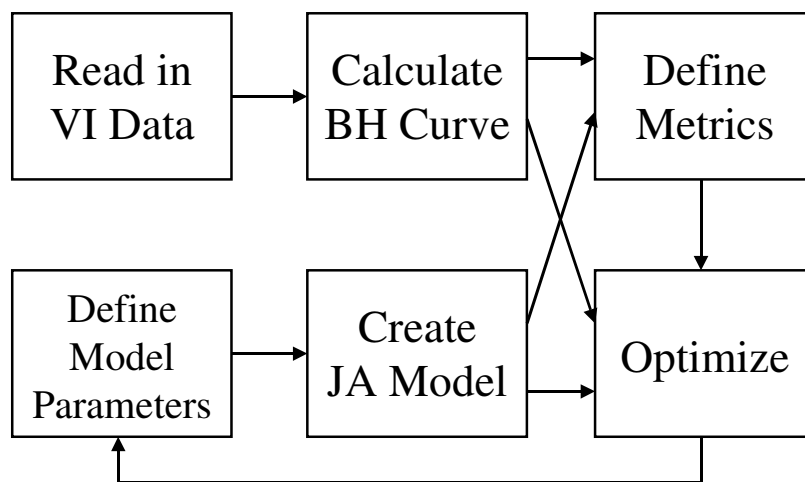


**Figure 4.22 : Virtual Scope Optimization Process Diagram**

### 4.6.3 Overview of Optimization Methods

Optimization techniques have been applied to the solution of engineering and mathematical problems for many years, and a plethora of methods exist with varying degrees of usefulness. Pierre [64] gives a good grounding in the broad spectrum of approaches including the *univariate*

*search method* while Laarhoven and Aarts [65] provide details for the *simulated annealing* approach and some practical examples. One exciting new area of progress is the development of *evolutionary* or *genetic* algorithms and a key text in this area is Goldberg [66]. Conventionally, the simulated annealing approach has been applied to the optimization of magnetic model parameters [40],[88] but comparisons in this thesis have been made between all the methods. The genetic algorithm has been successfully applied to topological optimization of transformers [85] but no published literature exists for the application of the method to material model parameters. This approach has therefore been studied in this thesis.

### 4.6.3.1  Univariate Search Methods

Univariate Search methods [64] are probably the simplest form of optimization algorithm to implement, and require that a set of parameters are varied, in turn, until the solution cannot be improved. Once all the parameters have been varied, the whole process is repeated until the solution goal has been achieved. The number of times a parameter is varied before moving onto the next one indicates the *depth* of the search, while the overall number of loops through the set of parameters is the *breadth* of the search. A flowchart of the Univariate Search Method is given in figure 4.23.
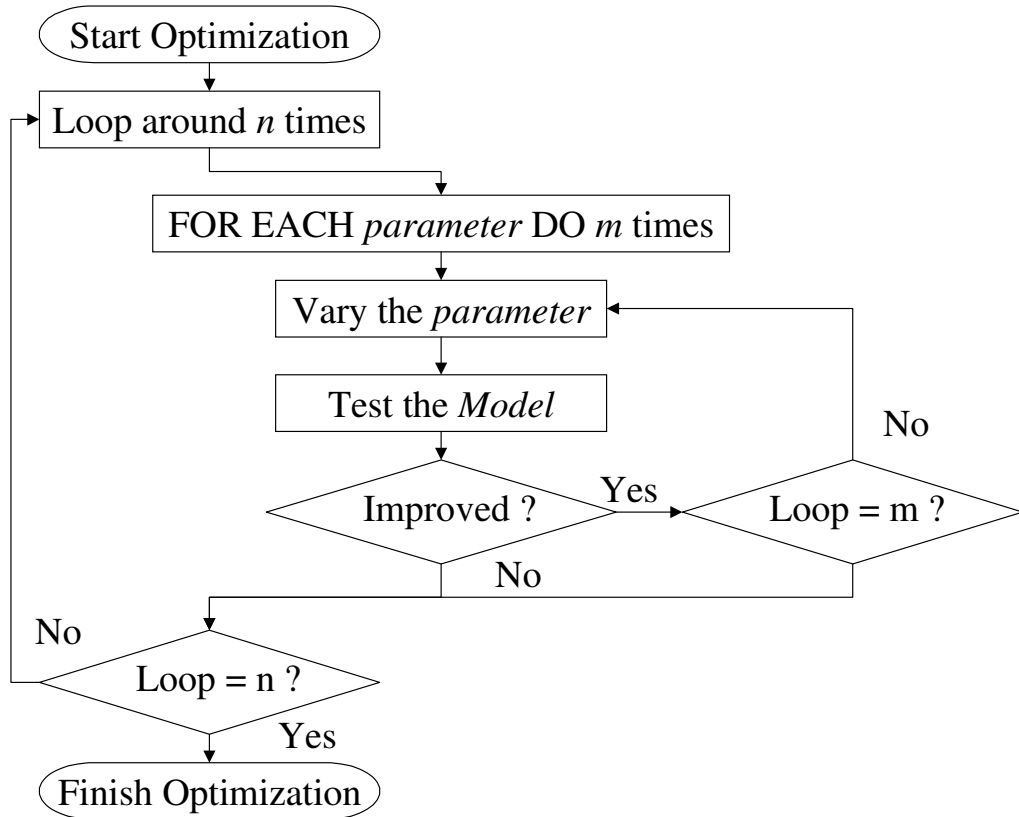


**Figure 4.23 : Univariate Search Method**

77

### 4.6.3.2  Simulated Annealing

The simulated annealing method [65] uses a mathematical analogy of the cooling of liquids into solid form to provide an optimal solution for complex problems. The method operates on the principle that annealed solids will find the lowest energy point at thermal equilibrium and this is analogous to the optimal solution in a mathematical problem. The equation for the energy probability used is defined by the Boltzmann distribution given by (4.8).

$$P(E) = \frac{1}{Z(T)} \cdot \exp\left(-\frac{E}{k_B T}\right)$$

(4.8)

$Z(T)$ is the partition function, which is a normalization factor dependent on the temperature $T$, $k_B$ is the Boltzmann constant and $E$ is the Energy. This equation is modified into a more general form, as given by (4.9), for use in the simulated annealing algorithm.

$$P(E) = \frac{1}{Q(c)} \cdot \exp\left(-\frac{C(i)}{c}\right)$$

(4.9)

$Q(c)$ is a general normalization constant, with a control parameter c, which is analogous to temperature in (4.8). $C(i)$ is the cost function used, which is analogous to the Energy in (4.9). The parameters to be optimized are perturbed randomly, within a distribution, and the model tested for improvement. This is repeated with the control parameter decreased to provide a more stable solution. Once the solution approaches equilibrium, then the algorithm can cease. A flowchart of the full algorithm applied is given in figure 4.24.
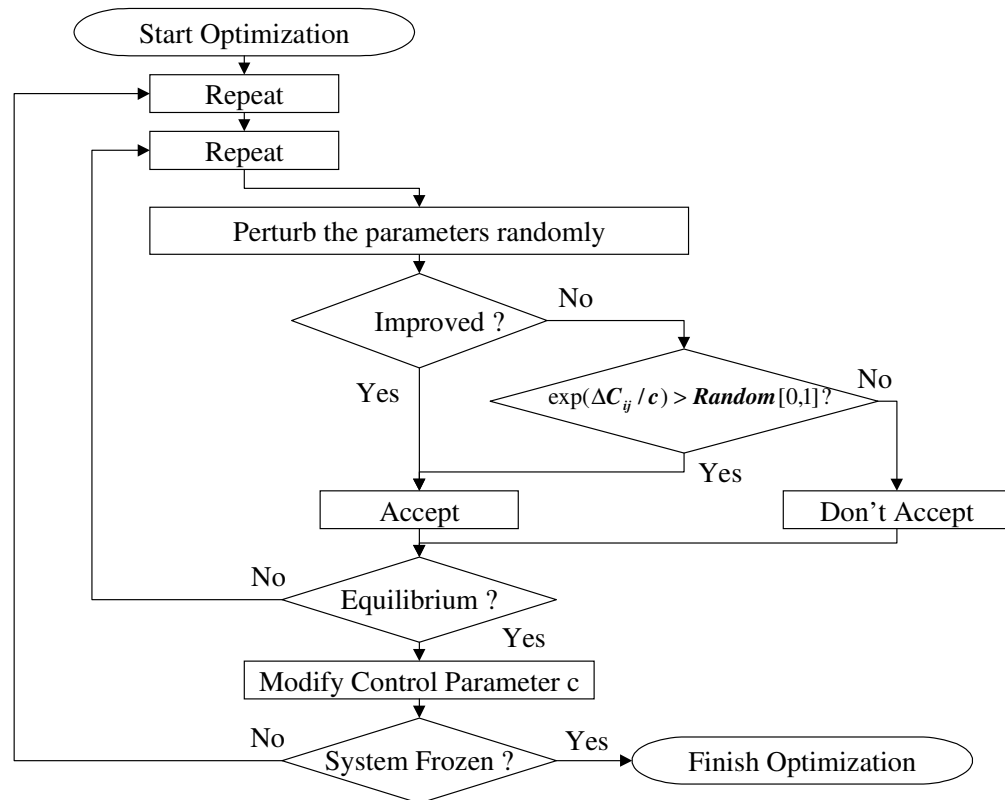
**Figure 4.24 : Flowchart of Simulated Annealing Method**

### 4.6.3.3  Genetic Algorithms

The use of Genetic, or Evolutionary, Algorithms to solve difficult engineering problems is a relatively recent innovation. Holland [86] and Goldberg [66] are two of the pioneers of this technique and the last ten years have seen a plethora of applications for Genetic Algorithms from systems design to topology analysis [87]. The fundamental difference between Genetic Algorithms and conventional optimization techniques, such as simulated annealing, is that in certain problems the computational effort involved in a standard exhaustive search method would be prohibitive. The random nature of Genetic Algorithms may not find the absolute best solution, but it has a greater chance of finding a good solution, quickly, for difficult problems. This randomness also works well for problems with chaotic or ill-defined behaviour difficult to classify and those problems with local maxima or minima that would perhaps trap a conventional search algorithm.

The first step in the Genetic Algorithm process, figure 4.25, is to define an initial population of individuals which becomes the first generation for the algorithm. For each generation there will be a number of children created by combining the characteristics of two parent individuals, determined by random and selective methods. Once the two parents have been selected, then their characteristics can be combined to create a new individual (child). The selection of characteristics from the two parents is random, and there is a risk of small mutations. Once the required number

of children have been created the population as a whole is adjusted by replacing the worst individuals in the population by the newly created children.
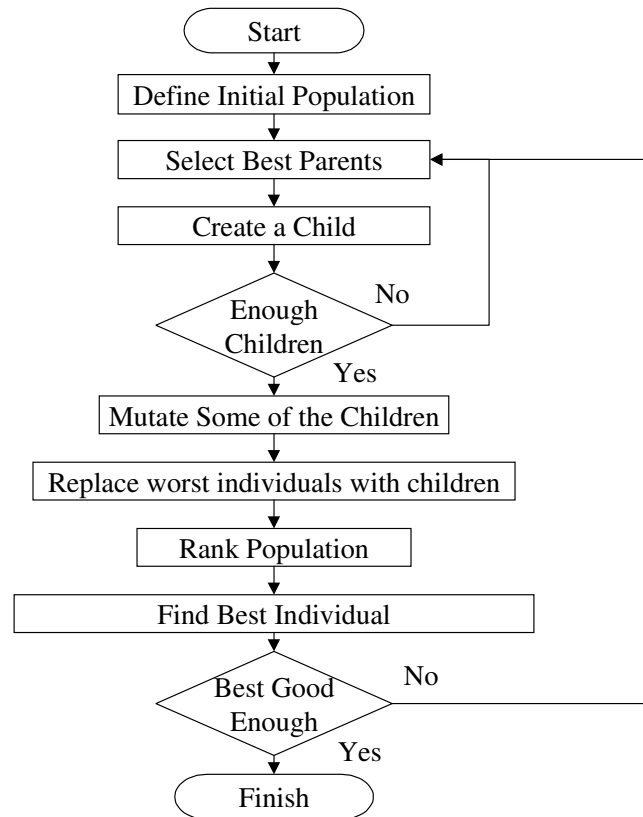


**Figure 4.25 : Flowchart of the Genetic Algorithm**

### 4.6.4   Comparison of Optimization Methods

A toroid made of the Siemens N30 material was tested and the resulting BH loop used for optimization. The Jiles-Atherton model was optimized using the classical model and also the improved model utilizing the variable $k$ parameter. The optimization was carried out using the well understood simulated annealing method as a control and also with a genetic algorithm approach. The simulated annealing approach was carried out with a variation of 10%, a control factor of 0.001 and 2500 iterations used. The genetic algorithm used 50 generations of a population including 50 individuals (50 times 50 giving a rough equivalent of 2500 iterations). Each generation produced 40 children of whom 20 were mutated. A variation of 10% was introduced in the mutation process. In each case the fitness function used the least squares error approach.

The resulting mean errors between the simulated and measured results are summarised in table 4.2 and figure 4.26. Table 4.2 shows that the error is significantly reduced for the genetic algorithm, and that the variable $k$ parameter makes a significant difference for both optimization methods. Figure 4.26 shows the error versus the number of iterations and again clearly the genetic algorithm with the gaussian modification of $k$ is the most accurate.

| Parameter | Genetic Algorithm | Genetic Algorithm Gaussian k | Simulated Annealing | Simulated Annealing Gaussian k |
|-----------|-------------------|------------------------------|---------------------|-------------------------------|
| a | 13.8 | 9.29 | 7.26 | 6.96 |
| c | 0.799 | 0.497 | 0.150 | 0.308 |
| k | 11.01 | 12.67 | 7.19 | 11.176 |
| $\alpha$ | 6.78e-6 | 29.1e-6 | 4.29e-6 | 4.54e-6 |
| $M_s$ | 293318 | 268562 | 264500 | 257479 |
| $\sigma$ | - | 16.55 | - | 15.54 |
| Error | 0.1416 | 0.019 | 0.188 | 0.035 |

**Table 4.2: Comparison of Simulated Annealing and Genetic Algorithm Optimization with and without Gaussian *k***
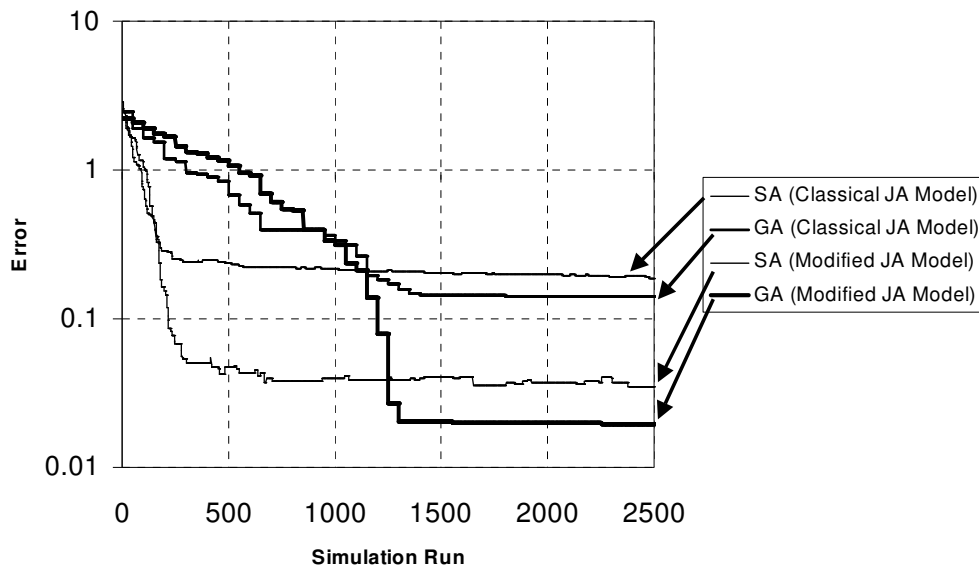


**Figure 4.26: Comparison of Simulated Annealing and Genetic Algorithm Error Functions**

Interestingly, when a combination of simulated annealing and the genetic algorithm was applied, the error was reduced further. This can be explained with the fact that the two methods have different strengths. The Genetic Algorithm is very good at finding the correct area of the solution, tolerant of local maxima and minima, and the simulated annealing method is excellent at refining a solution systematically to the nearest maximum or minimum. It is also worth noting the wide differences between some of the parameters obtained using different optimization approaches. The parameters in the Jiles-Atherton model are highly interdependent, and as such may produce similar BH curves for widely different parameter sets. The modification of the *k* parameter in the model

may also contribute to these differences, as in the original model, the improved modeling of the loop tip accuracy using a fixed $k$, may lead to a distortion of the parameters $a$, $c$ and $k$.

The results of the optimization are perhaps best visualized by observing the resulting BH Loops. Figure 4.27 shows the optimized BH loop using the original Jiles-Atherton model with no modification, and also the optimized curve with a gaussian variation of $k$ using a combination of Genetic Algorithm and Simulated Annealing optimization.



□  Measured    · · · · Original Jiles-Atherton    ⎯⎯ Modified Jiles-Atherton
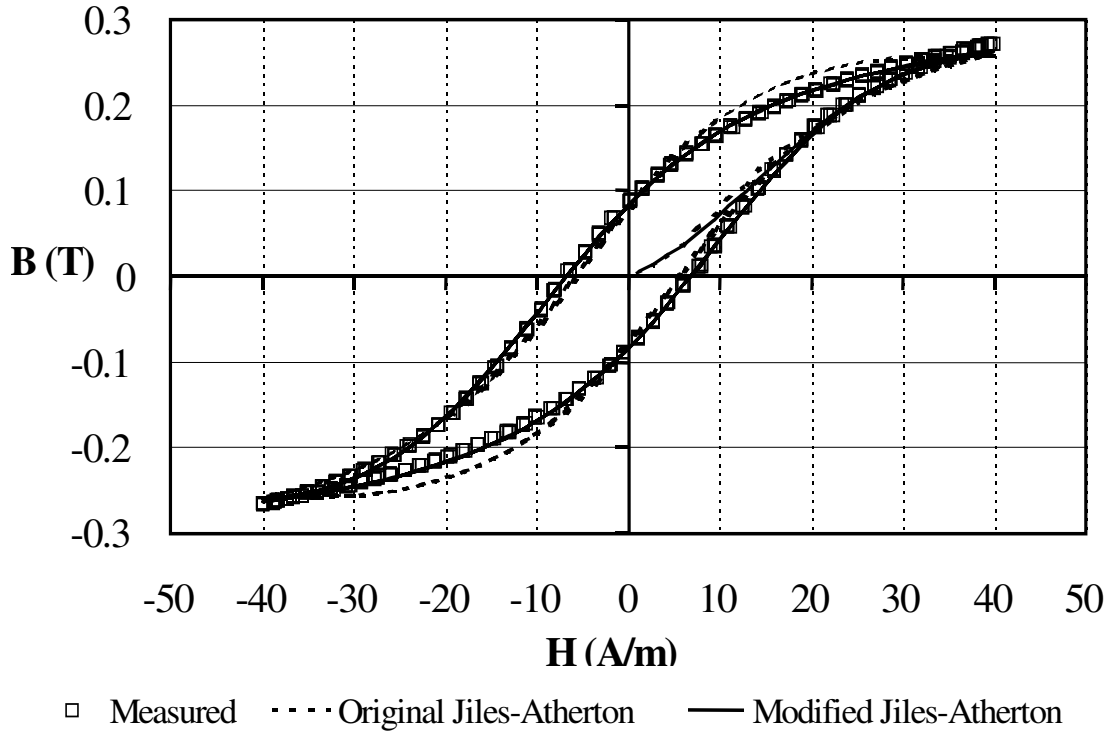
**Figure 4.27: Comparison of measured, optimized original Jiles-Atherton model and optimized modified Jiles-Atherton model BH curves**

## 4.6.5  Statistical Analysis of Optimization Methods

Although the individual optimization results previously shown are encouraging, due to the random nature of the optimization process in both simulated annealing and genetic algorithm approaches, it is appropriate to investigate the performance of the respective methods statistically. The optimizations were therefore repeated over a number of runs (20) and the resulting errors compared. The simulated annealing approach was carried out with a variation of 10%, a control factor of 0.001 and 2000 iterations used. The genetic algorithm used 40 generations of a population including 50 individuals (40 times 50 giving a rough equivalent of 2000 iterations). Each generation produced 40 children of whom 20 were mutated. A variation of 20% was introduced in the mutation process. The simulated annealing approach gave a mean value for the error of 0.0219, with a standard deviation of 0.003, while the genetic algorithm gave a mean value

for the error of 0.0148, with a standard deviation of 0.009. Figure 4.28 shows the histogram of the respective errors for the two methods.
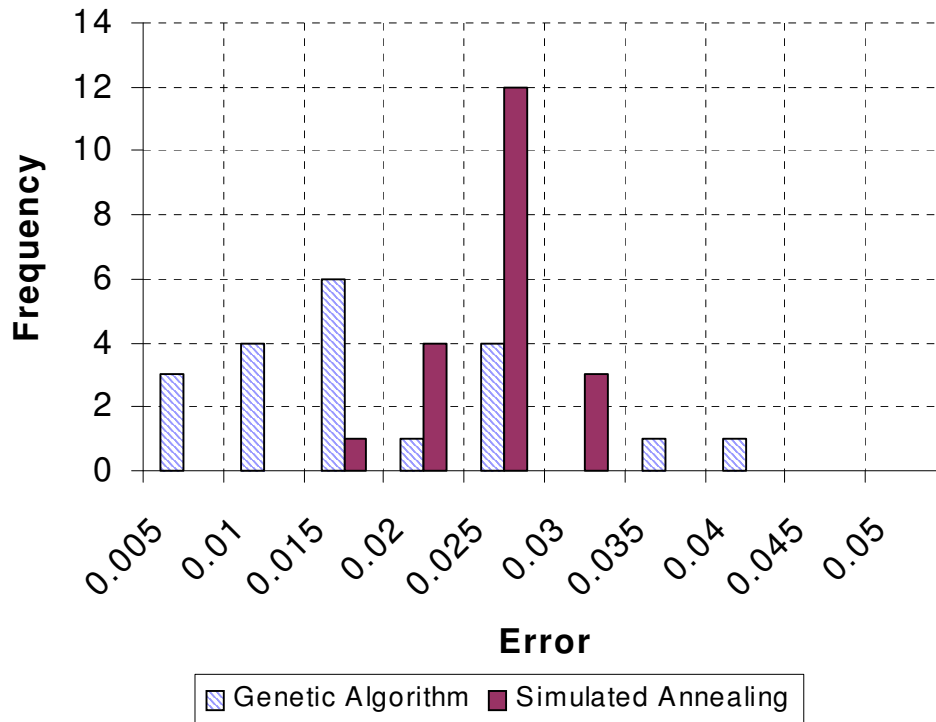


**Figure 4.28: Statistical Comparison of the performance of the Simulated Annealing and Genetic Algorithm Approaches**

It is interesting to note that although the genetic algorithm has a greater standard deviation (wider spread), the average error is less than that for the simulated annealing approach. This is partly expected, as the genetic approach will search on a wider array of possible solutions, some better and some worse. The strength of the method is that in some cases the error will be spectacularly better than the simulated annealing approach as shown in figure 4.28.

### 4.6.6  Multiple Loop Optimization

In practice, for circuit simulation, the resulting optimized model for a magnetic material must be accurate over a wide variety of operating conditions. To ensure this is the case, the optimization goal function was extended to allow the optimization of a set of BH loops rather than a single major loop. Each loop in the set has its own weighting, so if it is essential that the minor loop has a high level of accuracy, but the major loop is not significant, then the weighting can be increased for the minor loop accordingly. An example of this is shown in figures 4.29 to 4.31. The minor loop weighting was set to 5 to improve the relative optimization for the smaller loops. The resulting family of curves shows a good match for the minor loop, a reasonable match for the major loop, but a poor match for the medium sized loops.
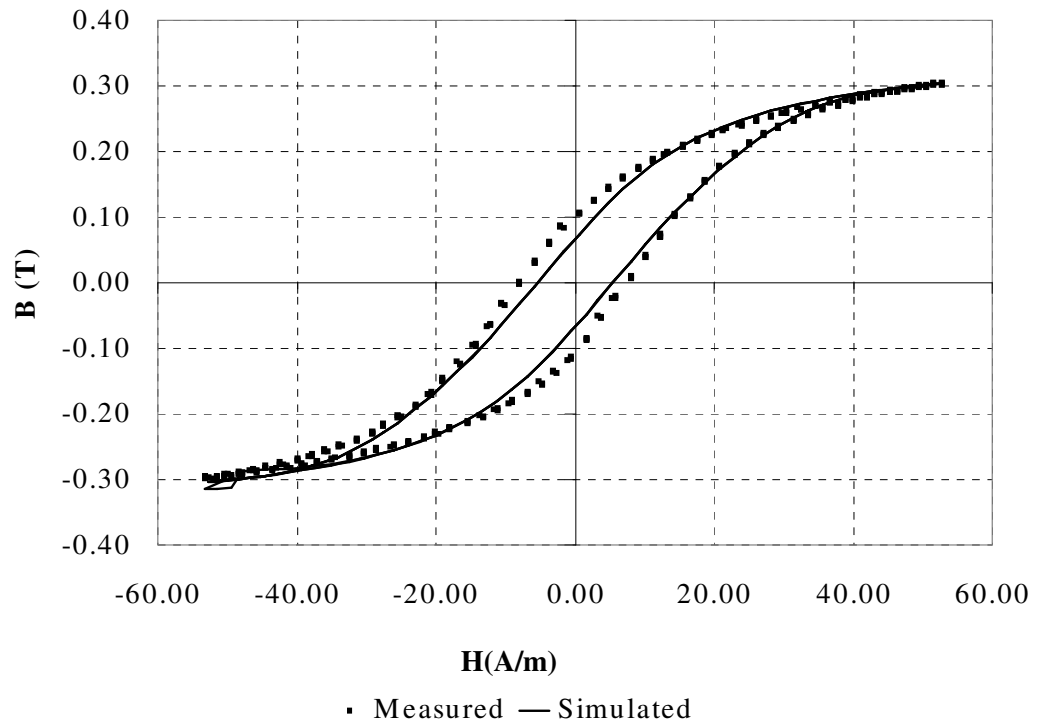
**Figure 4.29: Multiple Loop Optimization Results for Siemens N30 (Major Loop)**
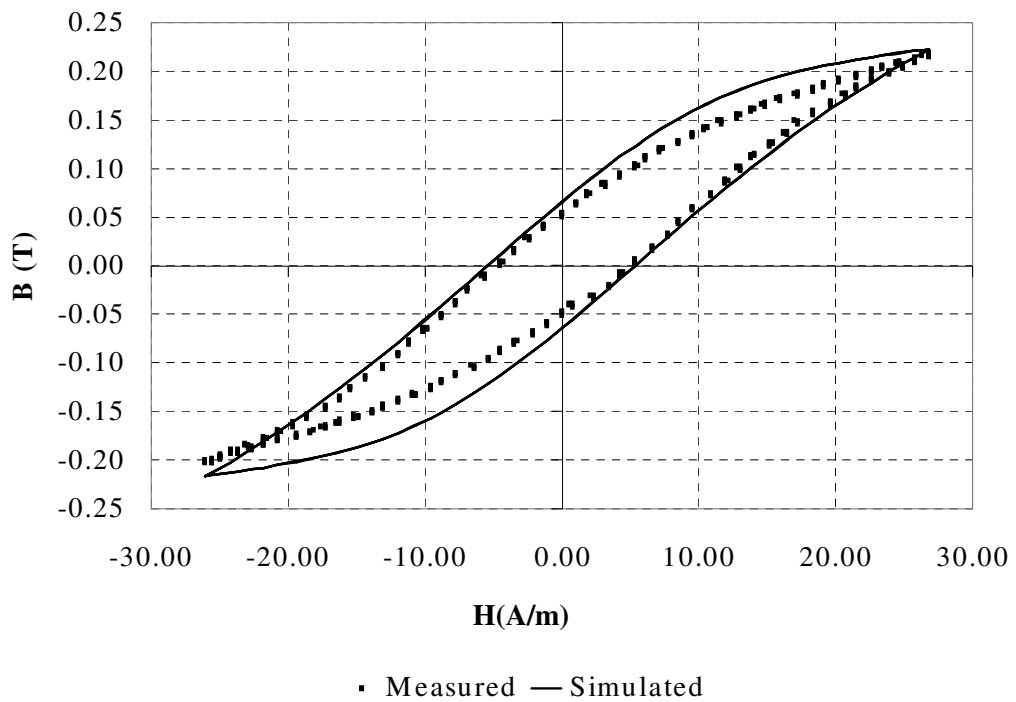


**Figure 4.30: Multiple Loop Optimization Results for Siemens N30 (Medium Loop)**

84
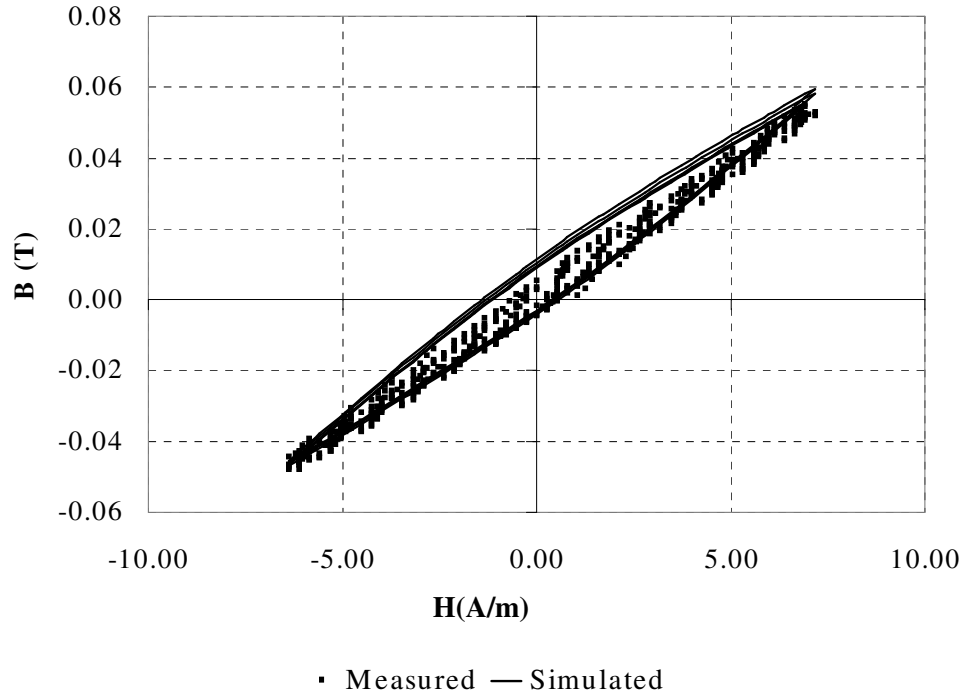
Figure 4.31: Multiple Loop Optimization Results for Siemens N30 (Minor Loop)

## *4.7 Dynamic Minor Loop Modeling*

### 4.7.1 Introduction

While the multiple loop optimization techniques described thus far are effective in the characterization of different fixed applied magnetic field strengths, a different approach is required for more general modeling of arbitrary loop shapes. The problem of modifying the original Jiles-Atherton model [20],[21] to address the minor loop issue has been tackled in a number of different ways. Carpenter [51] investigates the use of a new parameter *(Λ)* which effectively scales the slope and size of the minor loop depending on the last change of direction. Jiles [52] has also investigated the problem using a similar approach based on the two previous turning points (Jiles calls his modification parameter, *vf,* the *volume factor*). An implementation of this model is described in this section of the thesis. The difficulty with the implementation in circuit simulators of both of these methods is the necessity for knowledge of the turning points for accurate modeling of minor loops. There are three approaches to modeling this behaviour for use in circuit simulation (as opposed to direct coding, which is not particularly relevant in this thesis). These are to implement a C/Fortran model and recompile the simulator, develop a complex macro-model in SPICE using comparators, and sample-and-hold circuits or to use a mixed-mode Hardware Description Language. In general, the first option is not practical for anyone other than a seasoned simulator writer and is therefore not suitable for general-purpose application. Both the second and

85

third options are potentially useful depending on the availability of software, and are therefore discussed in this section.

### 4.7.2   Outline of Minor Loop Modeling using Turning Points

The key to both of the methods described by Carpenter [51] and Jiles [52] is to monitor the changes in direction of applied magnetic field strength ($H$). Carpenter's approach is to scale the irreversible magnetization using the last turning point of $H$. The strength of this approach is that only the last turning point is required to model the behaviour. Jiles [52] uses a slightly different method, which modifies the irreversible part of the magnetization using the last two turning points. Jiles refers to the factor that varies the irreversible magnetization as the *volume factor* and Carpenter refers to the factor as $\Lambda$ (in the remainder of this section I will use this notation). In both the Carpenter and Jiles methods, the models do not require any extra parameters, and are self-consistent.

### 4.7.3   Testing the modified Jiles-Atherton model behaviour

In order to test the basic behaviour of the volume factor modification for the Jiles-Atherton model, the original model was modified to include the volume factor as a parameter to the model. When a fixed amplitude $H$ was applied, then the effect of the parameter could be ascertained on the minor loop modeling performance. Firstly a Jiles-Atherton model was created based on the major loop characterization results, and then a magnetic field strength of ±30 A/m applied (about 20% of the major loop values) to create a minor loop. The value of $\Lambda$ was varied from 0.2 through to 1.0 (1.0 is the same as the original unmodified model). Figure 4.32 shows the results of the measured BH Loop, the unmodified Jiles-Atherton model and the modified model with $\Lambda$=0.4.
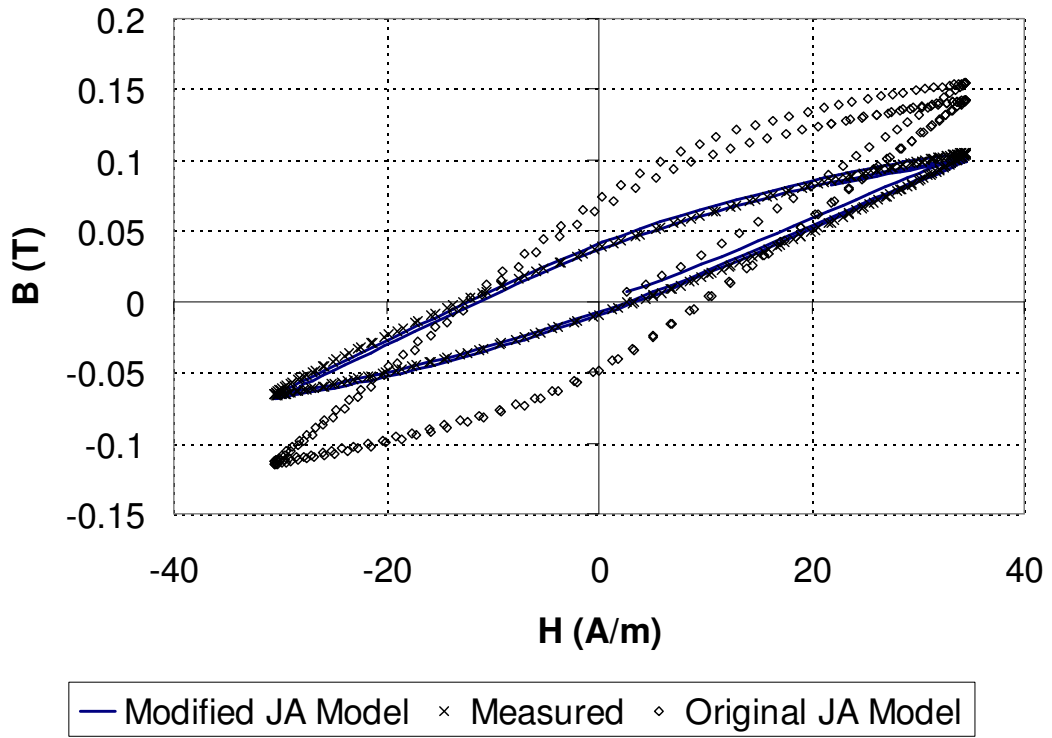
**Figure 4.32: Measured, original and Λ modified Jiles-Atherton BH Loops**

It is clear from figure 4.32 that making this modification can significantly improve the performance of the model for minor loops, without the need for different sets of parameters. The model is now extended to include the dynamic behaviour of modifying $\Lambda$ according to the recent $H$ turning points.

### 4.7.4   Implementation of the volume fraction modification using MAST

If  a device's behaviour includes discrete or state information, then the choice of modeling approach becomes straightforward. To implement this type of behaviour using a SPICE simulator, even with logic simulation capability is difficult, requiring comparators, sample-and-holds and leads to large, cumbersome models which may exhibit convergence problems. Conversely, using a mixed signal modeling language such as MAST or VHDL-AMS allows the direct implementation of event based behaviour, without large circuits or difficulties with convergence.

In this section, the modifications to the Jiles-Atherton model including the volume factor are outlined. The first step is to monitor the direction of $H$, by taking the derivative of $H$, and checking for when it crosses the x-axis. The model code to carry out this function is given in figure 4.33.

```
when(threshold(dhdt,0,last,next)) {
    if (last<next) {
        schedule_event(time,dir,1)
    }
    else {
        schedule_event(time,dir,-1)
    }
}

when(event_on(dir)) {
    if(dir<0) {
        hpos=h
    }
    else {
        hneg=h
    }
    schedule_event(time,hdiff,hpos-hneg)
}
```

**Figure 4.33: Obtaining the Turning Points of H in the Jiles-Atherton model**

The first when statement checks for when the derivative of *H* (*dhdt*) crosses the x-axis (*dhdt*=0), and the state variables last and next define the direction of the crossing. Using the direction (*dir*), the second when statement monitors this variable and sets the positive and negative turning points (*hpos* and *hneg*) to the current value of *H* depending on the direction of *H*.

At any time during the simulation, the volume factor can be calculated from the difference between *hpos* and *hneg*, and the major loop turning points. In this model, the assumption is made that the initial turning points are defined as the major loop turning points.

The dynamic behaviour of the model was tested by simulating 5 major loop cycles with $H_{max}$ =150A/m, then reducing the $H_{max}$ to 30 A/m (as compared previously with the measured results) and then returning to the full major loop for another 5 cycles.

Figure 4.34 shows the BH loops during the 3 phases, and it can clearly be seen how the model provides the same minor loop shape as the static test in the previous section. One disadvantage that only becomes apparent when using dynamic applied field strength, is that as the model changes from a minor to a major loop, the modified minor loops do not sit correctly inside the major loop. This is non-physical behaviour that does not happen in real devices. It is explained by the problem of obtaining the correct model parameters for major or minor loops, as has already been discussed. All that this modification does in essence is to modify the slope and area of the minor loop. This provides an apparent improvement in the loop matching, but the end points of the loop will be positioned, incorrectly, on the outside of the major loop.
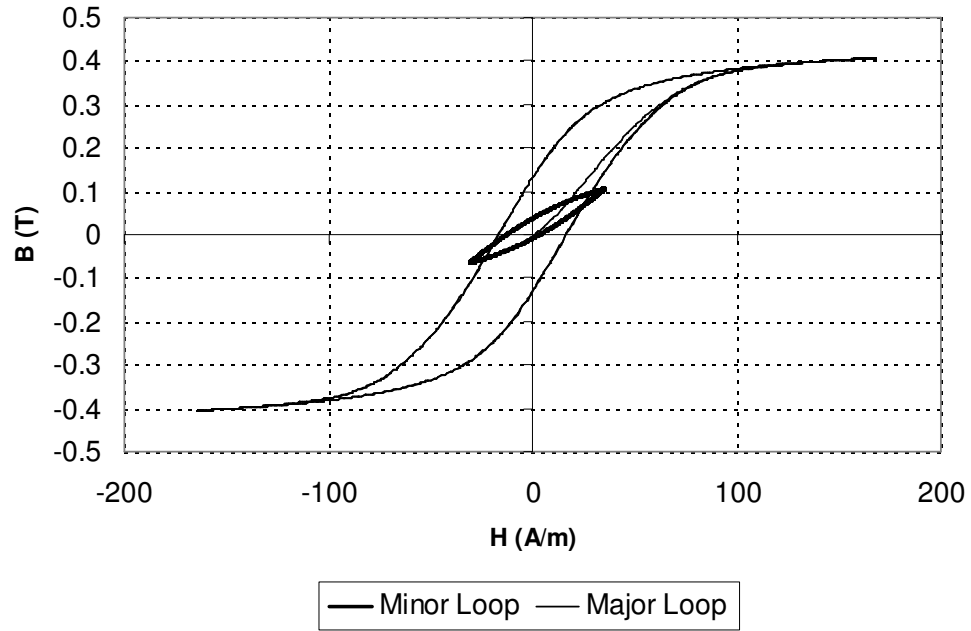
**Figure 4.34: Dynamic BH Loop Major and Minor Loops**

### 4.7.5 Summary of Dynamic Minor Loop Modeling

The results of the minor loop modifications to the Jiles-Atherton model demonstrate how Hardware Description Languages such as MAST or VHDL-AMS can take advantage of mixed signal methods to accurately represent dynamic BH loop variations that were previously not possible using standard analogue differential equation models. Even though a SPICE model was implemented using comparators, the increased level of complexity made the model much more unstable, slower and more difficult to use. The strength of a true mixed signal approach results in a robust, simple and extendable model. Despite the positive aspects highlighted in the modeling approach, there are some problems with the behaviour of the model, in particular reconciling the minor loop end points and the major loop.

### 4.8   Conclusions

Good progress has been made in the construction and application of a general purpose material test bench. A parallel testing configuration was made in simulation to enable direct comparisons to be made. Modifications to the Jiles-Atherton hysteresis model were proposed and have shown improved modeling of the loop tip closure behaviour. Methods of characterization of the BH Loop behaviour using metrics have been developed, and these have been used as an alternative to standard least squares curve fitting. An optimization procedure has been implemented and tested, with simulated annealing, univariate searching and genetic algorithms applied. Statistical analysis of the genetic algorithm and simulated annealing methods have highlighted the strengths and weaknesses of the approaches. It is clear that as the model becomes more complex, with a greater number of parameters, the genetic algorithm becomes more useful. If the model parameters are

well constrained, then the simulated annealing method is fast and efficient. An extension to optimization goal function of multiple loops has been tested, and although an individual loop may not fit as well, the overall performance of the model is better for the general case. Modeling of the minor loops using an approach based on the loop turning points demonstrates an effective method of representing the dynamic multiple loop behaviour of magnetic materials under realistic arbitrary conditions, although with limitations previously described.

# 5    Modeling Windings and Parasitics

## 5.1    *Introduction*

Many previous researchers have extensively studied the subjects of modeling windings and calculating parasitic effects. In this chapter of the thesis, a brief literature review and overview of the subject area are provided. After outlining the basic description of a winding from a modeling perspective, the main parasitic effects in windings are introduced, with the theoretical, empirical and numerical methods used to extract the parasitic values described.

## 5.2    *Introduction to Winding Models*

Using the fundamental laws of Faraday, Ampere, [1] and the duality transformations defined by Cherry [15] and Laithwaite [16], it is straightforward to define a model structure for the winding in a magnetic component. The model consists of two parts:

- Interface and Connections
- Equations and Energy Transfer

If the interface and connections are considered first, the winding model consists of two electrical connections, which have a voltage and current. The number of turns, and the resistance of the wire characterize the basic model. The model also has an interface with two connections to the magnetic circuit, which is enclosed by the windings, with an MMF and magnetic flux. The behaviour of the model is defined by the transfer of energy from the electrical to magnetic domains and vice versa, implemented using equations 5.1 and 5.2. Equation 5.1 defines the MMF resulting in the magnetic circuit from an applied electrical current to the winding, and equation 5.2 defines the EMF generated by a flux through the winding in the magnetic domain. The resulting model structure is given in figure 5.1 and using this basic structure winding models can be created for use in circuit simulation

$$MMF = NI \tag{5.1}$$

$$v = -N\frac{d\Phi}{dt} \tag{5.2}$$
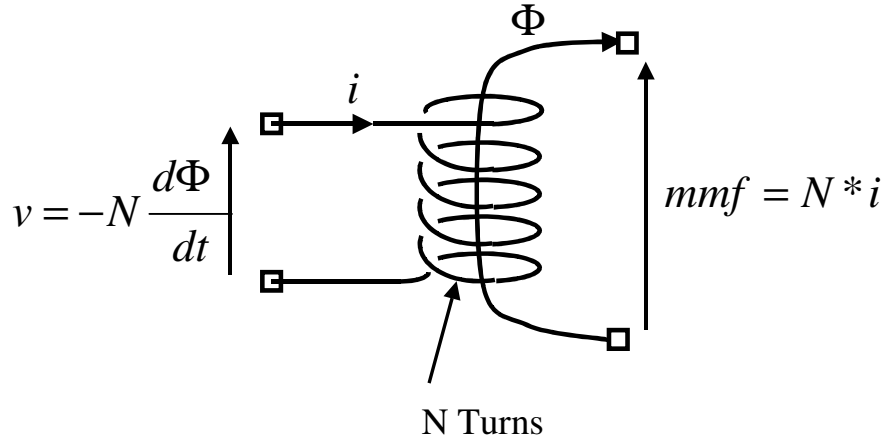
**Figure 5.1 : Ideal Winding Model**

This basic model can be implemented using a variety of approaches, and these are described in the next chapter of this thesis. The rest of this chapter is devoted to explaining the various parasitic effects and their derivation or extraction using a variety of methods.

### 5.3    Leakage Inductance

### 5.3.1    Definition

When a magnetic component is constructed from a number of windings and a core, the main design aim is usually to maximize the magnetic flux through the core, as this allows maximum energy transmission from winding to winding and the maximum inductance from the component. Unfortunately, not all the flux passes through the core and the flux that passes through the windings themselves, or the winding space is called the leakage flux. This flux gives rise to an inductance which is called the leakage inductance. Figure 5.2 shows a simple 2 winding transformer with the ideal and leakage flux paths defined.
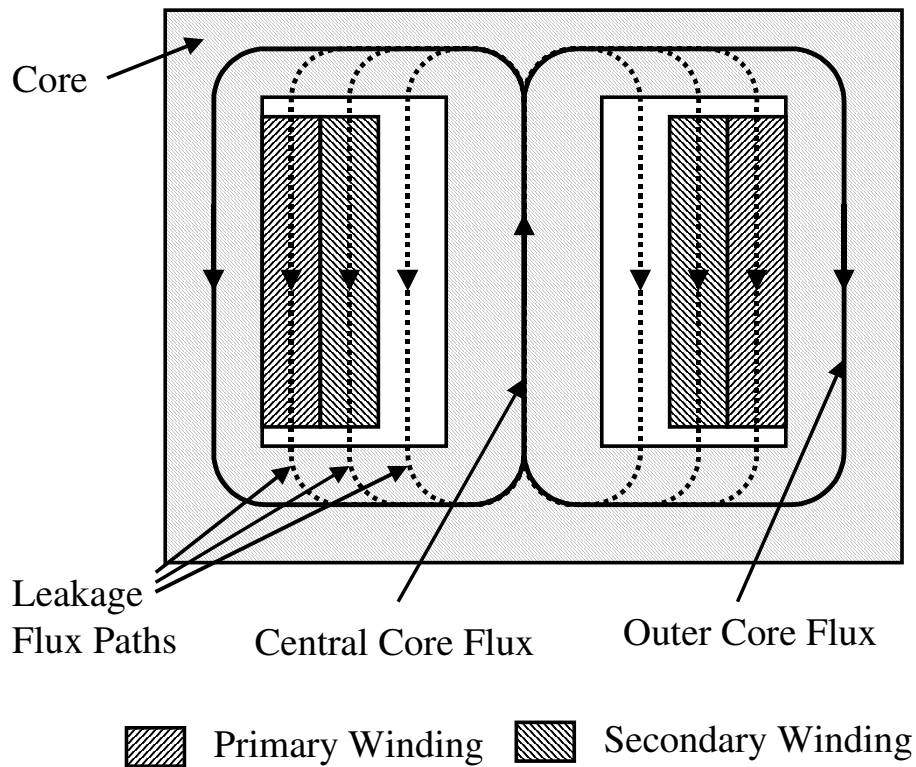
**Figure 5.2: Flux paths showing Leakage Flux**

The leakage inductance can be a vitally important parameter in switching power systems as it can give rise to resonance and ringing effects - causing losses. Equally leakage inductance can cause problems with line transformers as this parameter is crucial in defining the bandwidth attainable for a transformer.

### 5.3.2    Theoretical Methods

Using approximations such as that shown in 5.2, analytical expressions for the leakage inductance can be derived. Dowell [35], Snelling [27], Dauhajre & Middlebrook [31] and Dauhajre [112] use basically the same approach to derive expressions for the low frequency leakage inductance. By estimating the field strength over the winding area, integrating over the volume in question to obtain the magnetic energy stored, the leakage inductance can be calculated directly from the energy. Although there are other methods described in the literature such as Niemela *et al* [149], Hurley *et al* [151] and Evans *et al* [179]; they are generally derived using one of these basic techniques.

### 5.3.3    Measurement Methods

The standard method for measuring leakage inductance of magnetic components is based on the fact that if a winding is shorted, the field applied by another winding will then be automatically

cancelled out by the opposite field generated by the shorted winding (this is the assumption, but in practice the mutual flux is not cancelled out completely). The IEEE standard practice for the measurement of leakage inductance using this method is given in [116].

In practice the simplest method is to short the secondary winding(s), and measure the inductance across the primary winding using either an inductance bridge, or an impedance analyzer. It is important to ensure that measurements are taken across the frequency range of interest and at a low signal level to reduce the effect of core saturation reducing the effective inductance. These methods are applied practically in [174], [154]

### 5.3.4 Numerical Methods

The use of Finite Element Analysis to calculate the leakage inductance in transformers is in some ways even more accurate than measuring using the shorted winding approach described previously. In a Finite Element Analysis, it is possible to define the applied fields so that the mutual flux is *exactly* zero thus ensuring maximum accuracy of the calculated leakage inductance. The accuracy of the calculated value is primarily affected by the numerical accuracy in the basic Finite Element Analysis, and any approximations made in the construction of the model.

The procedure is well defined and has been applied successfully in a wide variety of applications [25],[28],[29],[30],[113] & [114] and is usually included by commercial Finite Element Analysis Software suppliers as a standard example [117]. The procedure is to apply the equal and opposite fields to the windings to make the mutual flux zero. This is obviously straightforward in the finite element analysis software as the applied winding currents can be specified exactly, and from the resulting energy stored in the finite element model, the leakage inductance can be directly calculated. This procedure will be applied and demonstrated practically later in this thesis.

### 5.3.5 Issues with unusual winding configurations

Multi-Wire, interleaved and split bobbin windings present a more difficult analytical problem. In these cases, instead of the winding consisting of an integral number of turns in a single section of the winding area, the winding topology may be much more complex. Multi-wire windings are where more than one wire is wound together to create a winding. For two wires this is bi-filar, three wires tri-filar and so on. Split bobbins are used to divide the winding area into lateral regions so that windings can be placed side by side. Interleaving can occur in a variety of ways, but the basic approach is to split the individual layers of a windings and intersperse the layers with those of another winding. This approach is sometimes called sectionalised winding. The main reason for this method is to reduce leakage inductance. Figure 5.3 shows the configurations for a 2 winding transformer with (a) a simple side by side arrangement, (b) bifilar windings, (c) split bobbin and (d) interleaving.

Calculation of the leakage inductance of windings in these configurations requires the use of finite element analysis techniques. The basic approach is described in [28],[29] & [30], with more recently specific analysis of interleaved windings by Prieto, Cobos, Garcia and Uceda [119],[121] and Prieto, Cobos, Garcia, Alou and Uceda [120].



(a) Simple  (b) Bi-Filar  (c) Split Bobbin  (d) Interleaved
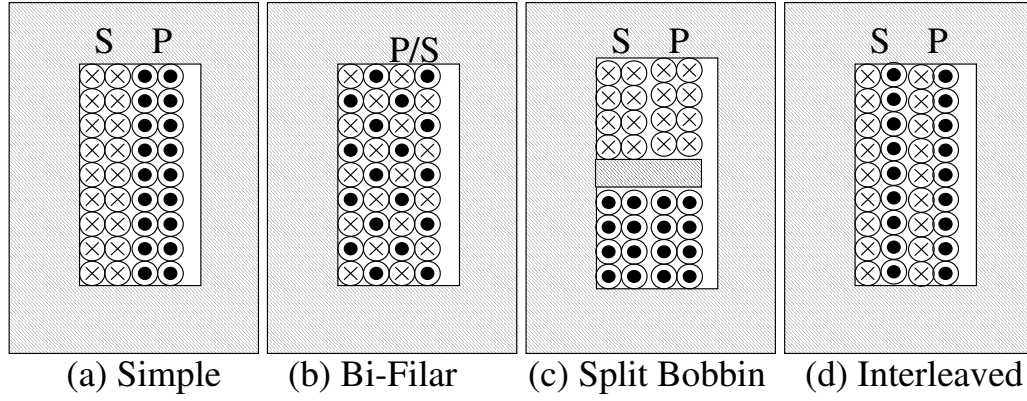
**Figure 5.3: Simple, Bi-Filar, Split Bobbin and Interleaved Windings**

### 5.3.6   Effect of Core Gaps and Geometry on Leakage Inductance

There has been quite an extensive series of studies into the effects of core gaps, winding location with respect to the gaps and core, and winding location with respect to other windings, mainly using finite element analysis techniques. An example is described by Prieto et al [150] during the optimization of a flyback converter transformer, with the specific analysis of air gap and filling factor effects [155]. Dai and Lee [173] have specifically investigated edge effects, and general geometric issues in [175]. The technique has also been used in the planar transformer optimization [172].

### *5.4   Capacitance*

### 5.4.1   Background

The modeling of transformers operating at high frequencies requires the accurate calculation and representation of the winding capacitances. The capacitances to be obtained consist of the following types.

- Winding to Core
- Winding to Winding
- Layer to Layer
- Turn to Turn

Generally the capacitances are not considered frequency or temperature dependent (i.e. the dielectric material is largely of a constant relative permittivity) within the range of interest of

SMPS and Communications components. This assumption cannot be made for higher frequency RF components however. It is also assumed for the purposes of calculation that the voltage across a winding is distributed evenly, proportional to the number of turns.

### 5.4.2   Theoretical Methods

Analytical methods for the calculation of winding capacitances have been in existence for many years with the development of wireless technology [123],[124],[127] and have generally been based on the premise that a winding can be treated as a plate of a parallel plate in a capacitor, where the other plate may be another winding, layer or even the core. Snelling [27]  and McLyman [67] provide basic summaries of the key equations for self capacitance of windings.

Empirical formulae have been used to modify the equation parameters such as the dielectric thickness depending on the winding arrangement to provide a more accurate value for the capacitance also described by Snelling [27] and originally by Zuhrt [126]. The accuracy claims for these equations to within 2% are only valid within defined parameter ranges however, and in some cases large errors may occur.

Collins [128] provides an energy based approach for the calculation of interwinding capacitances. In the case of a two winding transformer, where the windings are layered on top of each other, the winding capacitance is estimated by treating the layers as coaxial cylinders.

Other methods for analytical capacitance calculation include detailed turn to turn calculations as given by Leon and Semleyn [136], Popovic [139] and Massarini and Kazimierczuk [68]. In these cases, the turn to turn capacitance is calculated and a network model produced for the winding based on distributed inductors and capacitors. These approaches tend to apply where the winding is uniformly wound in a single layer.

### 5.4.3   Measurement Methods

The measurement of the winding capacitances of a transformer is not an easy task to perform, but can be carried out using the procedure defined in [116] for a two winding transformer. More Complex winding structures can also be measured using variations of this approach. The technique uses the resonant frequency of the transformer in various configurations to extrapolate the winding capacitances based on the equivalent circuit shown in figure 5.4, and using previously obtained values for the inductive elements.
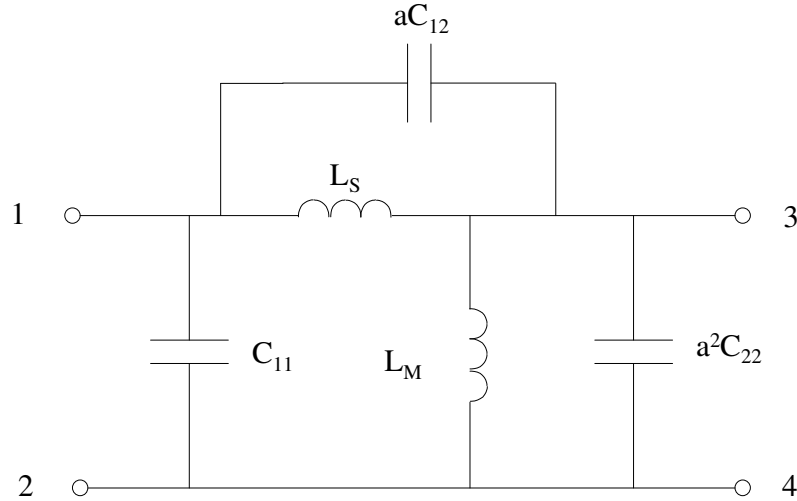
**Figure 5.4: Equivalent circuit assumed for measurement of winding capacitance**

### 5.4.4   Numerical Methods

The calculation of winding capacitances using finite element analysis is greatly simplified with the assumption that an ideal electrostatic analysis is an accurate method for the calculation. This assumes that the capacitances are essentially not dependent on frequency or voltage. In practise, this is not necessarily true, with dielectric losses contributing to some frequency dependence [142]. If the assumption are made however, then methods for the calculation of capacitance are well known [5],[12]. The basic approach is to apply voltages to the windings in question in the finite element analysis, calculate the stored electrostatic energy and calculate the capacitance directly. For example, to calculate the capacitance between two windings, 0.5V is applied to the first winding and –0.5V to the second. The capacitance can then easily be obtained by solving for the stored energy using a finite element analysis, and calculating ½ of the resulting energy.

This method has been automated using commercial finite element software by Prieto *et al* [28],[29],[30] and Wilson [60]. Alternative capacitive model structures have also been proposed by Prieto et al [132] to improve the accuracy of the capacitive model.

Extensive testing of the analytical and finite element techniques of capacitance extraction has been carried out using practical examples [119], [120], [121], [131], [134], and [136]. In general the finite element analysis provides good accuracy, and is not prohibitive in simulation time due to the static nature of the analysis.

### *5.5   Winding Losses*

### 5.5.1   Background

Losses in magnetic component's windings occur for a variety of reasons. The wires have a finite resistivity which causes a D.C. resistive loss. This can be quite easily calculated from the

resistivity of the wire and its dimensions. As the frequency of an applied signal increases eddy currents are generated inside the winding leading to further losses. These eddy currents occur in two forms, skin effect and proximity effect. The skin effect is a function of the frequency of the applied signal and is calculated easily. The effect occurs as the signal tends to flow nearer the surface of the conductor as the frequency increases. The second is the proximity effect of the conductor strands themselves. This is a result of eddy currents induced from the overall magnetic field, and is dependent on the wire layout, and whether stranding, twisting or bunching has taken place. This can be more difficult to calculate analytically as there may be a significant variation in the layout of the individual conductors.

### 5.5.2  Theoretical Methods

The low frequency resistance of a conductor can easily be calculated using the length of the conductor, the cross-sectional area, and the resistivity (for Copper this is $1.709 * 10^{-8}$ $\Omega$m). It is important to note that the resistivity is temperature dependent. For Copper the thermal coefficient is $Tc$=0.00393 $\Omega$m/°C. This is an important consideration for power devices where a 40°C temperature rise would not be uncommon. This approach can be used for a winding with $N$ turns and a Mean Turn Length $l_w$ to estimate the D.C. resistance as given by 5.3, where $d$ is the diameter of the conductor and $\rho_c$ is the conductivity.

$$R_{dc} = \frac{4\rho_c N l_w}{\pi d^2} = N l_w R_c \quad \Omega \qquad (5.3)$$

The losses due to eddy currents in windings can be divided into skin and proximity effects. As the frequency of an applied signal increases, the current flows in a progressively thinner layer at the surface of the conductor. The thickness of this layer is called the penetration depth, denoted by $\Delta$, and can be calculated using equation 5.4. Figure 5.5 shows the change in the penetration depth in a conducting copper wire at different frequencies. In equation 5.4, $\rho_c$ is the resistivity of the conductor, $\mu_c$ is the relative permeability of the conductor and $f$ is the frequency of the signal.

$$\Delta = \sqrt{\frac{\rho_c}{\pi \mu_0 \mu_c f}} \qquad (5.4)$$

(a) 10kHz                    (b) 100kHz
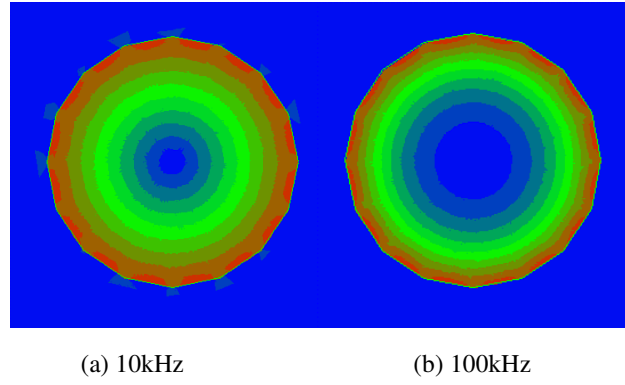
**Figure 5.5: Variation in conductor skin depth[5] with frequency.**

The skin depth is related to the conductor diameter d to obtain a relative measure of the skin depth that results in the 'skin effect factor' *F* as shown by Snelling [27]. If *d/Δ* is <2 then the skin effect is negligible and can be ignored. As *Δ* decreases, and *d/Δ* increases above 5 then the skin effect factor, *F*, can be approximated by equation 5.5.

$$1 + F \approx \frac{1}{4}\left(\frac{d}{\Delta} + 1\right) \tag{5.5}$$

### 5.5.3  Measurement Methods

In order to measure the winding losses, several steps need to be taken. The losses can be generally lumped into two parts, *Rdc* which is the D.C. winding resistance and *Rac* which is the frequency dependent loss, comprising mainly the eddy curent losses in the winding.

The *Rdc* measurement can be carried out easily using a measurement bridge or an impedance analyser at very low frequency. The *Rac* measurement can best be carried out using an impedance analyser, sweeping the frequency of the applied signal over the required range. The impedance and phase can be used to calculate the a.c. resistance, or the analyser may output the real and imaginary parts directly. All the measurements in this thesis were carried out either using a Wayne Kerr Impedance Bridge, or an HP4192A Impedance Analyser. Care must be taken to ensure that low applied signal levels are used so that the core of the device under test is not saturated.

### 5.5.4  Numerical Methods

There are numerous examples in the literature of methods using Finite Element Analysis (or a similar numerical approach) to extract the high frequency behaviour of winding resistance including [60],[34],[113],[114],[127],[153],[175]. Robert, Mathys and Schauwers [122] have

---

[5] The light colours indicate areas of high current density. The higher frequency shows a thinner layer of high current density than the lower frequency.

completed some comparisons of Dowell's methods with measured data and finite element analysis and have noted that there are discrepancies with underestimation of the losses at low frequencies and overestimation at higher frequencies. They propose modifications to the method to deal with these problems.

## 5.6   Proximity Effect

With more than one winding in the component, the magnetic field in other windings causes eddy currents in the winding of interest and this is called the proximity effect. This is illustrated with the finite element analysis of two windings with currents flowing in the opposite directions shown in figure 5.6. This shows the distribution of the magnetic field, and the current inside the conductors.
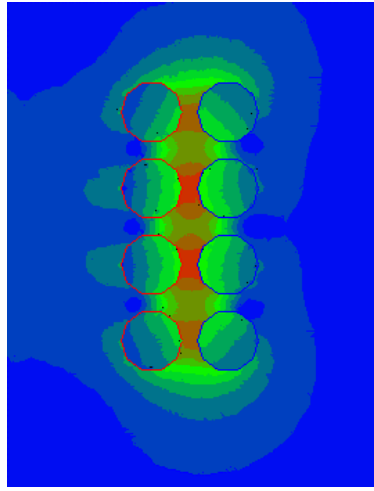


**Figure 5.6: The effect of proximity on the magnetic field distribution in windings[6]**

Snelling [27] shows how this can be approximated for idealised winding structures leading to the expression for the power loss due to the proximity effect for round conductors given by 5.6.

$$P_{pe} = \frac{\pi \omega^2 B_{\max}^2 \, l d^4}{128 \rho_c} \tag{5.6}$$

Further dependence on frequency in the form of a skin effect factor for this power loss is introduced similarly to the basic skin effect factor $F$, but this time alters the proximity effect. This factor, $G_r$, tends to unity for low frequencies, but as the ratio of $d$ to $\Delta$ increases beyond 4, the factor takes the form shown in 5.7.

---

[6] The light colours indicate areas of high current density.

$$G_r \rightarrow \frac{32}{(d/\Delta)^4}\left(\frac{d}{\Delta}-1\right)$$

<div align="right">(5.7)</div>

## 5.7  Summary

The area of modeling windings has been well covered in the literature from the theoretical, empirical and numerical analysis points of view, and in general offers limited opportunities for further research within the scope of this thesis. Some specific aspects of the parameter derivations have the possibility of improvement, especially in the area of model implementation, and at high frequencies (up to 10MHz). These issues are covered specifically later in this thesis.

# 6   Modeling Magnetic Components

## *6.1   Introduction*

So far in this thesis, the building blocks for constructing magnetic component models have been developed independently, including winding and material models. In this chapter the individual pieces are put together to provide component models for use in circuit simulation. Starting with basic macro-models of idealised components, the models are extended to include parasitic and geometric effects. The range of target simulators is extended to encompass Spice, Saber (using the MAST modeling language) and VeriasHDL (using VHDL-AMS - IEEE 1076.1).

## *6.2   Electrical vs Mixed Domain Modeling*

### 6.2.1   Introduction to Electrical Modeling

Magnetic modeling using Spice-based simulators has generally used electrical models of inductors and transformers. For example, a two-winding transformer could have each winding modeled as a separate electrical inductance and a mutual inductance to model the coupling between them. This is shown in figure 6.1.
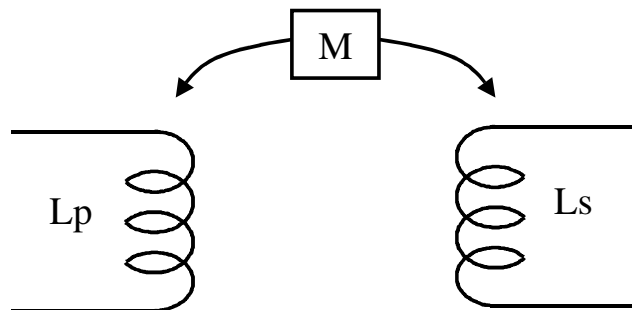


**Figure 6.1 : Electrical Magnetic Component Model - 2 Winding Transformer**

Non-linear modeling of the core material can be implemented using a non-linear inductor or special core models if they are available in the simulator. The difficulties of this approach include problems in specifying initial conditions for the flux and in modeling the hysteresis loop behaviour accurately. Although commercial core models allow limited modeling of the BH curve, the scope for development of more realistic models reflecting the physical geometry of the component is poor.

### 6.2.2 Mixed Technology Modeling

One of the goals of applying mixed technology modeling for magnetic components is to enable the development of more accurate physically based models. In the case of the two-winding transformer used previously, this could also be modeled using the mixed technology approach shown in figure 6.2.
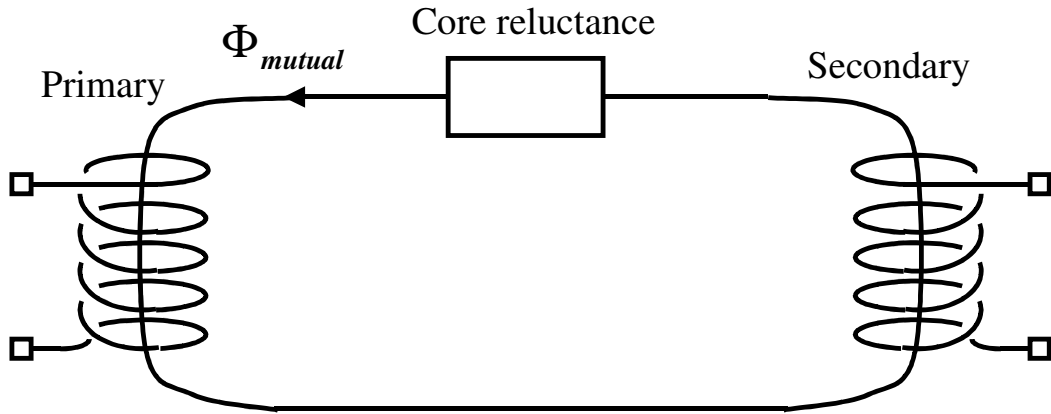


**Figure 6.2: Mixed Technology Model - 2 Winding Transformer**

With such a simple model, it is not clear where the advantages of this approach are, but when the model becomes more complex, then the relative merits of both approaches become clearer.

### 6.2.3 Units and Energy Conservation

While it may seem trivial to consider the unit of a variable to be important in simulation, after all it is all just numbers being solved, having direct implementation of the types in the model can greatly simplify the modeling process. All variables are automatically defined with the correct units removing any confusion (especially if Imperial and SI units are mixed). Using a consistent set of units also allows correct assumptions about energy transfer to be made. If the units are inherent in a model, then there is reduced risk of mistakes being made when units are translated from one domain to another.

### 6.2.4 Direct Physical Modeling

Using a true magnetic model allows a more direct relationship between the fundamental physical equations of the device and the simulation model. For example, if an inductor is to be modeled one of the two aproaches (electrical or mixed domain) could be taken. If the electrical route is taken, then the inductor is modeled directly as an electrical inductor. The information available to the engineer from the model is purely the electrical information such as the voltage, current and power. On the other hand, if a mixed domain model is used, with a winding and core model in the magnetic domain, the engineer has access to the electrical data as before, but also the Flux, Flux Density, MMF and Magnetic Field Strength. This aspect can become very important when

complex physical structures need to be analyzed, or the core model is non-linear. Another advantage of this type of approach is the ability to use a distributed model to encapsulate the behaviour of the physical structure more accurately.

### 6.2.5  Initial Conditions

Accurate modeling of initial conditions can be crucial in the simulation of magnetic components. Although in an inductor model, the current can be initialised, it is not generally possible to initialise the flux. Using a mixed technology approach, both the flux and MMF can be set at the start of an analysis and the BH trajectory can be highly accurate as a result.

### 6.2.6  Control of model complexity

Using the mixed technology approach, the model designer has direct control over how much or little accuracy is used in each section of the model. This can be much more difficult to accomplish with an electrical model. An example would be using a network of reluctances to model all the separate sections of a core model as individual reluctances. Although this could be achieved in the electrical domain using a transformation of the form described by Cherry [15] or Laithwaite [16], the ability to directly view the flux behaviour in each section of the core would be lost.

### 6.2.7  Mixing Electrical and Mixed-Technology Approaches

While the virtues of the mixed-technology method seem to be overwhelming from the magnetics point of view, for the circuit designer it is sometimes more convenient to think in terms of conventional circuit elements. This can make the choice academic, as the two methods can easily be mixed to use appropriate modeling techniques for a particular feature in the same model. A good example of this is the contrast between dealing with air gaps and leakage flux. The airgap is ideally suited to a mixed domain approach. If the air gap is to be included in the electrical model then some calculation is required but in the mixed domain model the air gap can be implemented directly using a linear core model with a relative permeability of 1.0. In contrast, while the leakage flux can be easily implemented in the magnetic domain, it is more useful from a circuit designer's perspective to see the leakage modeled as an inductance. It is therefore important to keep in mind the way the model feature is to be used in the simulation prior to selecting an implementation.

### *6.3  Incorporating parasitic effects in magnetic component models*

### 6.3.1  Introduction

In the previous chapter, methods of calculating the parasitic effects (leakage, losses, capacitance) were reviewed and discussed. In this section, the emphasis is more on how these can be implemented in simulation models.

### 6.3.2 Low Frequency Winding Resistance

Implementing the low frequency resistive winding loss in component models is simply a matter of inserting an electrical resistor model in series with an ideal winding, as shown in figure 6.3.
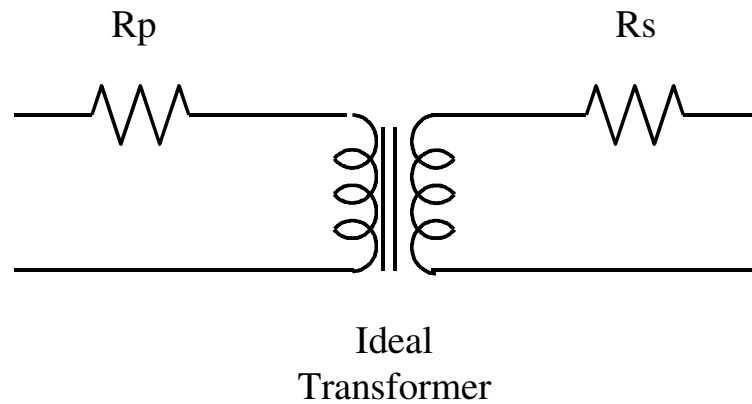


**Figure 6.3 : Implementing Low Frequency Winding Loss in a transformer**

Where Rp is the primary winding resistance and Rs is the secondary winding resistance.

### 6.3.3 Low Frequency Leakage Inductance

Implementing the leakage inductance in an electrical model is a simple matter of including the leakage as an inductor in series with the winding in question. Figure 6.4 shows how this can be accomplished for a two winding transformer (also including the winding loss).
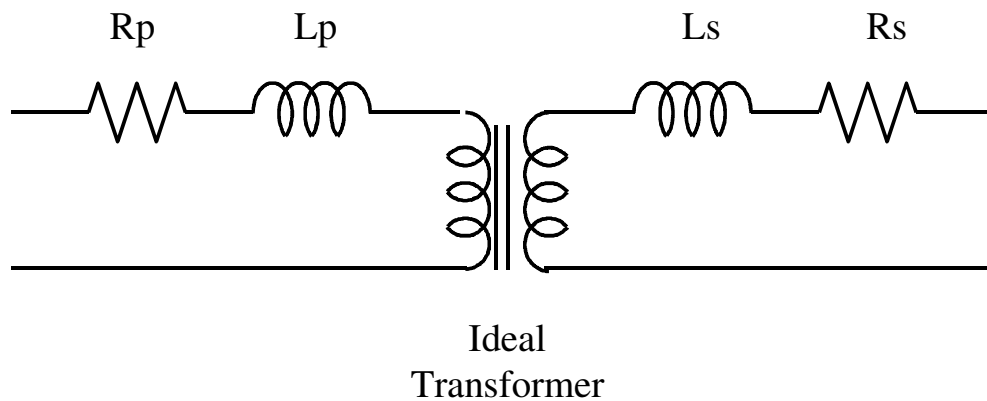


**Figure 6.4: Implementing Leakage Inductance in a transformer**

Where Lp is the primary leakage inductance and Ls is the secondary leakage inductance. Low frequency is defined as being where the eddy currents are insignificant.

### 6.3.4 Frequency Dependent Winding Loss and Leakage Inductance

As has been previously discussed, as the frequency of the signal in a winding increases, the effective winding resistance increases. Implementing this behaviour requires a complex impedance

model of the winding loss. As the frequency increases, the leakage inductance falls. These effects have been discussed in the previous chapter, and the method of implementation involves a complex impedance model encapsulating both the resistance and inductance variations. The model of the transformer then uses these impedance models instead of the simpler R and L in the low frequency case, as shown in figure 6.5.
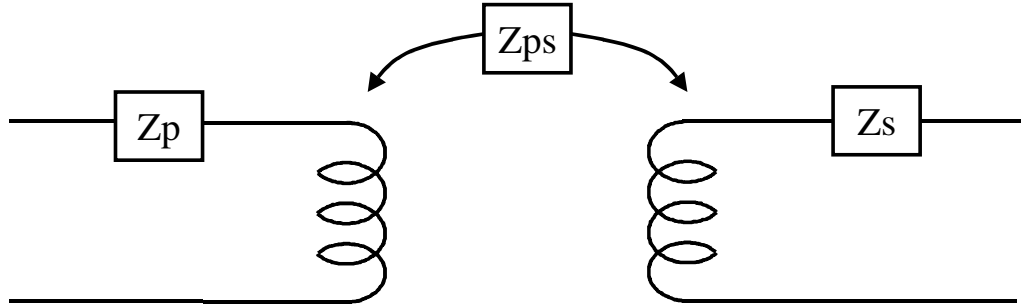


**Figure 6.5: Complex Impedance Leakage and Loss Winding Model**

Where Zp is the complex impedance representing the Primary Leakage and Loss, Zs is the secondary complex imedpance and Zps is the model of the coupling effects between the windings. The impedance model can be implemented using an RL network, as described by Lopera et al [63] or using a behavioural model as implemented by Prieto et al [119],[131],[156].

### 6.3.5   Core Loss Modeling

#### 6.3.5.1   Basic Core Loss Modeling

The approach used for modeling core loss partly depends on whether the model is linear or non-linear and whether the frequency is low or high enough to cause eddy current effects in the behaviour. The total core loss consists of two parts, the basic low frequency core hysteresis loss and the higher frequency eddy current losses.

In the low frequency case, the core behaviour can be implemented using a linear or a non-linear model. The non-linear case has been discussed extensively in chapters 3 & 4 of this thesis and has shown how the core loss is inherent in the BH loop of the model. If the core model used is linear, however, then a different approach is needed. (It is worth noting that for small signal analysis, i.e. frequency response analysis, a linear or linearised model must be used). The core loss can be implemented as a resistor in the electrical domain, averaging the core loss over a complete cycle, or as an inductor in the magnetic domain. This is shown in figure 6.6(a) and (b) respectively.
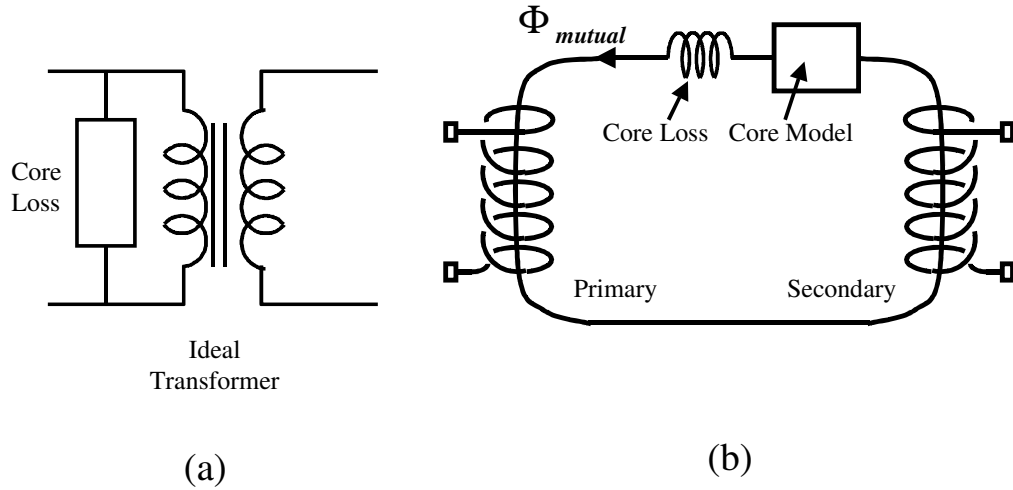
**Figure 6.6: Basic Core Loss Implemented in the electrical and magnetic domains**

The equivalence of the models in the two domains is described by Cherry [15] and Laithwaite [16].

### 6.3.5.2 Modeling High Frequency Behaviour

At higher frequencies, currents flow in loops inside the core material. These loops, called eddy currents, act against the externally applied magnetic field, causing losses. Konrad [34] discusses eddy currents in some detail and Zhu, Hui and Ramsden [42],[44],[45] propose methods of implementing the effects in a simulation model. In the previous chapter of this thesis, it was shown that as the frequency of a signal through a conductor increases, the current tends to flow more and more on the outside of the conductor. A similar effect occurs inside the magnetic core material, giving increased eddy current effects with increasing frequency.

The basic modeling concept is to treat the magnetic material as a series of laminations. These laminations approximate the eddy current behaviour as the frequency increases. Each lamination is modeled as an RL element, in a network in the magnetic domain - as shown in figure 6.7.
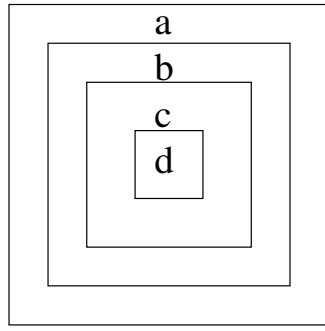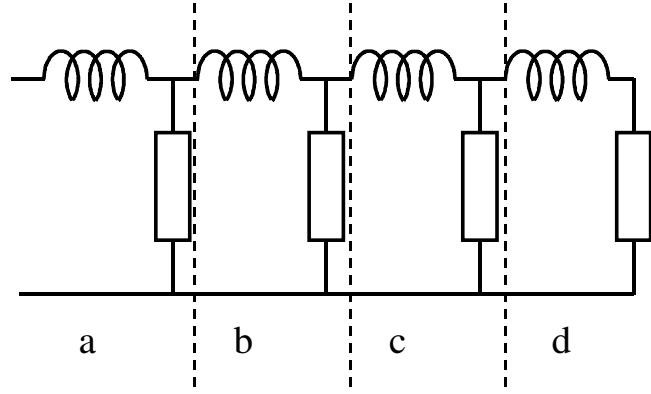
(a) Laminations　　　　　　(b) Equivalent Circuit Model

**Figure 6.7: Laminations and Equivalent Core Loss Circuit Model**

For each lamination, the eddy current loop can be considered to be a single turn winding around the cross section. In each cross section, the resistor represents the reluctance of the core material in the magnetic domain and is calculated using equation (6.1).

$$R = \frac{l}{A\mu_0\mu_r}$$
(6.1)

Where $l$ is the magnetic path length, $A$ is the cross sectional area of the lamination, and $\mu_r$ is the relative permeability of the core material. The inductance representing the core loss for the lamination is calculated using equation (6.2).

$$L = \frac{A_{cs}}{l\sigma}$$
(6.2)

Where $A_{cs}$ is the height of the lamination multiplied by the magnetic path length, $l$ is the length around the eddy current loop and $\sigma$ is the conductivity of the magnetic core material.

Using this approach, the number of laminations can be controlled for the required accuracy, and the RL components derived easily. This technique can also be used with non-linear core reluctances, simply by replacing the linear models with a suitable non-linear model with the correct physical dimensions of the lamination.

### 6.3.5.3 Behavioural modeling of high frequency losses

Another approach to implementing the eddy current behaviour described in the previous section is to modify the BH loop behaviour. As the frequency of the applied signal increases, the BH loop widens, and so to model this behaviour the magnetic field strength can be modified prior to calculating the BH function. The model structure is shown in figure 6.8.

108
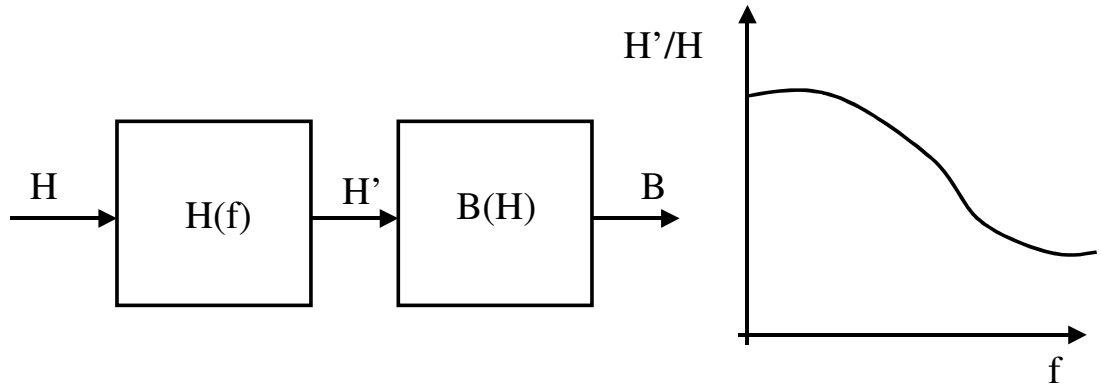
**Figure 6.8: Frequency Dependent Eddy Current Behavioural Model Structure**

The advantage of this type of approach (as implemented in the Saber simulator) is the simplicity of implementation, as opposed to the complex network of individual non-linear core models required in the network method. This gives a resulting increase in simulation speed and reliability due to the reduced number of equations and non-linearities to be solved.

## 6.4 Modeling Geometric Effects

Including geometric effects such as air gaps, fringing, structural variations and material variations can be accomplished using a variety of methods. Analytical approaches, such as those described by Snelling [27], are useful in estimating the basic effects on the component behaviour. More commonly, numerical methods such as Finite Element or Finite Difference Analysis are used to extract characterised model parameters from a geometric model (Asensi *et al* [28-30]).

These methods are essentially a priori, and as such if some aspect of the model changes, like a dimension or material, the model will require re-characterization. The other type of approach implements a model of the geometry using a psuedo-physical approach with lumped or distributed elements. An example of this method is implementing fringing or stray flux directly in a model using a linear core model (with $\mu_r=1$, representing air) in parallel with the main flux path. The model could consist of a network of elements, as well as a single model element, to obtain the necessary accuracy. This type of approach has been developed to the extent that a finite element analysis construction is made in the circuit simulator with a network of simple elements, as shown by Cherpentier *et al* [144], Abe *et al* [145], Hsu and Ngo [167]. A further extension to this technique is to integrate an FEA model into the circuit simulation. This technique is discussed specifically in chapter 8 of this thesis.

## 6.5   Implementation of Magnetic Component Models in Spice

A set of building blocks has been implemented for use in macro-modeling of magnetic components. The complete listings of the models created are provided in appendix A. The list of models and their descriptions is given in table 6.1.

| Model | Description |
|---|---|
| Winding | Winding Model |
| Winding_th | Winding model with thermal output based on winding losses |
| Core | Linear Core Model |
| Classicja, classicja2, classicja3 | Original Jiles-Atherton model of hysteresis. Minor variations included, based on original papers. |
| Xfr3, xfr4, xfr3_4a11 | 3 and 4 winding transformers including parasitic effects and material core characteristics |
| Vdslxfr3rx, vdslxfr3tx | Receive and Transmit VDSL transformer models |
| Expkja, expkja2 | Jiles-Atherton models with Gaussian K parameter variation |
| Thermalja | Jiles-Atherton with thermal output |
| Expja_th1-7 | Jiles-Atherton model with self heating and various configurations of parameter dependence. The only difference between the models is the gradual inclusion of thermally dependent parameters. The final model expja_th7 listing only is given as it includes all the parameter variations. |
| Emission, rconv, ctherm, rtherm | Thermal Elements for use in Electric-Thermal-Magnetic simulations |
| Pmlang, pmagnet, pmagnet2 | Permanent magnet models |

**Table 6.1: List of Spice building block models**

## 6.6   Implementation of magnetic models in Saber (MAST)

A useful set of basic building blocks for modeling magnetic components exist in the Saber simulator libraries. These have been extended, particularly with regard to minor loops, thermal effects and parameter variations. The full model listings are given in appendix B, and a list of the models with descriptions is given in table 6.2.

| Model | Description |
|---|---|
| Coreja | Original Jiles-Atherton implementation |
| Coreja2 | Modifications including gaussian K |
| Coreja3 | Minor Loop Modifications |
| Coreja_th | Thermal Extensions |

**Table 6.2 : Saber Model List and Descriptions**

## 6.7    Implementation of Magnetic Component Models in VHDL-AMS

A set of magnetic component models have been implemented in VHDL-AMS (IEEE 1076.1). Using the VHDL-AMS modeling language is a more sophisticated method of modeling, and will in the future be the standard Hardware Description Language across a wide variety of simulators and industries. The concept behind the language is to treat each device as consisting of two main sections, the entity and the architecture. The entity defines the connections points and parameters, while the architecture defines the behaviour. This is shown in figure 6.9. One of the strengths of this method is the ability to use a number of different architectures for a single entity, with different levels of complexity or functionality appropriate to the simulation requirements. This is shown in figure 6.10.
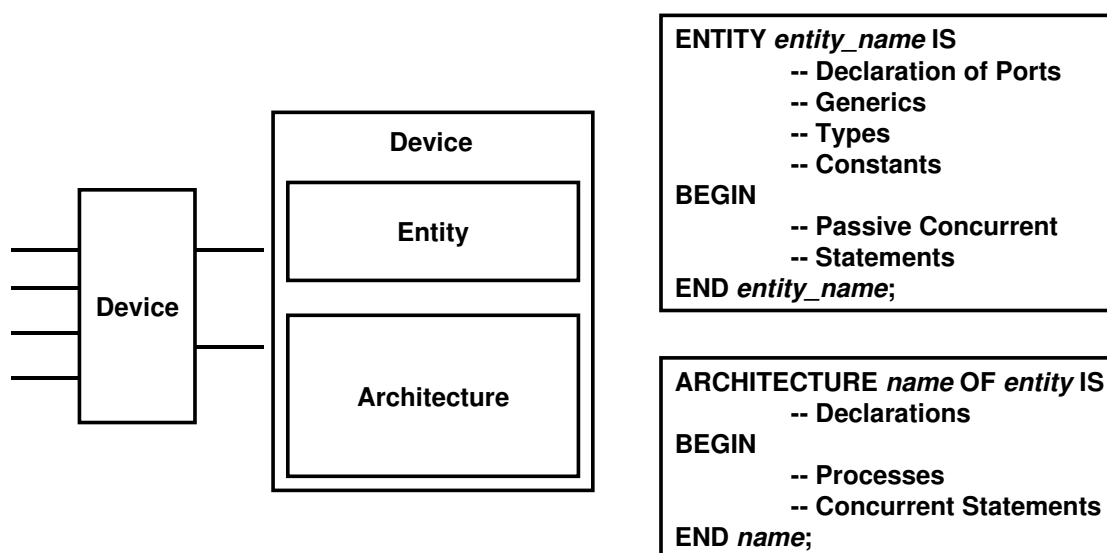


**Figure 6.9: Division of VHDL-AMS model into Entity and Architecture**
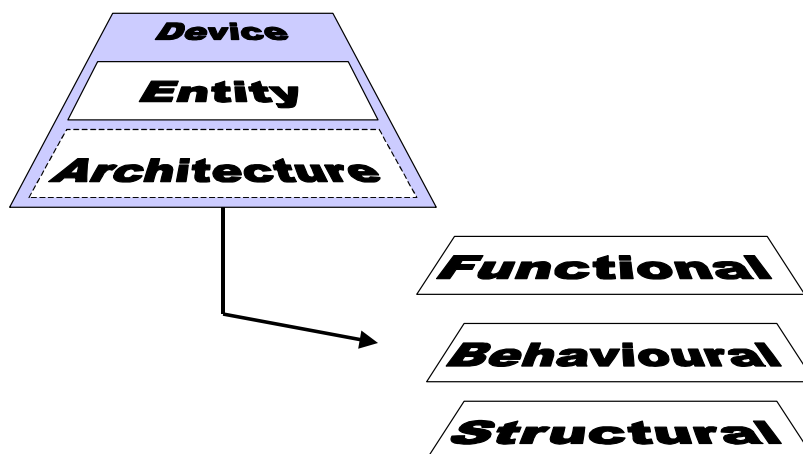


**Figure 6.10: Using different architectures in VHDL-AMS**

111

A penalty with using VHDL-AMS as ostensibly an analogue modeling language is the relative complexity of the model syntax. This comes from its roots in digital VHDL for ASIC design. The benefits of flexibility and compatibility can outweigh the syntax issue.

Another significant issue with VHDL-AMS is its practical use by non-software literate analogue engineers. To combat this a graphical modeling tool was developed in this project to simplify the modeling and debugging process. The editor configuration is shown in figure 6.11, and includes automatic code insertion from simple forms, colour highlighting of keywords, structure analysis and syntax checking.
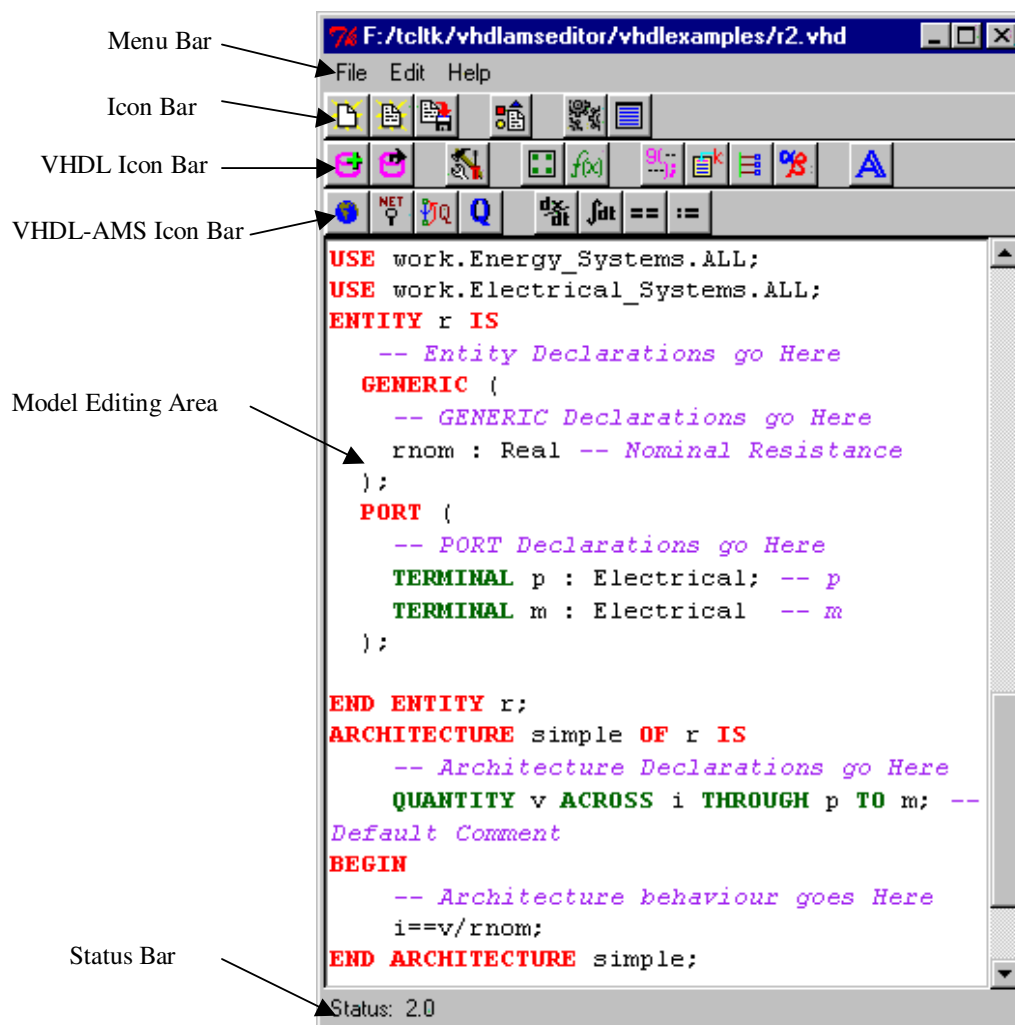


**Figure 6.11: VHDL-AMS Editor and Debugger**

The list of VHDL-AMS models and their descriptions is given in table 6.3, with the full model listings provided in appendix C.

| Model | Description |
|-------|-------------|
| wind | 4 terminal winding model entity and architecture |
| Core | Linear core model entity |

| Core_linear | Linear Core Model Architecture |
|---|---|
| Corenl | Non-linear core model entity based on Jiles-Atherton approach |
| Coreja | Non-linear core model architecture based on Jiles-Atherton approach |
| Core_langevin | Non-linear core model architecture based on Langevin Function |

**Table 6.3 : VHDL-AMS models and descriptions**

## *6.8 Magnetic Component Modeling Software*

There are currently three main dedicated magnetic component modeling packages for use with circuit simulators on the market today. These tools incorporate physical design, parameter extraction, model generation and model testing. The tools are OUM$^2$T [63], PEMag from Ansoft and SaberMMP[7] from Avant! [60]. These tools all have a similar basic methodology, with one difference being that PEMag and SaberMMP include links to the Ansoft FEA software.

UOM$^2$T is evaluated later in this thesis, and a screenshot of the SaberMMP modeling software is given in figure 6.12.

---

[7] SaberMMP was designed, developed and implemented by the author during 1996-1999 while working for Analogy, Inc., with the initial product release during 1998.
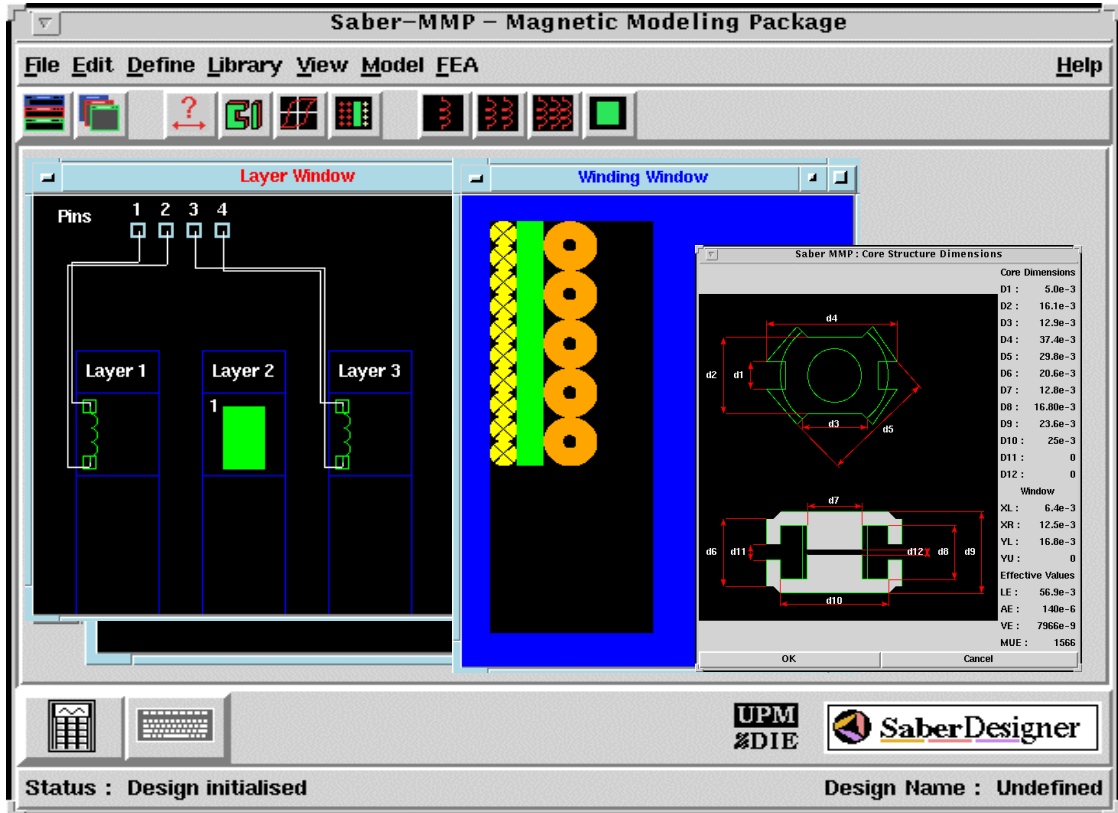
**Figure 6.12: SaberMMP Magnetic Modeling Software**

## 6.9   Conclusions

The combination of extensive analytical, empirical and numerical parameter extraction methods and the variety of modeling approaches available allow most magnetic component modeling requirements to be met.

This chapter has highlighted the main implementation methods, discussed some of the strengths and weaknesses and provided a comprehensive set of models for use at various stages of this project. Modeling software has been developed to greatly aid in the useability of the VHDL-AMS language and in the generation of models using a standard syntax form.

*Chapter 7*

# 7 Modeling a Simple Transformer

## *7.1 Introduction*

Extensive theoretical and empirical research has taken place to establish the variation of winding losses with frequency. Dowell [35] provides a theoretical framework for the calculation of losses in transformer windings, and this has been developed by a large number of authors since including Cheng and Evans [61],[62]. Roberts, Mathys and Schauwers [122] have studied the accuracy of the theory and have noted discrepancies between the theoretical and empirical values of losses obtained while Niemela et al [149] have extended the theory for general multiple winding topologies.

There has been much less effort applied to the equivalent theoretical calculation of leakage inductance, especially at higher frequencies where eddy current and proximity effects become significant. The modeling of the leakage inductance of magnetic components and its variation with frequency has been addressed theoretically by Dowell [35] and by Dauhajre [112], Dauhajre & Middlebrook [31] and Hsu, Middlebrook and Cuk [33]. Of these, however, only Dowell provides a theoretical approach for the estimation of the combined eddy current and proximity effects and the resulting leakage inductance variation with frequency. More recent work by Hurley and Wilcox [151] has provided an alternative approach, but is specifically for toroidal transformers. The problem with all of these methods is the inaccuracy of the predicted values for leakage inductance as the frequency increases.

In general, the focus of the effort to characterize the high frequency behaviour of windings, in particular leakage inductance, has been concentrated on the application of finite element analysis, with Silvester & Konrad [25], Tabaga, Pierratt & Blache [113], Skutt, Lee, Ridley & Nicol [114], Dai & Lee [146],[175] and Cherpentier, Lefevre & Lajoie-Mazenc [144] demonstrating the approach. The methodology is now well understood and is often provided as an application example in commercial finite element analysis software packages.

The development of the finite element analysis software as the integral part of a procedure to calculate the high frequency behaviour of magnetic components has been developed extensively by Asensi et al [28]-[30] and Prieto [119]-[121]. This procedure has the function of providing models for practical electric circuit simulation of power applications, and this has also been addressed by Okyere & Heinemann [138] and Evans & Heffernan [179]. Unfortunately the procedure requires exhaustive finite element analyses of the transformer models, which become more finely meshed as the frequency increases thereby either increasing the simulation time required, or reducing the accuracy of the result. It is not uncommon for a simple transformer to

require several hours of finite element analysis to obtain the leakage inductance variation with frequency. The resulting model obtained may also be cumbersome and exhibit convergence difficulties. Lopera et al [63] and Pernia et al [186],[166] have developed a one-dimensional approximation of the behaviour of the magnetic component windings including frequency variations. This has been developed into a software package UO-M$^2$T by Prieto et al [170] that produces a netlist model of the magnetic component for use in circuit simulation. There are two issues to consider with this type of approach. The first is the size and complexity of the resulting model. If the model consists of a large number of elements, then this may impact on the convergence and time of the circuit simulation. The second issue is the de-coupling of the model elements from the original physical geometry. If a model can be constructed which retains this link, then sensitivity of key parameters such as interlayer gap or winding size can be usefully investigated without the requirement for a remodeling of the device. This technique is discussed specifically in this chapter.

In this chapter, the difficulties of both the theoretical and numerical methods will be addressed from a practical perspective to provide a useful circuit simulation model in a reasonable time. Assessments are made of the theoretical models and various finite element analysis modeling techniques with respect to measured results to enable an informed choice to be made for the appropriate level of model required. Finally a resulting model structure is proposed which models the leakage inductance variation with frequency, and can be characterized with a relatively small number of measurements or finite element analyses.

## 7.2   *Evaluation of Dowell's Equations for the Prediction of leakage inductance*

If the theoretical equations of Dowell [35] and Dauhajre et al [112],[31] are evaluated, it can be shown that the low frequency leakage inductance is effectively obtained from the same equation, the apparent differences are purely a matter of nomenclature. If the two-winding transformer shown in figure 7.1 is taken as an example, Dauhajre provides the expression for the leakage inductance based on this geometry in (7.1).
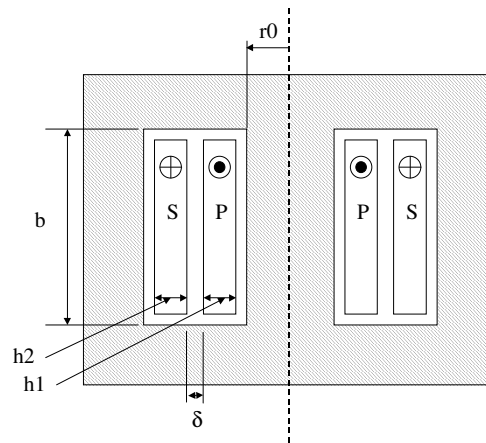
**Figure 7.1: Transformer Winding Structure**

$$l = 2\pi\mu_0 N_1^2 \frac{1}{b} \left[ \begin{array}{l} h_1\left(\dfrac{r_0}{3} + \dfrac{h_1}{4}\right) \\ + \delta\left(r_0 + h_1 + \dfrac{\delta}{2}\right) \\ + h_2\left(\dfrac{r_0 + h_1 + \delta}{3} + \dfrac{h_2}{12}\right) \end{array} \right] \tag{7.1}$$

This approach is fundamentally the same as Dowell's in that the energies stored in each winding space and the interwinding spaces are calculated independently and then combined to provide the complete leakage inductance value, referred to a single winding (e.g. the primary). Dauhajre stops at this point, but Dowell makes the point that by dividing the energy regions into winding and spaces, the winding regions are frequency dependent, due to eddy currents and proximity effects, but the spaces are not. For a two winding transformer, the overall expression for the leakage inductance is given from Dowell's equations by (7.2), where $L_{w1}$ is the leakage inductance in winding 1, $L_{w2}$ is the leakage inductance in winding 2, $F_{L1}$ and $F_{L2}$ are the frequency variations in the leakage indutances of winding 1 and 2 respectively, $L_g$ is the leakage inductance due to the interwinding gap and $L_U$ is the leakage inductance due to the interlayer gaps.

$$L_{leakage} = F_{L1}L_{w1} + F_{L2}L_{w2} + L_g + L_U \tag{7.2}$$

Where the frequency variation of each winding leakage inductance is represented by a lumped equation for all of the eddy current and proximity effects as shown by (7.3)-(7.6).

$$FL = \left\{ \frac{3M'' + (m^2 - 1)D''}{m^2 \left| \alpha^2 h^2 \right|} \right\} \tag{7.3}$$

Where $M''$ is the imaginary part of the function $M$ given in (7.4), and $D''$ is the imaginary part of the function $D$ given in (7.5). $\alpha$ is the expression for effective skin depth given in (7.6), $m$ is the number of winding layers and $h$ is the layer thickness.

$$\boldsymbol{M} = \alpha\boldsymbol{h}\coth\alpha\boldsymbol{h} \tag{7.4}$$

$$\boldsymbol{D} = 2\alpha\boldsymbol{h}\tanh\frac{\alpha\boldsymbol{h}}{2} \tag{7.5}$$

$$\alpha = \sqrt{\frac{jw\mu_0\eta}{2}} \tag{7.6}$$

To assess the accuracy of these equations, a 2 winding transformer was constructed using a Phillips RM12-3F3 core, and wound using 24 SWG (0.559 mm diameter) enameled copper wire

117

with both the primary and secondary having 2 layers of 21 turns each. The inter-winding gap was measured to be 1.2mm. The leakage inductance was obtained by measuring the impedance across the primary, while short-circuiting the secondary winding. An HP4192A impedance analyzer was used, varying the frequency from 100Hz to 1MHz. The short circuit wires on the secondary winding were kept to a minimum length to reduce the introduction of extraneous leakage due to the measurement set up. The correlation of the measured and calculated leakage inductance values at 1000Hz seems to indicate the shorting wires have little impact on the measured leakage inductance. The low frequency leakage inductance was calculated using Dauhajre's equation (1) and verified using Dowell's approach with the value estimated at 12.52uH. A Mathcad model was then created for equation (7.3) and the packing factor ($\eta$) varied using 1.0 (perfect winding area coverage), 0.866 (perfect round conductor packing) and 0.5 (practical estimate). The resulting variation of measured and theoretical values is given in figure 7.2.
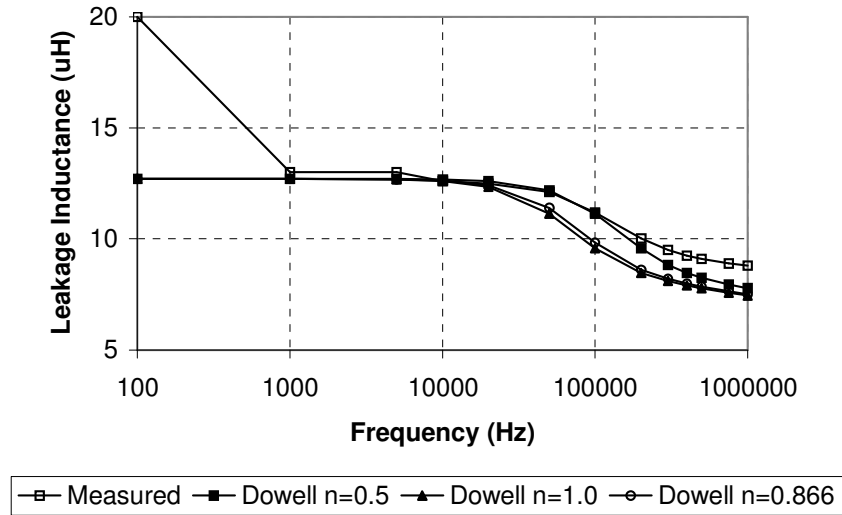


**Figure 7.2: Theoretical and empirical leakage inductance variation with frequency**

There are two interesting points to note from figure 7.2. The first is that as the frequency drops to around 100Hz, the apparent leakage inductance seems to increase. The explanation for this, is that as the frequency drops, the impedance of the magnetizing inductance falls and becomes comparable to the winding resistance. This has the consequence that the measured inductance can no longer be assumed to be an accurate measure of the leakage inductance alone. This causes the measured leakage inductance to apparently increase. The second point to notice is that as the frequency increases, the predicted leakage inductance decreases more quickly than the measured value. Niemela et al [149] and Robert et al [122] have also observed this difference. It is also noticeable that as the frequency tends to 1MHz, the leakage inductance flattens off to a high frequency value. In summary, therefore, it is clear that Dowell's theory is not always accurate at higher frequencies at predicting the roll off of the leakage inductance, or its final high frequency

value. This is probably due to the analysis by Dowell being effectively carried out in one dimension and not considering two dimensional effects.

## 7.3    Evaluation of Finite Element Analysis Methods

The use of finite element analysis for the estimation of leakage inductance has long been a standard technique, but there is a trade-off between the simulation time (depending on the complexity of the model) and the ultimate accuracy of the parameter derived. A study of the common model approximations used in the estimation of high frequency parameters was carried out, to establish the accuracy and simulation times for the example transformer previously used. In all cases an axis-symmetric approximation was used. Asensi, Cobos, Garcia, Prieto & Uceda [29] explain a procedure for applying two dimensional finite element analysis techniques to extract the parasitic parameters for magnetic components of the type used in this chapter.

### 7.3.1    Simple 2D Approximation with Lumped Windings

The first model uses the approximation that the complete winding can be modeled in a 2D finite element analysis as a single block. The resulting model, created using the MagNet software (Infolytica Corporation), is given in figure 7.3. The core model for 3F3 was modeled as a linear material with effective permeability 1583 (estimated from the Phillips datasheet).
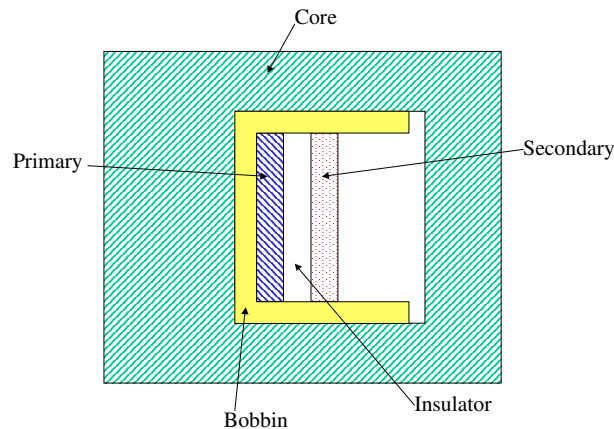


**Figure 7.3: Simple 2D Transformer Model**

The leakage inductance, referred to the primary winding can be estimated by applying equal and opposite field strengths to the primary and secondary windings (which if the number of turns are equal means equal and opposite currents). The resulting energy stored is effectively the energy stored in the winding area from which the leakage inductance can be directly calculated. The leakage inductance obtained using this model is shown in figure 7.4, along with the measured results and the values derived by Dowell for a packing factor of 0.5.
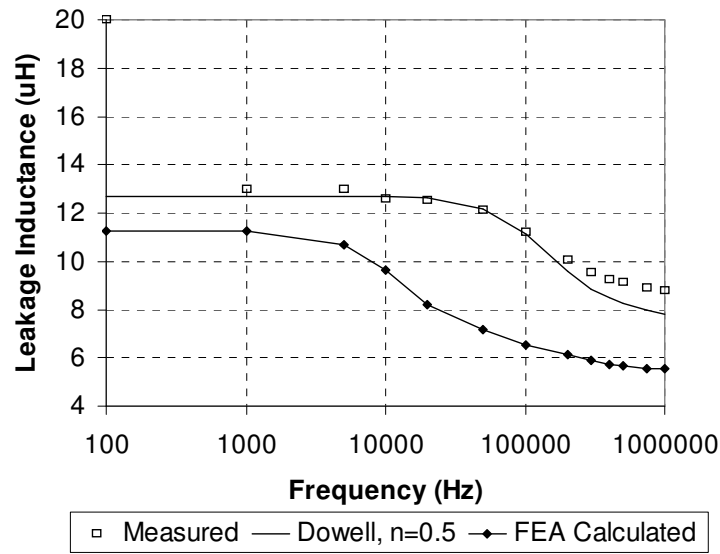
**Figure 7.4: Simple 2D Finite Element Model**

It is clear that this model does not accurately predict either the absolute value, or the frequency variation of the leakage inductance. However, it does show a less dramatic falling off of the leakage inductance with frequency than Dowell. The simple model of the winding does mean that the skin effect will be modeled differently than for individual turns, so that is not unexpected. This highlights that this commonly assumed model is clearly not adequate for accurate characterization of the parameters. At 1MHz, the leakage inductance calculated using the finite element analysis was 37% below the measured value. In this example, each analysis took approximately 4 minutes on a P133 PC.

## 7.3.2   Individual Layer 2D approximation

The second model lumped each layer as a separate entity in the finite element analysis, so in this case there are 4 discrete layers, with the correct diameter based on the wire gauge. The resulting model is given in figure 7.5.
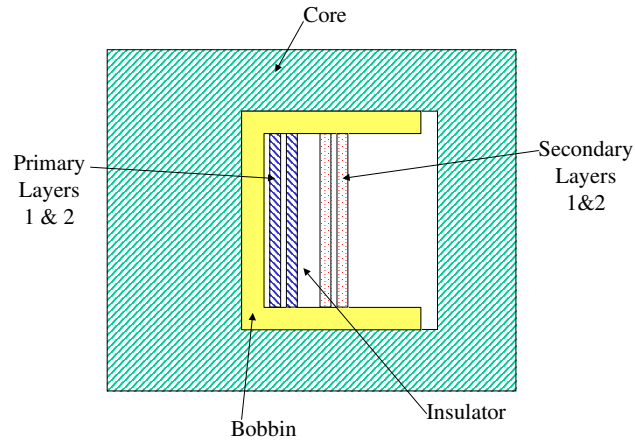
**Figure 7.5: 2D model using individual Layers**

The same tests were applied as for the simple 2D model, and the resulting leakage inductances shown in figure 7.6. As the complexity of the models increase, the corresponding simulation times also increase so fewer analyses were carried out. (In this case the simulations were still around 4 minutes on a P133 PC.
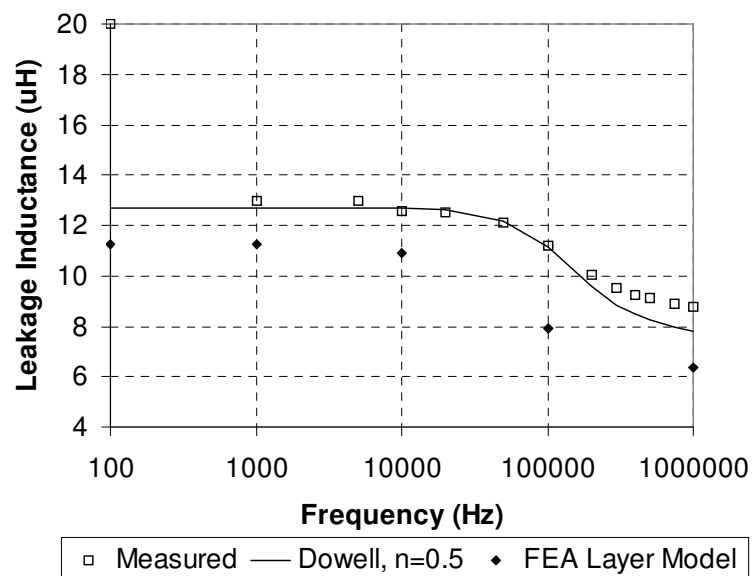


**Figure 7.6: Layer by Layer 2D Finite Element Model**

Using this model, the low frequency error was similar to that obtained using the simple 2D model, but the errors have decreased by about 10%. At 1MHz, the finite element calculated value of leakage inductance is 28% below the measured value.

121

### 7.3.3  Turn by Turn 2D Model

The final model is the most complex, and requires the modeling of each individual turn of the windings in the finite element model. The finite element model used is shown in figure 7.7.
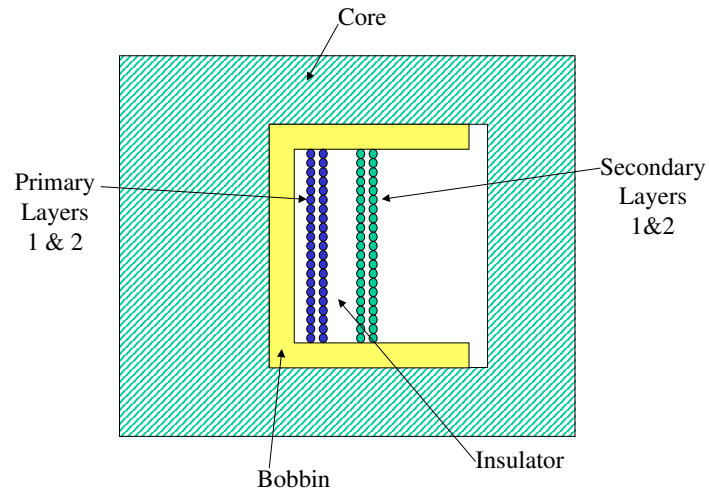


**Figure 7.7: Turn by Turn 2D Model**

The previous tests were carried out on this model, with a significant increase in simulation time observed. It was noticeable in this model that as the frequency increased, the simulation time increased dramatically from 33 minutes at 100Hz to over 2 hours for a 1MHz analysis (on the same P133 PC as before). The resulting leakage inductance results and measured values are shown in figure 7.8.
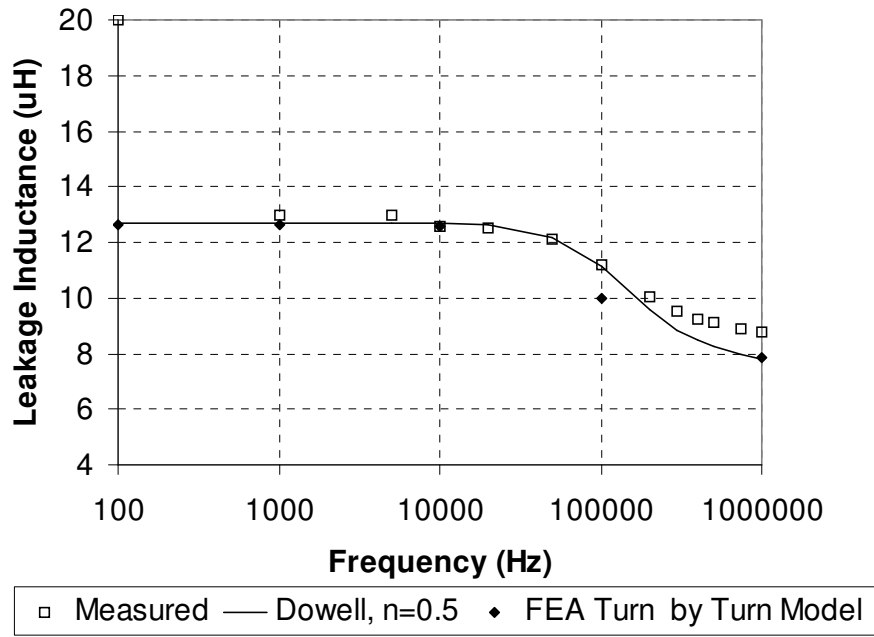
**Figure 7.8: Turn by Turn 2D Finite Element Model**

The results using this model are significantly better than the simpler 2D models, but at a heavy computational cost. To characterize this component using this approach would take many hours of simulation. The resulting error at 1MHz of leakage inductance of -10% is reasonable, given the tolerances in the materials and geometries.

## 7.4  *Evaluation of 1D modeling method*

Using a 1D approach to extract a detailed model of magnetic components has been well described by Lopera *et al* [63] and Pernia *et al* [186],[166] and implemented in the UOM$^2$T software by Prieto *et al* [170]. This software was used to generate a spice model of the RM12 transformer, with the resulting leakage inductance variations as shown in figure 7.9. The results were obtained using the built in analyzer, which creates and runs a PSPICE model and test circuit, then returns the required values of leakage inductance or winding resistance.
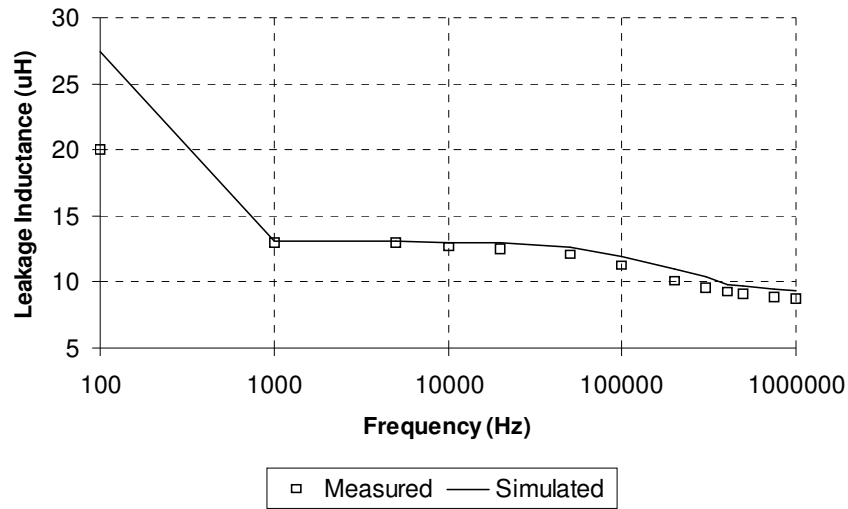
**Figure 7.9: UOM2T Model Leakage Inductance Calculation**

The comparison between measured and simulated results is good, but the resulting spice model in this case consisted of 71 elements. While this technique is extremely useful for designing the topology of devices, the resulting model is fairly cumbersome and does not provide the ability to vary parameters directly, without repeating the modeling procedure.

## 7.5   *Proposed new model for frequency dependent leakage inductance*

Given the deficiencies in both the theoretical and finite element analysis approaches demonstrated previously, there is the requirement for a simple model of the frequency variation of leakage inductance, which can reasonably accurately (to within 10%) model the behaviour of the leakage inductance with frequency which can be characterized with either a few measurements or finite element analyses. A further requirement of the model was to provide a simple approach that would allow direct understanding of the effect specific model parameters would have on the circuit performance with minimal simulation overhead. A new model structure is therefore proposed which reasonably models the low and high frequency behaviour of leakage inductance, and the transition between these two states. If the model of a transformer is considered in the magnetic domain, as shown in figure 7.10, the component consists of two windings, and a magnetic circuit containing the core and leakage reluctances.

124
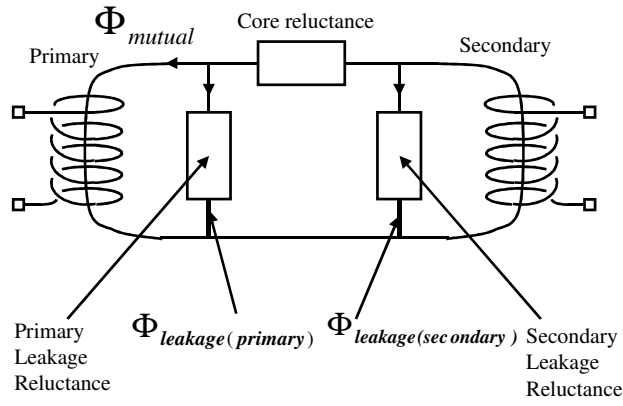
**Figure 7.10: Electro-Magnetic Transformer Model**

It is proposed to split each leakage reluctance into two parts, a d.c. or low frequency Reluctance ($v_{dc}$) and a high frequency Reluctance ($v_{hf}$). At low frequencies the total reluctance is the parallel combination of $v_{dc}$ and $v_{hf}$ while at high frequencies the effect of the d.c. reluctance is reduced by eddy currents represented by the inductance $L_{Loss}$, so the total reluctance tends towards the high frequency value $v_{hf}$. The inductance $L_{Loss}$ in the magnetic domain is equivalent to a closed turn linked to the flux as described by Cherry [15] and Laithwaite [16]. The time constant of the $v_{dc}$ reluctance and the loss inductor is effectively obtained from the conductor diameter. The resulting model of leakage reluctance is given in figure 7.11.
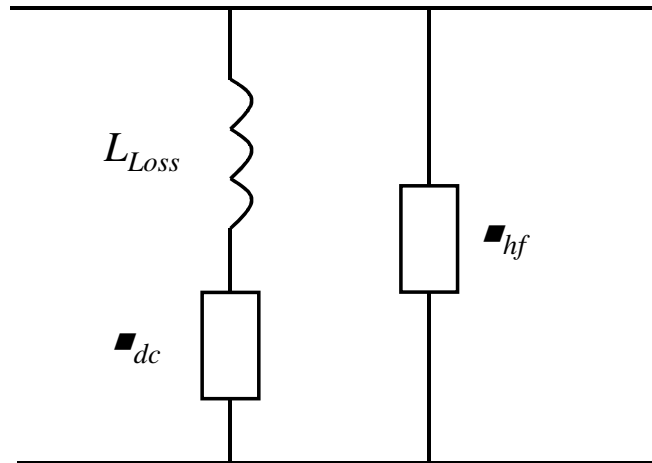


**Figure 7.11: Modified model of leakage reluctance**

This model can also be transformed into an equivalent in the electrical domain [24] using the configuration shown in figure 7.12.
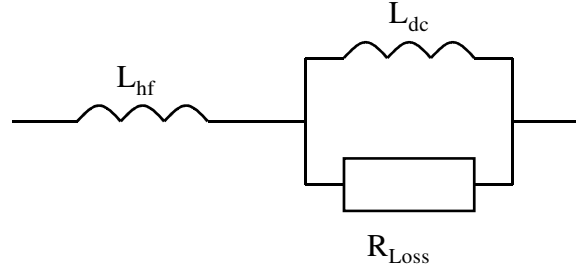
**Figure 7.12: Proposed Leakage Inductance Model in the electrical domain**

The $L_{Loss}$ & $v_{dc}$ (or $R_{Loss}$ & $L_{dc}$ using the electrical model) time constant can be estimated by using the frequency at which the skin depth is 0.5 the radius of the conductors used. This gives a reasonable estimate of the cut off frequency from which the loss component can be calculated. The low and high frequency leakage reluctances (or the inductances in electrical domain) can be measured or calculated using a high frequency and low frequency test thus reducing the number of tests (or finite element analyses) drastically. An alternative theoretical approach is to use Dauhajre's or Dowell's equations which separate the frequency and non-frequency dependent sections of the leakage inductance. Using this approach, the proportion of the leakage inductance due to the high frequency effect can be estimated.

## 7.6 Implementation of new model

The model of the transformer was constructed in SPICE as shown in figure 7.13, using the estimate of time constant based on the skin depth at half the conductor radius and the comparison with the measured leakage inductance given in figure 7.14. The ideal form of transformer model was used, with a measured magnetizing inductance of 10mH and perfect coupling ($k=1$). The low frequency leakage inductance was measured at 13uH, and the eventual effective high frequency leakage inductance was measured at 8.8uH. Thus $L_{hf}$ was set to 8.8uH and $L_{dc}$ was set to the difference between the low and high frequency leakage inductance measurements, giving a value of 4.2uH. In this model, the parasitic components were split evenly between the two windings, although the same value of leakage would be obtained by referring the values to one winding. The winding resistance $R_w$ was measured using a resistance bridge. The estimation of the $R_{loss}$ resistance, made with the skin depth at half the conductor radius, which can be estimated for 24 s.w.g. wire to be a depth of 0.13975mm, occurring at 223.6kHz. Using this frequency, and the previously measured leakage inductance of 13uH, the $R_{loss}$ value is estimated to be 2.9$\Omega$ using a simple RL time constant calculation. While this gives a reasonable estimate of the frequency variation, it is also the case that with such a simple model the accuracy of the final result may not be always optimal. It is an advantage of the simple model however, that improvements can be made in the matching with measured results by small variations in the value of $R_{loss}$. By including the magnetizing inductance and winding resistances in the model, the correct low frequency

behaviour was also observed. The test circuit shown in figure 7.13 used a current source on the primary side, and effectively shorted out the secondary winding using a 1mΩ resistor. The imaginary part of the input voltage *vin* was then divided by *2πf* to give the effective leakage inductance shown in figure 7.14. The magnetizing inductance was obtained by measurement, with a value of 10mH.
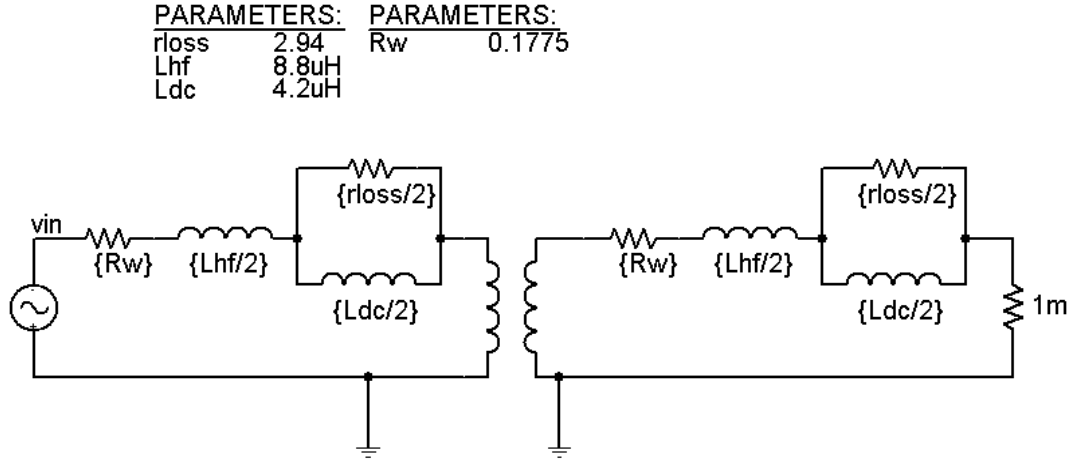


**Figure 7.13: Test Circuit for transformer, including the modified leakage inductance model, implemented in Spice**
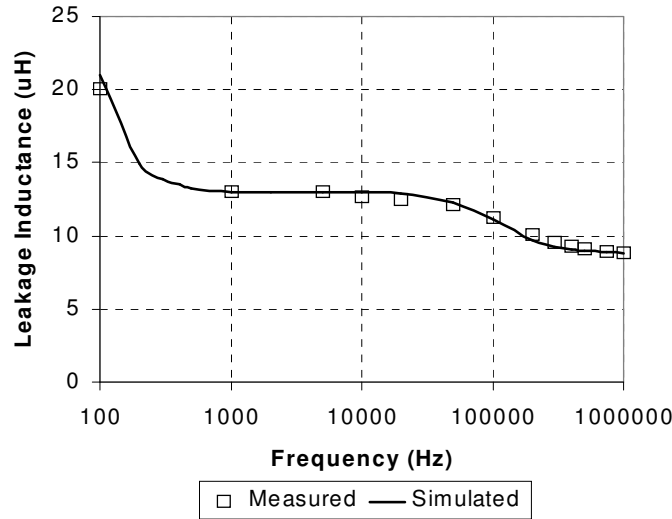


**Figure 7.14: Measured and Simulated leakage Inductance for RM12 transformer**

To demonstrate the technique more generally, another core was constructed, this time using an RM10-3F3 core, with two windings, each of 32 turns wound over two layers. The wire was 24 s.w.g as in the previous example. The resulting measured and simulated variations of leakage inductance with frequency are given in figure 7.15. The component values used in this case were $L_{hf}$=3.72uH, $L_{dc}$=4.58uH, $R_w$=0.125Ω and $R_{loss}$ =3.5Ω. The magnetizing inductance in this example was measured at 4.2mH.

127
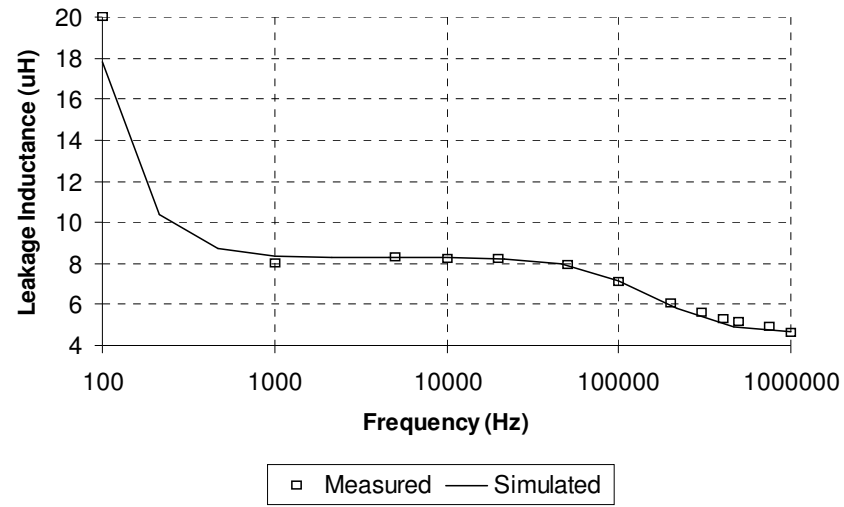
**Figure 7.15: Measured and Simulated leakage Inductance for RM10 transformer**

## 7.7 Evaluation of new Model

Testing of Dowell's theory of the variation of leakage inductance with frequency has demonstrated limitations in the accuracy of the method at high frequencies. Study of the finite element analysis approaches to the calculation of leakage inductance has also highlighted difficulties in the practical application of this method to the effective calculation of leakage inductance variation with frequency in a reasonable time. A new model structure has been presented which accurately models the variation of leakage inductance with frequency using a simple approach. The resulting model is simple to characterize, stable and fast to simulate.

*Chapter 8*

# 8   Coupled SPICE-Finite Element Analysis Simulation

## *8.1   Introduction*

It has been common practice for many years to attempt to simulate the behaviour of magnetic components in electric circuits using a combination of Finite Element Analysis (FEA) and circuit simulation techniques. These approaches can broadly be grouped into three main categories defined by the strength of the coupling between the analysis forms. The weakest coupling takes place when the FEA is used to characterize the parameters of the magnetic component and the resulting behavioural model used in a circuit simulation. The main purpose of this well documented technique has been to calculate static parasitic parameters such as leakage inductance or winding capacitance, as shown by Lyra, Cardoso, Braz, John & Lipo [197], Dai & Lee [146] and Asensi, Cobos, Alou, Prieto & Uceda [161]. The use of the same approach to calculate the behaviour of electromagnetic or electromechanical devices has also been applied by Affour,, Nachtergaele, Spirkovitch, Ostergaard &  Gyimesi [198], Dyck, Lowther, Malik, Spence, & Nelder [199] and Teegarden, Lorenz & Neul [200]. The drawback with this type of approach is the obvious difficulty of obtaining complete *a priori* knowledge of the component parameters under all possible operating conditions. To address this, much effort has been applied to combining the FEA and Circuit simulations in a way to allow complete access to both the FEA and circuit equations in a single simulation. This type of method can be implemented using either indirect coupling, with the FEA and circuit simulation in separate processes, or direct coupling where the equations of both models are incorporated into a single simulation of either FEA or circuit simulation form.

Direct coupling can be implemented either by including the external circuit model behaviour inside the FEA matrix as described and reviewed by Väänänen [201],[202], or implementing a form of pseudo-FEA within the circuit simulation.  In these cases, the drawbacks are twofold. Each model needs to be created from scratch and the strengths of either the circuit or FEA simulator are not fully utilized.

The indirect coupling method was long seen as completely impractical, but is now feasible with the increase in computing power available on the desktop and with the development of advanced modeling languages with external APIs, such as SABER's MAST modeling language [203]. For many engineers the circuit simulator of necessity or choice has been SPICE [204],[205] which does not have this external API. The author is aware of the commercial Simplorer (System Simulator) and Flux2D (FEA Solver) coupling, however one of the motivations in this chapter was

to produce a general-purpose link that was not bound by the restrictions of one or more proprietary software packages. Extensions to SPICE3 by Georgia Tech. Research Insititute [206] allow this possibility, and with the implementation in Windows of an open access version, SPICE-OPUS [207], SPICE can be investigated as a realistic simulator for coupling with an FEA solver without the requirement for direct access to the SPICE code itself. In this type of approach, the solvers are treated as a master-slave configuration, with the circuit simulator as the master. Another key motivation was to assess the practicality of such an approach in solving real-world problems in a reasonable time.

While the implementation is similar in architecture whichever simulators are used, practical considerations of availability and cost are important, so in this work the SPICE-OPUS simulator was chosen as the circuit simulator. The choice of FEA simulator is essentially a matter of preference for the end user, but there are some important considerations to take into account. It was considered that a modular FEA solver, with simple definitions of solver control and post-processing and easy access to non-proprietary data formats would be required, and so the SLIM FEA simulator [208] was used in this work. In this chapter, the mechanism of linking the FEA solver to a code model in SPICE-OPUS is described in detail. Examples are presented to show the results of the combined simulation technique for a simple inductor model and in the context of a switch mode power supply.

## 8.2  Extensions to Spice to interface to an External Finite Element Analysis Solver

### 8.2.1  Xspice extensions to Spice3

The Simulation Program with Integrated Circuit Emphasis (SPICE) was developed at the University of California, Berkeley in 1975 [204], and has become the standard for circuit simulation in the intervening time. More recent innovations, in Spice 3 [205], have included the development of mixed mode simulation. An important implementation aspect has been the translation into C from the original Fortran, and this has led to much more potential development, including the XSPICE program developed by Georgia Tech. [206]. In this software the ability to write customized behavioural models in C was added. This added a level of sophistication and power to Spice which had been lacking in the previous versions. A recent development has been the availability of a free version of XSPICE with optimization improvements on the PC Platform, SPICE-OPUS [207].

### 8.2.2  Interface Structure and Code Model Creation

There are two requirements for the code models, the node definitions and the model behaviour. The nodes may be defined using the existing library of analog and digital types in the library, or by creating new types. Similarly, a model's behaviour can use pre-defined models or new models can be written in C. If a new model is required, then a new Code Model needs to be created. A full

description of the procedure is provided in [206], but the essential components are a specification of the inputs, outputs and parameters in an ifspec.ifs file, and a C routine with the required behaviour defined in a cfunc.mod file. These are then compiled into a dynamic linked library that can then be loaded into the XSPICE simulator and used in a simulation.

### 8.2.3   Implementation of Xspice-FEA Interface Model

#### 8.2.3.1   Overview and model structure

Figure 8.1 shows the overall model structure of the XSPICE-FEA interface. At each time-step iteration, the required currents in the windings are passed down to a preprocessing routine which sets up the FEA control file with the winding current values. The FEA solver is then solved and post-processed using the standard FEA commands. A post-processing routine then extracts the winding flux for all the windings and returns these values to the XSPICE code model.
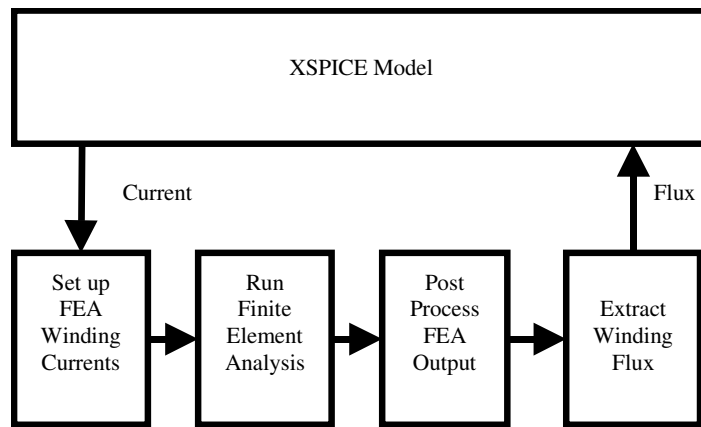


**Figure 8.1: XSPICE-FEA Model Structure**

In the iterative SPICE solving procedure at each time step, the model is treated as a standard non-linear model, and so the XSPICE simulator is the master for non-linear solving.

In the code model, the model is defined with a vector input representing the winding currents, and the return values are the winding flux. The winding number of turns is passed as a parameter to the underlying code model. This information is defined in the **ifspec.ifs** file. An excerpt of the definition for an inductor is given in Appendix D; figure D.1.

The winding current in the electrical domain is defined as a vector, as is the flux in the winding, in this specification file. This type of structure is easily expanded for multiple windings, by changing the size of the in and out vectors in this file.

The model behaviour is defined in the **cfunc.mod** file. The full C code listing for the FEA inductor is defined in Appendix D; Figure D.2. The functionality of the code is provided in figure 8.2.

131
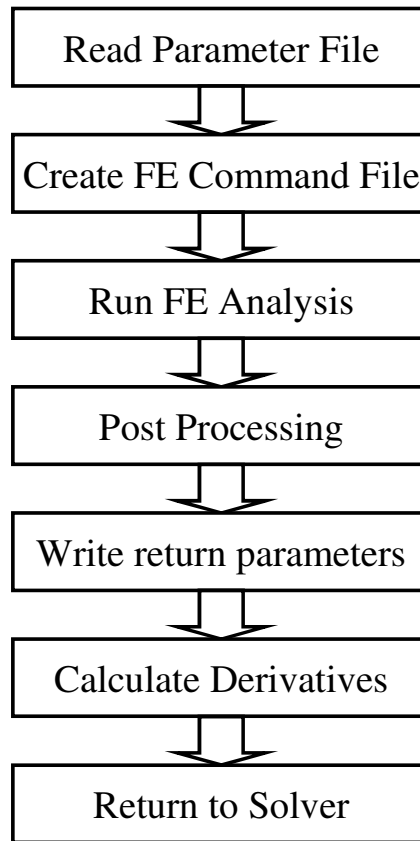
**Figure 8.2 : Spice-SLIM FE Analysis Procedure**

### 8.2.3.2  TCLTK FEA Pre-Processing and FEA Solution

The decision was taken to write out the winding currents into a generic format, and then use TCLTK [209] to format the data into the required form for the target FEA simulator so that changes could be made without requiring recompiling the code models. This of course could easily be incorporated into the Code Model C code with an increase in efficiency, but it was considered to be negligible compared to the FEA solution time. The TCLTK software reads in the values for winding current (equal and opposite values of the inductor current) and generates a SLIM control file (The full listing of the inductor control file is given in Appendix D;Figure D.3). Using this control file, the magneto-static solver in SLIM can be called in batch mode during each iteration

The magneto-static solver in SLIM creates two output files which require post-processing. The first is the nodal file, which contains the potential calculation at each node. The second file contains the flux density in each element.

### 8.2.3.3  FEA Solution File and TCLTK FEA Post-Processing

After the completion of the FEA solution, the batch post-processor in SLIM requires to be run using a control file, **basic.sp**. In this process, the FEA nodal solution file is used to integrate over

the winding regions and calculate the average integral flux in each winding. An example SLIM post-processing file is given in Appendix D; Figure D.4. (Notice the integration commands for the left and right halves of the winding.)

The log file for this process contains the resulting values required for returning to the XSPICE model, and so a final step is to parse this file using another TCLTK routine to create a generic data file that is read by the code model.

## *8.3 Simulation of Inductor using Spice-SLIM*

### 8.3.1 Introduction

A simple inductor was chosen to illustrate the concept of the SPICE-SLIM interface. The design was a basic double C core inductor, with 10 turns, on a core material of UNISIL 30M5. A current source was defined to apply a sinusoidal current of 1A peak at 50Hz to the inductor, with a combined winding and load resistance of 1Ω. The resulting XSPICE netlist is given in figure 8.3 and a schematic showing its structure in figure 8.4.

```
Test Circuit for SLIM Inductor in XSPICE

I1      1       0       dc      0       SIN     0       1       50
X1      1       0       SLIMINDUCTOR

.SUBCKT SLIMINDUCTOR     P       M
R1              P               MID     1
V1              MID     WP              0
H1              IL              0               V1              1
H2              IR              0               V1              -1
A1      [IL     IR]
+       [PHIL   PHIR]
+       foo1
.model foo1  slim1 (n=10.0)
E3              PHI     0               PHIL            PHIR            1
A2              PHI     VOUT            foo2
.model foo2 d_dt (out_lower_limit=-1.0e6 out_upper_limit=1.0e6)
E4              WP              M       VOUT            0       10.0e-3
.ENDS
.END
```

**Figure 8.3: Slim-XSPICE test circuit netlist**
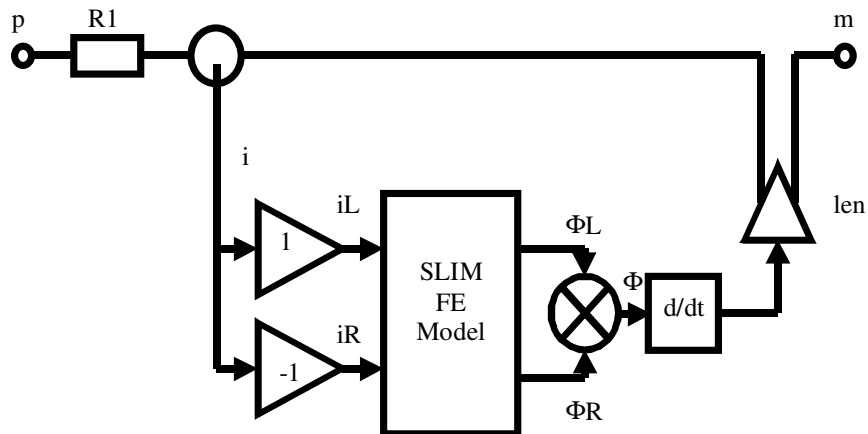


**Figure 8.4: SLIM-XSPICE inductor schematic**

The finite element model of the inductor was based on the mesh defined as shown in figure 8.5.
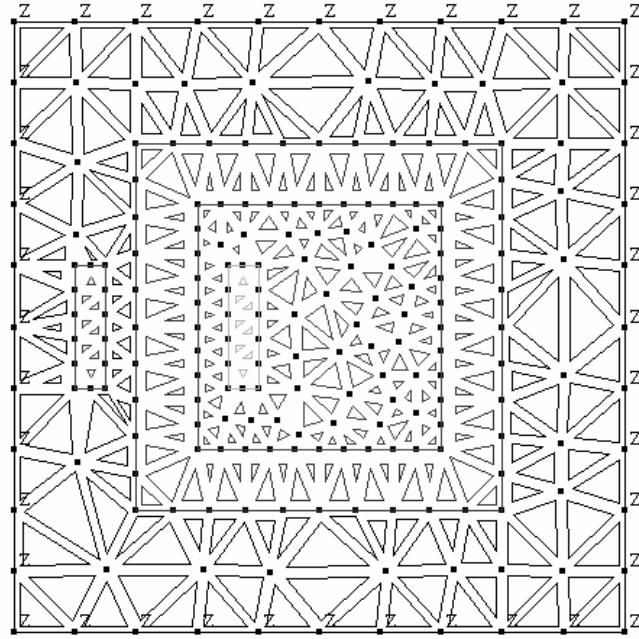


**Figure 8.5: SLIM inductor FEA Mesh**

## 8.3.2  Simulation Results

The test circuit for the inductor was simulated using XSPICE and SLIM 3.1.3, over 2 complete cycles of the input current, 40ms. The maximum time step was defined as 500us, and after an initial startup where the time-step was reduced to 1us, the solver stabilized quickly to an even time step of 500us. The total number of time-steps taken was 87. The resulting current and voltage waveforms are shown in figure 8.6. Notice that with the 1A peak current, the inductor voltage is saturating, causing the distortion in the voltage waveform.
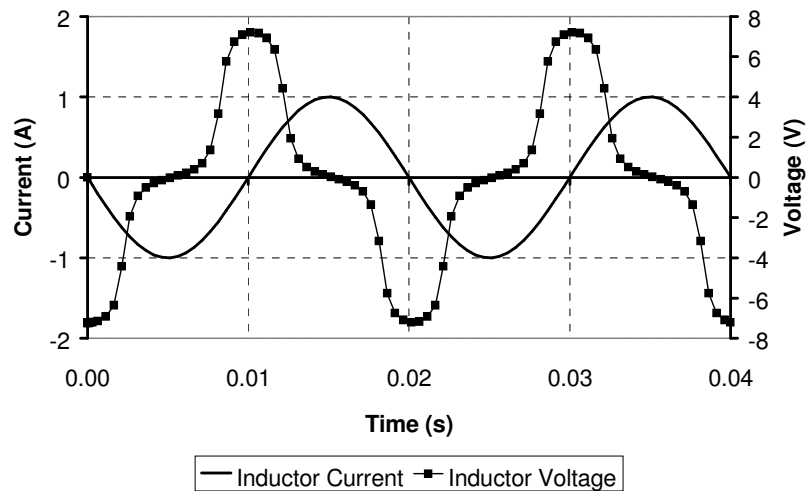


**Figure 8.6: Inductor Current and Voltage**

The advantage of this type of approach is that if a problem such as saturation is identified in the circuit waveforms, it is possible to use the Finite Element model to establish if there is a geometric problem, such as a weak link, in the core design. For example in this case, it is interesting to examine the peak flux density obtained with this core configuration at the maximum current levels. In this case, the corners of the core show increased flux density on the inside of the corner and reduced on the outside. This non-uniform flux distribution indicates that the core will saturate earlier on the inside of the corner. This is illustrated by a vector plot of the flux density through the core given by figure 8.7 (The size of the vector arrows represent the relative flux density magnitude).
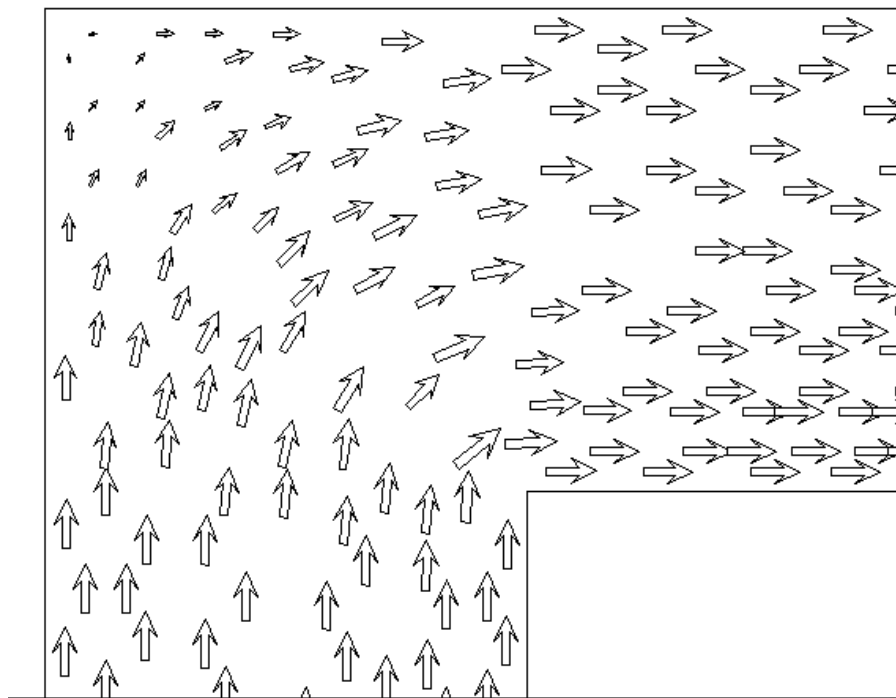


**Figure 8.7: Vector Plot of Flux Density in Core Corner**

## 8.4 *Simulation of a Switch-Mode Power Converter*

### 8.4.1 Introduction

While the simulation of individual components, such as inductors and transformers, may be useful; this type of analysis can easily be carried out using the alternative approaches of direct coupling previously discussed. The technique becomes increasingly powerful when the external electrical circuit is complex, and less easily integrated into FEA solver code directly. The ability to connect two models without the significant effort required to integrate them into one or other simulation technique offers a useful general purpose approach for a huge variety of circuits. To demonstrate this a switch mode power supply example was simulated with the combined Spice-Slim software. The circuit under test is shown in figure 8.8, with the corresponding SPICE netlist given in figure 8.9.
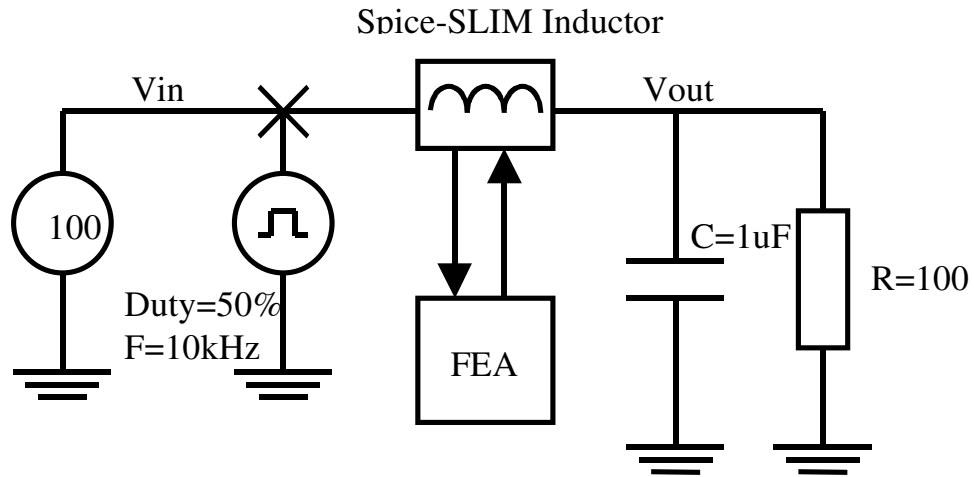
**Figure 8.8: SPICE-SLIM Inductor in Switch Mode Power Supply**

```
V1      1       0       DC      0       PULSE   0       100     0       100U    100u    1
        2
AS      SC      (1      2)      switch1
.model switch1 aswitch(r_on=0.1       r_off=100k log=TRUE)
VC      SC      0       DC      0       PULSE   0       1       10u     10u     10u     50u
        100u
X1      2       3       SLIMINDUCTOR
R3      3       0       100
C1      3       0       1u

.SUBCKT SLIMINDUCTOR   P       M
V1      P       WP      0
B1      IL      0       V=I(V1)
B3      IR      0       V=-I(V1)
*...Finite  Element Analysis Function
A1      [IL     IR]
+       [PHIL   PHIR]
+       foo1
.model foo1  slim1 (n=10.0)
E3      PHI     0       PHIL    PHIR    1
A2      PHI     VOUT    foo2
.model foo2    d_dt(out_lower_limit=-1e12 out_upper_limit=1e12)
B2      WP      M       V=V(VOUT)
.ENDS
.END
```

**Figure 8.9: SPICE Netlist for Switch Mode Power Supply**

The analog switch model uses a logarithmic transition between the on and off states for ease of convergence, with values of ron=0.1Ω and roff=100kΩ. The circuit was simulated for 10 cycles (1ms) till a steady state on the output was reached.

### 8.4.2   Simulation Results for Switch mode Power Supply

The simulation of this circuit, including the FEA inductor, took many hours on a P133 PC. The time step reduced to 1us to achieve reasonable accuracy, with several iterations required at each time step. The resulting output voltage waveform is shown in figure 8.10.
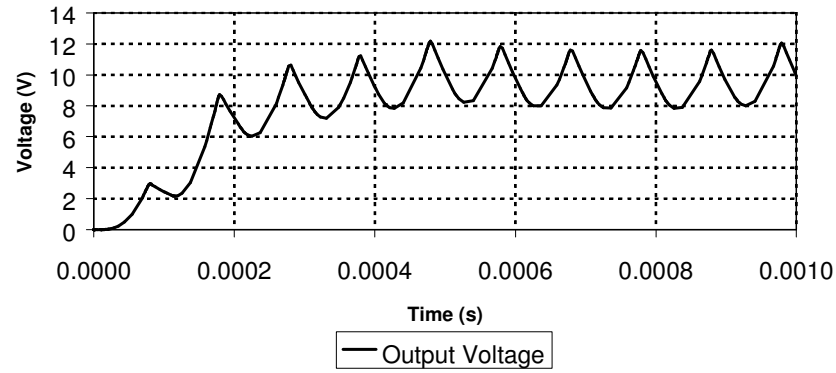
**Figure 8.10: Output Voltage Waveform of SPICE-SLIM simulation of switch mode power supply**

The corresponding current drawn from the supply is shown in figure 8.11.
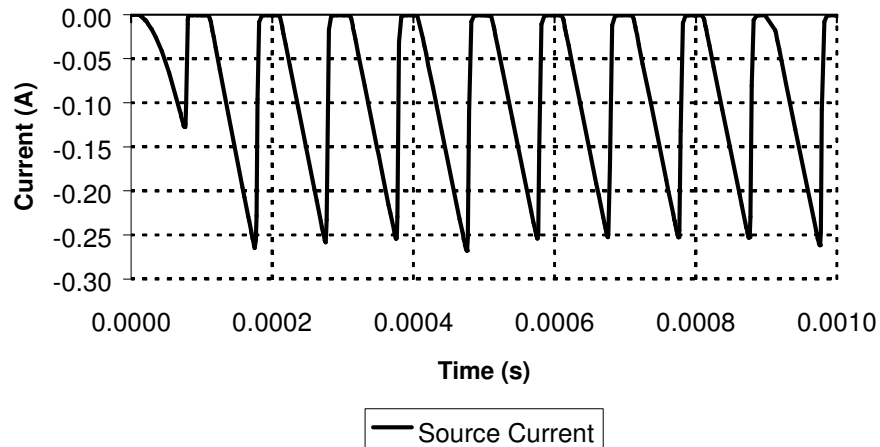


**Figure 8.11: Current drawn from the supply during SPICE-SLIM simulation of switch mode power supply**

## 8.5   *Discussion of Convergence Issues*

It has been noted in this chapter that the use of an external coupled Finite Element Analysis solver in conjunction with a circuit simulator may lead to convergence difficulties. The circuit simulator is attempting to solve non-linear equations with values returning from the 'black box' FEA software. The circuit simulator relies on information about not just the absolute values, but also the first derivative to allow a Newton-Raphson iterative process to converge to a stable solution. During this section of the work, it was found that an implementation of just the interface model, or in fact any non-linear model, without the calculation of the relevant partial derivatives gave severe convergence problems. In this case, the c*m_analog_auto_partial()* function was used to automatically calculate the model partial derivatives.  Despite the success of the examples used, it

is envisaged that lack of convergence could be a potential problem to be overcome in applying this technique on a day to day basis.

## 8.6 Conclusions

A complete method of integrating a Finite Element Analysis routine inside a model for use in the SPICE simulator is presented. The software architecture is outlined, and examples are presented to demonstrate the effectiveness of the technique.

While it is reasonably straightforward to obtain good results with a simple circuit, it is envisaged that great care will be required for more complex circuits to ensure convergence and accuracy. Other significant issues that have not been addressed in this work thus far are eddy currents and hysteresis.

Eddy current analysis in a Finite Element Analysis (FEA) is a linearized frequency domain analysis, therefore its use in a non-linear time domain simulation is of questionable value, except under tightly controlled conditions. The coupling method also assumes a quasi-static configuration, and this has implications when hysteresis is considered. A static FEA does not take into account the initial magnetization of the material, or its dynamic hysteresis behaviour. This is a major issue when considering the complexity of an interface between circuit and FEA simulators, and may fundamentally affect the behaviour of the dynamic circuit. The eddy current limitations become significant as the frequency of the application increases.

Despite these limitations, the method offers a systematic approach to modeling detailed magnetic effects in a standard circuit simulation. The method is also not limited to complete magnetic components, but could be used in conjunction with a magnetic circuit model of a core to model just the magnetic behaviour of a critical section of the core geometry. The extension of the technique to other domains such as thermal and mechanical is also possible using a similar approach.

*Chapter 9*

# 9 Dynamic Electric-Magnetic-Thermal Modeling

## *9.1 Introduction*

With the advent of higher switching frequencies and power densities in power electronic circuits, it is becoming ever more important to ensure that the magnetic components in the design operate within their specified thermal, magnetic and electrical safe operating regions and performance limits. It is also becoming standard design practice to use circuit simulation software, such as SPICE or SABER, to analyze and refine the behaviour of the circuit design as shown by Chwirka [187] and Wilson [188],[189].

Much effort has been applied to the detailed modeling of individual components in the design, especially switching power devices such as IGBTs, Power Mosfets and Diodes [190],[81],[192],[193]. Models for magnetic materials for use in power circuit simulation have included the Jiles-Atherton model [100],[20] &[21] (implemented in many SPICE simulators and Saber), the Chan-Vladirimescu model [23] (implemented in I-Spice), the Preisach model [19] & [101]  (implemented in Saber) and the Hodgdon model [22],[53],[54] (also implemented in Saber). The integration of the magnetic material models into a magnetic component model for use in a circuit simulator has been based on equivalent  circuit techniques using the duality concept. Duality and the theoretical development of equivalent circuit models have been described by Cherry [15], Laithwaite [16] and Carpenter [17]. The techniques have been applied in practical examples by Zhu, Hui and Ramsden [44],[42] and Brown, Ross, Nichols and Penny [18].

A similar approach has been used to model the relationship between power switching devices and thermal components, such as heatsinks, as shown by Hefner [190] and Hefner and Blackburn [81]. Hsu and Vu-Quoc [195],[196] have developed the use of Finite Element Analysis to characterize detailed models for dynamic electro-thermal simulation. The effect of temperature on magnetic component behaviour has been examined using finite element analysis techniques, such as Jesse [36]. The development of magnetic material models that are thermally dependent has also been undertaken by Hsu and Ngo [103] and Tenant, Rousseau and Segadi [104]., but these don't take self heating into account. Maxim, Andreu and Boucher [164],[160],[168] have implemented a lookup table hysteresis model in SPICE, with thermal behaviour, but the power losses are calculated analytically and effectively restricted to fixed waveform shapes. In this chapter the energy aspects of the Jiles-Atherton model of hysteresis are considered to produce the correct dynamic power loss for arbitrary applied waveforms. Winding losses and eddy current losses are also included to ensure the correct overall power loss. The resulting power loss is used as the

stimulus to a lumped element thermal model including core conduction, thermal capacitance, and convection to the air. The parameters of the Jiles-Atherton model have been characterized over a wide temperature range (27ºC to 154ºC) and implemented in the model to vary with respect to the component temperature.

To demonstrate the accuracy and effectiveness of the model, a standard core material was characterized (Philips 3F3) and used to create a model of a transformer for use in circuit simulation. Test cases were constructed and measured results compared with simulations.

### 9.2    Proposed Magnetic Component Model Including Dynamic Thermal Behaviour

### 9.2.1    Proposed Model Structure

It is proposed to extend the non-linear core model by modifying the model parameters dynamically depending on the temperature of the magnetic material. The outline of the approach is given in figure 9.1. Hsu and Ngo [103] and Tenant, Rousseau and Segadi [104] have shown how to modify the model parameters depending on the material temperature, but the temperature has been specified as a static variable. In this model, the temperature is calculated dynamically from a thermal network representing the thermal behaviour of the magnetic core. The input power to the thermal network is calculated dynamically from the non-linear core model. It must also be noted that the power loss due to the hysteresis in the core is not the only loss to be considered, but that eddy current loss and winding losses need also be taken into account. For the moment, the eddy current and winding losses will be ignored to keep the initial model structure simple, but will be discussed later in this chapter. Using this approach allows the use of arbitrary waveshapes to be applied to the model and an accurate power loss estimated regardless of the waveform. This contrasts with analytical methods of power loss calculation as described by Maxim, Andreu and Boucher [164],[160],[168] for sinusoidal waveforms, which are therefore restricted in applicability.
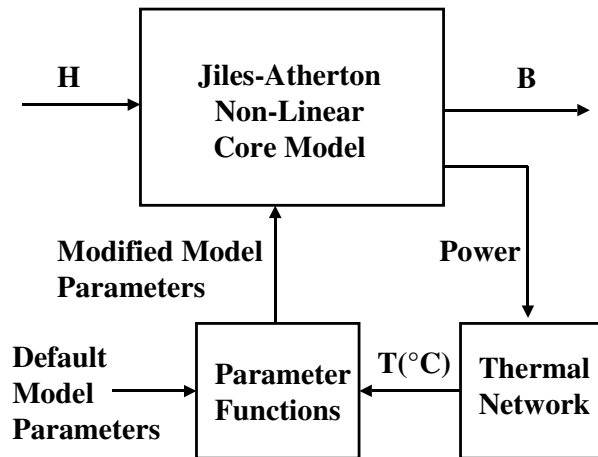


**Figure 9.1: Modification to the Jiles-Atherton model including temperature dependence**

### 9.2.2 Modeling Power Loss in Magnetic Components

Hefner & Blackburn [81] and Hsu & Vu-Quoc [195],[196] have described how electrical semiconductor devices can be linked dynamically with a lumped thermal network for simulation. This method operates on the principle that the power in the electric circuit can be instantaneously calculated from the resistive elements directly. The resulting power is then connected to a thermal network as a heat source. The solving of the network equations results in a change of temperature which is then used to control the electrical properties of the device, providing dynamic self-heating and behaviour variation depending on temperature. In this chapter a similar approach has been implemented, with the power loss calculated for the magnetic component.

The conventional method of calculating the hysteresis loss requires the measurement of the area of the BH loop. The energy lost per cycle is obtained by integrating the field strength (H) with respect to the change in flux density (dB). The mean power loss is found by multiplying this energy by the frequency. Unfortunately, this procedure does not provide the instantaneous power dissipated inside the material. It is possible to make the assumption that the thermal network time constant is several orders of magnitude greater than that for the magnetic circuit and effectively averages out the effect of the cyclic power applied. This assumption allows the approach to be used in practical examples, but the instantaneous power will still only be valid on average over the period of the simulation, not at every simulation point.

The Jiles Atherton model is based on fundamental energy considerations as explained by Feynman [194] and Jiles [47] which implies that the instantaneous power loss can be derived directly from the model. The Jiles-Atherton model uses an anhysteretic function to represent the stored energy, and so the instantaneous energy loss can be approximated as shown in fig. 9.2. The instantaneous power loss can be obtained by differentiating the energy loss with respect to time. This power loss can be used as the input to a thermal circuit for a more accurate representation of instantaneous power loss. While this method is not an exact derivation of the power loss, it is an improvement over the cycle based approach and permits a more accurate estimation of the energy loss in the magnetic material for an arbitrary applied magnetic field (H) at all points in the simulation. The power is the same as the previous approach over the complete cycle, but the instantaneous power at each simulation point during the cycle will be more accurate.
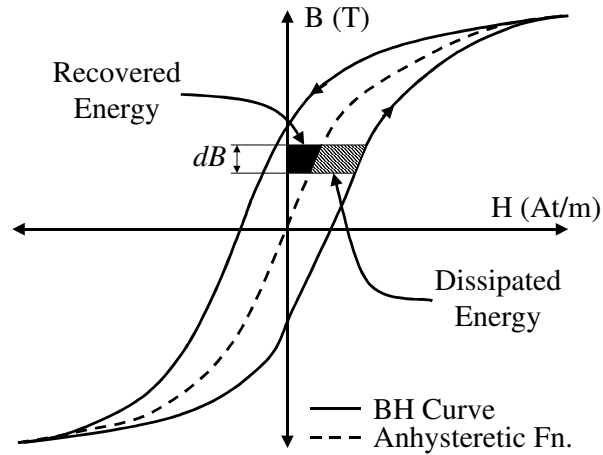
**Figure 9.2 : Recovered and Dissipated Energy in the BH Loop**

### 9.2.2.1  *Modifications to the Jiles-Atherton model to include dynamic self heating effects*

The Jiles-Atherton model was modified as shown in fig. 9.3  to use the generated temperature
based on the heat flow into the thermal network to dynamically modify the model parameters. The
dependence on the temperature was modeled using the polynomial approximations calculated from
the experimental data. The heat flow into the thermal circuit was calculated using the integral of
the BH curve to evaluate the area inside the loop.

```
.SUBCKT expja_th7         1     2     3      PARAMS:       AREA=10E-6
LEN=10E-3
+ MS=430K A=33.5 K=27.98 C=0.406 ALPHA=3.28U ECRATE=54.1
+ MSTC=-1138.2 KTC=-0.073 CTC=1.63m ATC=-1.11e-3 ALPHATC=5.28e-9
+ ECRATEATC=0
* CONVERT MMF TO HE
E1    HE   0      VALUE={V(H)+ALPHA*V(TALPHA)*MS*V(TMS)*V(M)}
R1    HE   0      1MEG
* ANHYSTERETIC MAGNETISATION
E2    MAN  0      VALUE={IF(ABS(V(HE))>1E-3,1/TANH(V(HE)/(A*V(TA)+1u))-
(A*V(TA))/V(HE),0.333*V(HE)/(A*V(TA)+1u))}
R2    MAN  0      1MEG
* 1DH/DT
E3    5    0      1     2     1
C1    5    6      1M     (IC=0)
RD    6    7      1M
V1    7    0      0V
* DELTA*K
E4    8    0      VALUE={K*V(TK)*EXP(-
(V(H)*V(H)/(2*ECRATE*ECRATE*V(TEC)*V(TEC))))*SGN(I(V1))}
R3    8    DELTAK       1K
C2    DELTAK       0      1PF
* INTEGRATE MAGNETISATION
E5    10   0      VALUE={V(MAN,M)/(V(DELTAK)-
ALPHA*V(TALPHA)*MS*V(TMS)*V(MAN,M)+1M)/LEN}
D1    10   DMDH   DMOD
R4    DMDH 0      1K
E6    M    0
      VALUE={SDT(1000*I(V1)*V(DMDH)/(1+C*V(TC)))+C*V(TC)*V(MAN)/(1+C*V(T
C))}
R5    M    0      1K
```

```
E7     FLUX   0      VALUE={AREA*1.258E-6*(MS*V(TMS)*V(M)+V(H))}
R6     FLUX   0      1MEG
G1     1      2      FLUX   0      1
*
* Calculate thermal Output
*
E8     MIRR   0      VALUE={V(M)-V(MAN)}
E9     PLOSS  0      VALUE={V(1,2)*1.258E-6*(MS*V(TMS)*V(MIRR) + V(H))}
G10    3      0      PLOSS  0      1
E10    T      0      3      0      1
*
* Thermal Variables
*
* MS
EMS    TMS    0      VALUE={(MS+(V(T)*MSTC))/MS}
RMS    TMS    0      1000
* K
EK     TK     0      value={(k+(v(t)*ktc))/K}
RK     TK     0      1000
* C
EC     TC     0      value={(c+(v(t)*ctc))/c}
RC     TC     0      1000
* A
EA     TA     0      value={(A+(v(t)*ATC))/A}
RA     TA     0      1000
* ECRATE
EEC    TEC    0      value={(ECRATE+(v(t)*ECRATEATC))/ECRATE}
REC    TEC    0      1000
* ALPHA
EALPHA       TALPHA     0      value={(ALPHA+(v(t)*ALPHATC))/ALPHA}
RALPHA       TALPHA     0      1000
*
* Calculate B and H for postprocessing
*
E21    B      0      VALUE={V(FLUX)/AREA}
E22    H      0      VALUE={V(1,2)/LEN}
.MODEL       DMOD   D(N=0.01)
.ENDS
```

**Figure 9.3: Spice Listing of Jiles-Atherton model extended to include parameter variations with temperature**

### 9.2.3 Including Eddy Current Losses

The eddy current loss can be implemented in two forms. The first uses the existing Jiles-Atherton model for the core, but the model parameters are characterized with the behaviour including the eddy currents. This is apparent in a larger BH loop. This approach is fine for a single sinusoidal frequency, but less useful in the general case for arbitrary waveforms. The second form is to dynamically include the eddy current behaviour in the model. This can be achieved using inductors to model power loss in conjunction with resistors to provide the correct frequency response, or by using a filter on the applied field variable to provide a larger apparent BH loop area at higher frequencies. In this chapter, fixed frequency sinusoidal waveforms were used, and the frequencies were chosen to minimize the effect of eddy currents on the eventual thermal

behaviour. In this chapter the a.c. resistance variations have not been included, but this could be easily implemented using an RL ladder network with the same principle.

### 9.2.4   Winding Losses

To include the d.c. winding losses, a winding model was modified as shown in fig. 9.4 to extract the instantaneous power dissipation from the winding for inclusion as a power source in the thermal circuit.

```
.SUBCKT winding_th     1     2     3     4     5      PARAMS: N=1
RD=100MEG RW=1M
RP    1     8     {RW}
V1    9     2     0
V2    6     4     0
E1    8     9     VALUE={N*V(7)}
E2    3     6     VALUE={N*I(V1)}
R2    3     6     {RD}
F1    7     0     V2    1
R1    7     0     {RD}
L1    7     0     1
E3    MMF   0     VALUE={V(3,4)}
E5    FLUX  0     VALUE={I(V2)}
*
* Thermal Circuit
*
ETH   PLOSS 0     VALUE={I(V1)*I(V1)*RW}
GTH   5     0     PLOSS 0     1
.ENDS
```

**Figure 9.4: Winding model with thermal pin connection**

### 9.2.5   Modeling the thermal behaviour of  the magnetic component

#### 9.2.5.1   Thermal Modeling Concepts

The thermal model for the magnetic core consists of the core thermal conduction, the thermal convection to the atmosphere and radiated emissions as described by Snelling [27]. The governing variables for the thermal system are the heat flow (or power) and the temperature. In the thermal network models, the heat flow is defined as the through variable and the temperature as the across variable, analogous to the electrical current and voltage respectively. Each of the elements in the thermal network can be represented by an equivalent electrical circuit model for simulation, as described previously by Hefner & Blackburn [81] and Hsu & Vu-Quoc [195],[196].

#### 9.2.5.2   Thermal Conduction Model

Snelling [27] provides the general expression for the calculation of the conduction of heat through a lamina and hence the effective thermal resistance for a magnetic core as given in equation (9.1), where $\delta x$ is the elemental lamina thickness, $\lambda$ is the thermal conductivity and $A$ is the cross sectional area.

$$R_{TH} = \frac{\delta x}{\lambda * A} \qquad (9.1)$$

Practical magnetic materials are usually of a more complex shape and this requires some analysis, again described by Snelling [27], to calculate the effective thermal resistance of the material. In the magnetic core, the power source is distributed throughout the volume. To calculate the thermal resistance of a toroid, for example, requires the integration of the heat flow over the volume of the toroid. The thermal resistance relates the integration between the centre of the core and the core surface to the total power input. Equation (9.2) shows that the thermal resistance is dependent on the cross-section diameter $d$ of the toroid.

$$R_{TH} = \frac{d^2}{\lambda * 16} \qquad (9.2)$$

The implementation of a thermal resistor in spice can be achieved using a standard resistor component, with the resistance equal to the thermal resistance.

### 9.2.5.3 Thermal Capacitance

The definition of the thermal capacitance is given by equation (9.3), where $\delta P_{TH}$ is the incremental Power Loss, $C_{TH}$ is the thermal capacitance and $\frac{d\theta}{dt}$ is the rate of change of temperature.

$$\delta P_{TH} = C_{TH} * \frac{d\theta}{dt} \qquad (9.3)$$

The thermal capacitance can be modeled in a circuit simulator using an electrical capacitance, where the value of capacitance is the thermal capacitance for the material. The value of thermal capacitance for a material can be calculated using the volume, density ($\rho$) and specific heat ($c$) in equation (9.4).

$$C_{TH} = Volume * \rho * c \qquad (9.4)$$

### 9.2.5.4 Thermal Convection

The major loss of heat from the core material is by convection heat transfer. Estimates of the loss are given by Snelling [27], with the expression for the power loss per unit surface area from a cylinder given by equation (9.5). If the toroid is assumed to be of approximately circular cross-section then the convection of heat from a toroid is considered to be approximately the same as that from a cylinder, where $\theta_{tc}$ is the temperature difference across the boundary and $d$ is the toroid diameter. In most cases a thermal resistance model is of adequate accuracy.

$$P_{convection} = 6.3 * \frac{\theta_{tc}^{1.25}}{d^{0.25}} \tag{9.5}$$

The thermal convection was modeled in spice using the model given in fig. 9.5.

```
.SUBCKT RCONV     1      2 PARAMS: AREA=1.0 D=10.0e-3 K=6.3
*
G1      1                          3
        VALUE={K*(V(1,2)**1.25)/(D**0.25)*AREA}
V1      3     2                          0
E2            POWER     0      VALUE={I(V1)}
E3            DELTAT    0      VALUE={V(1,2)}
.ENDS
```

**Figure 9.5: Thermal Convection Model**

### 9.2.5.5 Radiated Emissions

The radiation of heat from the core is generally disregarded as it can be much smaller than the other forms of heat transfer, but can be included in a model if necessary for improved accuracy. The standard Stefan-Boltzman law given in equation (9.6) defines the rate of heat dissipation, where $E$ is the emissivity of the material.

$$P_{radiation} = 5.67 * 10^{-8} * E * (T_{Surface}^4 - T_{ambient}^4) \tag{9.6}$$

The thermal emission was implemented in spice using the model given in fig. 9..

```
.SUBCKT EMISSION 1      2 PARAMS: AREA=1.0 E=1.0
*
G1     1     3      VALUE={5.67e-8*E*(V(THETAS)**4-V(THETAA)**4)*AREA}
V1     3     2     0
E2           POWER 0      VALUE={I(V1)}
E3           THETAS    0      VALUE={V(1)+273.0}
E4           THETAA    0      VALUE={V(2)+273.0}
.ENDS
```

**Figure 9.6: Thermal Emission Model**

### 9.2.5.6 Thermal Network Model Implementation

In this section, the temperature was assumed to be constant across the volume of the core material, and therefore the thermal resistance of the core material can be ignored in this instance. If the heat transfer behaviour across the core material is required, then a ladder network of thermal resistances and capacitances is necessary. The transfer of heat from the core to the surrounding atmosphere takes place primarily through surface convection and radiated thermal emissions. The thermal capacitance of the TN10/6/4 core is based on the volume, specific heat and density of the core material. Using the Philips data book density $\rho$ value of 4750 kg/m$^3$, the specific heat of MnZn Ferrites given by Snelling [27] as 700-800 JKg$^{-1}$°C$^{-1}$, and the volume of the core (188e-9 m$^3$) the thermal capacitance was calculated to be 0.7 J°C$^{-1}$. The parameters for the convection model were

based on the surface area of the toroid's ferrite material 293 mm$^2$ and diameter of 4.4mm (see fig. 9.8 for the toroid's dimensions) The resulting thermal circuit is shown in fig. 9.7. If more detail is required in the thermal model, a distributed approach can be implemented using the same basic models, as described by Hefner & Blackburn [191] and Hsu & Vu-Quoc [195],[196]. The penalty for using a distributed approach would be a considerable added complexity to the circuit simulation.
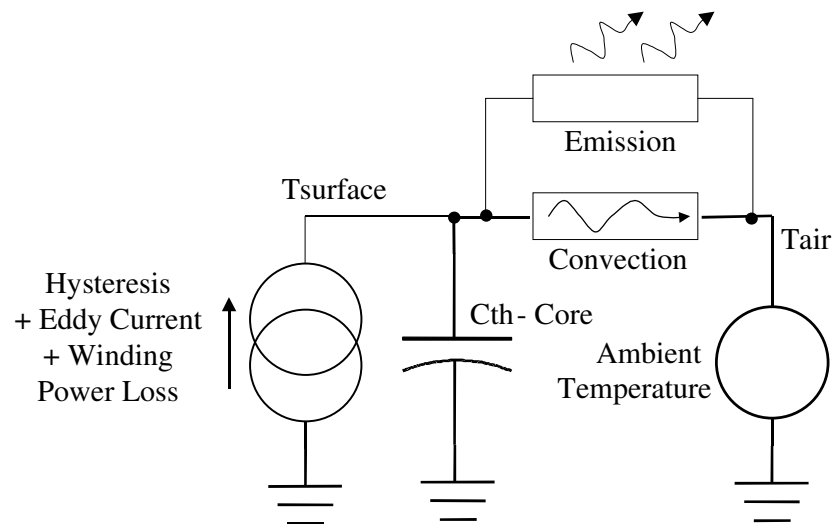


**Figure 9.7: Thermal Circuit**

## *9.3   Derivation of Magnetic Material Model Parameters*

### 9.3.1   Measurement of Material Behaviour

A test transformer was made by winding  primary and secondary coils on a Philips TN10-3F3 toroid core (dimensions given in figure 9.8).  This component was then used to extract the required magnetic material model parameters. Each winding has 40 turns of 28 S.W.G. copper wire. The transformer was tested using the configuration shown in fig. 9.9. The stimulus waveform was defined to provide a maximum applied magnetic field strength (H) of 100 A/m. The power amplifier was configured as a current amplifier to ensure that the applied current and hence applied magnetic field strength was the same for each temperature (under no-load conditions). Initially the frequency was set to 80Hz to minimize any eddy currents. The primary current sense and secondary voltage waveforms were captured using a digital oscilloscope and transferred to a personal computer for post-processing. The flux density (B) was derived from the (no load) secondary voltage by using numerical integration (4th order Runga-Kutta) and the applied magnetic field strength (H) derived from the voltage across the primary current sense resistor. The environmental temperature was varied across the range 27ºC to 154ºC in 10ºC steps by setting the oven temperature. The temperature was verified using a temperature probe attached to the surface of the core. The temperature was allowed to stabilize between measurements for a minimum of 10

minutes. Examples of the resulting BH curves obtained can be seen in fig. 9.9. This clearly shows that as the temperature increases, the saturation flux density decreases, as does the coercive force. There is also increased loop tip closure, as has been previously investigated in this thesis. Testing of the material beyond the Curie temperature (220ºC) gave rise to complete thermal demagnetization as expected for this material.
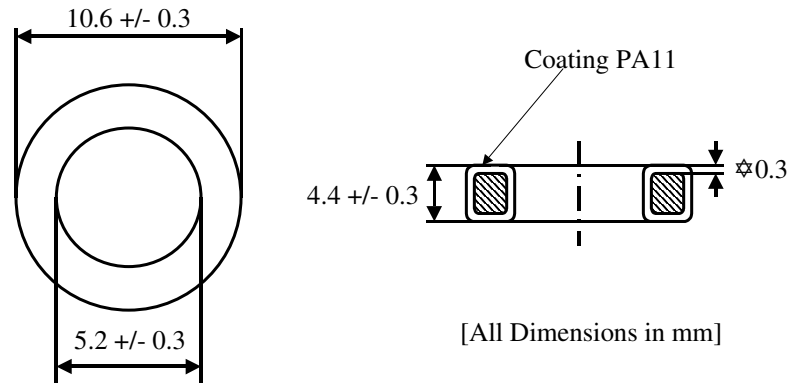


**Figure 9.8: TN10/6/4 Physical Dimensions**
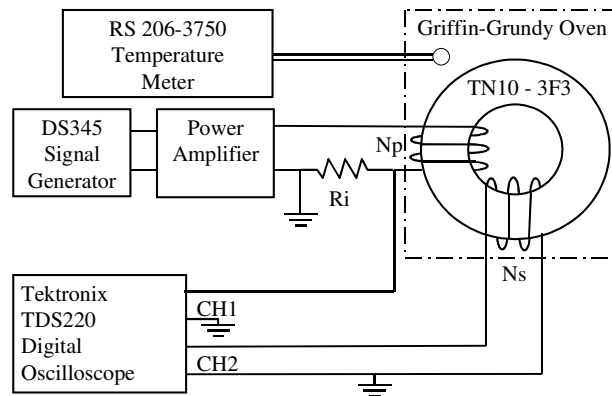


**Figure 9.9: Test Configuration for Temperature Characterization**
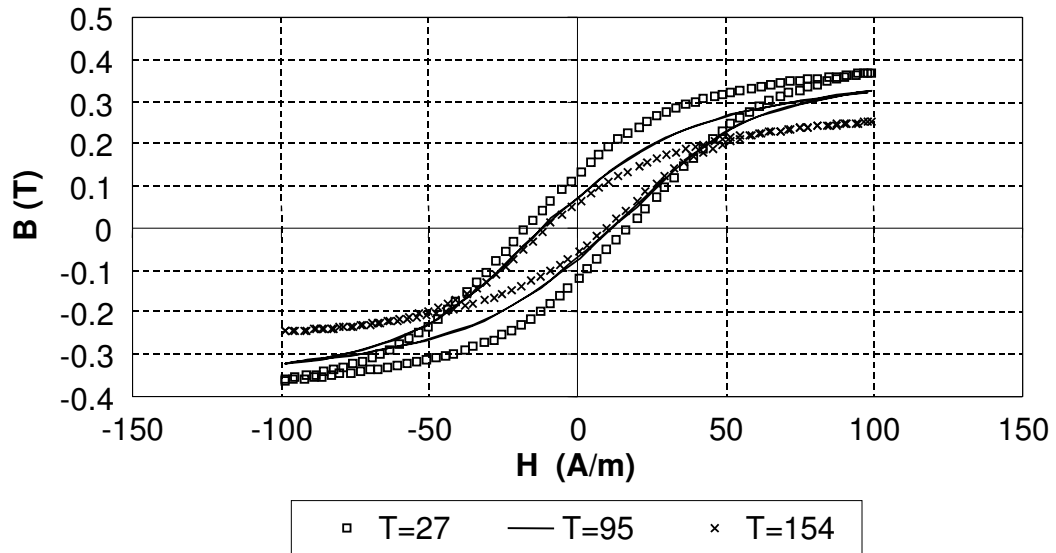
**Figure 9.10: BH Characteristic variation with temperature**

### 9.3.2 Extraction of the model parameters including temperature variations

The Jiles-Atherton model parameters were extracted from the BH hysteresis curves obtained at each test temperature, by optimizing the model to fit the measured data at each point. A Genetic Algorithm was used in this case, as has been described previously in this thesis. Regression analysis was applied to the resulting model parameters to obtain functions for each model parameter with respect to temperature. The resulting extracted parameters, regression analysis curves and estimated errors are shown in figs. 9.11 to 9.15. It is important to note that the Jiles-Atherton model parameters may be highly interdependent, therefore care must be exercised in constraining the optimization process to achieve consistency of parameter change across the temperature range. Any discontinuity in characteristic should be analyzed for 'rogue' optimization results.
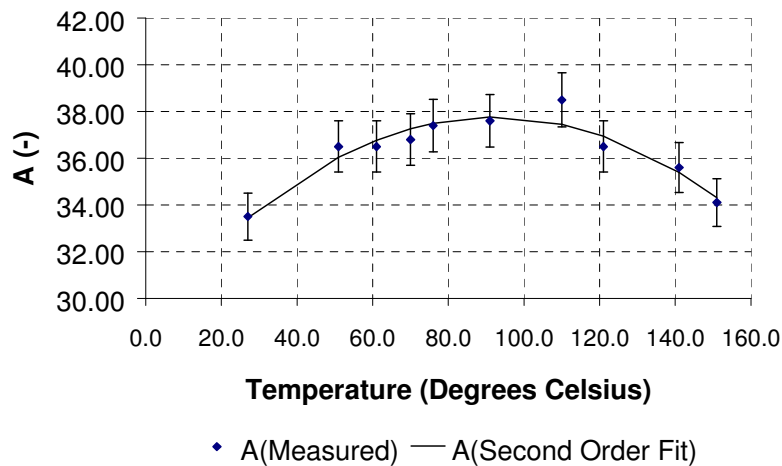


**Figure 9.11: Variation of A with Temperature optimized to within 3% error**
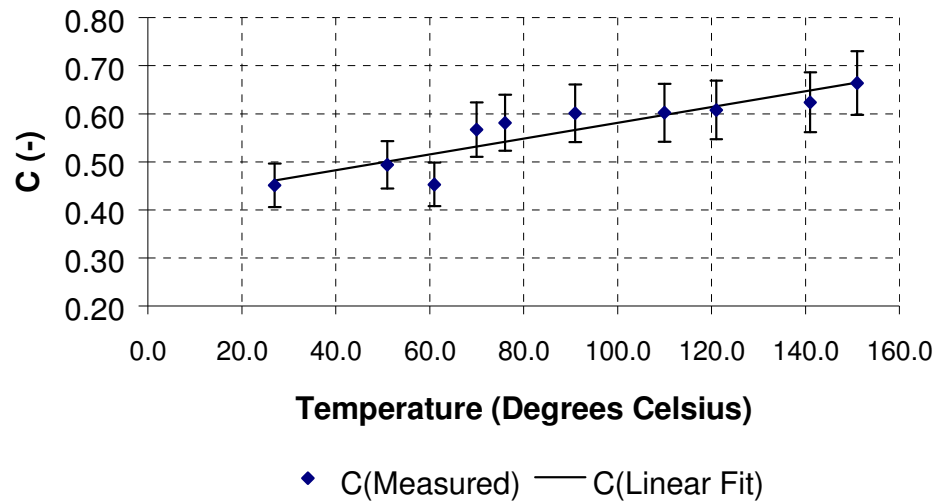
**Figure 9.12: Variation of C with Temperature optimized to within 10% error**
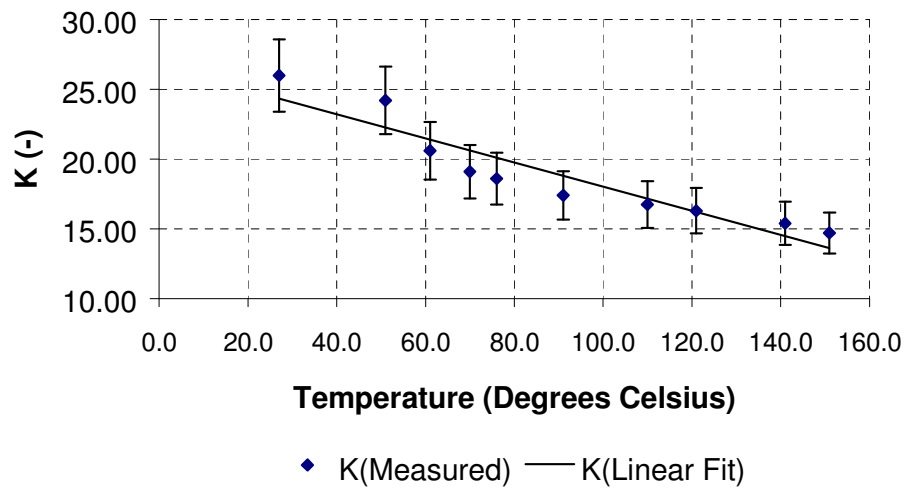


**Figure 9.13: Variation of K with Temperature optimized to within 5% error**
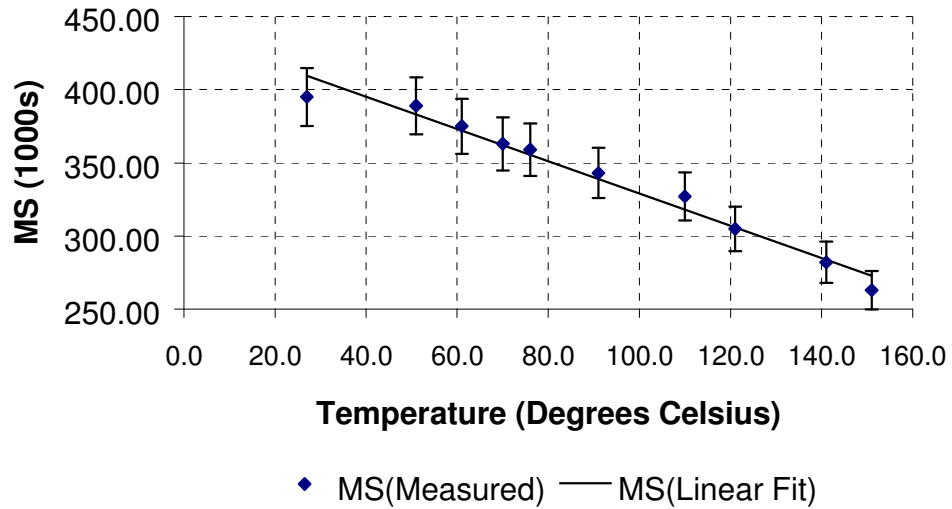
**Figure 9.14: Variation of MS with Temperature optimized to within 5% error**
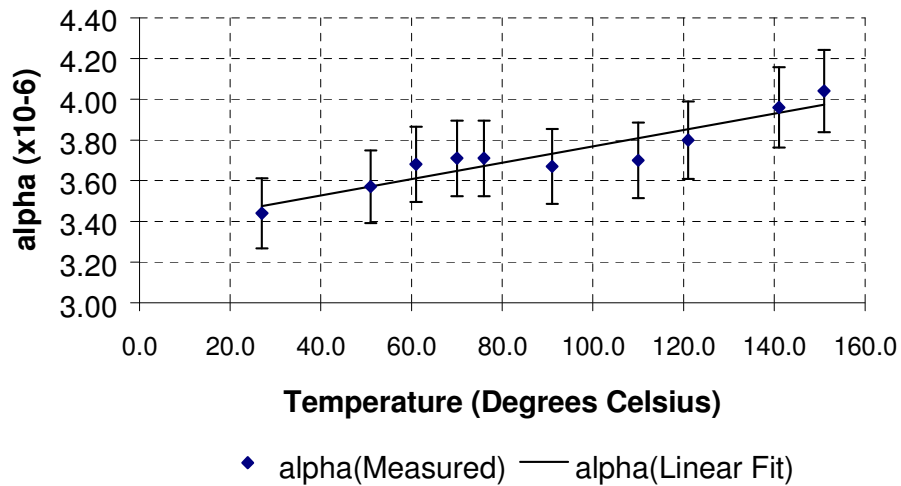


**Figure 9.15: Variation of Alpha with Temperature optimized to within 5% error**

### 9.3.3 Parameter Validation - Static Thermal Testing of Magnetic Material Model

The original Jiles-Atherton model was implemented in PSPICE using a behavioural modeling approach, with the modification for improved early closure modeling as outlined previously in this thesis. The parameters were modified to include temperature dependence as characterized previously. The test circuit shown in fig. 9.16 was used to test the behaviour of the model. The comparison of the measured and simulated BH curves at 27ºC, 95ºC and 154ºC can be seen in figs. 9.17, 9.18 and 9.19 respectively. It is clear from these figures that there is an excellent correlation between the measured and simulated waveforms.

151
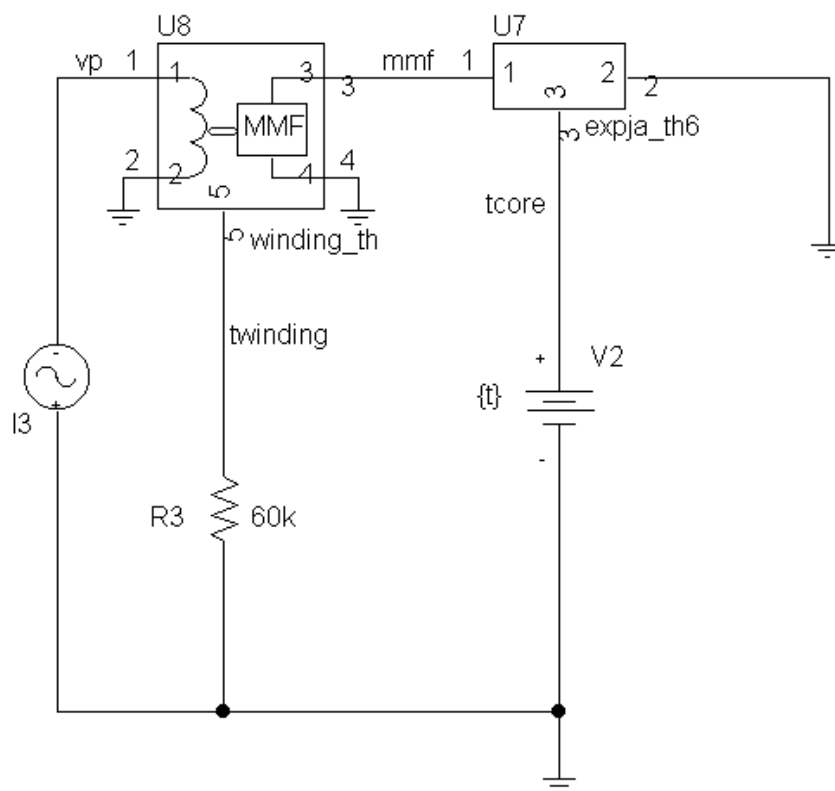
**Figure 9.16: Magnetic Material Model Static Temperature Test Circuit in PSPICE**
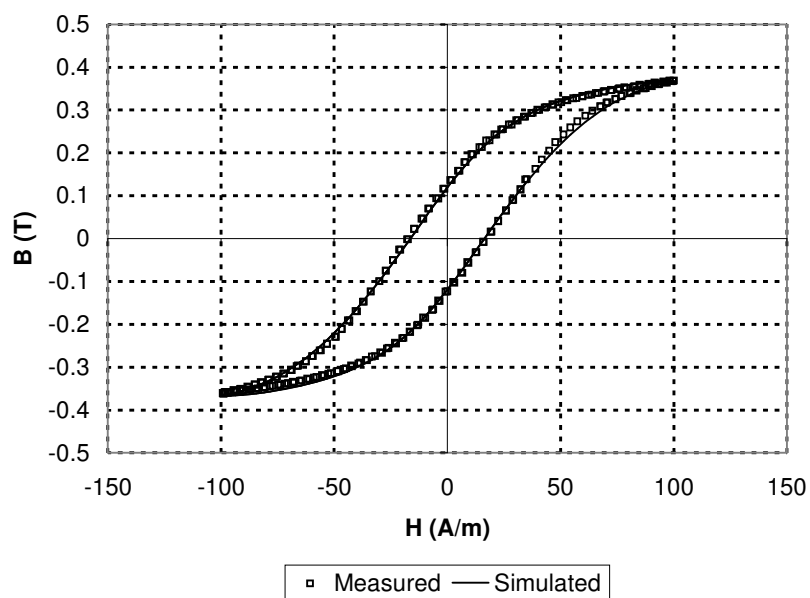


**Figure 9.17: Measured and Simulated BH Curves at 27ºC.**
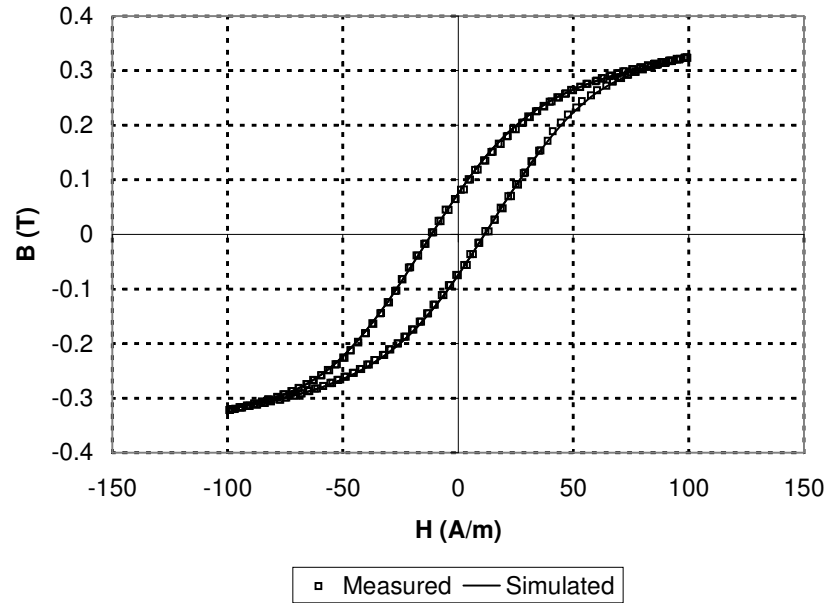
**Figure 9.18: Measured and Simulated BH Curves at 95ºC.**
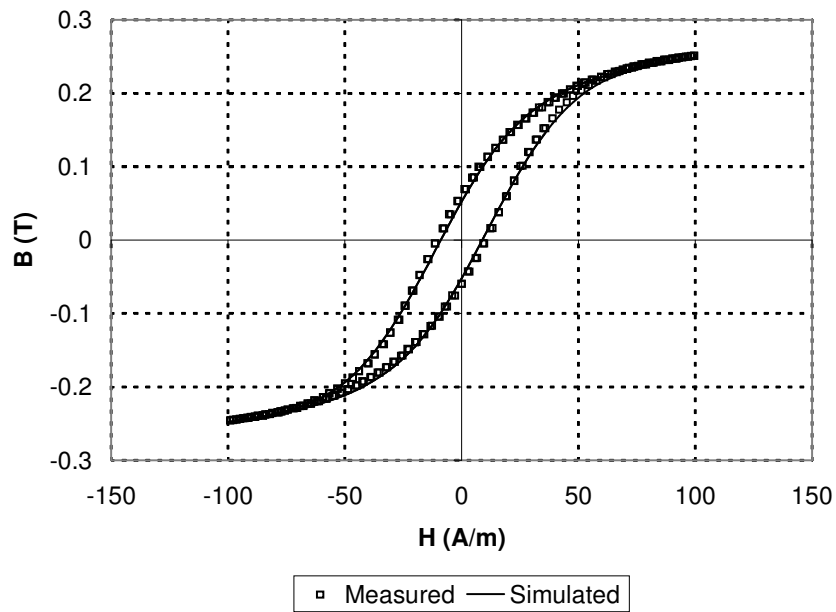


**Figure 9.19: Measured and Simulated BH Curves at 154ºC.**

## *9.4    Example: Modeling A Transformer With Dynamic Self-Heating Effects*

### 9.4.1    Static Thermal Behaviour Testing

To demonstrate the electrical behaviour of the model, including the effects of the thermally
dependent magnetic core, an example transformer was modeled including eddy currents, winding
losses and hysteresis losses, with a thermal circuit to complete the electric-thermal-magnetic
model. The complete model of the transformer, thermal circuit and electrical circuit is shown in

fig. 9.20. A voltage was applied to the primary of the transformer at 80Hz at 27ºC and 70ºC driving the transformer into saturation for a short time with the resulting simulated and measured waveforms shown in figs. 9.21 and 9.22. The initial difference between the measured and simulated waveforms is primarily due to differing initial conditions and the waveforms correlate better after one cycle has been completed. The simulations correctly predict the reduced amplitude of the secondary voltage of the transformer windings at the higher temperature, and accurately predict the electrical behaviour of the transformer at different temperatures.
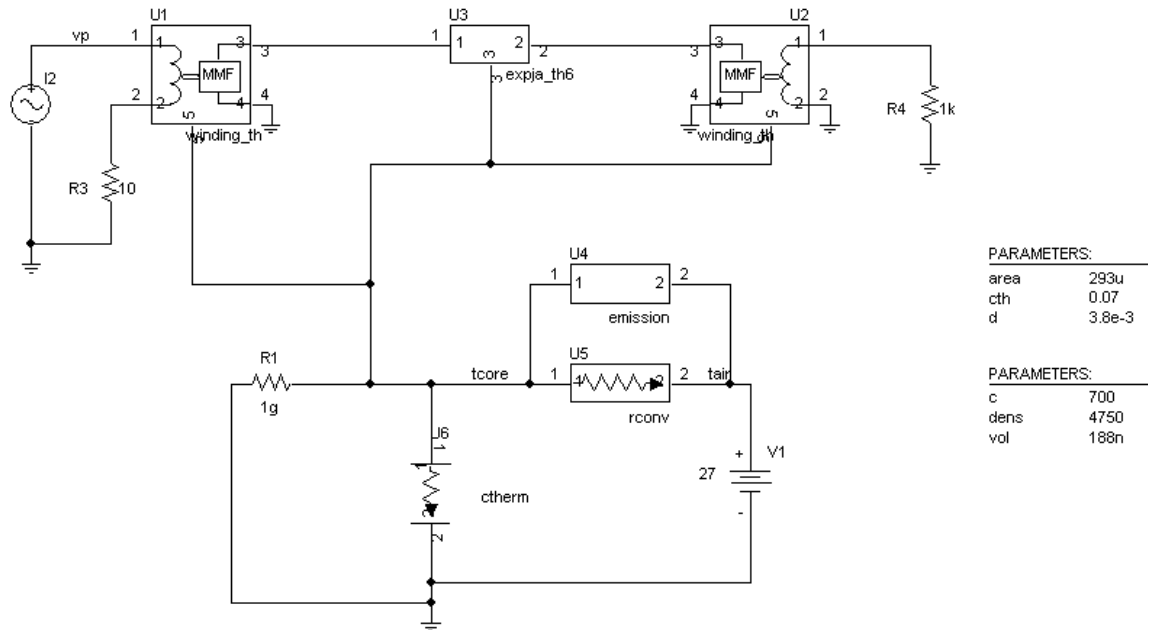


**Figure 9.20: Electrical-Thermal-Magnetic Transformer Model in PSPICE**
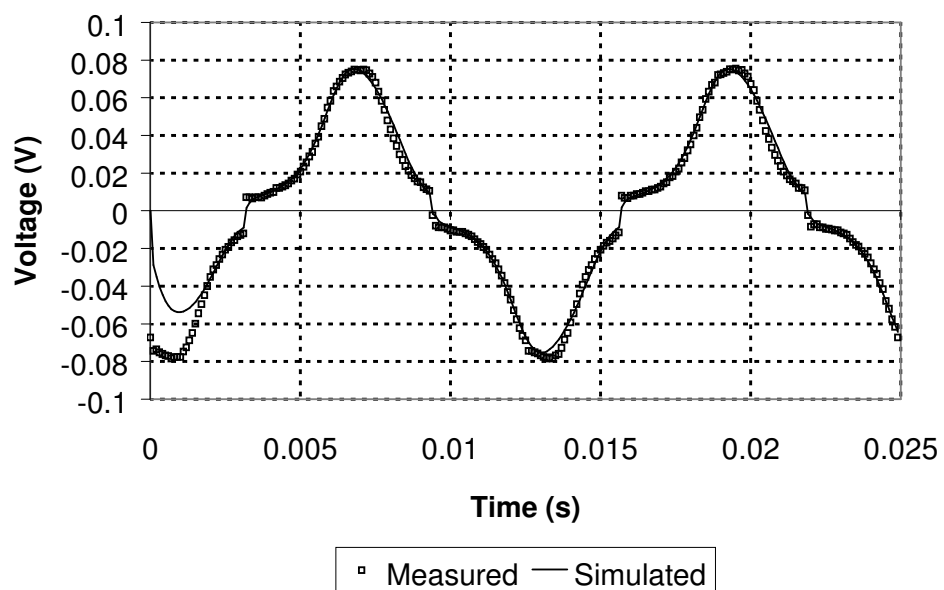


**Figure 9.21: Measured and Simulated Transformer Secondary Voltage at 27ºC**

154
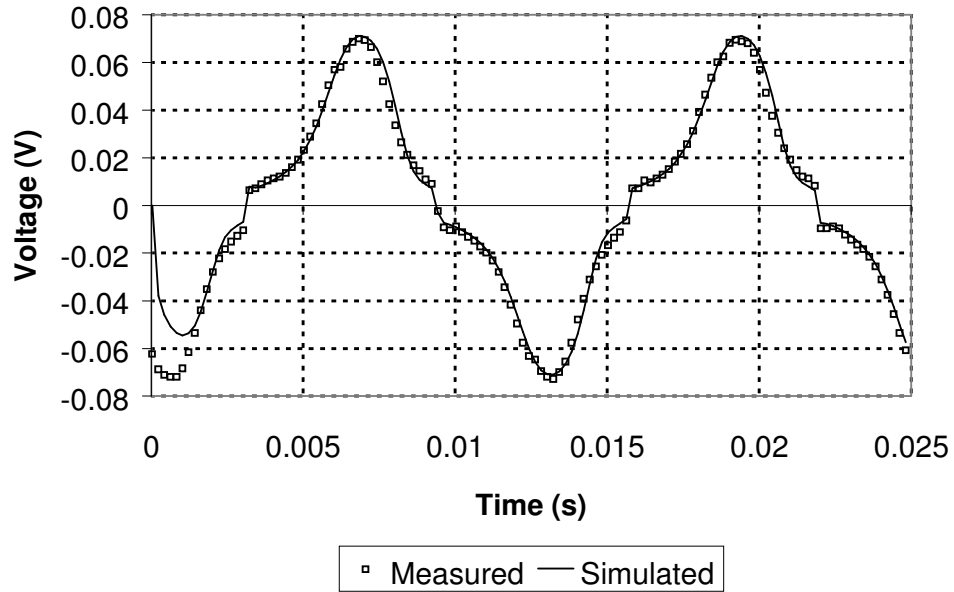
**Figure 9.22: Measured and Simulated Transformer Secondary Voltage at 70ºC**

## 9.4.2   Self-Heating and Dynamic Magnetic-Thermal Testing

With the static results showing a good correlation between measured and simulated results at a variety of environmental temperatures, the core temperature was measured and simulated due to the self heating of the core itself. For the TN10-3F3 core, a simulated temperature rise of 3.5ºC corresponded well with a measured rise of 3.2ºC. Measurements on a range of core types showed a thermal time constant in seconds making full real-time simulations time-consuming and memory intensive. The results of the overall temperature rise measurements and simulations are given in table 9.1. By reducing the thermal capacitance in the thermal model, the simulation times could be reduced but still keeping the overall temperature changes correct.  An RM12 core was used to investigate the accuracy of the approach for a more complex core type.

| Core | Material | Frequency | Measured Temperature Change (ºC) | Simulated Temperature Change (ºC) |
|------|----------|-----------|----------------------------------|-----------------------------------|
| TN10/6/4 | 3F3 | 1KHz | 3.2 | 3.5 |
| RM12 | 3F3 | 10KHz | 30.5 | 34.4 |

**Table 9.1: Measured and Simulated Temperature Rises**

### 9.4.3  Simulation of Dynamic Magnetic Material Behaviour

Investigation of the self-heating behaviour of components using measurements demonstrated a significant time for thermal changes to take place, in the order of several seconds using the test waveforms described previously.  To show the transition of the material behaviour as the temperature increases, it is valid to reduce the time constant in the thermal circuit by reducing the value of the thermal capacitance. Using this approach it is possible to observe the dynamic behaviour of the flux in the core as the temperature increases (with the time axis effectively scaled by the reduction of the thermal capacitance). This allows reasonable simulation times to be achieved without significant loss of overall accuracy. An example of this is the variation of flux density as the core heats up (as shown in figure 28). In this case the simulated results of the RM12 core show a reduction in the peak flux density of 10%, which is consistent with measured values. The advantage of the simulation is the ability to observe the dynamic behaviour, which is difficult to see on a real-time measurement.
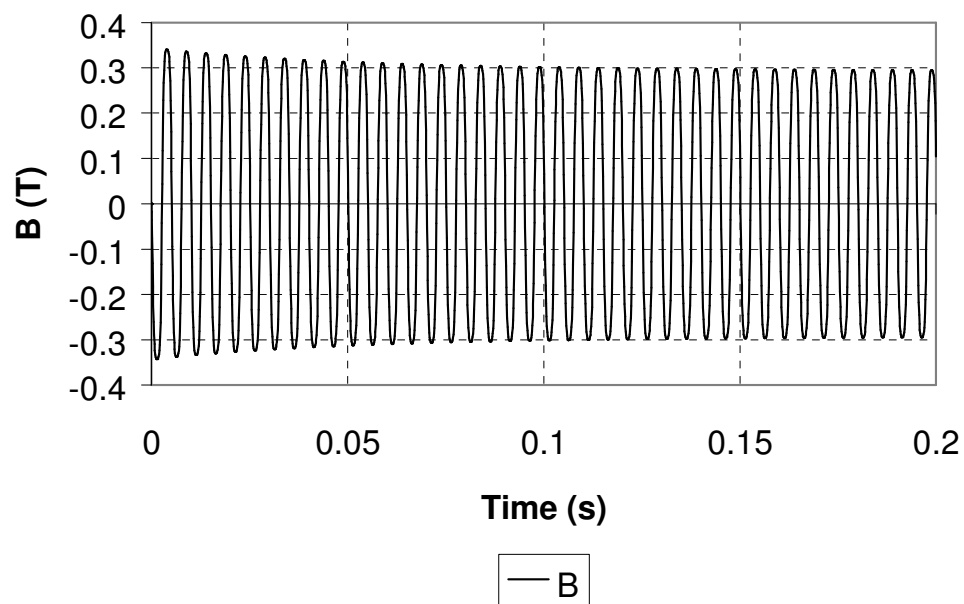


**Figure 9.23. : Variation of B with time as Core Temperature Increases**

The core surface temperature can also be observed in the same context as the flux density variation using this time-scaling approach.  Fig. 9.24 shows the core surface temperature rise for the RM12 core, with the time constant reduced by a factor of 10000.
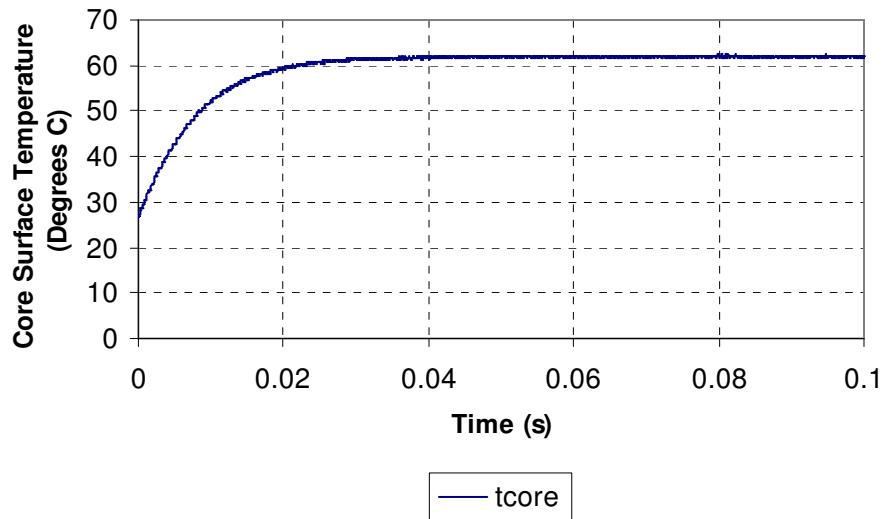
**Figure 9.24: Core Surface Temperature Rise for insulated core**

### *9.5  Conclusions*

### 9.5.1   Overall Conclusions

This chapter demonstrates how self-heating and dynamic thermal effects can be implemented in magnetic component models for application in circuit simulators. Modeling methods have been presented to show how the Jiles-Atherton hysteresis model can be made temperature dependent and characterized. Lumped element models of thermal components were derived, and these were used to accurately model the thermal aspects of the core material and its effect on both the magnetic and electrical behaviour. Good correlation between the simulated and measured results of the magnetic component in the electrical, magnetic and thermal domains has been observed, for static and dynamic temperature variations. Analysis of the methods for the calculation of power losses in magnetic materials has highlighted the need for care in the assumption of the behaviour of energy losses in magnetic materials, particularly when applied to circuit simulation.

### 9.5.2   Validity of the model

The model in its present form has only been tested for sinusoidal waveforms at low frequencies (<10kHz). Although the model is theoretically valid for arbitrary waveforms and higher frequencies, these have not been tested thus far, and will be the subject of future work.

### 9.5.3   Simulation Issues

This work has raised issues with simulating this type of mixed-domain system, the most important of these being large differences in time constants. If simulations are carried out over long periods, then it is possible for cumulative accuracy to be very poor. This chapter has highlighted this issue and demonstrated that by judiciously reducing the thermal time constants, reasonable predictions of the overall performance can be obtained.

157

*Chapter 10*

# 10 Modeling a Passive Fault Current Limiter

## *10.1 Background to Passive Fault Current Limiting*

The development of Passive Fault Current Limiting devices (FCL) for the protection of electronic systems has been required due to the increase in load growth in conjunction with a requirement for increased reliability.  The basic technique uses a magnetic core that has been magnetically offset such that the material is fully saturated. When a winding around this core is connected as an inductor in series with a line as shown in figure 10.1, the inductance (and hence the impedance) is small and so the line current is allowed to pass through unhindered. If the current reaches a level high enough to bring the core material out of saturation, then the inductance will increase dramatically and block the current, thus providing current limiting.
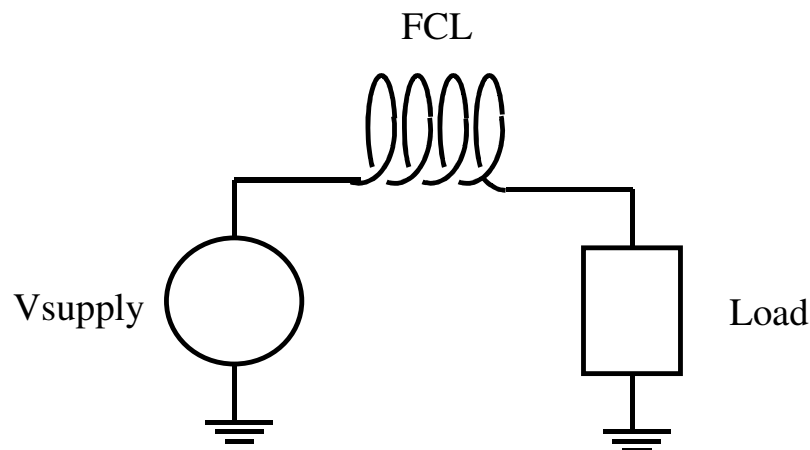


**Figure 10.1 : Basic Passive Fault Current Limiter**

The regions of low and high permeability are illustrated by Figure 10.2, which shows how the inductance increases as the current deviates from its nominal operating condition in the low permeability region. One aspect of this type of approach is that if the Limiter is magnetically offset, then it can only limit the current deviations in one direction. To achieve bi-polar current limiting requires two of these devices in series, with the opposite magnetic offset.
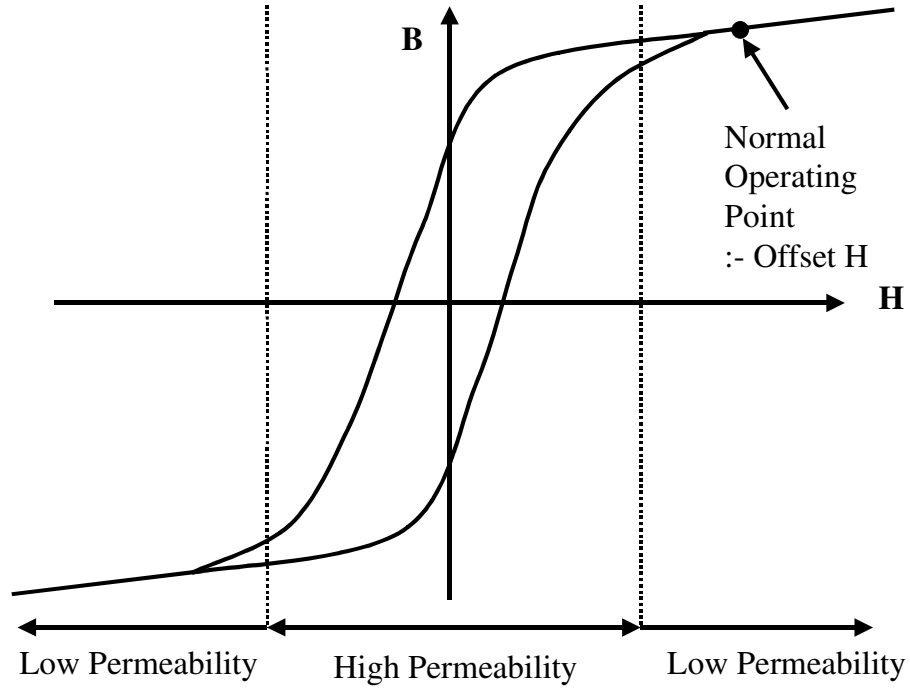
**Figure 10.2: Fault Current Limiter Operating Regions**

It is clear from figures 10.1 and 10.2 that if accurate models for the core material behaviour could be obtained, then reliable predictions about the performance of the Passive Fault Current Limiter could be achieved.

A variety of techniques exist to accomplish the protection with the overall requirements for such systems discussed in [220]. The literature has extensive discussion of the range of approaches including Microprocessor control [219], an Electromagnetic method [212], Direct Cooled Tubular Element [213], a tuned LC circuit [218] and numerous papers investigating the use of superconductors including [214]-[216]. These techniques all suffer to some extent from being complicated, expensive and difficult to implement. The use of permanent magnets to provide a cheap and simple alternative approach for magnetic offset in inductors has been developed by Mukhopadhyay *et al* [210], Dawson, Yamada and Iwahara [211], with specific tableau numerical methods introduced by Iwahara and Miyazawa [217]. The permanent magnet approach has potential merit due to the low cost, simple construction and potentially good transition characteristics to and from the fault region of operation. The previous work by Mukhopadhyay *et al* has modeled these devices using a simple piece wise linear (PWL) approximation of the non-linear behaviour of the core material, however the comparison of simulated with measured results has been quantitatively deficient. The authors themselves make no claims in this regard with both the overall current limiting effect subject to large tolerances, and the comparison between measured and simulated curves shows significant differences.

## 10.2 Modeling Philosophy

In this chapter of the thesis, the magnetic material and component modeling techniques previously developed are applied to provide a much more accurate representation of the passive Fault Current Limiter behaviour. The modeling was approached from a mixed-domain point of view, using a Jiles-Atherton magnetic material model including hysteresis and power loss. By modeling the hysteresis of the core material, the limit and recovery cycle can be predicted more accurately than previously obtained using the simple PWL approach. Measured and Simulated results were obtained for FCL components using an exter permanent magnet Aspects of the FCL component are discussed including eddy currents, and the behaviour of the permanent magnet.

## 10.3 Proposed Passive Fault Current Limiter Model

The basic idea of the passive fault current limiter proposed in [210] is to use a magnetic core with a permanent magnet inserted in the gap between the core halves to provide a magnetic offset. The physical configuration for an E type core is shown in figure 10.3.
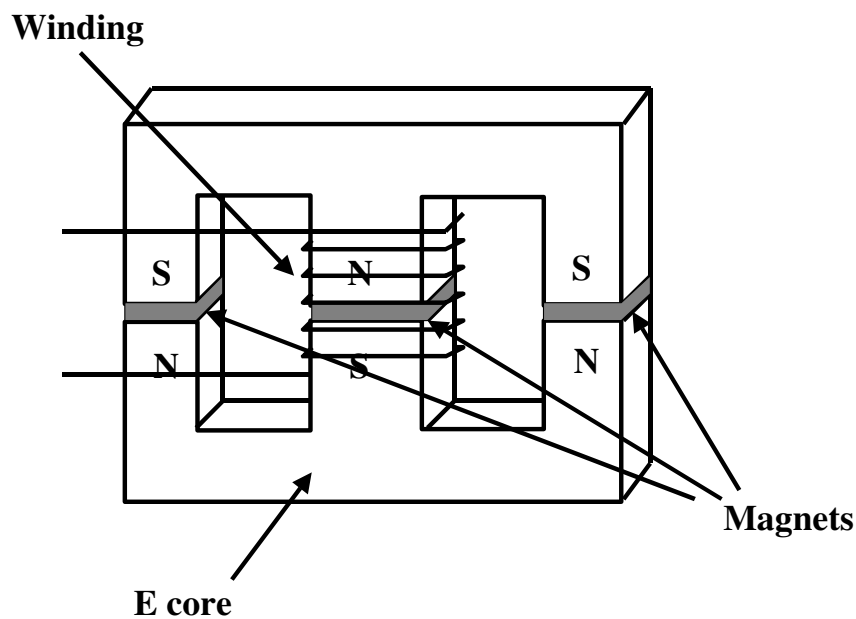


**Figure 10.3 : Passive Fault Current Limiter Physical Configuration**

To model this type of component using a behavioural model requires three main elements, the non-linear magnetic core, the winding and the magnets. We can simplify this physical model into the three primary elements as shown in figure 10.4.
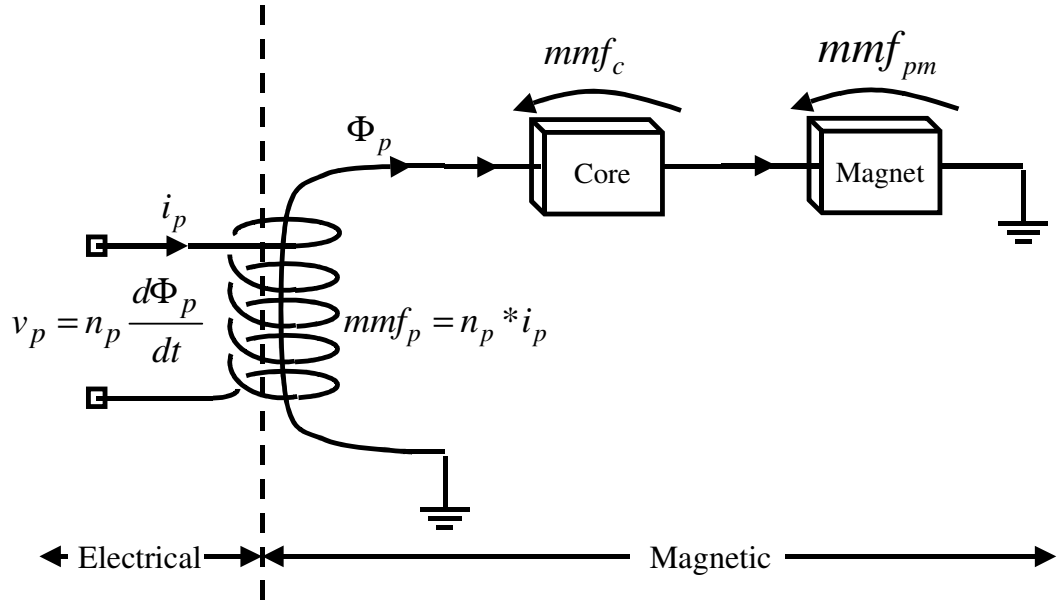
**Figure 10.4 : Proposed Model Structure**

The model structure shows how we model the FCL using the electrical and magnetic domains. The advantage of this approach is that we can see in the simulation results how the flux and mmf behaviour compares with the measured FCL directly. The non-linear core model is based on the Jiles-Atherton approach previously described in this thesis, and the winding model is again the same as has been used previously. Modeling permanent magnets can be achieved using a simple magnetic offset model of the form shown in figure 10.5
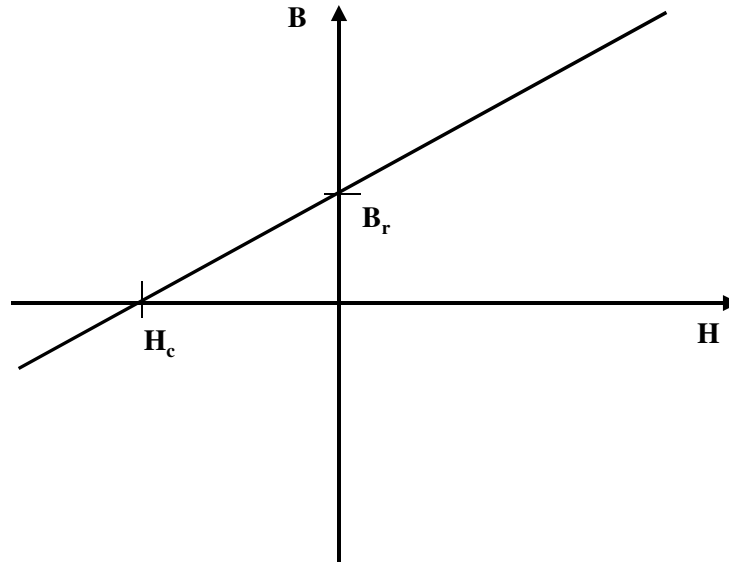


**Figure 10.5 : Basic Permanent Magnet Model**

Using this method a simple linear reluctance model, with a d.c. MMF source of -Hc will give the required behaviour. The model used in this work is given in figure 10.6, showing how the effective magnetic field strength He, is calculated internally to the model.

```
.SUBCKT pmagnet   1     2 PARAMS: UR=1000 HC=-100
+ AREA=10e-6 LEN=10e-3
E1    B     0      VALUE={V(HE)*(12.8e-7*UR)}
E2    MMF   0      VALUE={V(1,2)}
E3    H     0      VALUE={V(MMF)/LEN}
E4    FLUX  0      VALUE={V(B)*AREA}
E5    HE    0      VALUE={V(H)-HC}
G1    1     2      FLUX  0     1
.ENDS
```

**Figure 10.6 : Linear Permanent Magnet Model**

Of course, permanent magnets have a non-linear behaviour just like any other magnetic material and if necessary a more accurate representation of the demagnetization curve of the material can be implemented as shown in figure 10.7.
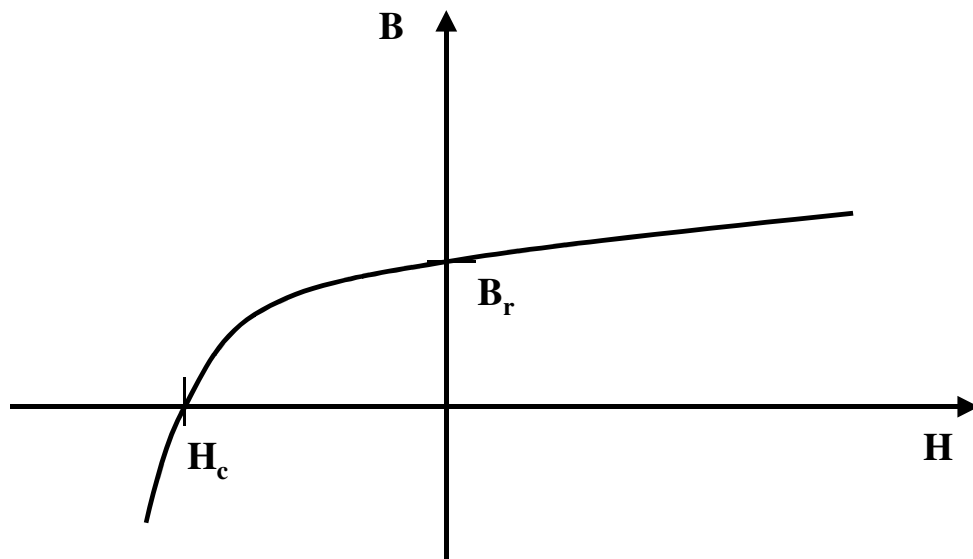


**Figure 10.7 : Permanent Magnet Demagnetization Curve**

In order to characterize this behaviour, a langevin function was used, with an H axis offset added to provide this behaviour. The listing of this model is given in figure 10.8.

```
.SUBCKT pmlang    1     2 PARAMS: UR=40 HC=300k BR=1.1 A=10
+ AREA=10e-6 LEN=10e-3
E1    B     0      VALUE={(1+V(BEFF))*(IF(ABS(V(HE))>1e-
3,1/TANH(V(HE)/A)-A/V(HE),0.333*V(HE)/A))}
E2    MMF   0      VALUE={V(1,2)}
E3    H     0      VALUE={V(MMF)/LEN}
E4    FLUX  0      VALUE={V(B)*AREA}
E5    HE    0      VALUE={V(H)-HC}
E6    BEFF  0      VALUE={ABS(V(HE))*UR*12.58E-6}
```

162

```
G1      1      2      FLUX   0      1
.ENDS
```

**Figure 10.8: Permanent Magnet Model based on the Langevin Function**

These approaches are fine for most cases, and were used successfully in this project, but in fact the magnet behaviour shown thus far is just a small section of an overall BH hysteresis loop which can be modeled using standard models such as Jiles-Atherton. This becomes important when the effect of magnet recoil is relevant to the behaviour of the device. Figure 10.9 illustrates this aspect of the magnet's behaviour. As the magnet is demagnetized (Path AB), if the applied field strength changes direction, then the magnet does not return back the same way, but traverses the BH loop across to the other side directly (Path BC and then to D). Thus the effective permeability is the same, but the flux density is much lower.
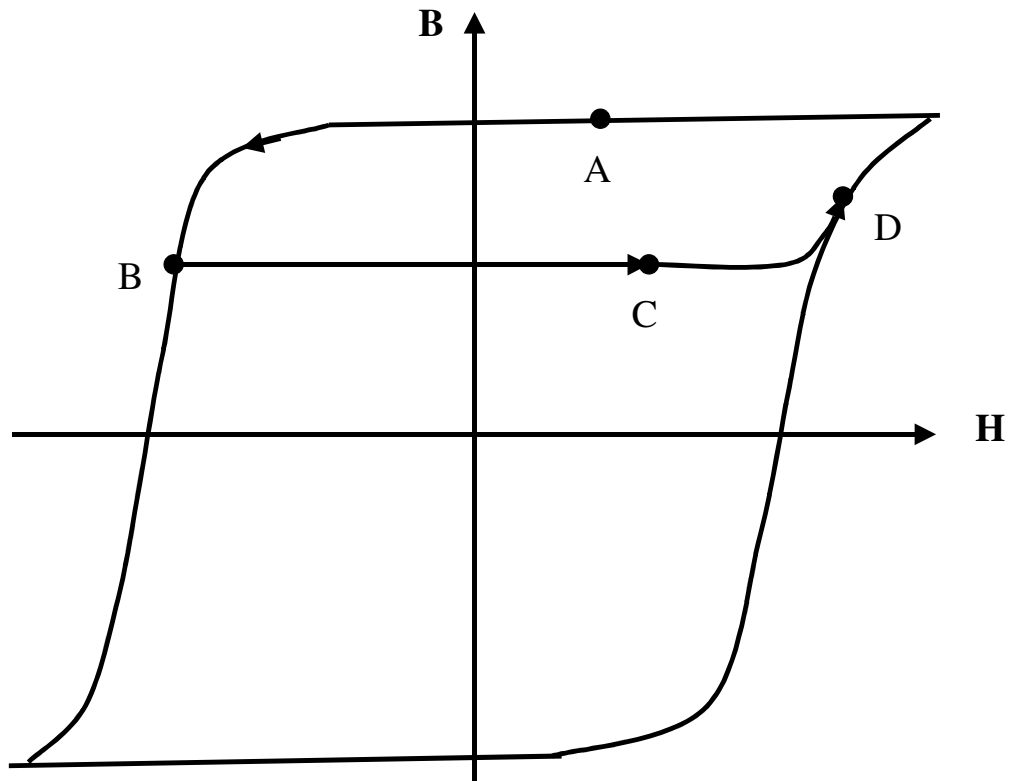
**Figure 10.9 : Illustration of Magnetic Recoil Trajectory**

Implementing a very wide square loop of the kind shown in figure 10.9 using the standard Jiles-Atherton model is not easy, as the equations are not designed for a Coercive Force of 10e6 At/m, and will become very unstable. To improve the robustness of the model therefore, the effective field strength was scaled in the magnet model by a large factor (e.g. 1e5 At/m) to keep the model within a sensible numerical region.

With the range of models defined from a simple linear magnetic offset to more complex non-linear and hysteresis approaches, the application can be modeled with the required level of accuracy. As

a benchmark and comparison, a single offset winding was added to the same core material to provide an alternative modeling representation. This was then compared, both with measured and simulated results, to establish the relative merits of the models used in each case.

## 10.4  Fault Current Limiter Using A Permanent Magnet Offset

### 10.4.1  Introduction

In this section a practical Permanent Magnet FCL was constructed, tested and the results compared with the simulation model.

### 10.4.2  Circuit Design

Using the averaged BH curve and corresponding Impedance curve in figure 10.10, the characteristics of the FCL can be designed.
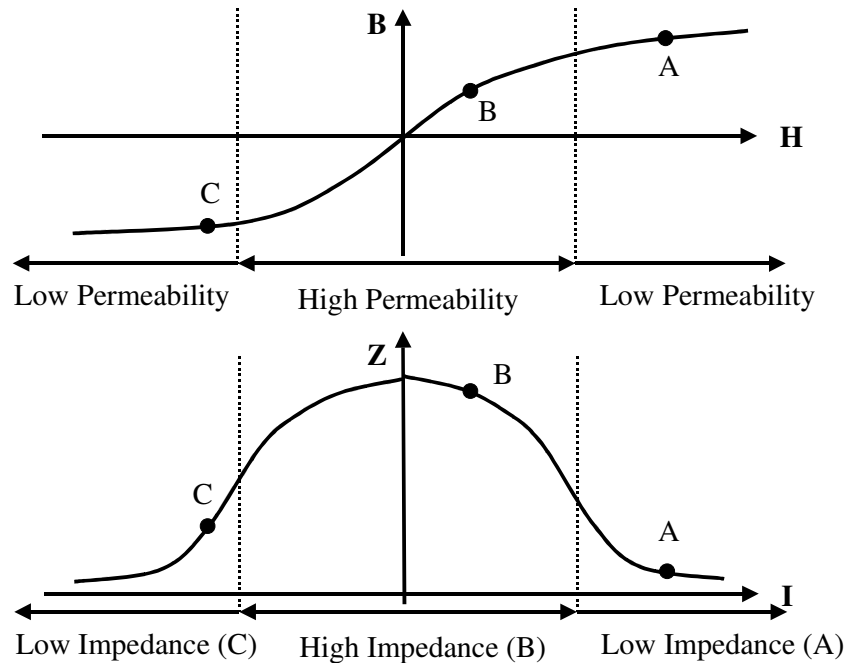


**Figure 10.10: FCL Averaged BH and Impedance Curves**

If the nominal operating point is at A, then it can be seen that the slope of the BH curve is low, therefore the corresponding impedance at A is also low. This is the normal operating condition and the FCL does not limit the current. If the current is perturbed around this point, for small values of current perturbation there will be no impact on the waveform due to the FCL. If the current perturbation increases, however, to the extent that point B is reached, then the slope of the BH curve increases as does the impedance. This is the region (B) in which the impedance of the FCL causes limiting of the current. If the current continues to rise, despite the efforts of the FCL, and continues further into region C, the magnetic core will go back into saturation, with the result that the BH slope decreases, as does the impedance of the FCL. It is also clear from these graphs that to

164

obtain bi-polar current limiting, two of these devices need to be placed in series, with opposite magnetic offsets.

The basic design methodology uses the basic inductance equation given in (10.1).

$$L = \frac{\mu_0 \mu_r N^2 A}{l} \qquad (10.1)$$

Where A is the cross sectional area of the core, l is the effective magnetic path length, N is the number of turns, $\mu_0$ is the permeability of free space, and $\mu_r$ is the relative permeability of the core material. When the material is in saturation (i.e. normal operation) the relative permeability is much lower, hence a lower inductance and impedance results than for the fault condition.

### 10.4.3 Construction and Measurement Configuration

The choice of a toroidal core type was made for a number of reasons. Primarily, the need to keep the modeling structure as simple as possible to reduce the probability of errors due to the complexity of the structure of say, a multiple section E core. This also allows simple analytical calculations to be carried out, estimating magnetic path lengths, and keeps the cross sectional area of the magnetic flux path constant. The choice of magnet also enables the flux path area to be the same shape and area as that of both the core and the magnet, reducing the errors introduced by fringing and leakage fluxes.

By reducing the complexity of the core/magnet combination to a toroid, the number of air gaps and magnets is also reduced, thus increasing the confidence in the model and simulation results. The prediction of the model parameters is also made simpler by this design decision.

The FCL design layout used in this chapter is shown in figure 10.11. The core was based on a Philips 23/14/7 toroid, made of the 3F3 material. A 1mm gap was cut in the toroid, as shown in figure 10.11, enabling the magnet (1mm thick) to fit exactly into the gap.
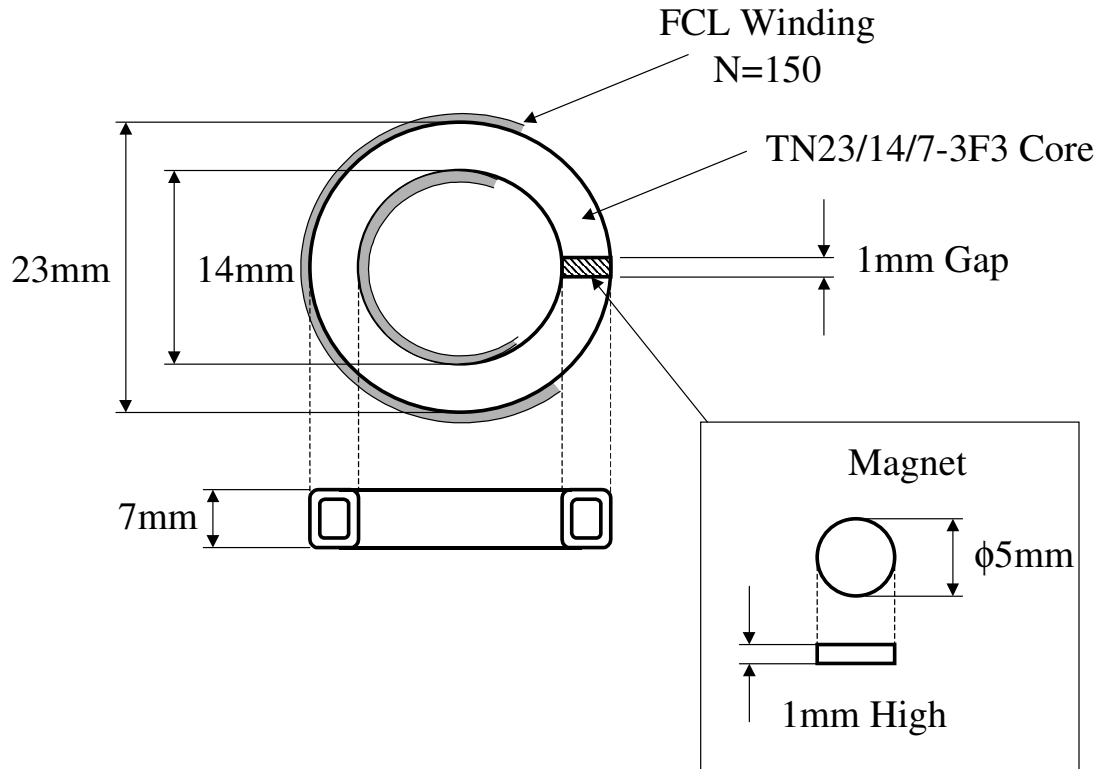
**Figure 10.11 : FCL Based on TN29/19/17.6-3F3 Toroid**

The toroid was wound with 150 turns, cross sectional area of 30.9mm$^2$, magnetic path length 55.8mm. The effective inductance was measured with and without the magnet in place. The magnet used was a NdFeB permanent magnet, 5mm diameter and 1mm thick.

A secondary winding was wound around the outside to monitor the voltage across the toroid for the purposes of BH curve estimation (in all the measurement graphs, the initial Flux Density, *B*, has been assumed to be 0T, although in practice it will be a non-zero value. It is not possible from the voltage measurements alone to calculate any steady state initial flux conditions, unless the full start up transients are taken into the calculation). A current sense resistor was used in series with the winding to derive the current through the FCL inductor, and the line voltage from the source was also measured.

### 10.4.4 Measurement Results

To test the basic behaviour of the FCL, a current sense resistor doubling as a load of 10Ω was used in series with the toroidal FCL. The secondary winding of 100 turns was used to measure the voltage and derive the flux density through the core. Using this configuration, a line voltage was applied to the FCL & Load combination, with the amplitude gradually increased until the FCL began to limit the line voltage and the frequency set to 100Hz. With low levels of voltage, the line current and sensed voltage across the FCL are nearly sinusoidal as shown in figure 10.12. This

indicates that the FCL is operating in the saturated (linear) region, and has minimal effect on the waveform shape of the line voltage. This is confirmed when the Flux Density (*B*) and Magnetic Field Strength (*H*) in the core are calculated, the resulting BH curve is shown in figure 10.13. This shows that the permeability is effectively constant.
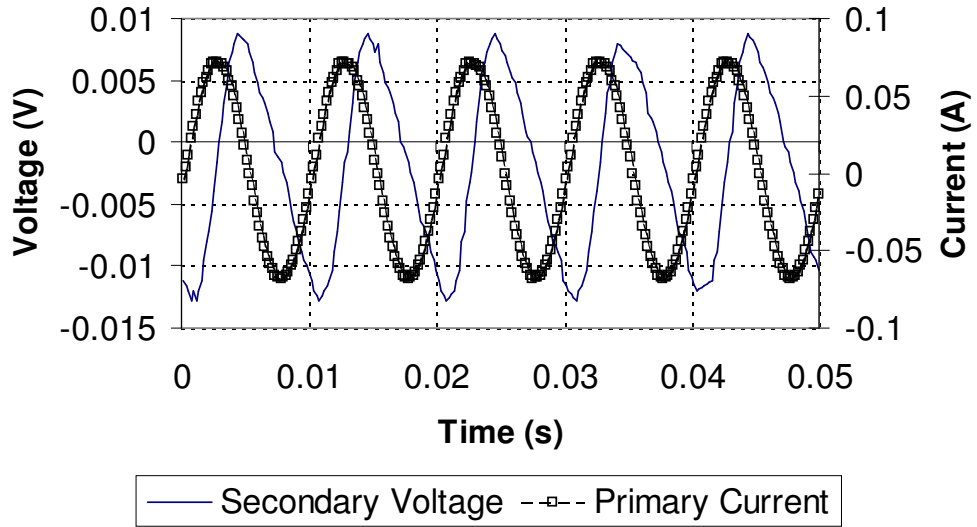


**Figure 10.12: FCL Sensed Line Current and Secondary Voltage**
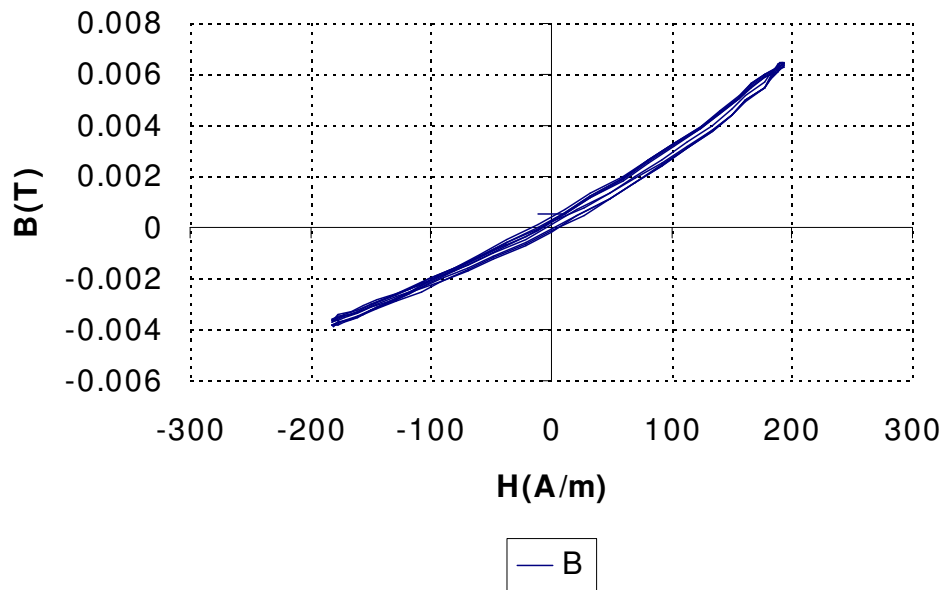


**Figure 10.13: BH Curve derived from FCL operation under nominal load conditions**

As the line voltage increases, or the load resistance is reduced to simulate the effect of a fault condition, the deviation of the current will push the core material out of saturation and cause a distortion of the line current, and provide effective fault current limiting. Using the same test configuration, the line voltage was increased, with the resulting line current and sensed voltage waveforms obtained in figure 10.14.
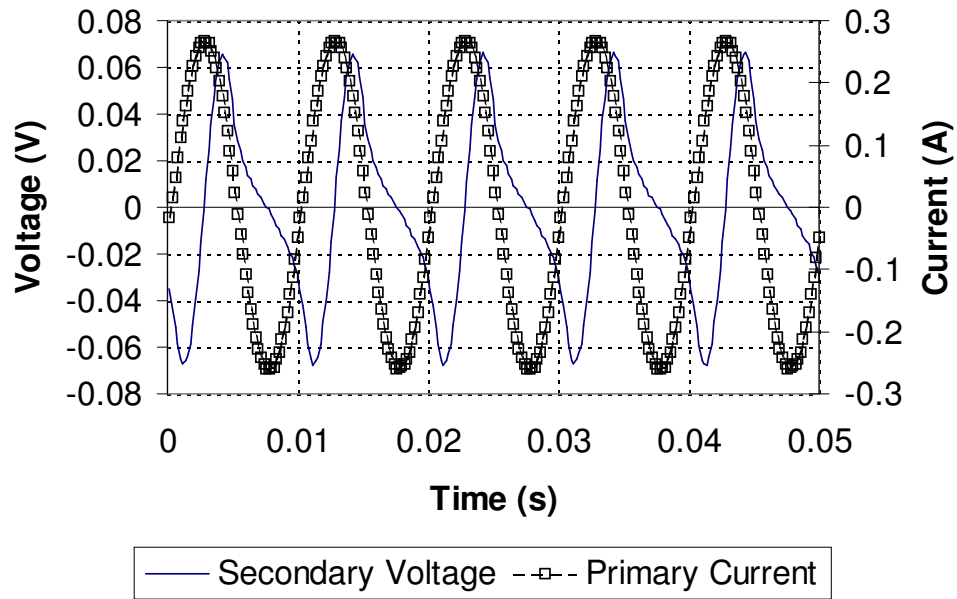
**Figure 10.14: FCL Sensed Line Current and Secondary Monitor Voltage Waveforms**

As can be seen from Figure 10.14, during the positive half cycle of the line current, there is a phase shift of the voltage, but no significant distortion, however, during the negative half cycle, the sensed voltage is limited and is due to the magnetic material coming out of saturation. This is clearly seen in figure 10.15, which shows the BH curve of the magnetic material under the same load and line conditions.
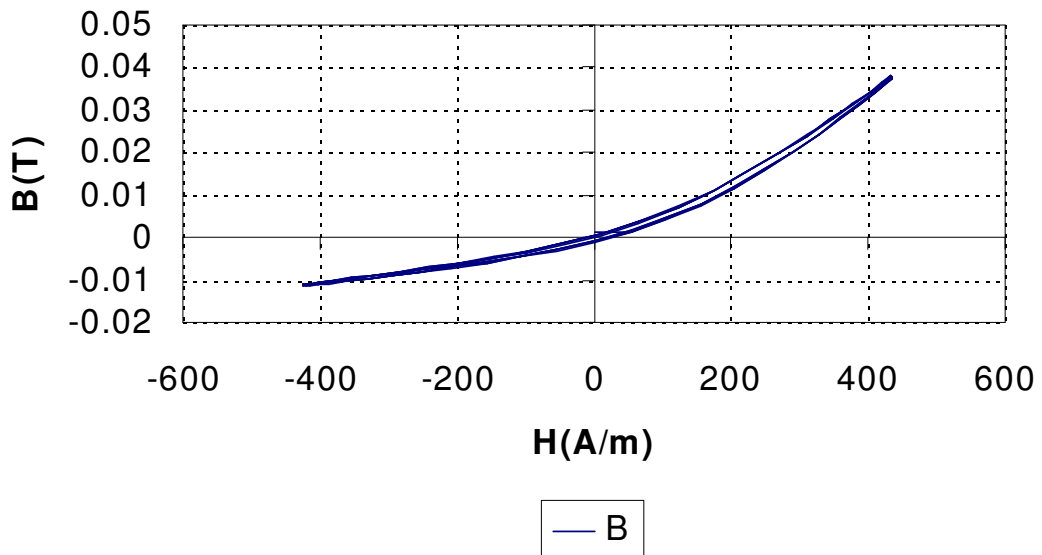


**Figure 10.15: BH Curve for FCL under increased Line Voltage Conditions**

It is noticeable that the graph is no longer nearly, linear, and that the area of the BH curve is beginning to become visible, i.e. the core is moving into hysteresis.

The load was then reduced to 0.5Ω, resulting in a simulation of a fault condition, such as a short across the line. When the BH curve is plotted under these conditions, the hysteresis behaviour becomes pronounced as shown in figure 10.16. The frequency of the line voltage was reduced to 5Hz to reduce eddy currents in the magnet (and the resulting self-heating).
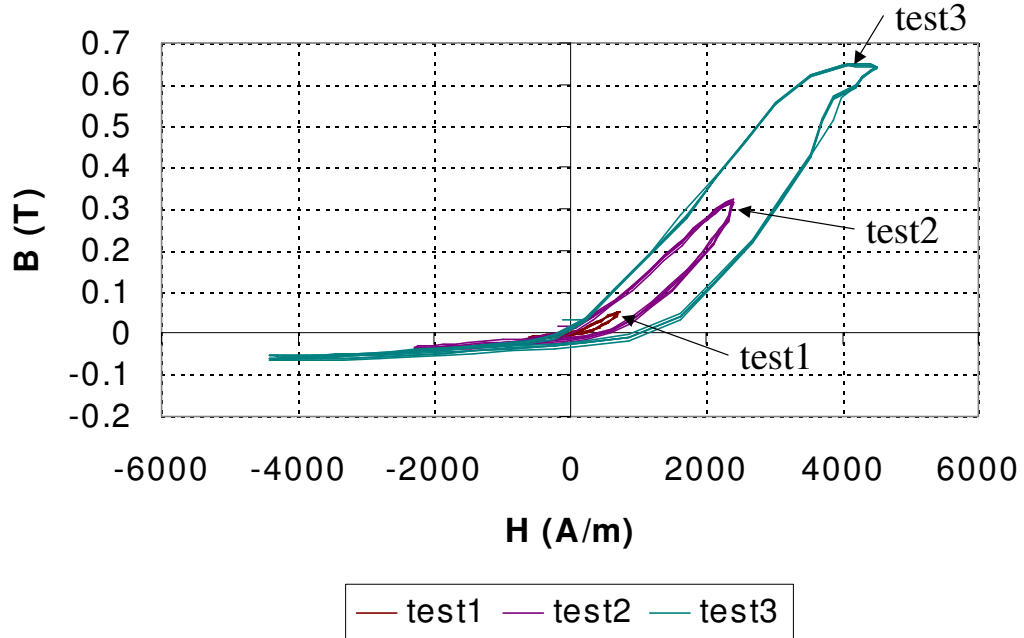


**Figure 10.16: FCL BH Curve under Fault Conditions (Load = 0.5Ω)**

Figure 10.16 illustrates one of the reasons why using a simple PWL model of the magnetic core is not adequate for predicting the behaviour of a practical FCL. The hysteresis behaviour defines the loss in the component, and also directly influences the voltage and current waveforms in the limiter. By implementing a model with this behaviour, a potentially highly accurate model may result.

### 10.4.5 Model Implementation and comparison between simulated and measured results

In order to model the fault current limiter used to obtain the measurements, the structure previously described in figure 10.4 was used. A non-linear model of the magnetic core material (3F3) was used, characterized using the techniques described previously in this thesis. This was then combined with a simple linear model of the permanent magnet in the first instance and the measured line voltage was used as the stimulus to allow a direct comparison with the measured results. The BH curve shown in figure 10.17 shows the comparison between the BH curves and the measured and simulated flux densities (*Bmeas* and *Bsim* respectively) are shown plotted against time in figure 10.18. In both cases an offset was added to the derived, measured flux density (Bmeas) for easy comparison with the simulated equivalent.
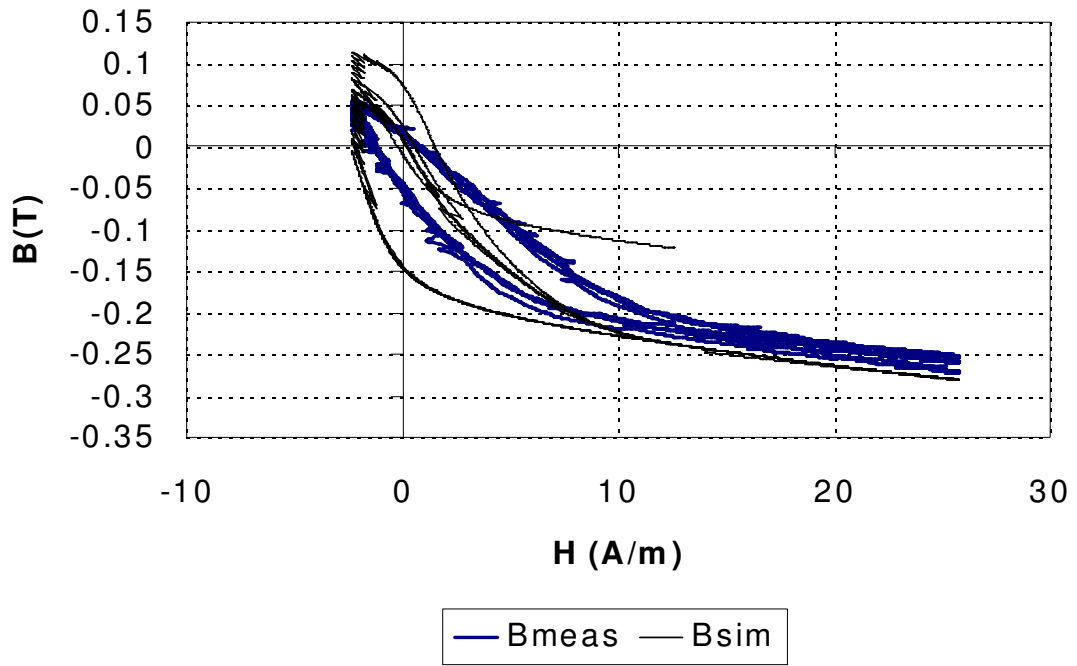
**Figure 10.17: Measured and Simulated BH Curves**
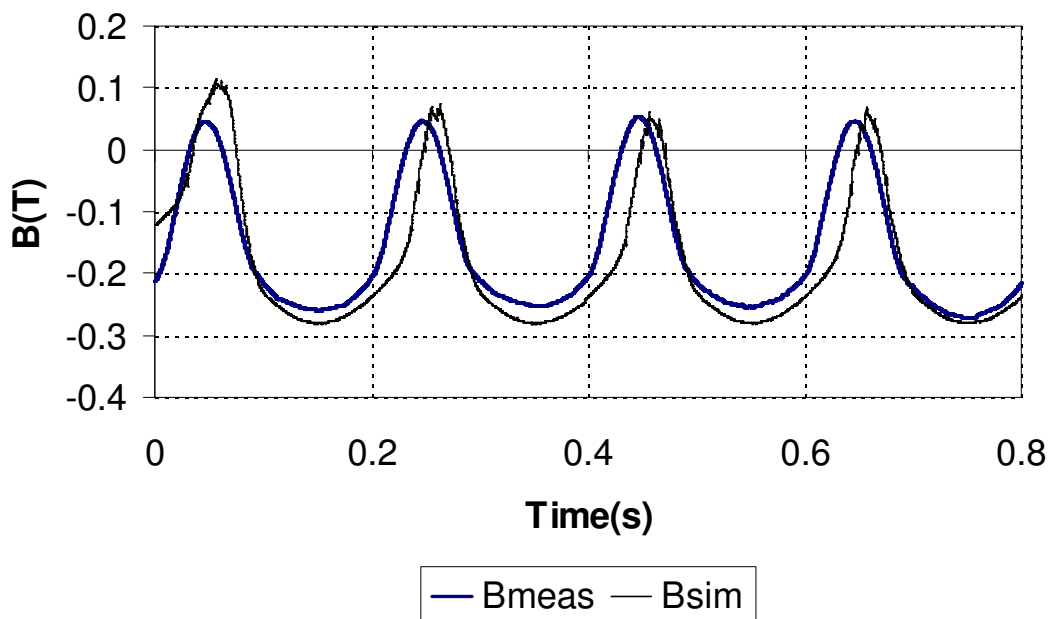


**Figure 10.18: Measured and Simulated Flux Densities**

It is clear that despite accurate material modeling of the 3F3 material, and a simple configuration, there were some problems with the results. Looking at the BH curves, it is clear that the simulated BH curve is fatter and steeper than the measured equivalent. This seems to indicate an aspect of the FCL behaviour not considered in the model. When the time domain plot in figure 10.18 is observed, it appears that there also may be a phase shift introduced that is not included in the model.

170

The material model characterization software was therefore modified to allow the charaterization of the Jiles-Atherton model in combination with a permanent magnet offset. Tests using this approach improve the matching of the BH curve, but the phase difference in the time domain remains.

## 10.5 Magnet Model Modification

The magnet model was modified using the model structure shown in figure 10.19. This extends the basic linear model of a reluctance in series with a magnetic field strength (H) offset in the magnetic domain, by including a magnetic capacitor element across the reluctance of the magnet. This combination gives a dependence of the magnetic reluctance with frequency, that can provide a phase shift commensurate with the measured data.
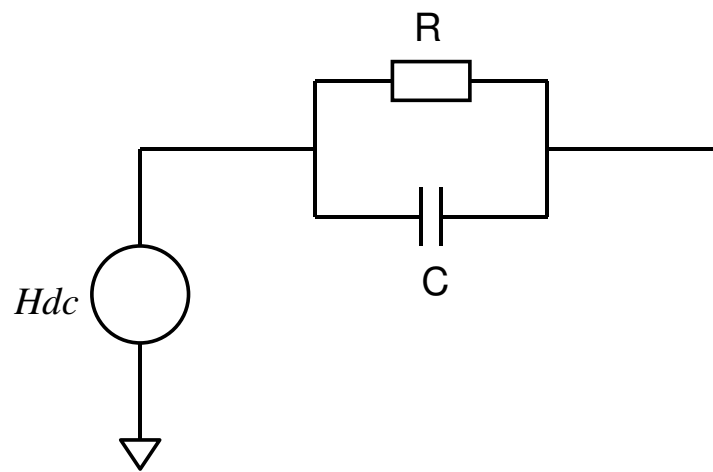


**Figure 10.19 : Modified Magnet Model with Frequency Dependent Reluctance**

Using this modified model, with a reluctance of 100k, and a magnetic capacitance of 0.5u, the phase shift error was corrected as shown in figure 10.20. These values were obtained by optimizing the reluctance and capacitance values using iterative simulations in SPICE.

Using this modification is clearly non-physical, as a magnetic 'capacitance' is a pure energy source, but it is a simple method of improving the phase behaviour of the model compared to the measured results. It is clearly a weakness of the existing magnet models that needs to be addressed, and could be the subject of future work.
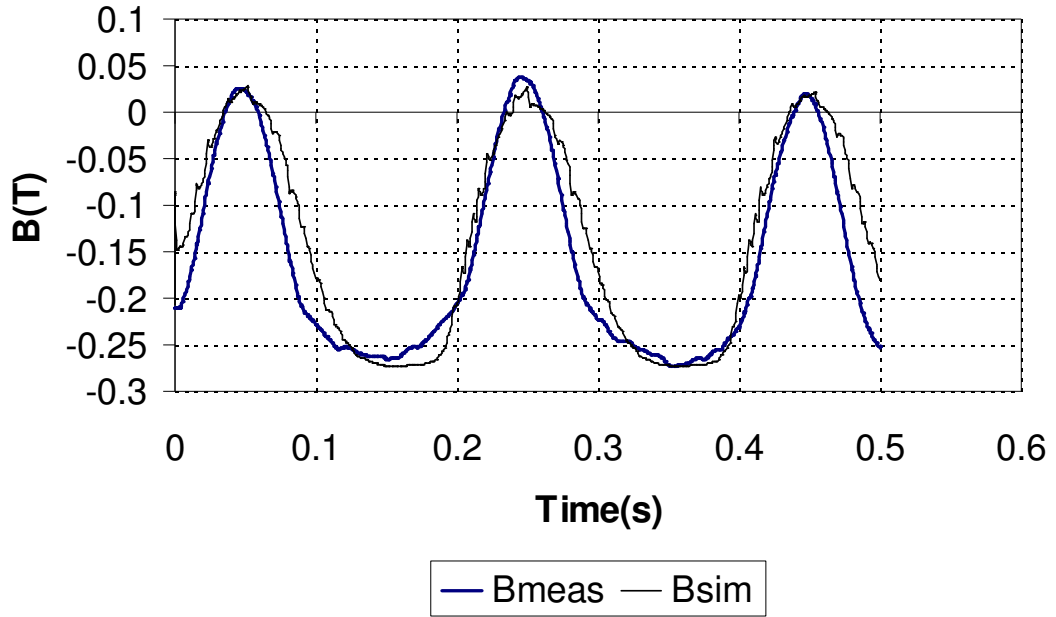
**Figure 10.20: Flux Density of the FCL with corrected phase shift.**

## 10.6 Conclusions

The results obtained of the behaviour of the fault current limiting inductor using a non-linear Jiles-Atherton core model have shown that by using a true hysteresis model, the BH trajectory of the FCL can be predicted using simulation and matched closely to the physical device under fault and nominal conditions. With reference to the previous work in [210] and [211], one of the deficiencies with the models used was the lack of true hysteresis behaviour, leading to discrepancies between the simulated and measured results – showing up as asymmetry in the line voltage and current waveforms. The authors did not explain these discrepancies, but it is clear from BH curves in the tests carried out in this chapter that such asymmetry could result from hysteresis in the magnetic core material.

By using a mixed-technology approach to modeling the magnetic elements in the FCL, this aspect of the component can be modeled more accurately, and allows a higher level of confidence in the design of the FCL.

It is worth noting that if an external winding is used to provide the magnetic offset, rather than a permanent magnet, some of these problems in the FCL design are eliminated immediately, and the modeling process becomes relatively straightforward.

## 10.7 Potential for further work

The modeling effort has primarily concentrated on the magnetic core material behaviour, while using a fairly simple linear magnet model. The FCL design in this chapter was also primarily for

172

use at low frequencies (<100Hz), and modeling of eddy currents in the magnet has been neglected. Despite these omissions, the results have had adequate accuracy for this application.

Experimental work previously carried out at higher frequencies, however, has highlighted the potential problems of eddy currents in the magnet, to the extent of thermal demagnetisation occurring. Useful future work could therefore be carried out in this area, extending the magnet model to include the hysteresis model described in the introduction of this chapter, and using eddy current models also previously described in this thesis.

## *Chapter 11*

# 11 Modeling broadband ADSL transformers

## *11.1 Introduction*

As a design application, the ADSL broadband line transformer offers interesting challenges somewhat different to those in Power Supply design. In this chapter the primary issues for designing ADSL line transformers are addressed, modeling techniques applied and several design techniques investigated. Simulation is used to predict key performance criteria of the transformer component, such as Total Harmonic Distortion, Insertion Loss, Inter Modulation Distortion and Trans Hybrid Loss. Finally, simulations are carried out on example ADSL hybrids investigating the effect of the transformer on hybrid performance and demonstrating the potential of modeling and simulation for predicting hybrid performance in the application area.

## *11.2 Introduction to ADSL*

Asymmetric Digital Subscriber Line (ADSL) technology is used as a high-speed modem link with asymmetric up- and down-stream data rates as the name suggests. The current primary application is for very high-speed internet access, but the goal of the technology is not restricted to purely internet applications, but also video-streaming (for commercial video-on-demand), fast data transfer, and fully integrated network services for companies and home use.

A significant differentiator between ADSL and current cable television access is the ability to utilise the existing infrastructure (i.e. copper twisted-pair wires) of the telephone network. Figure 11.1 shows the outline of a typical network configuration, with a Central Office (CO) connection at the service provider, and a number of remote Customer Premises Equipment (CPE) installations.
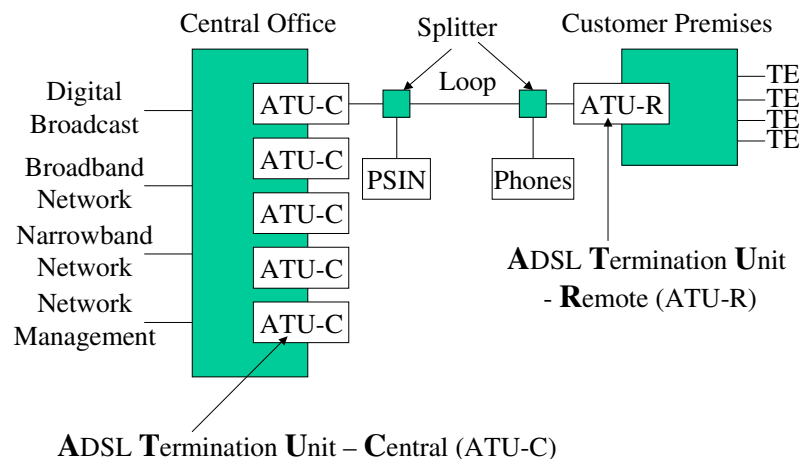


**Figure 11.1: ADSL Network Configuration Outline**

ADSL has proved a significant step in the development of Digital Subscriber Line (DSL) technology, as it has probably the best defined standard (IEEE T1.413-1995 [223]) that is actually implemented de facto in the telecommunications industry, by both service providers and chip manufacturers alike. Bingham [224], Cioffi [225] describe the development of the philosophy for ADSL and similar broadband approaches and Goralski [226] or Chen [227] provide background to the technology area to high-speed communications. It is beyond the scope of this thesis to go into detail of the mechanism of the ADSL system, but it is necessary to describe some details of the transmission scheme and the analogue interface to understand the requirements for hybrid line transformers.

ADSL is based on a broadband modulation scheme, with multiple carriers placed at 4.3125kHz intervals. With 256 carriers a 1.1MHz bandwidth is required. These sub-carriers may also be referred to as sub-channels. Figure 11.2 shows how the bandwidth is divided into areas for the standard telephone communications (POTS), up-stream and down-stream bandwidth. In figure 11.2, with the distinct gap in the bandwidth between the up- and down-streams, there is no requirement for echo cancellation. If echo cancellation is used, then a more efficient use of the bandwidth occurs where the up- and down-streams overlap.
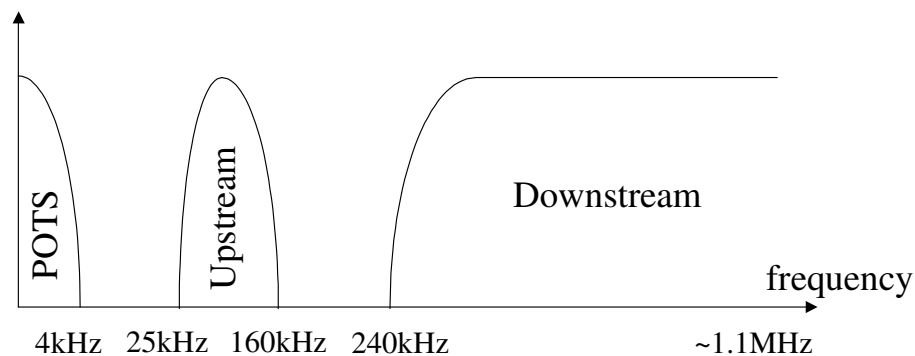


**Figure 11.2: ADSL Bandwidth Allocation**

Two methods of modulation can be used in ADSL, CAP and DMT. Carrier-less Amplitude/Phase Modulation (CAP) is very similar to QAM (Quadrature Amplitude Modulation), except that the carrier itself is not transmitted. The carrier does not actually hold any information and is therefore recreated at the receiver for efficiency. The phase is synchronised using phase sequences in the data. Discrete Multi-Tone Modulation (DMT) is the method described in the ANSI standard T1.413, and uses intelligent allocation of the different channels to send the appropriate number of bits to achieve maximum overall throughput. Each individual channel uses QAM, so although both CAP and DMT use QAM at the lowest level, the difference is the dynamic allocation of data to individual channels using DMT that provides a potentially better data rate.

## 11.3 Overview of the Analogue Interface and Modeling Line Transformers

As has been described in the previous section, the signals to be transmitted between two ADSL modems are modulated using some form of QAM, with an interface between the modem hybrid and the line of a 1:1 line transformer, as shown in figure 11.3.
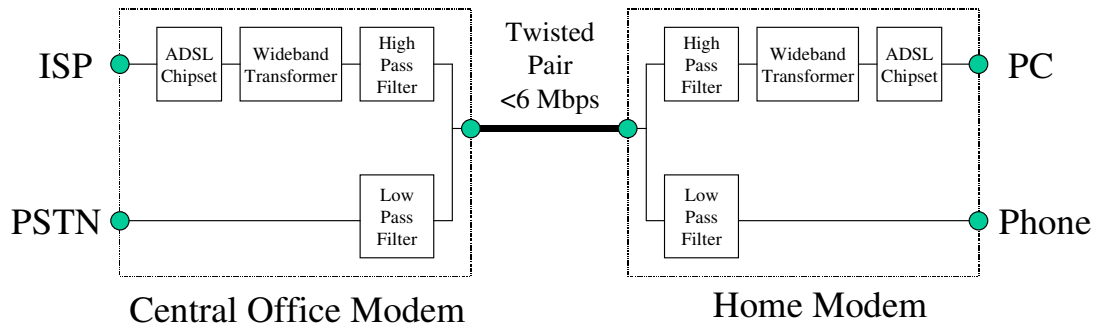


**Figure 11.3: ADSL Analogue Interface**

Day, Wurcer and Hoffman [228] provide an excellent primer in the design of ADSL hybrids, and address some of the rudimentary aspects of the transformer design. Other useful and practical sources of design information can be found in Cornil [229] and Cabler [230]. The key issues are loss, matching, parasitic effects and distortion. The frequency response is limited at low frequencies by the magnetising inductance. The parasitic leakage inductance and winding capacitance reduce the bandwidth at higher frequencies. Resistive losses in the windings also provide a source of loss in the device across the whole range. The overall effect on the insertion loss is summarised in figure 11.4.
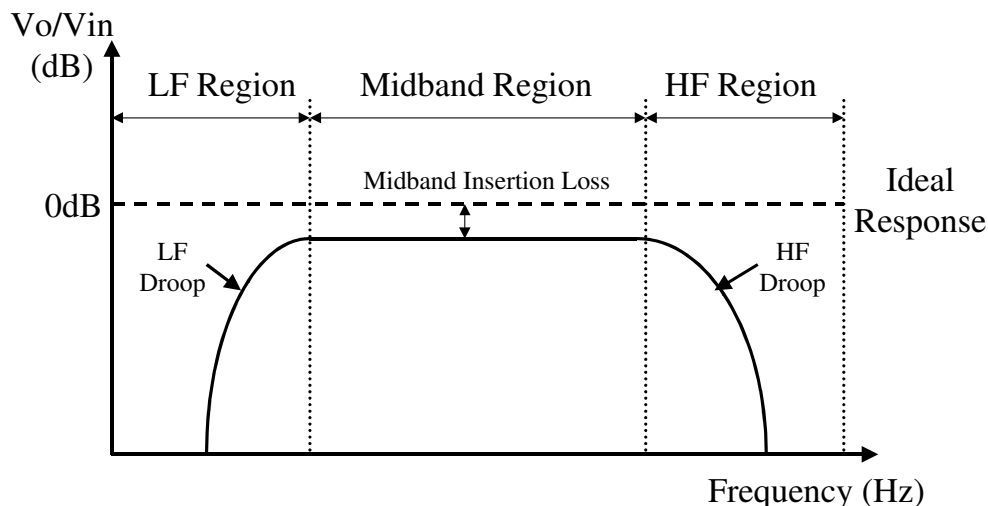


**Figure 11.4 Transformer Insertion Loss with non-ideal model**

Steffes [246] and Nash [247] demonstrate how simulating the line driver and its associated circuitry can predict the performance of the analogue interface in general. Day and Wurcer [228]

and Dean [245] have shown specifically how a simple model of a transformer, including the parasitics as shown in figure 11.5, can be used to predict the frequency response and insertion loss of the device. This is shown in figure 11.6, with a graph of the simulated insertion loss for a realistic ADSL device.
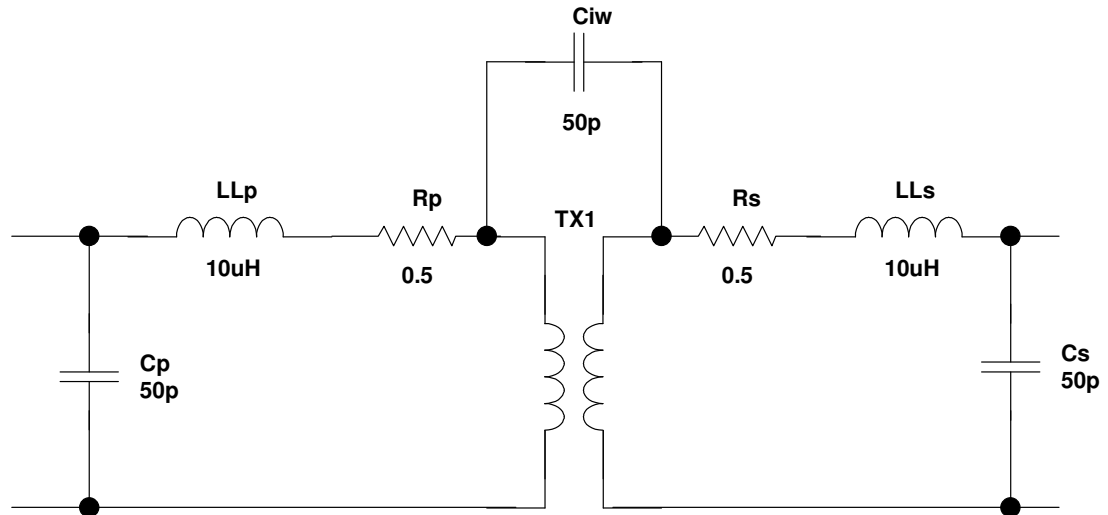
**Figure 11.5 : Transformer Model Used for Simulation of Insertion Loss**
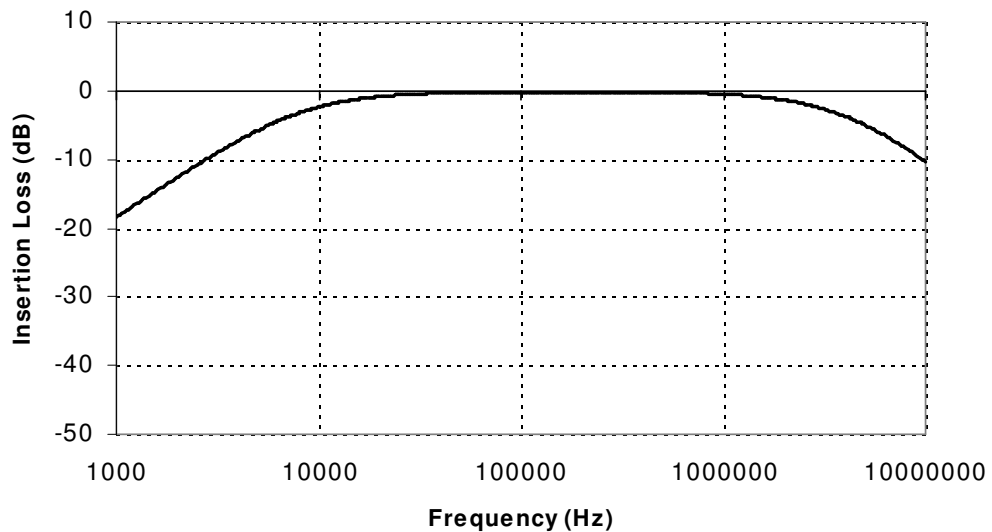
**Figure 11.6: Simulated Insertion Loss using Pspice**

Using simulation in this way is an effective tool in identifying critical parameters, defining parametric limits and optimising device performance. This is illustrated in figures 11.7-11.9, where the winding resistance, leakage inductance and magnetizing inductance are varied respectively.
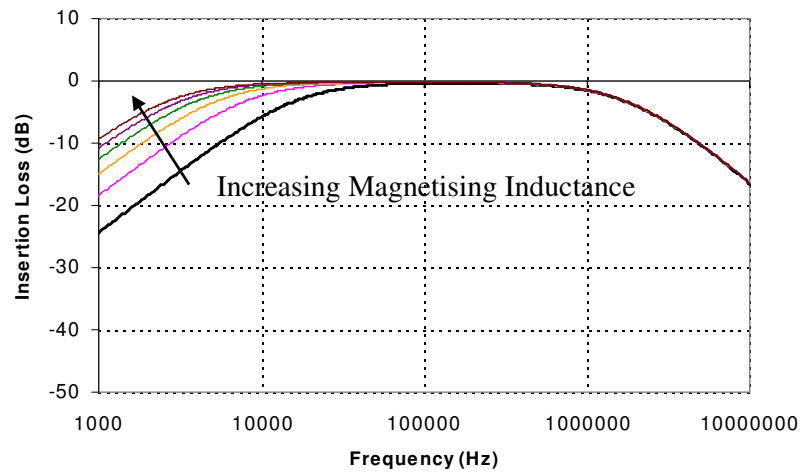
**Figure 11.7 : Simulated bandwidth increase with increasing Magnetising Inductance**
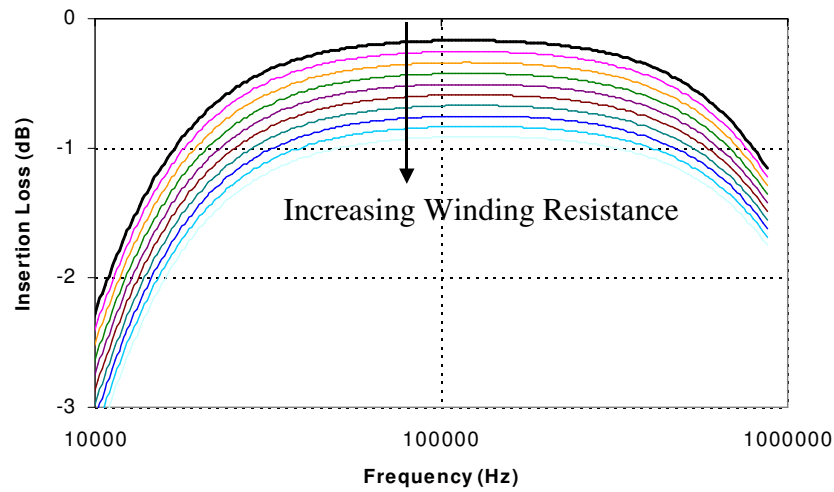


**Figure 11.8 : Simulated increase in Insertion Loss with Winding resistance**
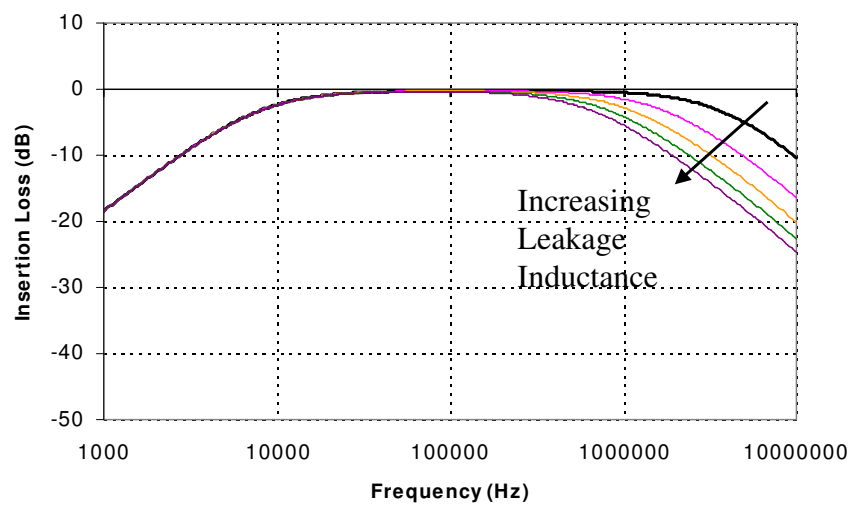


**Figure 11.9: Simulated decrease in bandwidth with increasing Leakage Inductance**

In order to achieve effective and accurate simulation results, it is necessary to characterise these parameters accurately as has been discussed previously in this thesis. The range of methods employed range from analytical approaches, such as those proposed by Dowell [35], Dauhajre [31] & [112] and Snelling [27], through to integrated modeling procedures involving multiple Finite Element Analyses [FEA], such as those described by Asensi *et al* [28]-[30], Wilson [60], Lopera *et al* [63] and Prieto *et al* [118]-[121]. These various approaches have been discussed extensively previously in this thesis.

The other issue with the transformer is its effect on signal distortion. If distortion occurs in a sub-carrier or channel, then degradation of the signal may occur, giving rise to loss of signal integrity and data errors. A further side effect of non-linearities in the core is the possible introduction of inter-modulation products in other sub-carriers or channels. Even if the transformer is designed to operate largely in a linear region, due to the nature of the modulation scheme used in ADSL, large Peak-to-Average Ratios (PAR) may occur giving rise to significant magnetic offsets and possible non-linear behaviour. Tellado [231] discusses the potential for large PAR in ADSL systems in some detail, and also methods for its reduction. Due to the broadband nature of the signals, phase shifts may also occur in the transmitted signal, as a result of different frequencies across the range having a different phase response in the core material. This may also result in phase shifts in the recovered ADSL signals.

It is important therefore in a simulation model to include the non-linear core model to ensure that the transformer does not degrade the performance of the system as a whole. The remainder of this chapter will therefore concentrate on this aspect of the transformer design, with investigations carried out into the trade-offs of material characteristics and air gaps, the effect of core size and number of windings on performance, and comparisons between different winding configurations and core types. Previous work [232] describes the basic design procedure for DSL transformers, but relies on 'rule of thumb' calculations and simplification of the THD (Total Harmonic Distortion) figures. It is proposed in this thesis to apply circuit simulation to more accurately predict the effect of non-linear ferrite cores on the transformer's performance. The proposed model will have a similar parasitic model to that described previously, but will include an accurately characterised non-linear core model. In this chapter the original Jiles-Atherton model has generally been used. The modifications to the Jiles-Atherton model that have been proposed previously in this thesis refer to heavily saturated cores, and in general the ADSL transformers operate at low signal levels implying minor BH loops.

### 11.4  Distortion Performance Criteria

There are several criteria that are used to measure the performance of DSL transformers including Total Harmonic Distortion (THD), Signal to Noise Ratio (SNR), and Intermodulation Distortion (IMD). This section defines these criteria as they have been used in this work. The THD figure is

of primary interest to ADSL system designers and is usually the only distortion figure given on a data sheet.

Total Harmonic Distortion (THD) is used to establish the effect on an ideal sinusoidal test tone of non-linearities in the transformer. The THD is calculated using expression 11.1, where $V_1$ is the peak harmonic, the voltage at the ideal tone frequency, and $V_2$, $V_3$, $V_4$, $V_5$ are the second to fifth harmonics respectively.

$$THD = \frac{\sqrt{\sum_{i=2}^{5} V_i}}{V_1}$$

(11.1)

A variation on the THD is the THD+Noise figure, which extends the range of harmonics to include all the harmonics measured. This is similar to the signal to noise ratio (SNR) and is calculated using equation 11.2.

$$SNR = \frac{V_1(rms)}{\sum_{i=2}^{n} V_i(rms)}$$

(11.2)

Both the THD and SNR give an indication of the single tone performance, but real problems can result in DSL system from a number of signals giving rise to Inter-Modulation Distortion (IMD). In a linear (ideal) system, the output signal will be a proportion of the input signal. If the system is non-linear, such as a real transformer with a ferrite core, then the output signal can be represented as a Taylor series expansion of the input signal, as given in 11.3.

$$V_{out}(t) = a_1 V_{in}(t) + a_2 V_{in}^2(t) + a_3 V_{in}^3(t) + ... + a_n V_{in}^n(t)$$

(11.3)

Where $a_1$ to $a_n$ are the amplitudes of the individual harmonics of the output signal (for a sinusoidal input waveform). If the input waveform is the sum of 2 sinusoidal waveforms as given in 11.4, then the output harmonics become more complicated to calculate due to the higher order products of the two input signals.

$$V_{in}(t) = A\cos(\omega_1 t) + A\cos(\omega_2 t)$$

(11.4)

With a non-linear system, the input voltage given by 11.4 can be substituted into 11.3 and the output harmonics calculated. Considering the second order harmonics, the output voltage due to the second term in 11.3 can be calculated using 11.5, expanded into 11.6.

$$V_{out(2)}(t) = (A\cos(\omega_1 t) + A\cos(\omega_2 t))^2$$

(11.5)

$$V_{out(2)}(t) = A^2 \cos^2(\omega_1 t) + A^2 \cos^2(\omega_2 t) + 2A^2 \cos(\omega_1 t)\cos(\omega_2 t) \qquad (11.6)$$

This can be rearranged using simple algebraic relations into the alternative form given in 11.7.

$$V_{out(2)}(t) = A^2\left(1 + \frac{1}{2}\cos(2\omega_1 t) + \frac{1}{2}\cos(2\omega_2 t) + \cos((\omega_1 + \omega_2)t) + \cos((\omega_1 - \omega_2)t)\right)$$

$$(11.7)$$

This shows how as well as the 2nd harmonics of each input signal frequency, product and difference terms appear also. These are known as inter-modulation products (in this case 2nd order). A similar exercise can be carried out for other orders, with 3rd order products of particular interest, as products are generated at frequencies close to the original signal frequencies.

The intermodulation distortion IMD can be calculated using the expression in 11.8.

$$IMD = \frac{\sum RMS(distortion\ products)}{\sum RMS(input\ signals)} \qquad (11.8)$$

The second order IMD is calculated using the second order products, third order IMD from the third order products and so on.

## 11.5 Distortion in transformers due to non-linear materials

Having defined the measurement criteria for distortion, it is useful at this stage to consider the sources of distortion, and how simulating transformers could predict the level of distortion. Due to the non-linear nature of the transformer ferrite core, the voltage waveforms on the windings will have a non-linear relationship with respect to the current through the driving (primary) windings. This is due to the non-linear relationship between $B$ and $H$ in the core, as has been discussed previously in this thesis. Figure 11.10 illustrates how the $BH$ characteristic changes as the applied field strength ($H$) is increased, introducing non-linear behaviour.
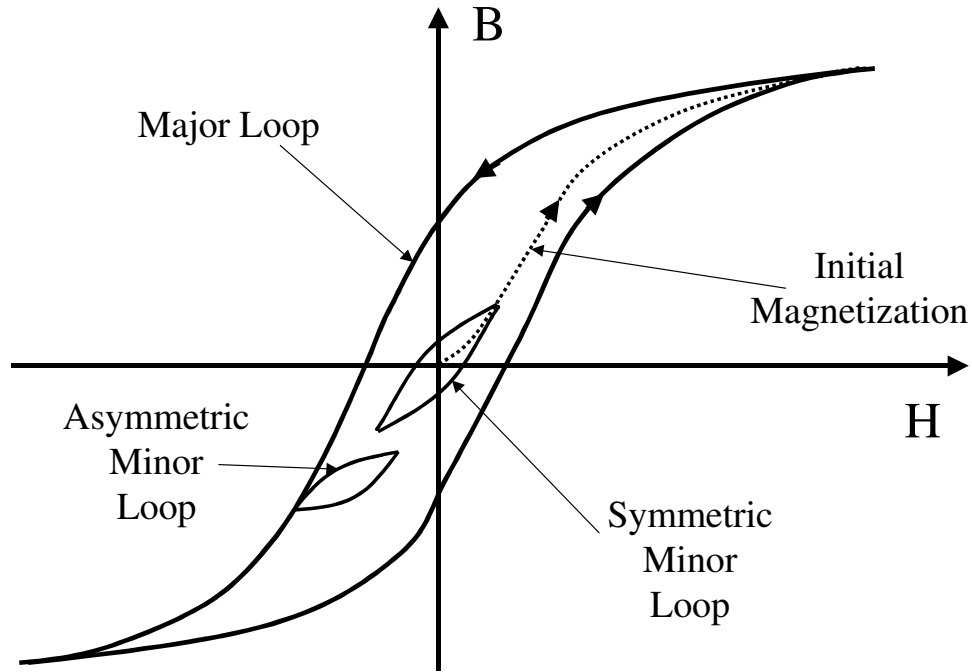
**Figure 11.10: Non-Linear BH Behaviour in Transformer Core**

Near the origin, the relationship between *B* and *H* is essentially linear, but as *H* increases, the slope of the *BH* curve steepens until saturation occurs, at which point the slope reduces once again (This is clearly seen on the initial magnetization curve). This illustrates how there are two potential sources of distortion, at low and high field strengths. Figure 11.10 also shows how any magnetic offset conditions may cause different slopes and sizes of loop, as shown with the minor loop variations.

This behaviour can be modelled in transformers using a mixed-domain approach as has been described earlier in this thesis, with the resulting voltage waveforms reflecting the effect of the non-linear behaviour of the core. As long as accurate models of the core non-linearity are used, then it is possible to estimate the effect on distortion of the voltage waveforms. A common assumption in the available design guides from manufacturers such as Ferroxcube[8] [232] indicates that the 3rd harmonic is the only significant problem in DSL transformer design, but this assumes that hysteresis is not taking place in the core. If hysteresis is included, then the 2nd through to the 5th harmonic may have an impact on the transformer performance. In the testing and simulation that follows, all the harmonics are considered, not just the 3rd.

---

[8] During the course of this work, Philips Components spun off its Magnetic Component group to form a new company called Ferroxcube.

## 11.6 Predicting Total Harmonic Distortion (THD) with Simulation

### 11.6.1 Introduction

In order to investigate the techniques required to simulate the THD performance of a line transformer for ADSL, a series of transformers were constructed, THD measured, models derived and simulated. Comparisons were made between the measured and simulated results to assess the accuracy of the simulation model and its usefulness for predicting the THD figure for a variety of transformer configurations. Gapped and un-gapped cores were chosen to establish the effect of air gaps on the performance, and similarly toroidal (ring) cores were compared with two-piece (ER11) cores. The types of core used in this section were a TN10/6/4 toroid and ER11 (gapped and un-gapped). The EP13 (gapped and un-gapped), Intgrated Inductive Components (IIC) and planar E cores are considered in the next section of this chapter. All of the cores were made of the materials 3E5 or 3E6 (Philips), or T38 (Siemens).

### 11.6.2 Toroid TN10/6/4-3E5 Line Transformer

The first test case was a TN10/6/4 toroid made of 3E5 material. The component was a two-winding transformer, each winding wound with 60 turns of 28 s.w.g wire. To ensure accurate results, a 12-bit oscilloscope was used to enable more accurate definition of small signal harmonics (the Tektronix TDS220 oscilloscope used previously in this thesis has only 8-bit resolution) therefore the ADC-212 Picotech Virtual Instrument was used. To ensure that spectral leakage of the FFT results was minimized, the frequency of the source was specified at 9732Hz[9], to produce a sampled waveform with an integral number of cycles for a sample size of 4096.

Using the optimization software previously described in this thesis, the 3E5 ferrite material was characterized using the original Jiles-Atherton model (previously described in this thesis in chapter 3), with the parameters given in table 11.1. The model was optimized to measured results obtained at approximately the same operating conditions as the THD test circuit to ensure a like-with-like comparison.

---

[9] The test frequency was initially set at 10kHz as a realistic low end ADSL signal frequency, and refined to the specific 9732Hz value. If the frequency is set much higher than 10kHz, then problems may occur in the accuracy of the measured THD (Philips [232]).

| Parameter | Value |
|:---------:|:-----:|
| $a$ | 5.245 |
| $k$ | 20.022 |
| $c$ | 1.1675 |
| $\alpha$ | 4.1u |
| $M_s$ | 241k |

**Table 11.1: 3E5 model parameters**

The transformer was tested using the circuit shown in figure 11.11, with the peak input voltage varied from 2V to 10V in 2V steps. A similar test circuit was created using the **winding** and **classicja** models described previously in this thesis in chapter 4 as shown in figure 11.12.
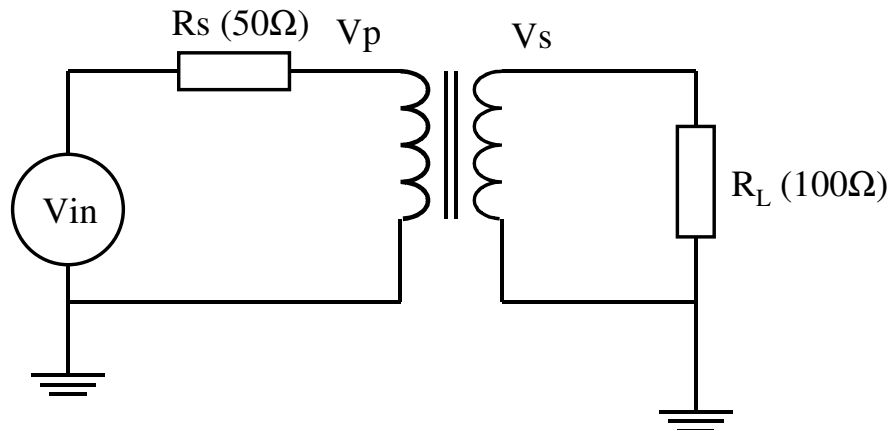


**Figure 11.11: Transformer THD Test Circuit**
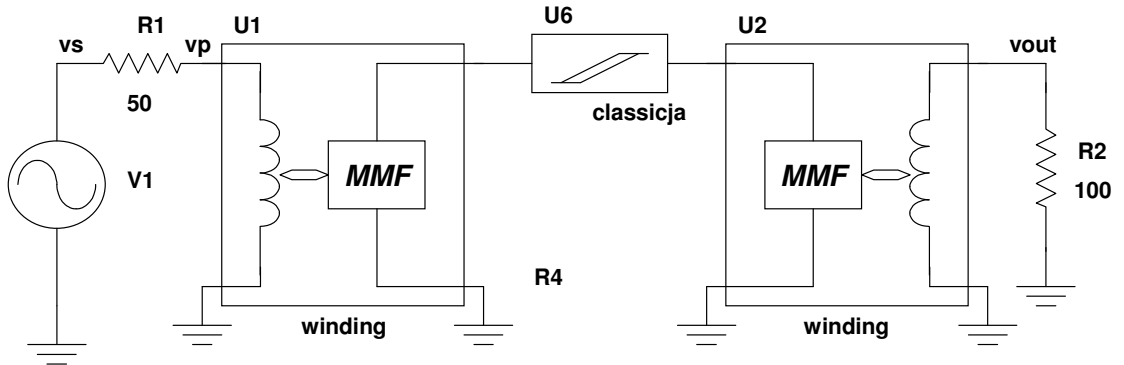


**Figure 11.12: Pspice Transformer THD Test Circuit**

The THD calculated for the measured and simulated test circuits is given in figure 11.13.
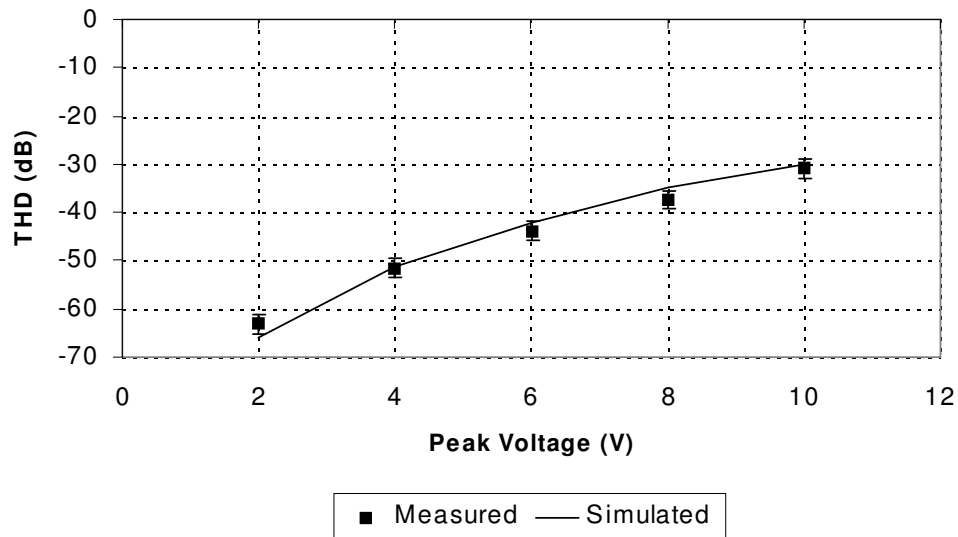
**Figure 11.13: TN10/6/4-3E5 Comparison of Measured and Simulated THD**

Using this approach it is clear that accurate estimates of the Total Harmonic Distortion for transformers can be obtained with the use of suitably characterized material models of the core. In this case, the difference between the measured and simulated results is within 4dB (worst case) and often within a fraction of a dB. It was found that if the material was not characterized for the general operating conditions of the transformer, that much less accurate results were obtained, highlighting the necessity for specific material models, or models that change behaviour accurately depending on the applied field strength levels.

### 11.6.3  ER11-3E6 Line Transformer

Obviously the toroid analysed in the previous section would not be used in practice, but rather a gapped core such as EP13 or ER11. The EP13 cores have been well used in commercial applications but are becoming a significant cost of the hybrid design due to their relatively large size and weight. It was therefore considered useful to investigate the performance of ER11 cores. These cores are significantly smaller, and also offer the potential to be used in planar or thick film constructions as well as the conventional wire wound form.

The first test case was a two winding transformer, wire wound on an ER11 two piece un-gapped core made of Philips 3E6. Each winding was wound with 9 turns of 28 s.w.g wire to give an inductance of 230uH. This transformer was tested using the same test circuit as used previously (shown in figure 11.11). The core was characterised in the same way as the toroid previously described, with the resulting model parameters given in table 11.2.

| Parameter | Value |
|-----------|-------|
| $a$ | 15.0 |
| $k$ | 40.0 |
| $c$ | 1.06 |
| $\alpha$ | 3.6u |
| $M_s$ | 224k |

**Table 11.2: ER11-3E6 model parameters**

The parameters are in a similar range to those for the 3E5 toroid, but it is worth noting that the characterization includes the small gap between the two core halves. The THD of the transformer was measured using the circuit shown in figure 11.11, with the peak input voltage varied from 1V to 10V in 1V steps. A simulation test circuit was created in the same fashion as for the toroid example using the **winding** and **classicja** models as shown in figure 11.12.

The THD calculated for the measured and simulated test circuits is given in figure 11.14.
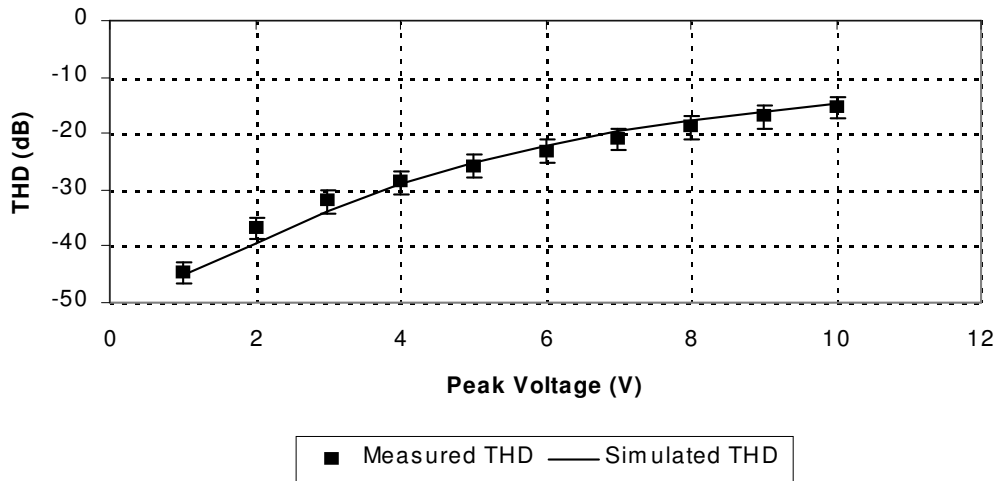


**Figure 11.14 : ER11-3E6 Comparison of Measured and Simulated THD**

In this case, the core is un-gapped, so the THD is relatively poor for this range of input voltage. The addition of a core gap will have the effect of storing energy in the gap rather than the core and hence reducing the effect of the core material non-linearities on the signal through the transformer.

In order to compare the gapped and un-gapped behaviour, the ER11-3E6 core was tested using the same current applied to the primary winding, with no load attached to the secondary. This method, while not replicating the line conditions, allows a direct comparison of the gapped and un-gapped core for a specific current applied to the primary. The primary current was applied across the range 1-7mA at 10kHz (approx) as before. The secondary voltage was used to measure the resulting THD of the transformer for the applied current input. This method also allows the calculation and comparison of the BH curves for each case. In this case a larger number of turns was chosen

(20:20), and a small gap implemented by grinding the centre leg flat using emery paper. The change in measured winding inductance was 2.1mH (ungapped) to 326uH (gapped).

The resulting measured waveforms were used to characterise the gapped and ungapped core models, with the resulting Jiles-Atherton model parameters given in Table 11.3 (The ungapped core parameters are slightly different to the previously used parameters, due to the different stimulus levels used to characterise the model)

| Parameter | Ungapped | Gapped |
|-----------|----------|--------|
| $a$ | 60.0 | 15.0 |
| $k$ | 45.0 | 20.0 |
| $c$ | 0.15 | 1.06 |
| $\alpha$ | 3.6u | 3.6u |
| $M_s$ | 224k | 224k |

**Table 11.3: ER11-3E6 model parameters**

The measured values of THD and the values calculated from simulations are summarised in figure 11.15 and figure 11.16.
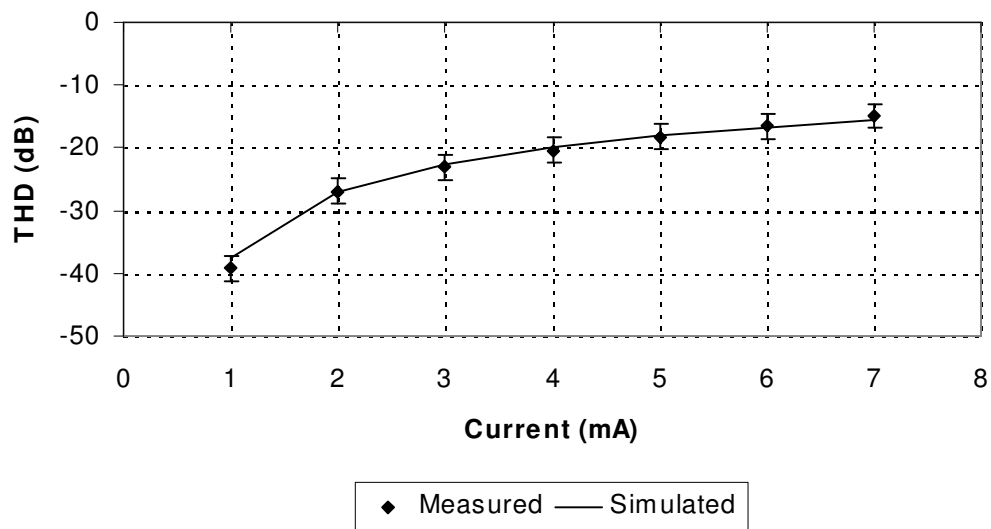


**Figure 11.15: ER11-3E6 Ungapped Core (20 turns) Measured vs Simulated THD**
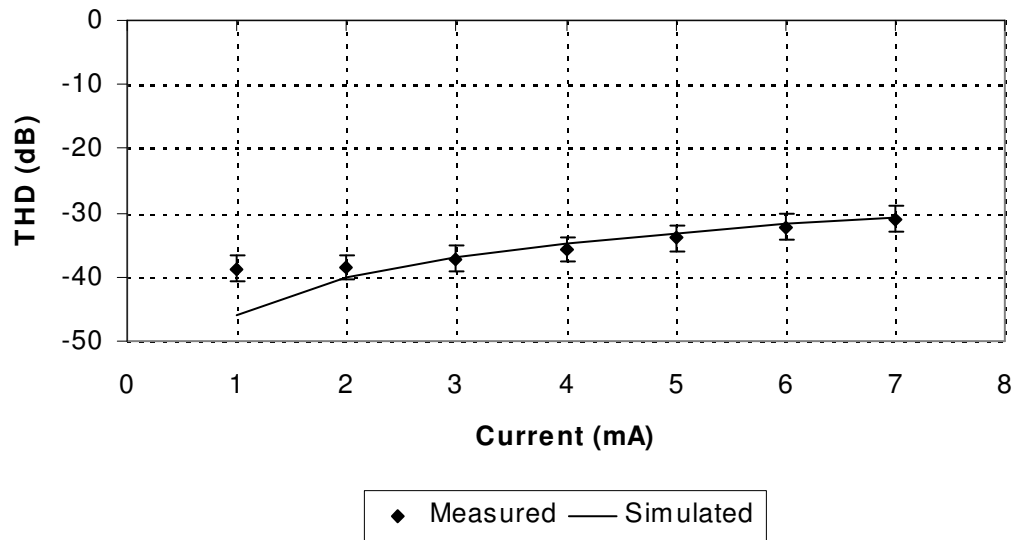
**Figure 11.16 : ER11-3E6 gapped Core (20 turns) Measured vs Simulated THD**

In both cases the correlation is good (within 2dB), apart from the gapped core at very low current levels. Investigation of this showed that the measured source signal was introducing some noise, limiting the THD achieved. The use of the mixed technology models for measuring the THD from a simulation has been demonstrated to be of usefulness, with the added benefit of insight into the magnetic behaviour inside the core. As an illustration of this, figure 11.17 shows the simulated BH curves inside the gapped and un-gapped core models for the same applied current level (7mA).
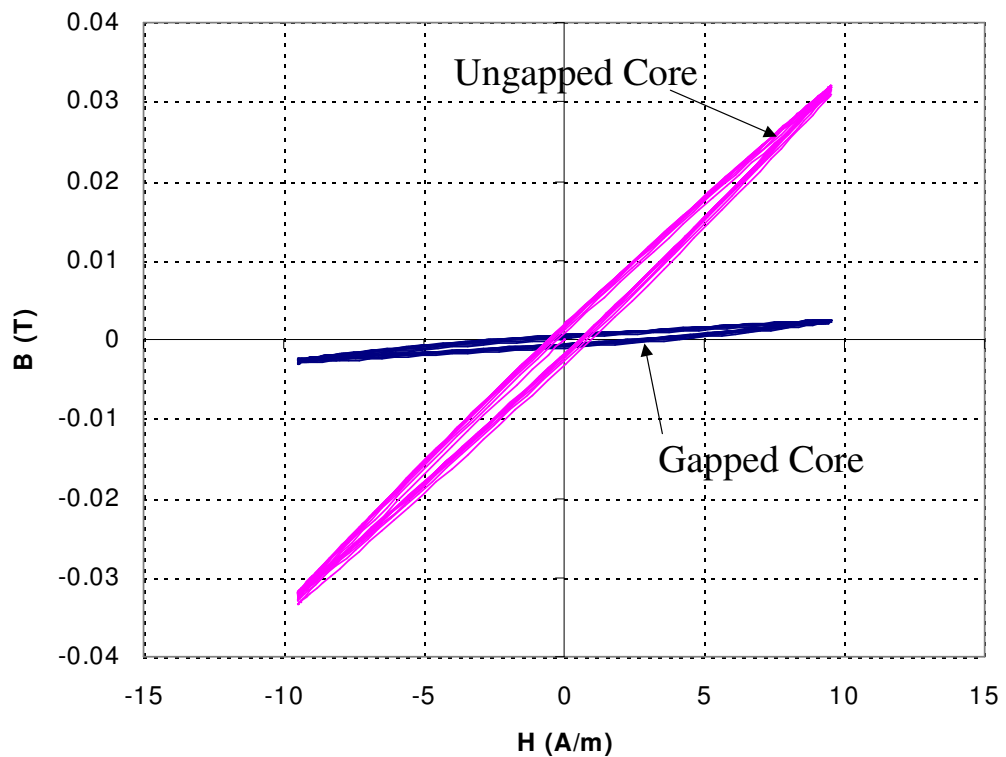


**Figure 11.17: ER11-3E6 Gapped and Un-gapped Core Simulated BH Curves**

As can be seen from the figure, the area of the ungapped core BH loop is greater and also steeper. This illustrates the effect of the air gap, effectively reducing the effective permeability of the overall core & gap combination. One effect of the introduction of a gap is to effectively reduce the distortion, as more of the energy is stored in the gap.

## 11.7  Planar Line Transformers for use in DSL Applications

### 11.7.1 Introduction

With the higher level of integration in DSL hybrids, requirements for space reduction and also reduction in manufacturing costs, it is becoming important to investigate new methods for the implementation of transformers. The wire-wound EP13 transformers widely used in the DSL hybrid market are now generally the largest single component on the hybrid, in height, board area and weight. The complexity of designs also requires a heavy investment in terms of manpower to manufacture these devices. It is also true to say that wire wound transformers suffer from relatively poor repeatability. This applies both in the prototype to production transition and also across a large number of devices in a production environment.

These issues have been successfully addressed to a certain extent in the Power Supply industry with the use of Planar Magnetics, and as part of this thesis, the potential use of planar devices in DSL applications is considered. As has been discussed in this chapter, there are several key issues that need to be considered when designing DSL transformers, and these require trade-offs of the parameters of the component. The basic insertion loss of the transformer in the mid-band range is a direct function of the winding resistance. While the cross sectional area of planar windings is relatively large (giving a low resistance), the effective high frequency resistance may be more susceptible to change due to eddy currents (As has been discussed previously in this thesis). The low and high frequency behaviour of the transformer is dominated by the magnetizing and leakage inductances respectively. A potential problem may exist in achieving the required number of turns to attain the necessary magnetizing inductance, while still having a large enough gap in the core to reduce THD. This implies that multi-layer Printed Circuit Board (PCB) or Thick Film implementations would be required for a final production model.

The goal was to assess the potential applicability of this technique to DSL transformers, and the performance and manufacturing merits of the approach. One of the attractions of a planar implementation is the precision with which parameters can be estimated due to the repeatability of the structure. This has obvious benefits when taken in the context of a design methodology that relies heavily on simulation. If the model parameters are estimated accurately early in the design phase, then predictions can be made about the performance of the design prior to prototypes being manufactured. The other benefit is the repeatability when the design progresses into a full production phase. Using existing wire wound techniques, there exists the risk of the production

component exhibiting different characteristics to the prototype part, and also potentially wide variations in performance due to the tolerances in a wire wound design. In order to use simulation to compare the wire wound and planar approaches using simulation, benchmark prototypes were constructed. The methods used to develop these prototypes are also discussed in this section, and while it may seem to be a digression from the main focus of simulating these transformers, it is useful to understand the physical geometries used compared with a conventional wire wound approach.

Extensive work has been carried out previously implementing planar (PCB) transformers for power supply applications. Cuk *et al* [240]-[243] have developed the methods for use with coupled inductors, power supply design and complete integrated magnetics (where the transformer and inductor is implemented as a single magnetic component).

More recently, this technique has been extended to a thick film process, offering the ability to create effectively full-customization of the ferrite and winding structure. Varsheney et al [235] describe this technique for ultra low profile transformers, and Tang et al [234] and Arshak et al [233] & Park et al [236],[237] discuss using ferrite sheets and screen printing of ferrites to achieve a completely integrated thick film process. Barnwell [238] has investigated the use of a ferrite substrate. This alternative approach has the major advantage of simplifying the production process significantly.

Both the printed circuit board and thick film methods require a customized design of the magnetic component, but another approach is to use an integrated inductive component (IIC) [244]. These commercially available devices consist of a ceramic package containing a ferrite core with a number of tracks impregnated in the package attached to the device pins. By using a simple PCB track layout magnetic components can be easily constructed with minimal design effort.

The magnetic component designer therefore has the choice of 3 basic planar approaches, PCB custom, Thick Film or IIC. Investigation into the manufacture possibilities of PCB and Thick Film has provided the information that in most cases the same minimum track widths are achievable. Thus there is not an immediate benefit for one technology over the other in terms of achieving more turns for a specific core geometry. Also, the good heat transfer properties of a thick film substrate are not a significant benefit for low power communications transformers in general. Assessment of prototype costs demonstrated that the PCB route would be the most cost effective for prototyping, therefore with no demonstrable technical differentiator between the PCB and Thick Film methods, PCB prototyping was chosen. The next choice is whether to use custom PCB or an integrated component (IIC) [244]. As has been discussed previously, inclusion of a gap to improve THD performance is usually necessary in DSL applications, and this in turn leads to a larger number of turns required. The standard IIC from Ferroxcube [244] was able to

accommodate 10 turns maximum with no gap. Tests were carried out on a 5:5 turn transformer in any case to assess the performance of the device, with particular regard to the THD.

The remainder of this section on planar transformers will concentrate on various proposed DSL designs using PCB planar components, assessing their performance versus the cost in terms of board area and height. Comparisons are made with approximately equivalent wire wound devices[10]. Tests are also carried out on the IIC devices to demonstrate their comparative performance.

### 11.7.2 DSL transformer using Integrated Inductive Component (IIC)

The basic outline of an IIC is shown in figure 11.18. This shows the basic component and an accompanying PCB design for an interleaved 5:5 two winding transformer. The package is 14.4mm long and 4mm high, with 10 surface mounting pins.
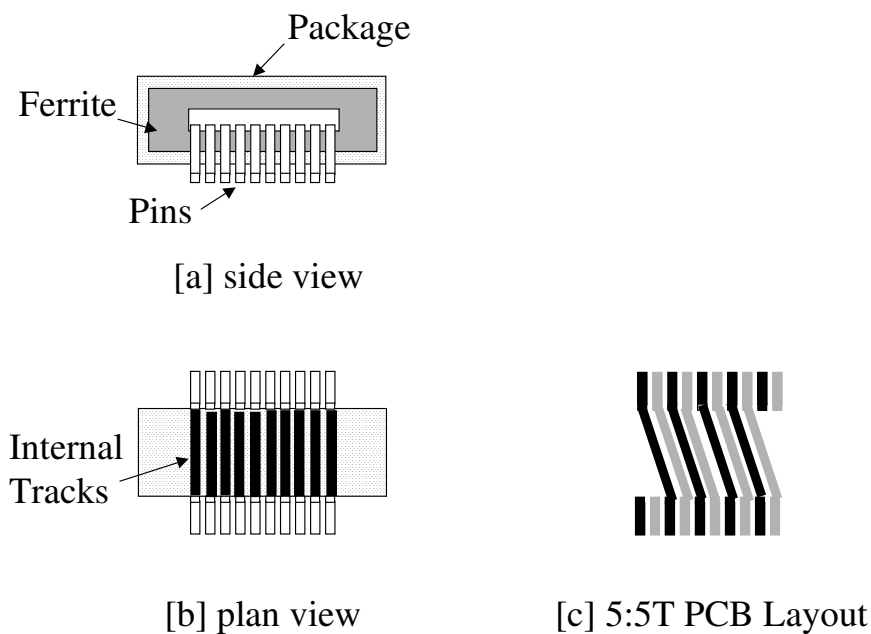


**Figure 11.18: IIC Construction Details**

As can be seen from figure 11.18, the 10 pin IIC has 10 tracks passing horizontally across the component, through a ferrite core. By defining alternate tracks (shown with black and grey colours), a 5T:5T transformer is defined. Note also that the ferrite core is completely encapsulated inside the ceramic or plastic case and therefore cannot include an air gap. When this component was constructed using the 3E6 ferrite material, the magnetizing inductance was measured at 1kHz

---

[10] Commercially available parts from APC were used, such as the APC41199 transformer based on an EP13 ferrite core.

as 215uH (which is acceptable compared to some smaller DSL devices), Leakage Inductance 0.6uH (which is excellent) and a winding resistance of 0.17Ω (Also very good). The effective core length is 28.9mm and cross sectional area is 11.7mm$^2$, leading to a core factor of 2.47mm$^{-1}$.

This device was tested by applying a range of input voltages to the primary winding and measuring the THD across the secondary winding. This test is for comparison between transformers, and will give a worse value of THD than with a load across the secondary as all the primary current will pass through the primary winding. The input voltage was varied from 1V pk-pk to 10V pk-pk at 10kHz, and measurements carried out on an EP13 wire-wound transformer (APC41199) and the IIC10-14/4 transformer. The THD results are summarised in figure 11.19.
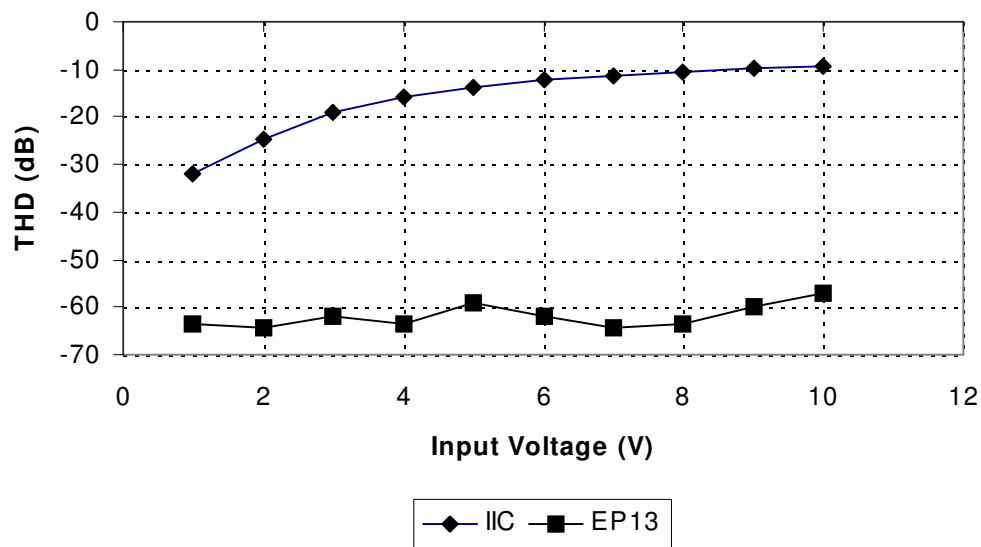


**Figure 11.19: IIC and APC41199 THD versus Input Voltage @ 10kHz**

These results indicate that the IIC approach is not adequate for DSL applications. With a THD of –9.4dB at 10V input, the output voltage is heavily saturated and distorted. In order to test the performance at 100kHz, the test was repeated, this time with the voltage at 100kHz to investigate whether the THD performance was any better. The results of this test are shown in figure 11.20.
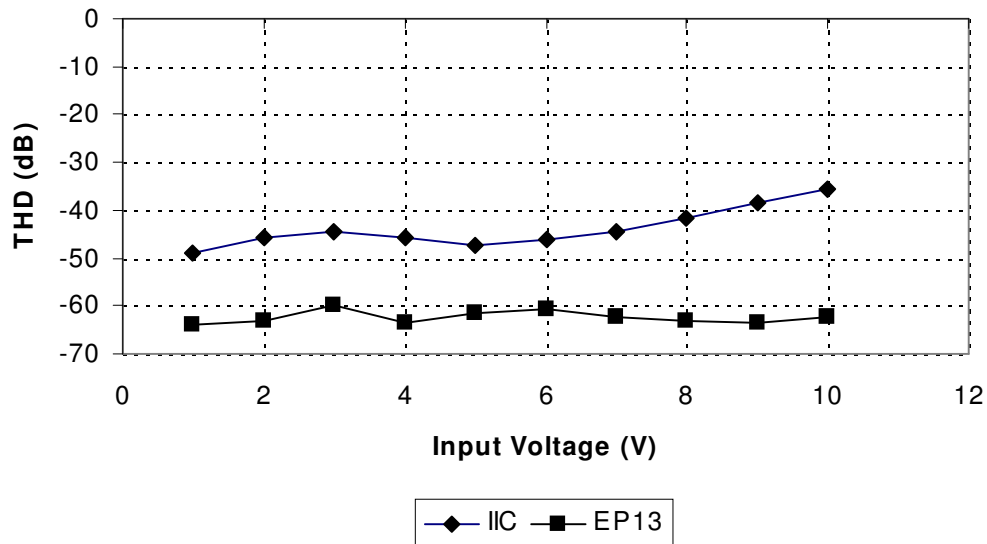
**Figure 11.20: IIC and APC41199 THD versus Input Voltage @ 100kHz**

It is clear that the THD performance is improved, but still significantly worse than the EP13 wire wound component. The conclusion drawn from these tests was that the IIC was not going to provide an 'off-the-shelf' solution for DSL transformers in general that would provide the THD performance necessary for communication systems. The two main problems with the approach are insufficient turns to achieve an inductance high enough to ensure good low frequency performance, and with no gap, the THD performance will not be as good as a gapped EP13 core without a much larger number of turns. This implies that a custom made planar component will be required to provide the necessary performance.

### 11.7.3 DSL Transformer using Custom Planar Magnetics

As has been discussed already in this chapter, the choice for custom planar magnetic components is essentially between PCB and Thick Film implementations, and for reasons of low cost and prototype turn-around speed, the PCB implementation was used in this thesis. The basic methodology behind a planar magnetic component involves defining a winding using a spiral track on a PCB, which has a hole (or number of holes) routed for the core material to pass through. Figure 11.21 shows an exploded view of a simple planar magnetic component using a multiple layer PCB and planar E core. The two halves of the Planar core will be clamped (as shown), glued or taped together.
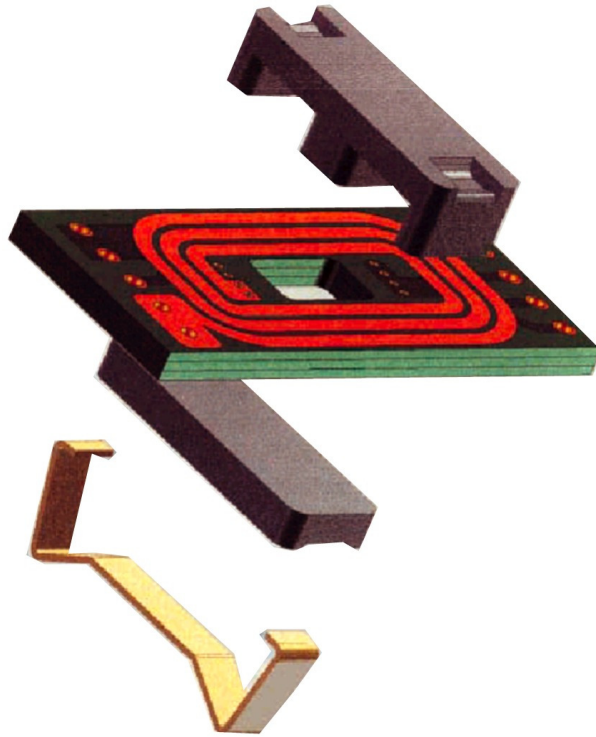
**Figure 11.21: Planar PCB Construction**

In order to decide on the best planar core for the DSL application, the key parameters to be considered from a geometry point of view are the core factor (effective core length divided by effective cross sectional area) and the area available for winding. Using the standard EP13 core as a reference, some of the possible cores available, their core factors, winding areas, winding window width and height are provided in table 11.4. The EP cores are not suitable for planar designs, so have no planar parameters, the ER cores can be used with a bobbin, or planar, and the planar E cores are only used with planar designs and so have no wire-wound parameters.

| Core | Core Factor $(mm^{-1})$ | Area (Wirewound) $(mm^2)$ | Area (Planar) $(mm^2)$ | Width (mm) | Height (mm) |
|---|---|---|---|---|---|
| EP10 | 1.7 | 11.3 | - | - | - |
| EP13 | 1.24 | 13.5 | - | - | - |
| ER9.5 | 1.67 | 2.8 | 5.76 | 1.8 | 3.2 |
| ER11 | 1.23 | 2.8 | 5.625 | 1.875 | 3.0 |
| ER14.5 | 1.08 | 5.1 | 10.85 | 3.5 | 3.1 |
| E14/Plt | 1.16 | - | 8.0 | 4.0 | 2.0 |
| E14/EE | 1.43 | - | 16.0 | 4.0 | 4.0 |
| E18/Plt | 0.514 | - | 10.0 | 5.0 | 2.0 |
| E18/EE | 0.616 | - | 20.0 | 5.0 | 4.0 |

**Table 11.4: Table of core factors and winding area parameters**

The figures in table 11.4 show for example that an ER11 core has the same core factor as an EP13, but significantly smaller winding area using a wire wound approach. However, using the planar technique, potentially double the winding area becomes available (as there is no bobbin taking up space). The dedicated planar cores (E14 and E18) have a comparatively better winding area and core factor (especially E18), and look to be the most promising components.

In order to calculate the potential number of turns using a particular core is simply a matter of simple arithmetic based on the track size, track spacing and window width (given in table 11.9). This can be expressed using the equation given in 11.9.

$$n = Round\left(\frac{W - 2*osp + sp}{tw + sp}\right) \tag{11.9}$$

Where $n$ is the number of turns (rounded down to the nearest integer), $W$ is the window width, $osp$ is the spacing on the outside and inside of the PCB, $sp$ is the spacing between tracks and $tw$ is the track width. Using this basic approach, minimum numbers of turns per layer could be calculated for each of the core types in table 11.4.

In implementing planar windings, individual windings can be defined on separate layers or interleaved (for example 2 tracks side by side on the same layer). In either case the windings spiral from the outside of the PCB to the centre. To make a connection to the external circuit requires the winding to be connected back to the edge of the PCB. This can be done using a direct, straight track, or by using a mirror spiral from the inside back out to another via on the edge of the PCB. Both these approaches have been implemented during this work. Details of the implementation method, further test results and a description of automatic layout software are provided in appendix E.

A transformer constructed using 2 double sided PCB windings was tested in the same fashion as the IIC previously in this section and compared with the benchmark APC41199 EP13 based component. The E18 planar component was tested with no gap (Inductance = 2.99mH), and gapped (Inductance = 140uH). The resulting comparison of THD measured at 10kHz is given in figure 11.22.
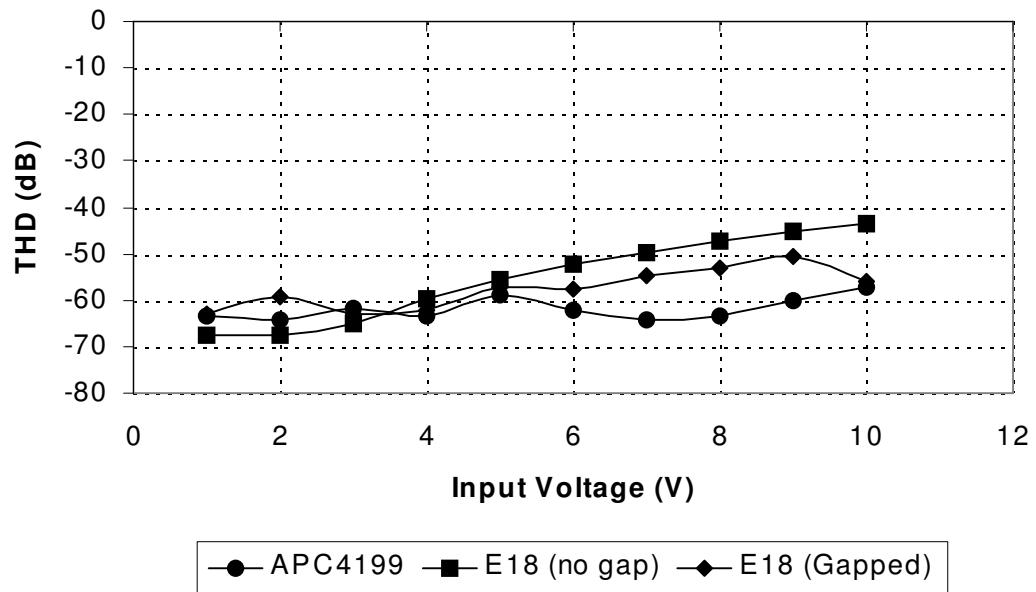
**Figure 11.22: E18 and APC41199 THD versus Input Voltage @ 10kHz**

It is clear from these results that the performance of the Planar transformer using the E18 core is substantially improved from the IIC. The THD at 100kHz is given in Appendix E.

These results indicate a level of performance that is getting close to the benchmark case, with a non-optimal physical construction (i.e. two separate stacked 1.6mm FR4 PCBs). The E18 core size is relatively large in terms of its PCB footprint, and an alternative option is to use an ER11 core. Unfortunately the number of turns possible with this core size is much reduced compared to the E18 core, especially when using a double sided prototype PCB.

Using the same approach as for the E18 core, a 4T:4T transformer implementation was constructed using a double-sided FR4 (1.6mm thick) PCB and the resulting inductance measured with an ER11-3E6 core. The resulting inductance at 1kHz was measured as 11.5uH with a leakage inductance of 2.5uH. This is much lower than the benchmark value of ~200uH (Minimum) and even if the layers were doubled up by connecting the inner vias, the inductance only increased to ~35uH. It was therefore clear that with this implementation, a practically useful ADSL line transformer was not realistically possible. I therefore made the decision to concentrate on E18 and E14 cores for this application.

The initial double-sided PCB planar magnetic components indicated that comparable results in terms of the THD performance could be obtained when compared to an existing wire wound component on an EP13 core. It is also clear that by using a stacked double-sided PCB implementation excessive leakage inductance would result. In order to combat this, a 4 layer implementation was then constructed for the previously used E18 core and also the E14 core size.

Tests were then carried out to evaluate the THD in the E14 core size and to compare the insertion loss for the APC41199 benchmark transformer with those of the E14 and E18 implementations. The resulting measured E14 THD compared with the benchmark APC41199 THD is given in figure 11.23. Again, the performance is comparable with the benchmark APC41199 device, but in this case it is clear that the un-gapped core introduces significant levels of distortion as the voltage level increases. The gapped core (gap ≈100um) shows a level of performance that is comparable with the benchmark APC41199.
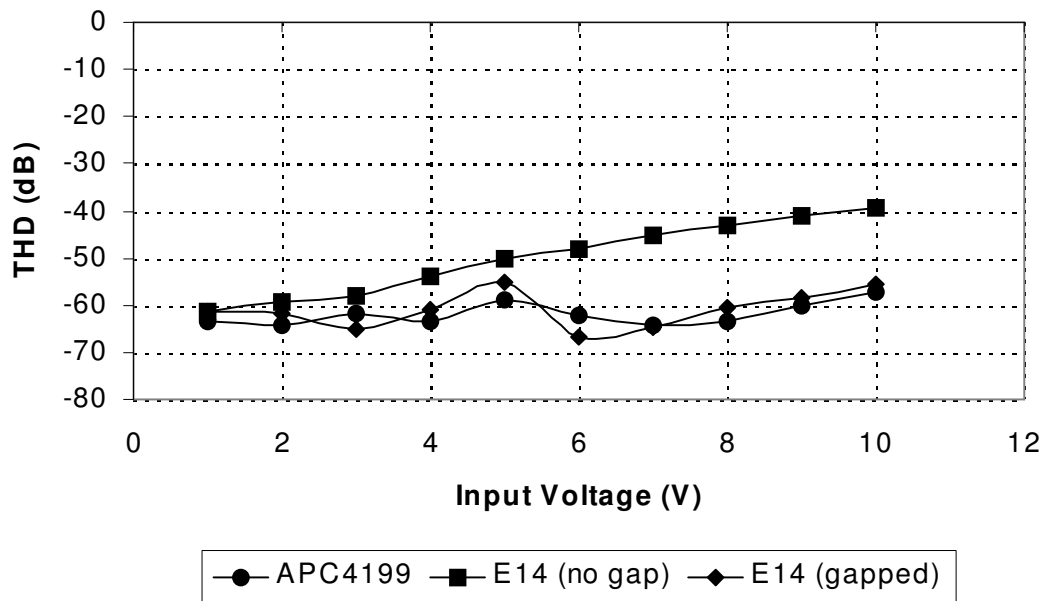


**Figure 11.23: E14 and APC41199 THD versus Input Voltage @ 10kHz**

The measured insertion losses for the APC41199, E14 (E14 NIL), E18 - Single winding per layer (E18 NIL) and E18 (Double winding per layer E18 IL) are given in figure 11.24. The E14 and E18 transformers used un-gapped cores for this test.
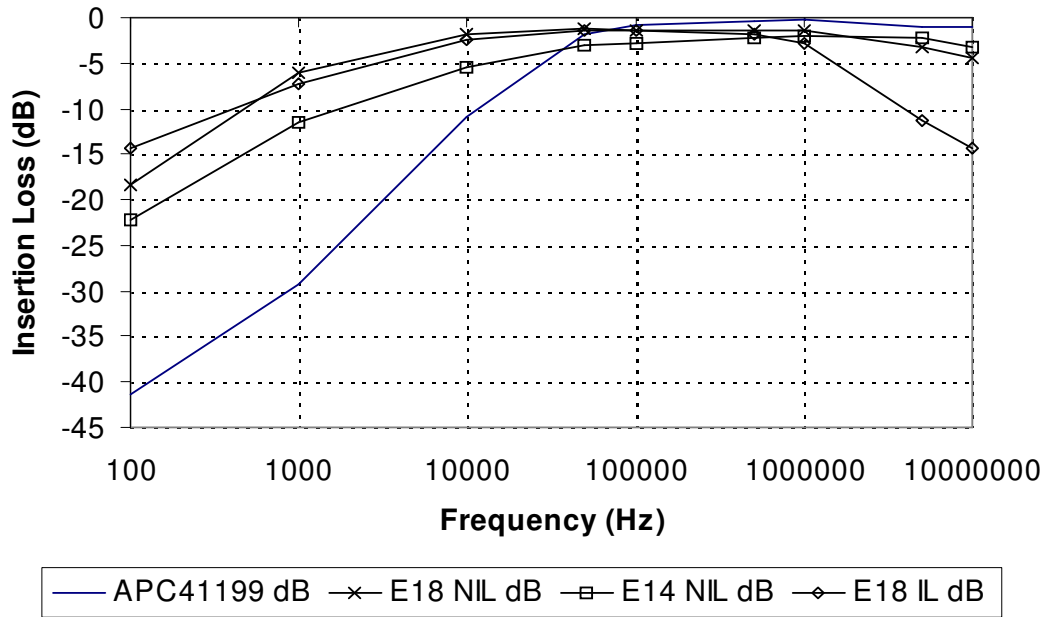
**Figure 11.24 : Measured Insertion Loss for APC41199, E14 and E18 based transformers**

It is clear from figure 11.24 that the low frequency performance in terms of bandwidth is much better than is required. The audio range is effectively filtered out prior to this point in the ADSL hybrid as a whole and so some gap could be introduced to reduce the variability of the magnetizing inductance with respect to the core material and also improve the THD. The insertion loss in the mid band is quite poor for all the planar implementations, primarily due to the relatively high winding resistance (1.4Ω to 9.7Ω) compared to the APC41199 component (<0.5Ω). The winding resistance in the wire wound component (APC41199) is reduced by using bifilar windings, and a similar method could be applied for the planar implementation. The high frequency bandwidth (~1MHz) of the transformers using single windings per layer is acceptable, due to the relatively small leakage inductance (1.3uH for the E14 for example, compared to 0.5uH for the APC41199). When the double winding per layer approach was used, the leakage inductance increased to 11uH, thereby reducing the bandwidth significantly as shown in figure 11.24.

## 11.8  Predicting Insertion Loss with Simulation

### 11.8.1 Introduction

Insertion Loss is one of the most important parameters in assessing the basic performance of broadband transformers. In this section the insertion losses for the benchmark EP13 based device APC41199 and the E14 and E18 planar magnetic prototype transformers are compared using measurements and simulations.

### 11.8.2 Insertion Loss Test Bench

The definition of insertion loss is the ratio of the measured output signal when the transformer is in the line to the measured output signal with an ideal connection. It is expressed in dB across the frequency range of interest. In this case the applied signal was set to 5Vpk-pk across the frequency range 100Hz to 10MHz. The Source impedance was 50Ω and the load impedance was matched to this 50Ω.

### 11.8.3 APC41199 Insertion Loss Measurements and Simulation

The measured values of magnetizing inductance, winding resistance and leakage inductance over the 100Hz to 1MHz range are given in figure 11.25
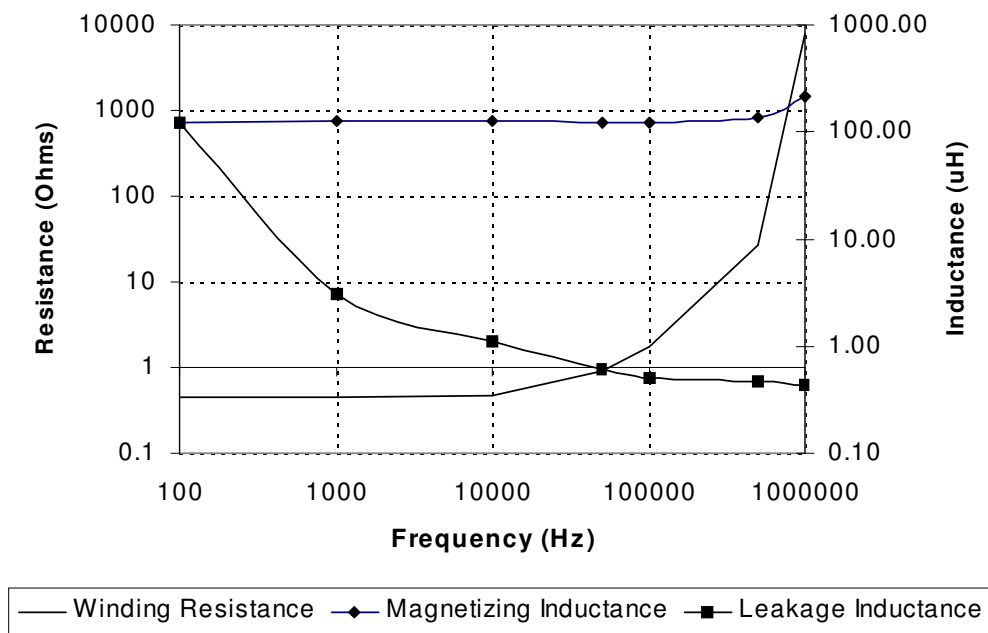


**Figure 11.25 Measured Parameters for APC41199 transformer vs Frequency**

Using these values in the model previously shown in figure 11.5, the insertion loss was simulated using Pspice and compared with the measured values as shown in figure 11.26.
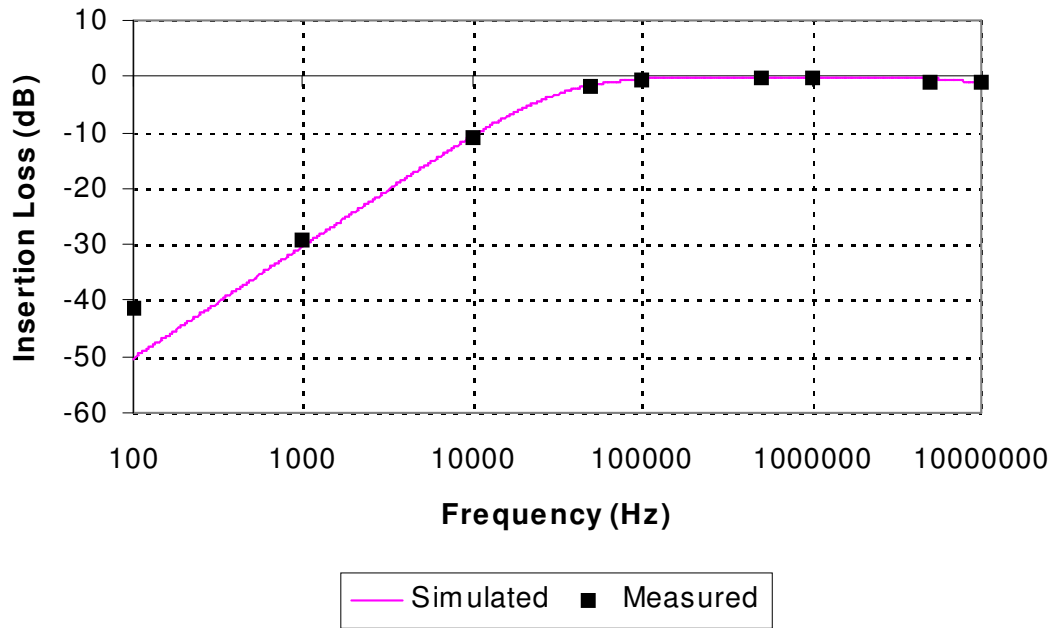
**Figure 11.26 : Measure and Simulated Insertion Loss for APC41199**

The insertion loss in the mid band range (~500kHz) was measured at –0.3dB with a simulated value of –0.11dB.

### 11.8.4  E14 Insertion Loss Measurements and Simulation

The measured values of magnetizing inductance, winding resistance and leakage inductance over the 100Hz to 1MHz range are given in figure 11.27
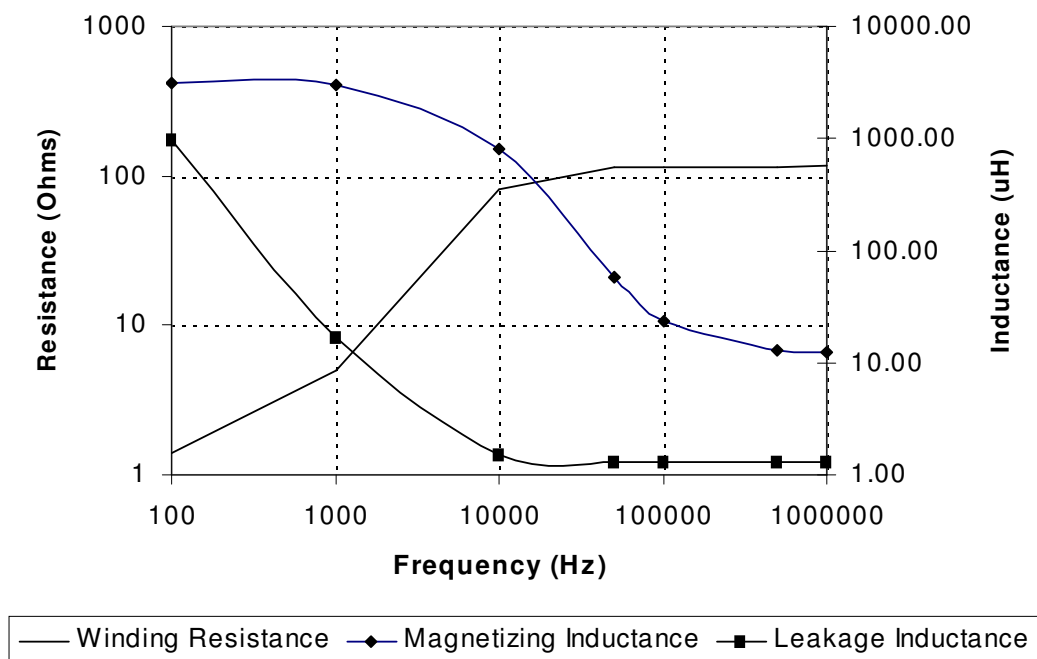


**Figure 11.27 Measured Parameters for E14 transformer vs Frequency**

Using these values in the model previously shown in figure 11.5, the insertion loss was simulated using Pspice and compared with the measured values as shown in figure 11.28.
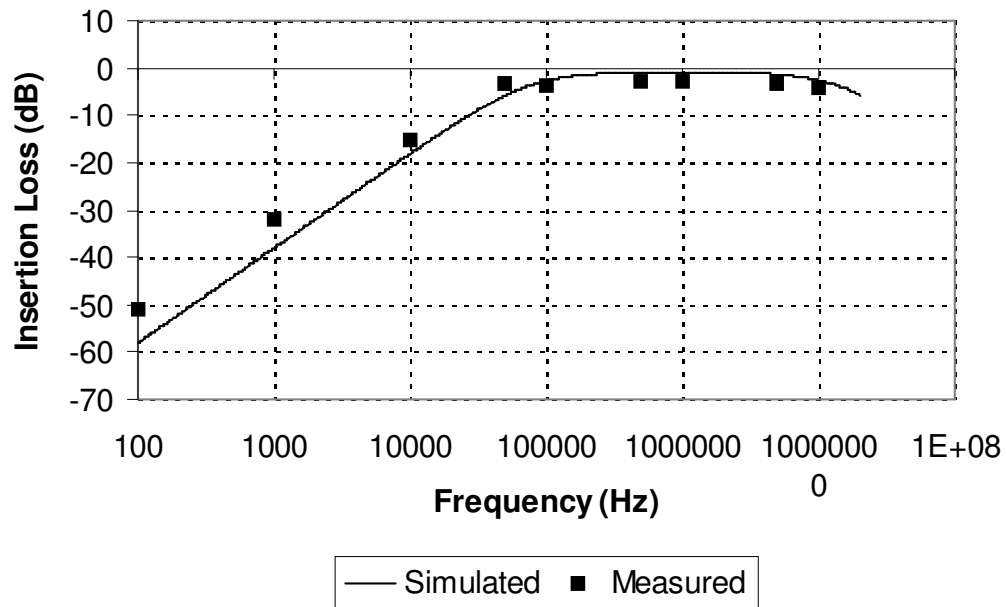


**Figure 11.28 : Measure and Simulated Insertion Loss for E14**

The insertion loss in the mid band range (~500kHz) was measured at –2.7dB with a simulated value of –1.76dB (The increased insertion loss is primarily due to the higher resistance in the prototype planar windings compared to the wirewound component, as has been discussed previously).

### 11.8.5 E18 Insertion Loss Measurements and Simulation

The measured values of magnetizing inductance, winding resistance and leakage inductance over the 100Hz to 1MHz range are given in figure 11.29
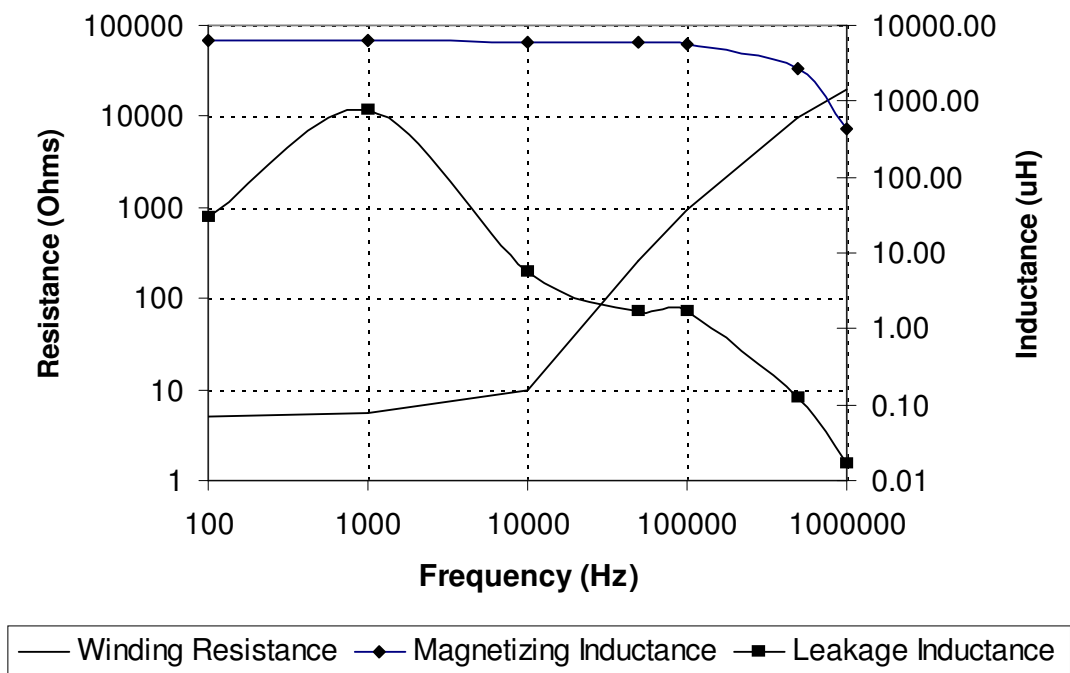
**Figure 11.29 Measured Parameters for E14 transformer vs Frequency**

Using these values in the model previously shown in figure 11.5, the insertion loss was simulated using Pspice and compared with the measured values as shown in figure 11.30.
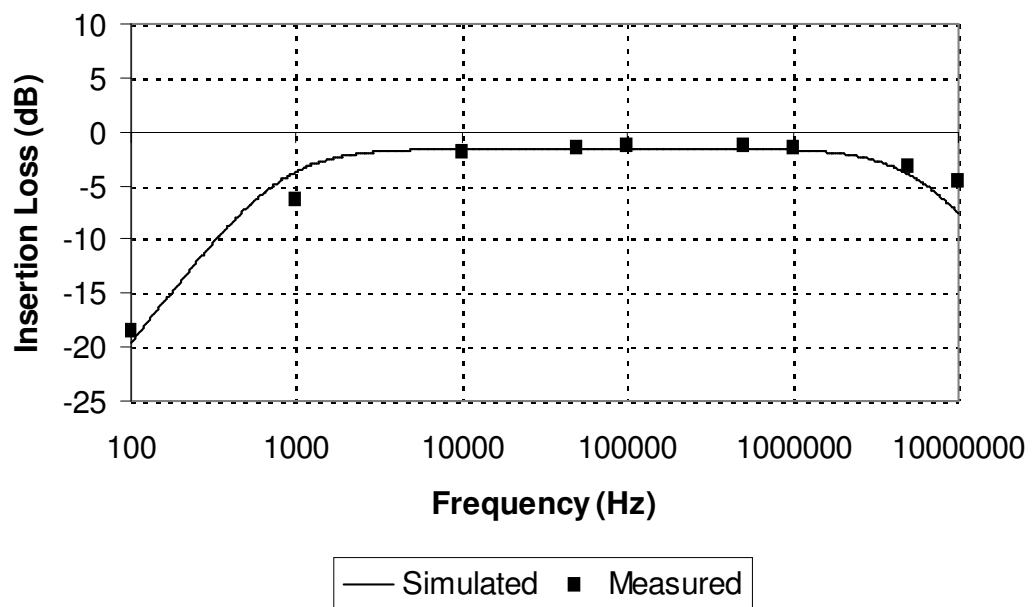


**Figure 11.30 : Measure and Simulated Insertion Loss for E18**

The insertion loss in the mid band range (~500kHz) was measured at -1.3dB with a simulated value of –1.6dB.

## 11.9 Predicting Inter-Modulation Distortion using Simulation

### 11.9.1 Introduction

The definition of inter-modulation distortion has been made previously in this chapter, with the second and third order products being of particular interest. In a typical broadband application, such as ADSL, there is the scope for a large number of signals to be transmitted through the hybrid at a 4.3125kHz separation. It has previously been highlighted how distortion of single tone signals may occur due to the non-linearities in the line transformer. In this section it will be demonstrated how simulation can be used in a very similar fashion to predict the potential inter-modulation behaviour of the line transformer.

### 11.9.2 APC41199 Measured and Simulated IMD Results

To measure the effect of Inter Modulation Distortion (IMD) due to the non-linearities in the magnetic component a two tone signal was applied to a 50Ω load, with and without the APC41199 benchmark transformer in place. The basic test configuration is shown in figure 11.31, with two low distortion signals summed using a simple opamp circuit and applied to the DUT. The DUT is a straight wire connection in the first instance to establish the distortion due to the opamp circuit and then this is replaced by the magnetic component under test (in this case the APC41199). The two signals applied are 1V sinusoidal signals 4.3125kHz apart (the spacing between ADSL signals). The tests were applied at frequencies of 10kHz and 14.3125kHz with the resulting spectrum shown in figure 11.32.
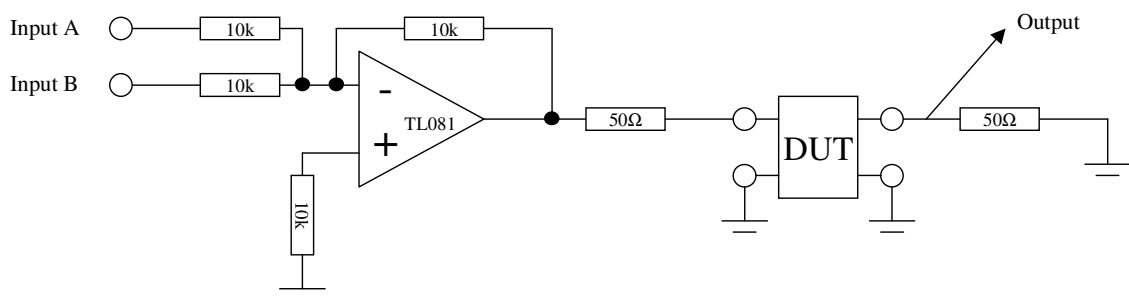


**Figure 11.31: IMD Test Circuit**
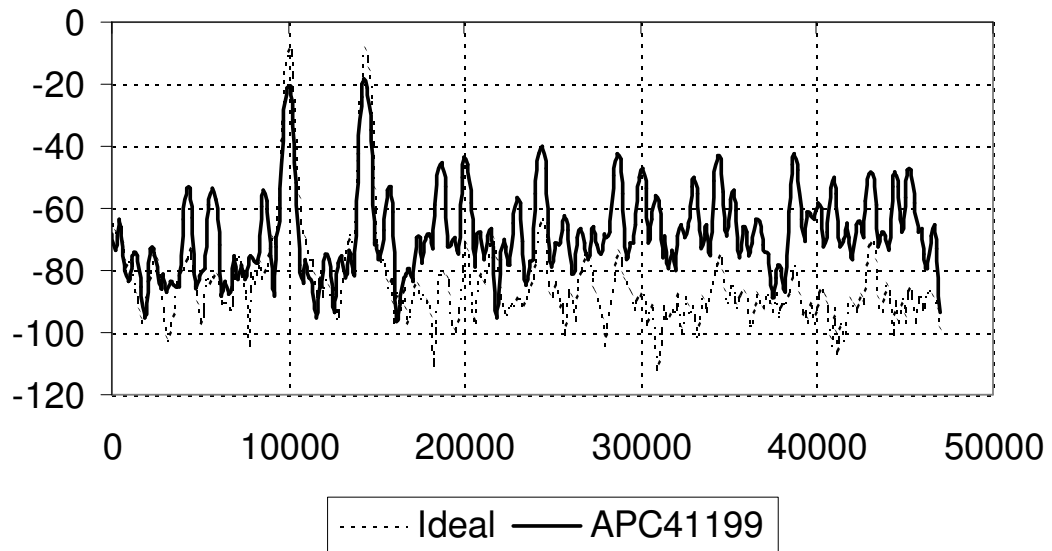
**Figure 11.32: Measured Frequency Spectra for APC41199 with two tone input**

The definition of IMD was given previously in this chapter and the third order products measured at 5.7kHz, 18.6kHz, 34.3kHz and 38.6kHz. It is possible to largely predict these harmonics using simulation models including the non-linear core models used previously in this chapter. Carrying out a simulation and measuring the $3^{nd}$ order IMD allows the comparison to be made. The simulation analysis was carried out in two stages. The first stage being a 7ms transient (time domain) analysis followed by a Fast Fourier Transform (FFT) of the output signal to calculate the harmonics of the output voltage, with the resulting frequency spectrum is given in figure 11.33 and the measured and simulated third order harmonics summarised in table 11.5.
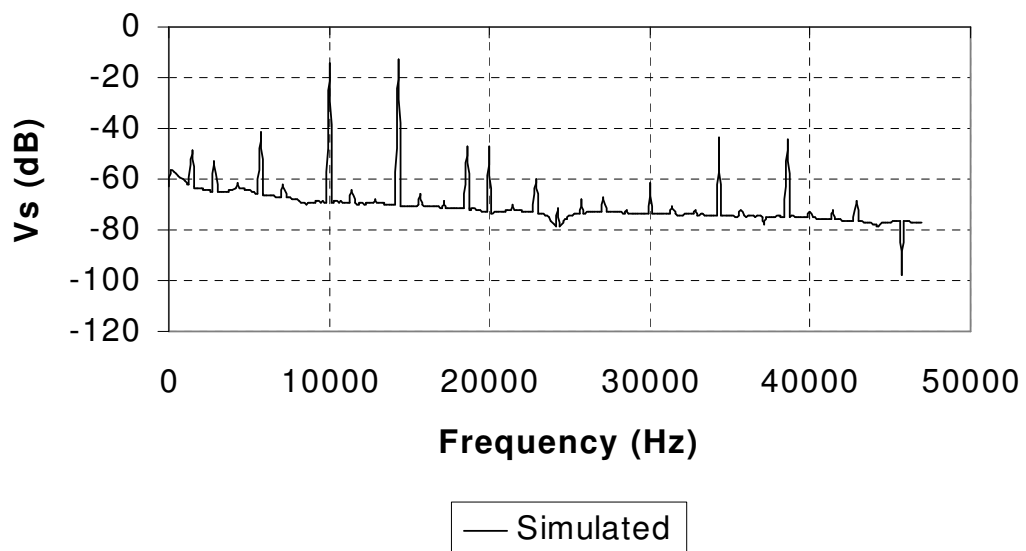


**Figure 11.33: Simulated Frequency Spectrum for APC41199 with two tone input**

204

| Frequency (Hz) | Measured (dB) | Simulated (dB) |
|:---:|:---:|:---:|
| 10k | -22 | -22 |
| 14.3k | -20 | -20 |
| 5.7k | -53 | -41 |
| 18.6k | -45 | -47 |
| 34.3k | -43 | -43 |
| 38.6k | -42 | -44 |

**Table 11.5: Measured and Simulated third order IMD products and input signals**

Using these values and equation 11.8 the third order IMD for the measured transformer was calculated to be –17.9dB and the simulated as –16.5dB.

While this simulation shows the principle of predicting the IMD products using simulation, it is clear that further investigation is required into the link between specific non-linear behaviour in the magnetic core and the resulting IMD. It is beyond the scope of this thesis to investigate the nature of ADSL signals in general, but the behaviour of multiple carrier systems with modulated waveforms implies extremely complex inter-modulation characteristics. It can be seen clearly from figure 11.32 that higher order products exist and that other interactions between the $2^{nd}$-$5^{th}$ harmonics of the fundamental signals are also taking place.

## 11.10 Predicting Trans-hybrid Loss using Simulation

### 11.10.1 Introduction

To illustrate how the transformer models developed in this chapter can be applied to the complete ADSL hybrid to estimate system parameters such as the THL (Trans Hybrid Loss), an example electronic hybrid is simulated in this section. Realistic transformer models are included in the simulation to estimate the effect of component parasitics on the performance of the hybrid as a whole. The basic configuration of one channel of the hybrid is shown below in figure 11.34 (In this case the low pass filter for the POTS telephone circuit has not been included). In the full hybrid there are a number of these channels, which are identical. The hybrid consists of the high pass filter for the higher speed transmit path, the low pass filter for the receive channel and the line driver. The output of each line driver is connected to a line transformer. There are also line protection circuits on the line side, but these have been neglected in this model.
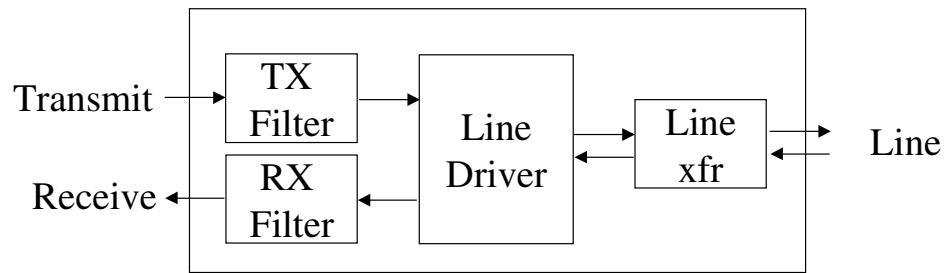
**Figure 11.34 : Block Diagram of ADSL Hybrid Channel**

Nash [247] provides a set of example ADSL driver circuits which can be modified to fit the requirements of the individual line driver and line impedance. The line impedance will generally be either 100Ω or 135Ω, and the driver circuit must be matched to this impedance. The Receive (RX) and Transmit (TX) filters are used to match the impedance to the line across the ADSL bandwidth, and to ensure that the signal from the Transmit to Receive path is attenuated (ideally to zero) and similarly from the line to the transmit port in the receive band. The general form of the electronic hybrid circuit is shown in figure 11.35.
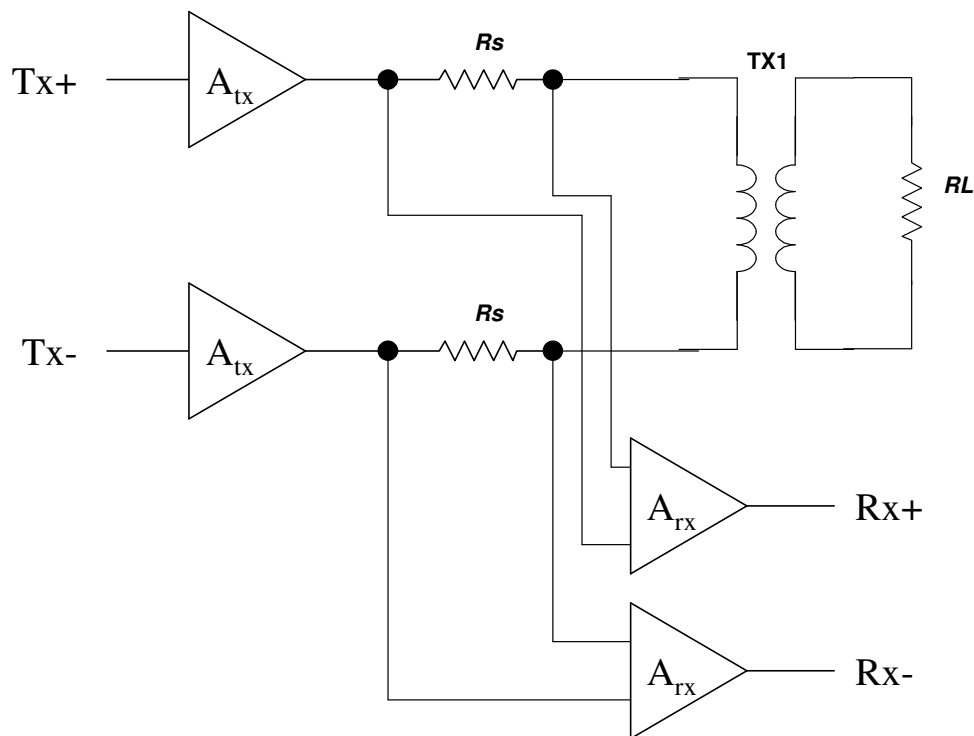


**Figure 11.35 ADSL Electronic Hybrid Circuit**

The component values for this basic driver circuit are derived from the load impedance and the driver gain requirements. The simplest approach could be to use amplifiers with unity gain and a transformer turns ratio of 1:1, therefore $R_s$ will be 50Ω and a gain of say, 2. Generally, however, the gain of the driver circuit will be higher (for example 10), and the transformer used to step up

206

the voltage from the Transmit to the Line side. This ratio is usually between 1.3 and 2. The design decision to be made is whether to have a higher power amplifier and a step down ratio, or a lower power amplifier and a step-up turns ratio. One advantage of a step-down ratio from the device to the line is that the line to receive path then has a step-up ratio, potentially improving the Signal to Noise Ratio (SNR).

The detailed design of the transmit and receive filters is beyond the scope of this thesis, however Nash [247] describes one method of implementing a receive path filter. The passbands of the filters depend on the type of ADSL used. Full rate ADSL allows the use of the same bandwidth area, but ADSL G.Lite clearly separates the transmit and receive bands. The full passband range for ADSL is 25.875kHz to 1.104MHz (Transmit from Central Office to Customer Premises) and 25.875kHz to 138kHz (Received at Central Office from Customer Premises). The hybrid can also be implemented using splitter transformers and balanced impedances as described in the next section.

### 11.10.2        Definition of the Trans-Hybrid Loss

The Trans-Hybrid Loss (THL) is defined in this application as the loss or isolation between the transmit and receive ports of a two-wire to four wire hybrid. The THL also includes the loss from the transmit-to-line and line-to-receive ports respectively. If the example magnetic hybrid shown in figure 11.42 is considered, the THL is obtained using the expression given in 11.9. This assumes that all the impedances are matched, but if the transmit, receive and line impedances do not match, then the appropriate impedance transformations must also be included in equation 11.9. Equation 11.10 shows the method of calculating the receive-to-transmit loss including the impedance transformation.
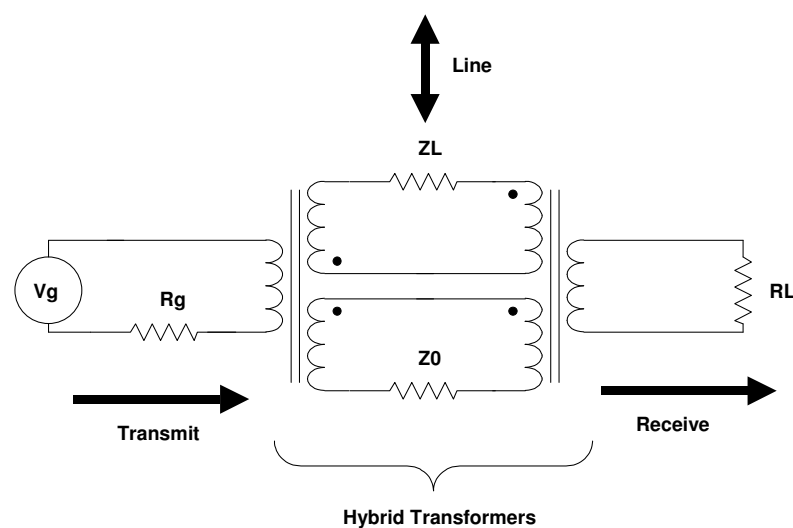


**Figure 11.36: two-wire to four-wire hybrid schematic diagram**

$$THL_{dB} = Rx \rightarrow Tx_{dB} - Line \rightarrow Rx_{dB} - Line \rightarrow Tx_{dB} \qquad (11.9)$$

$$Rx \rightarrow Tx_{dB} = 20\log_{10}\left(\frac{V_{RX}}{V_{TX}}\right) + 10\log_{10}\left(\frac{Z_{TX}}{Z_{RX}}\right) \qquad (11.10)$$

In may cases the Trans Hybrid Loss is just taken as the Transmit to Receive loss, not including the line losses.

### 11.10.3 APC78155 ADSL Hybrid Simulation

In order to test the usefulness of predicting the behaviour of the hybrid as a whole, containing the full transformer model, an example APC ADSL hybrid was measured and simulated to obtain the Trans Hybrid Loss and the Line to Transmit transfer function. The hybrid chosen was the APC78155 (Central Office) electronic hybrid, for use with the Centillium Octal Flite Chip Set. The Line Transformer was the APC41240S.

The detailed schematics of the hybrid cannot be published in this thesis due to commercial reasons, but the form of the hybrid follows the general structure in figure 11.35. The line transformer has a turns ratio of 1.8:1 (Line:Device), with an inductance of 450uH on the line side, Leakage inductance of 5.5uH (Max) and winding resistance of 0.5Ω on the device and 1.6Ω on the line side). The transformer model (including parasitics) described early in this chapter was implemented using the measured parasitic values, and the hybrid modelled using the schematics provided by APC. The transfer functions from transmit port to the Line (terminated with 100Ω) and also to the receive port were measured[11] and simulated with the results given in figures 11.37 and 11.38 respectively.

---

[11] The measured transfer functions were supplied by Advanced Power Components Ltd (APC) using an HP Network Analyser.
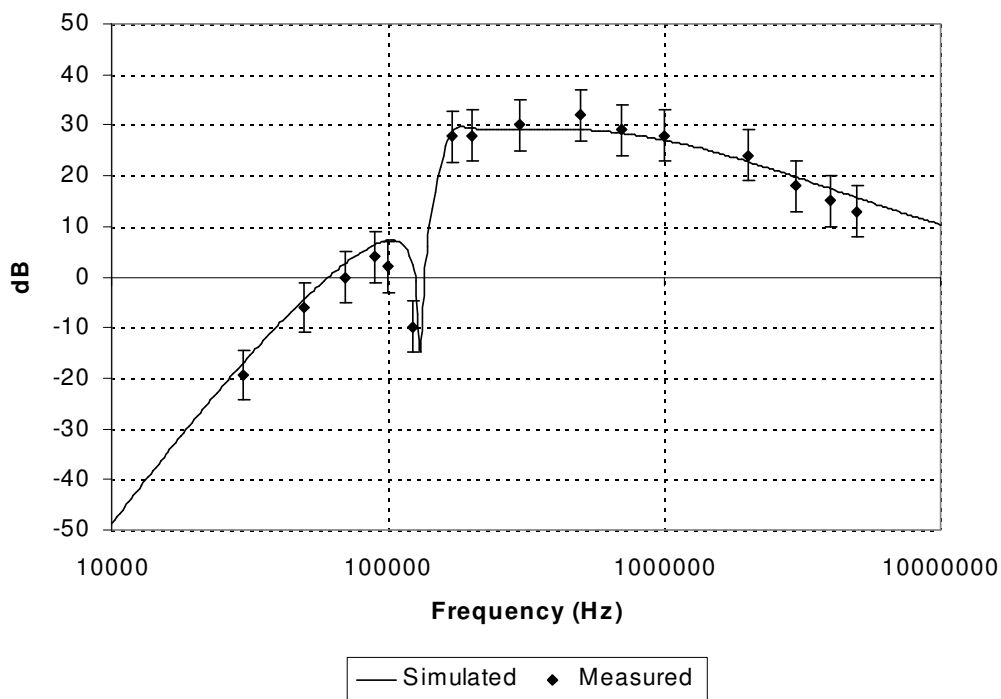
**Figure 11.37: APC78155 Measured and Simulated Transmit to Line Transfer Function**
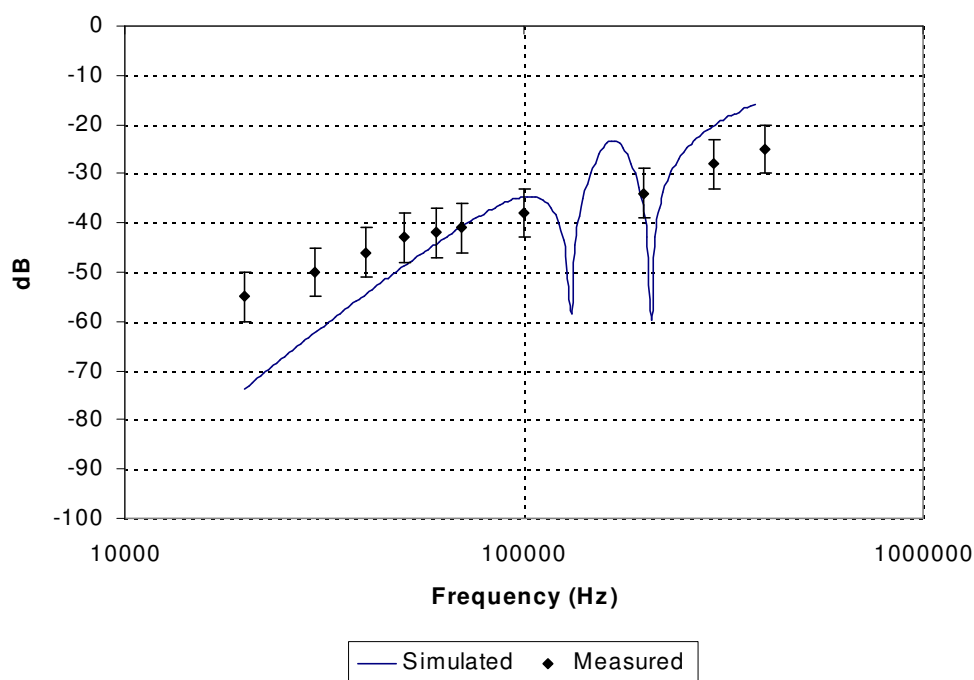


**Figure 11.38: APC78155 Measured and Simulated Transmit to Receive Transfer Function**

The effect of having an accurate transformer model can be clearly seen if the same simulations are carried out using an ideal (standard) transformer model with the same test circuit and hybrid model. The results are shown in figure 11.39.
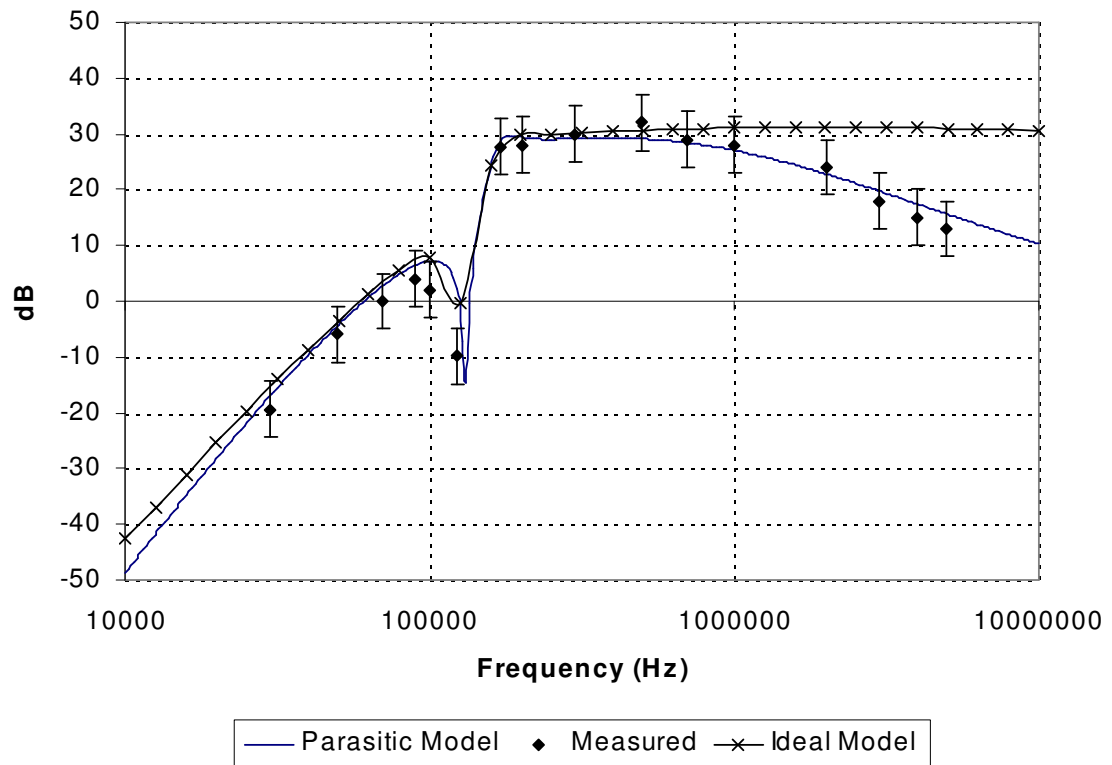
**Figure 11.39: APC78155 Line Transfer Function (measured, ideal and parasitic model)**

The difference the accurate line transformer model makes is clear from 11.39. The winding resistance causes added insertion loss across the range of operation, and the leakage inductance causes the transfer function to fall off rapidly at the upper end of the passband (~1MHz).

## 11.11 Simulating Transformer Parameter Variations

### 11.11.1 Introduction

All of the simulations carried out in this chapter have used a set of nominal (or in some case worst case) parameter values to predict the behaviour of the device (transformer) in isolation or in a circuit context. One of the powerful aspects of simulation is the ability to include statistical variations into the model parameters and assess the likely behaviour for a large number of devices in a production environment. This is especially important for magnetic components as the material and geometric tolerances may be large (up to 40% or more). With more and more companies adopting a 6σ approach to design, where the ±3σ variations are taken into account as well as the nominal and tolerance values, the use of simulation to predict the design behaviour is becoming an essential tool in the design process.

In this section, an example device (APC41199) will be simulated with the model parameters including statistical variations, and the variations of the performance resulting assessed.

### 11.11.2 Including Variations in Model Parameters

Most simulators allow model parameters to include statistic variations. In SPICE, for example, the standard models include a DEV parameter that defines the variation in a parameter (e.g. 5%). One limitation in SPICE is that this only applies to a predefined set of models, and is not able to be used in all cases (such as user defined models). Other simulators that use a Hardware Description Language (such as Saber) allow more flexibility in the definition of tolerances and distributions. To define a normal Gaussian distribution of 1% with a nominal value of 1 requires the parameter to be described using ***normal(1.0,0.01)*** rather than just 1.0. Due to this flexibility, the Saber simulator was used to obtain the simulation results in this section.

### 11.11.3 Monte Carlo Simulation

Monte Carlo simulation is a method of incorporating parameter tolerances in simulation. Vlach and Singhal [9] provide further background on this subject, but the approach is essentially to run a number of simulations with a randomly varied set of parameters, where each parameter has a variation within its own tolerance limits. The result is a family of curves, one for each analysis run, that reflects the statistical variations in the response of the circuit as a whole.

### 11.11.4 Simulating insertion loss statistical variations

The APC41199 transformer model was constructed using the mixed domain approach described in this chapter, and parasitics also included. The core material was modelled using a linear core model, with a statistical variation of 30% on the material permeability. 5% tolerances were included on all the parasitics. Using an AC analysis to simulate the insertion loss, a Monte Carlo simulation was carried out over 100 individual simulations to include the parasitic parameter variations. The resulting 100 insertion losses obtained are shown in figure 11.40.
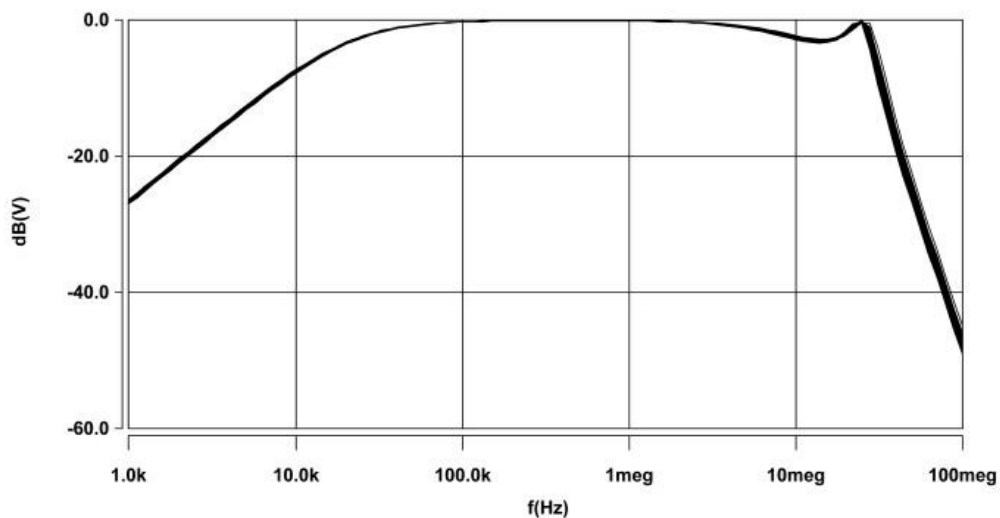


**Figure 11.40: Insertion Loss Simulation Results over 100 runs**

The differences between the simulation runs are relatively small making it difficult to quantify the effect on performance due to the parameter variations. It is therefore useful to carry out specific measurements (such as the 3dB points) and show those either as scatter plots versus simulation run, or as a histogram. Examples of this are shown in figures 11.41 and 11.42 respectively.
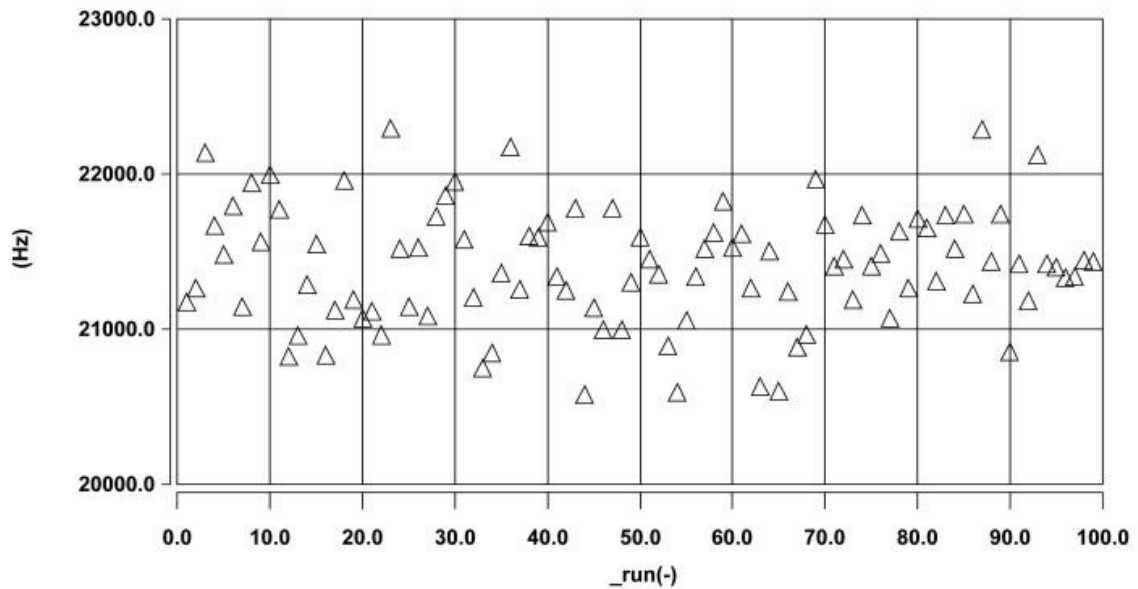


**Figure 11.41: High Pass Response –3dB point over 100 simulation runs**
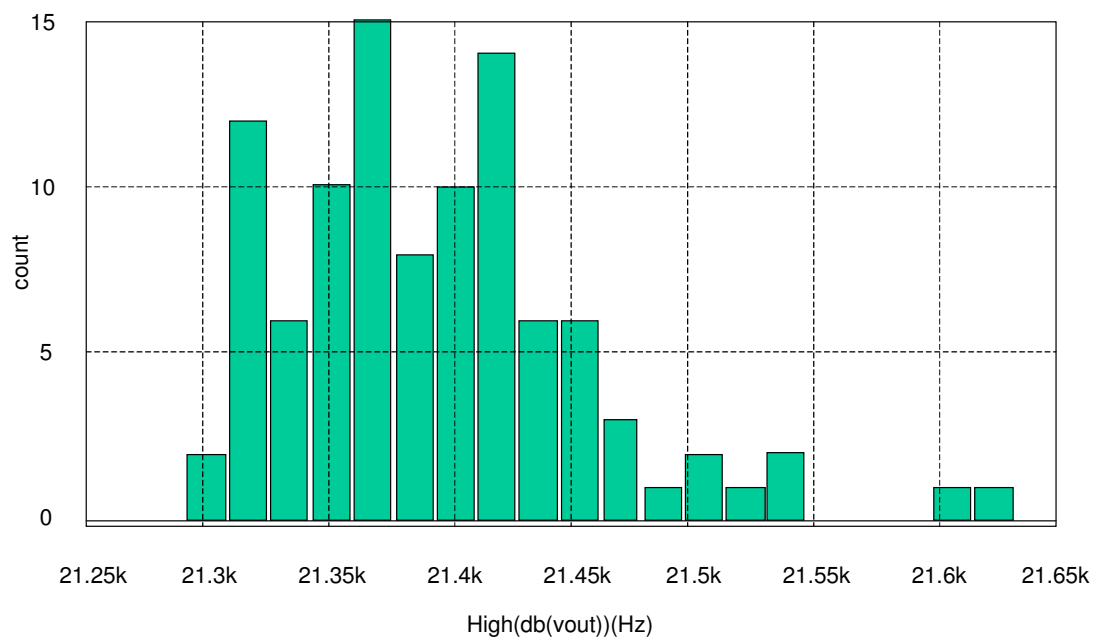


**Figure 11.42 Histogram of High Pass Response –3dB point**

The advantage of having the Monte Carlo simulation results available in this form and being able to carry out measurements statistically is that the mean and standard deviations for the results can be obtained directly. If the parameters are also stored, then regression analysis can be carried out

212

to establish the correlation between a particular parameter and the measurement in question. To demonstrate this the insertion loss in the passband was obtained from the Monte Carlo simulations, as shown in figure 11.43.
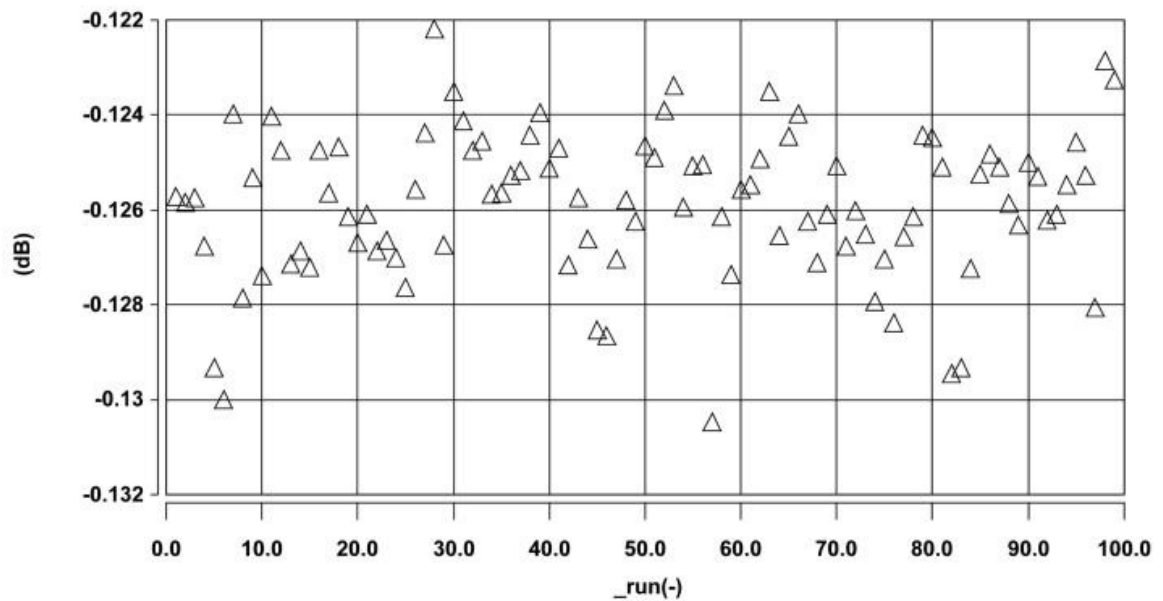


**Figure 11.43: Insertion Loss over 100 Monte Carlo Simulation Runs**

These results can then be plotted with respect to the stored value of particular parameters to establish their correlation or otherwise. In this case the insertion loss in the passband is directly related to the winding resistance, as shown in figure 11.44.
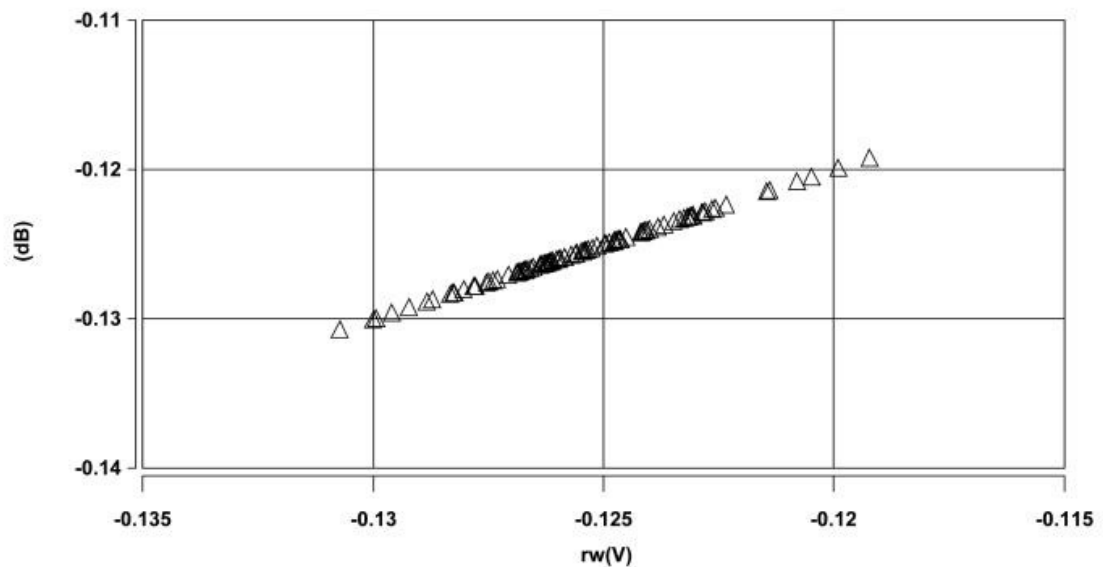


**Figure 11.44: Correlation between insertion loss and winding resistance (rw)**

### 11.12 Conclusions

This chapter has concentrated on the aspects of modeling transformers relevant to their application in ADSL systems. The modeling and simulation of the Total Harmonic Distortion has demonstrated how accurate non-linear core models are required to obtain practically useful results. The introduction of multiple tones and subsequent measurement of Inter Modulation Distortion revealed that there were limitations with the Jiles-Atherton model in this context, however many important modulation products were predicted accurately. In general the extension of existing techniques to include a non-linear core model has been demonstrated to provide further insight into the non-linear behaviour of the transformer in communications systems, such as ADSL, as this has been generally neglected.

The use of planar magnetics for the implementation of ADSL transformers has been proposed, simulated and tested against the existing wire wound approach. While there still remain issues to be resolved to obtain the level of performance required for a commercial application, the technique has been demonstrated to be generally feasible. An elegant approach for the efficient utilisation of winding space has been used to increase the effective use of the winding area.

With the accurate modeling of the line transformer, predictions were made of the Insertion Loss of the device, and this was extended to include the complete ADSL hybrid. Simulations and measurements of the Trans Hybrid Loss, and the transfer functions across the hybrid show a good match, and have been used in practice to optimise the hybrid and transformer combination.

Finally, statistical methods were demonstrated that allow prediction of the performance of devices in a production environment. By using a mixed domain approach for the basic transformer, in conjunction with parasitic elements, geometric and parasitic variations were able to be considered in assessing the performance of transformers in a virtual production environment.

*Chapter 12*

# 12 Discussion and Conclusions

## 12.1 *Discussion of Results*

### 12.1.1 Core Modeling

A significant portion of this work has been devoted to the effective and accurate characterization of magnetic material models for use in circuit simulation. After taking the decision to primarily use the Jiles-Atherton model of hysteresis as the basic model, several key developments were made. The original equations include a directional parameter ($\delta$) that indicates the direction of the magnetic field strength ($H$) in a binary fashion (+1 or –1). A modification to this behaviour was proposed that removes the discontinuity and hence improves the ability of simulations to converge using this model.

Investigations into the behaviour of magnetic materials showed that for materials driven heavily into saturation, the BH loops tended to close at high levels of $H$. This 'loop closure' behaviour could not be controlled independently in the original Jiles-Atherton model, and so two modifications were proposed to remedy this fact. The first method proposed was to modify the effective $H$ inside the Jiles-Atherton model using an exponential function that would be activated when a threshold value of $H$ was reached. The second method was to include a variation of the $k$ parameter in the model using a Gaussian function of $H$. The $k$ parameter essentially controls the width and curvature of the BH curve as the material saturates. This second method is alluded to in the original paper in general terms, but this elegant modification seems to provide a simple and accurate approach with minimal convergence difficulties.

At the other end of the model range, for small (minor) loops, the behaviour of the Jiles-Atherton model becomes different from measured behaviour. Modeled minor BH loops tend to have an incorrect slope (too steep) and to have an area that is larger than the equivalent measured BH loop. Modifications to the Jiles-Atherton model have been proposed to correct this problem, but investigations in this thesis have demonstrated that although this approach can be effective for static situations, in situations where the stimulus may be dynamic or arbitrary the model modifications may cause un-physical behaviour.

Further work has been done on the characterization of magnetic core models and the development of thermal dependencies of model parameters, but this is referred to specifically later in this chapter.

### 12.1.2 Characterization Methods

To utilize the magnetic core models developed it was necessary to produce effective methods of characterization. Software was developed that could accurately characterize the Jiles-Atherton model parameters from measured BH data. A test bench methodology was developed using a test circuit, DSP stimulus and software post-processing to semi-automate this procedure. Integral to this work was the development of optimisation techniques and goal functions.

Initial optimisation using Univariate Search methods proved effective, but rather slow. Alternative methods were therefore investigated including Simulated Annealing (SA) and the Genetic Algorithm approaches. The Genetic Algorithm (GA) method proved particularly effective for optimisation of the magnetic core model parameters. Statistical comparison of the GA and SA approaches demonstrated that over time the GA method could produce models of a significantly higher accuracy than the SA method.

Other developments in the characterisation procedure included the use of multiple loop optimisation to allow the model parameters to be applicable over a much wider range of operation. Existing methods tend to use the major loop, but in cases where the signal peak to average ratio (PAR) is high (such as ADSL applications) it becomes important for the model to be able to cope with this range of operation. Another development has been the use of metrics to define the goal function for the optimisation procedure. Existing methods use a least squares approach to define the goal function, but the use of metrics allows specific aspects of the BH curve to be used to accurately characterize the model for the eventual requirements of the application.

### 12.1.3 Magnetic Component Modeling

The use of a building block approach for the development of complete magnetic component models allows the individual pieces of the model to be developed separately and re-used in multiple applications. A library of models was therefore developed for use in the SPICE, Saber and VHDL-AMS simulation environments. A mixed domain approach was used so that magnetic core models would operate in the magnetic domain, with flux and MMF as variables, and connect via interface winding models to electric circuit models. This allows access to not only electrical information in the simulation, but also internal magnetic behaviour in the core models. This aspect of the modeling approach has been essential in the understanding of the magnetic component behaviour in the applications used in this thesis work.

While some aspects of the magnetic component are relatively well understood (such as the windings), there are limitations in the existing models. Investigations into the use of Finite Element (FE) Analysis to characterise the leakage inductance of the windings at high frequencies has demonstrated potential problems with particular FE approximations. This work has also

realized a simple model structure for leakage inductance that can be used to replace the more complex existing models generated by analytical or FE methods.

The use of VHDL-AMS models has also resulted in the development of a language based model editor and debugger, that has been used on other projects and for teaching purposes.

### 12.1.4 Hybrid Finite-Element and Circuit Simulation Methods

A technique that was tested during this thesis work was linking circuit simulators to Finite Element Analysis solvers. This idea uses the circuit simulator to model the electrical circuit, and the FE solver to model the magnetic component. A prototype hybrid simulator was implemented using the Xspice simulator and the SLIM FE solver and tested with a simple inductor and also a Switch Mode Power Supply example.

While the concept operated correctly for these examples, and the technique offers the ability to combine the understanding of the circuit behaviour with the field behaviour of the magnetic component in a single simulation there are some problems that have been highlighted by this work. The first obvious point to note is the time required to carry out significant simulation times. If the FE solver is required to be called at every iteration then the simulation times can be prohibitive. There is also the risk of non-convergence that is essentially out of the control of the circuit simulator - due to the FE analysis being a separate process. Tests were carried out using the Saber simulator to test whether the convergence problems were a function of the Spice simulator, but while the convergence was better than Xspice, problems still occurred.

Another issue with this method is the inability of this approach generally to cope with hysteresis. Each iteration initialises a new FE analysis and this has no knowledge of the previous analyses carried out. This simple decoupled approach does not allow the accurate modeling of hysteresis behaviour or other initial conditions.

### 12.1.5 Multiple Domain Modeling

One of the purposes of the use of multiple domains has been to include thermal behaviour into the magnetic core models. By using the multiple domain approach, the circuit can be divided into electrical, magnetic and thermal sections and appropriate interface models developed. The complete system can then be simulated in a single integrated simulation.

In order to carry this simulation out, thermal models were developed for the thermal conduction, convection and emission of heat and extensions to the Jiles-Atherton model made to estimate the heat loss from the core. Other extensions included the winding model having a thermal output for the resistive winding loss.

Measurements were carried out on magnetic materials to characterize the variation of model parameters with temperature. This behaviour was included in the Jiles-Atherton model by adding a thermal pin and thermal parameters. The model was tested statically using an oven to control the temperature and the resulting model behaviour correlated well with the measured results. Dynamic model tests were also carried out to measure the effect of self-heating in the core, and the resulting change in behaviour.

### 12.1.6 Applications Simulation

#### 12.1.6.1 Passive Fault Current Limiters

In this application the use of magnets required the development of a range of magnet models from simple linear magnetic offsets to non-linear hysteresis models. A Passive Fault Current Limiter (FCL) was constructed and tested, then the results compared with an equivalent simulation model. A good correlation between the measured and simulated results was observed. The use of the multiple domain models allowed the magnetic behaviour to be analysed in some detail. The BH behaviour of the magnetic core in particular showed the transition of the FCL component in and out of its limiting region.

#### 12.1.6.2 ADSL Broadband Transformer Modeling

Existing methods of predicting the behaviour of broadband transformers have generally assumed a linear core model and concentrated on winding parasitics such as leakage inductance and resistance. The models were extended in this thesis to include non-linear core models of the form previously described to allow prediction of key distortion parameters such as Total Harmonic Distortion (THD), Inter Modulation Distortion (IMD) and the Insertion Loss (IL) across the frequency range. The models were also used to model the complete analogue hybrid in order to predict the Trans Hybrid Loss (THL).

In general, the existing commercial implementations of broadband transformers use an EP13 core (or similar) with a wire wound construction. As part of this section of the work a series of planar transformers were developed, modelled and tested to investigate their potential applicability in this application. Software was developed to automatically generate PCB designs for specific cores in a number of winding configurations (2 layer, 4 layer, interleaved, bi-filar etc). Initial results demonstrate the THD performance is acceptable, even for these initial prototypes. While there still remain issues to be resolved to obtain the level of performance required for a commercial application, the technique has been demonstrated to be generally feasible. An elegant approach for the efficient utilisation of winding space has been used to increase the effective use of the winding area.

With the accurate modeling of the line transformer, predictions were made of the Insertion Loss of the device, and this was extended to include the complete ADSL hybrid. Simulations and measurements of the Trans Hybrid Loss, and the transfer functions across the hybrid show a good match, and have been used in practice to optimise the hybrid and transformer combination.

Finally, statistical methods were demonstrated that allow prediction of the performance of devices in a production environment. By using a mixed domain approach for the basic transformer, in conjunction with parasitic elements, geometric and parasitic variations could be considered in assessing the performance of transformers in a virtual production environment.

## 12.2  Conclusions

### 12.2.1 Project Objectives Achieved

The original project hypotheses are reviewed in this section and an assessment of the progress made given for each hypothesis.

*Hypothesis 1 :* Existing magnetic material models have inadequacies that need to be addressed including minor loops, loop tip closure and dynamic thermal behaviour.

This thesis has made significant progress in the areas of loop-tip closure and dynamic thermal behaviour with the provision of models that include this behaviour. Extensions to the existing models that claim to provide improved minor loop modeling have been tested and found to be effective in static cases, but problems still exist in dynamic minor loop modeling.

*Hypothesis 2 :* Parameter extraction methods are weak and new techniques require to be developed

*Hypothesis 3 :* Characterized model parameters are generally poor and new techniques are required for optimization and assessing performance.

Hypotheses 2 & 3 are closely related and are therefore combined. A complete magnetic model parameter extraction and characterisation software environment has been developed including metric and least squares goal functions, Univariate, Simulated Annealing and Genetic Algorithm optimisation routines, and multiple loop optimisation.

*Hypothesis 4 :* Magnetic component modeling approaches for high frequency circuits are limited and inaccurate.

Tests have quantified the errors obtained from Finite Element Analysis parameter extraction models and provide insight into the type of geometric approach required. Alternative models for modeling leakage inductance variations with frequency are presented.

*Hypothesis 5 :* Limited use is made of mixed domain modeling techniques to provide more insight into the behaviour of magnetic components in their target applications.

Multiple domain model libraries have been created and applied in Fault Current Limiter and Broadband applications.

*Hypothesis 6 :* Simplistic modeling approaches used for high-speed digital communications do not take into account magnetic component parasitics or non-linear behaviour.

An integrated non-linear broadband transformer model is presented and tested including parasitics and a non-linear core model. Standard performance tests including THD, IMD and THL have been carried out with the measured and simulated results correlating well.

*Hypothesis 7 :* The application of new modeling technology such as VHDL-AMS will allow detailed integrated modeling of systems including mixed technology aspects such as magnetic and thermal behaviour.

Integrated Electrical, Magnetic and Thermal domain simulations have been carried out using a variety of simulation approaches. Modeling Languages such as Saber's MAST and VHDL-AMS allow direct modeling of multiple domains without the need for 'equivalent' electrical models as used in the SPICE simulators.

Overall, all of the original hypotheses have been addressed. Progress has been made in all areas, with significant contribution in specific aspects of the work.

## 12.2.2 Specific Conclusions

In general, significant progress has been made in the area of core modeling and characterisation. The good results obtained in the final application tests are testament to this, and the model library has been extensively used in this work.

The modifications to the Jiles-Atherton model of hysteresis have provided a useful extension to the model, but this work has also indicated that the model is near the limits of its effective use. Recent work referred to has highlighted the view that of the range of available models, none will provide a completely accurate solution under all conditions. The goal of a 'unified' model of hysteresis that satisfies this ultimate requirement is therefore still outstanding. Nevertheless, it is true to say that for the applications used, the modified Jiles-Atherton model has proved very effective. One outstanding problem with the model, however, is the inaccurate modeling of dynamic minor loop behaviour. Tests on published methods have highlighted potential problems that require further investigation, but that is beyond the scope of this thesis and would be a useful piece of future work.

The development of optimisation methods for the characterization of magnetic model parameters has led to the first use of the Genetic Algorithm in this context. Comparisons between the Genetic and Simulated Annealing approaches show the differing results obtained, with the Genetic

Algorithm ideally suited to large problem spaces. The work on the use of a metric based goal function has demonstrated that for specific applications this can be more appropriate than the generally used least squares fit goal function.

The development of a software environment that can automatically carry out the majority of the characterization process from a simple measurement is a major improvement in the extraction of model parameters.

Much of the core modeling work would be effectively useless if there were not the building blocks to allow a complete magnetic component to be constructed and used in an electric circuit simulation. The development of building block libraries for use in the SPICE, Saber and VHDL-AMS simulation environments has made the process of including advanced non-linear core models in a circuit simulation straightforward.

The extension of the models to include thermal effects is important for many applications, including Power Supply design, where the temperature change in the core may be significant. The simulations in this thesis clearly show how the behaviour of the magnetic component can change significantly with a moderate temperature rise.

Advanced hybrid techniques linking circuit simulation to a Finite Element Analysis has demonstrated a 'curate's egg' outcome. The power of integrating an abstract circuit simulation, with a highly detailed physical component model has attractions, especially if insight into the field behaviour is required, but the practical limitations of the method have also been identified. If the simulation time is not a significant issue, and the whole system maintains convergence, then the approach has merit. If, however, time is critical and there is limited time to spend on analysis and simulation, then this method is just not practical.

An interesting sub-topic that has resulted from this thesis work is the development of a new planar implementation of ADSL transformers. A novel winding approach is described that allows a 4 layer implementation which can be integrated into the existing 4 layer analogue hybrid. This has the potential to significantly reduce the manufacturing costs associated with a separate wire-wound transformer component.

The ultimate goal of the modeling work has been to provide accurate magnetic component models for simulation in electric circuits. Several applications have used the proposed models, including a Power Application (Fault Current Limiter), where the analysis of the basic performance of the device relies on the accuracy of the core model. The other main application, ADSL broadband transformers, relies on the model to predict the non-ideal aspects of the component performance including the Losses, Distortion and Bandwidth. In each case, the main goals of the simulation have been achieved and demonstrated to be consistent with measured results.

### 12.2.3 Overall Conclusion

The overall conclusion made at the end of this project is that the main goal of being able to simulate magnetic components accurately in electric circuits has been achieved. The wide ranging nature of this subject has meant that it has been impossible to investigate every aspect of modeling magnetic components in this project, however significant progress has been made in a number of key areas, as described in the previous section. The results of the simulations of the individual applications correlate well in general with the equivalent measured results, demonstrating the effectiveness of the models and techniques developed.

### *12.3 Contribution*

### 12.3.1 Specific Contribution

The specific contributions made by this work include:

- Improved Jiles-Atherton Model of Hysteresis

- Development of Integrated Magnetic Core Model Characterisation Software

- First Genetic Algorithm Optimiser for Magnetic Models

- Development of Magnetic Component Model Libraries in Spice, Saber and VHDL-AMS

- Dynamic Thermal Extensions to Jiles-Atherton Model

- Spice-Finite Element Analysis Hybrid Simulation Method Development

- Prediction of ADSL transformer total harmonic distortion, inter modulation distortion and trans hybrid loss using simulation

- New planar implementation of ADSL transformers

### 12.3.2 Publications

As a direct result of this work, 4 journal papers have been published or accepted for publication, with a further 2 papers submitted for review. 3 papers have also been presented at conferences, with a further 3 papers presented that have indirect links to this thesis work. The complete list of publications is provided in the 'List of Publications' section of this thesis.

### 12.3.3 Contribution to Sponsoring Company (APC Ltd)

The most useful aspect of this work for APC (Advanced Power Components Ltd) has been the development of simulation techniques to predict the distortion and losses in transformers and hybrids as a whole. Several other designs, not described in this thesis, have been modelled and simulated using the techniques described in this work. In particular a VDSL hybrid design was re-

designed to include a matching network and the performance of the hybrid in practise exactly matched the simulation results. This work directly resulted in the solution to a significant design problem that would probably not have been solved without the use of simulation techniques.

The work on planar transformers has also provided a useful starting point for an ongoing research project into this area at APC, and has a promising future in this application.

## *12.4 Future Work*

### 12.4.1 Core Models

While progress has been made in improving the Jiles-Atherton model of hysteresis, it is also true that limitations still exist. Adequate general-purpose models including accurate dynamic minor loop behaviour require development. The goal of a unified model of hysteresis that can correctly model the macroscopic material behaviour under all conditions is still outstanding. A model that combines knowledge of the microscopic behaviour of individual grains of the magnetic material with the structural arrangement of the crystals would be a useful step.

### 12.4.2 Multiple Domain Modeling

The work completed on multiple domain modeling has made significant steps to allow complete integerated thermal-electrical-magnetic simulations, but further work is still required. The obvious application for this technique is in Power Supplies or Systems, and useful further research could be undertaken in this area. Of particular value would be the investigation into the use of arbitrary waveforms, such as the pulse waveforms commonly used in Switch Mode power Supplies, and the resulting thermal dependencies. Other extensions to the model include more accurate eddy current modeling.

### 12.4.3 Genetic Algorithm Extensions

The successful application of the genetic algorithm to the optimisation of magnetic material models suggests that the same approach could be used in more general applications. The use of the same method for other circuit elements or even complete circuits is an obvious next step.

### 12.4.4 Hybrid Finite-Element and Circuit Simulation Methods

The prototype hybrid Finite Element & Circuit Simulation approach is potentially useful, and as the computing power of PCs increases, becoming more practical for general use. The further development of this technique, perhaps with a tighter integration to the circuit simulation, would be a useful subject for future work. Modern Finite Element Analysis packages that already include limited time-stepping capability could be better equipped to link directly to circuit simulators with a more efficient algorithm than the simple connection illustrated in this thesis.

### 12.4.5  Broadband Transformer Modeling and Simulation

As the frequency of transmission increases, the models used for all the components in hybrids will need to be improved and their ranges extended. This will necessitate improved high frequency core models, with perhaps a more complex structural approach to model the effect of eddy currents in the core more accurately.

### 12.4.6  Planar Magnetics for Broadband transformers

The initial prototypes of planar magnetic broadband transformers indicate that this may be an extremely useful approach. Much further work could be undertaken in this area to investigate the relationship between the physical geometry and the device parameters and parasitics. A complete planar hybrid model including a number of planar transformers and inductors would be a good target for this work, with alternative implementations in Silicon or Thick Film as well as the current PCB approach.

# List of References

[1] J.C.MAXWELL, "A Treatise on Electricity and Magnetism", Clarendon Press Oxford, 1873, 3rd Edition.

[2] "Soft Ferrites Databook -MA01", Philips Components, 1998

[3] B. D. CULLITY, "Introduction to magnetic materials", Addison-Wesley, 1972

[4] J.D. KRAUS, "Electromagnetics", McGraw-Hill, 3rd Edition, 1984

[5] P.P. SILVESTER AND R.L. FERRARI, "Finite Elements for Electrical Engineers", Cambridge University Press, 3rd Edition, 1996

[6] K.J. BINNS, P.J. LAWRENSON AND C.W. TROWBRIDGE, "The Analytical and Numerical Solution of Electric and Magnetic Fields", Wiley, 1995.

[7] R. S. TEBBLE & D. J. CRAIK, "Magnetic Materials", Wiley-Interscience, 1969

[8] R. BOLL, "Soft Magnetic Materials", Heyden, 1978

[9] J. VLACH & K. SINGHAL, "Computer methods for circuit analysis and design", Van Nostrand Rheinhold, 2nd Edition, 1994

[10] R. KIELKOWSKI, "Inside SPICE, overcoming the obstacles of circuit simulation", McGraw Hill, 1994

[11] R. J. HOSKING, S. JOE, D. C. JOYCE & J. C. TURNER, "First steps in numerical analysis", Arnold, 2nd Edition, 1996

[12] D.A. LOWTHER & P. P. SILVESTER, "Computer-aided Design in Magnetics", Springer-Verlag, 1985

[13] S. R. H. HOOLE & P. R. P. HOOLE, "A modern short course in Engineering Electromagnetics", Oxford University Press, 1996

[14] P. HAMMOND & J. K. SYKULSKI, "Engineering Electromagnetism - Physical Processes and Computation", Oxford Science Publications, 3rd Edition, 1999.

[15] E. C. CHERRY, "The duality between inter-linked electric and magnetic circuits", *Proceedings of the Physics Society*, Volume 62, 1949 pp101-111

[16] E. R. LAITHWAITE, "Magnetic Equivalent Circuits for electrical machines", *PROC. IEE*, Vol. 114, November 1967, 1805-1809

[17] C.J. CARPENTER, "Magnetic Equivalent Circuits", *PROC. IEE.,*Vol 115,No 10, October 1968, 1503-1511

[18] AD BROWN, JN ROSS, KG NICHOLS AND MD PENNY, "Simulation of Magneto-Electronic Systems using Kirchoffian Networks", *European Conference on Magnetic Sensors and Actuators*, Sheffield, July 1998

[19] F PREISACH, "Über die Magnetische Nachwirkung", *Zeitschrift Fur Physik*, 1935, 277-302

[20] DC JILES & DL ATHERTON, "Theory of Ferromagnetic Hysteresis (invited)", *Journal of Applied Physics*, Vol. 55 , No 6, Mar 1984, 2115-2120

[21] D.C.JILES & D.L.ATHERTON, "Theory of Ferromagnetic Hysteresis", *Journal of Magnetism and Magnetic Materials*, 61, 1986, 48-60

[22] M.L. HODGDON, "Mathematical Theory and Calculations of magnetic hysteresis curves", *IEEE Transactions on Magnetics*, Vol. 24, No. 6, Nov 1988, 3120-3122

[23] J.H. CHAN, A. VLADIRIMESCU, X.C. GAO, P. LIBMANN AND J. VALAINIS, "Non-linear transformer model for circuit simulation", *IEEE Transactions on Computer Aided Design*, Vol. 10, No 4, April 1991, pp476-482

[24] D.C. JILES, J.B. THOELKE AND M.K. DEVINE, "Numerical Determination of hysteresis parameters for the modeling of magnetic properties using the theory of ferromagnetic hysteresis", *IEEE Transactions on Magnetics*, Vol. 28 , No 1, Jan1992, pp27-35

[25] P.P. SILVESTER & A. KONRAD, "Analysis of transformer leakage phenomena by high order finite elements" , *IEEE PES*, 1973, p1843

[26] Z. CENDES, D. SHENTON & H. SHAHNASSER, "Magnetic Field Computation using Delaunay Triangulation and Complementary Finite Element Methods" ,*IEEE Transactions on Magnetics*, Vol. 19, No 6, 1983, pp2551-2554

[27] E.C. SNELLING, Soft Ferrites, Butterworths, 2nd Edition, pp330-335

[28] R. ASENSI, J.A. COBOS, O. GARCIA, R. PRIETO & J UCEDA, "New Modeling Strategy for high frequency transformer windings", *IECON Proceedings*, 1994, pp246-251

[29] R. ASENSI, J.A. COBOS, O. GARCIA, R. PRIETO & J. UCEDA, "A full procedure to model high frequency transformer windings", *IEEE Power Electronics Specialist Conference Proceedings*, 1994, Vol. 2, pp856-863

[30] R ASENSI, J.A. COBOS, O. GARCIA, R. PRIETO & J UCEDA, "A CAD tool for magnetic components modeling", *American Power Electronics Conference (APEC)*, 1996, Vol 1, pp427-433

[31] A. DAUHAJRE & R.D. MIDDLEBROOK, "Modeling and estimation of leakage phenomenon in magnetic circuits", *PESC '86*, 1986, pp213-226

[32] C.J. CARPENTER, "A network approach to the numerical solution of eddy current problems", *IEEE Transactions on Magnetics*, vol. Mag-11, No 5, Sep 1975, pp1517-1522.

[33] S.P. HSU , R.D. MIDDLEBROOK & S. CUK, "Transformer modeling and design for leakage control", Advances in Switch Mode Power Conversion, 2nd Edition, TESLACo., 1983, Chapter 13, pp205-218.

[34] A. KONRAD, "Eddy Currents and Modeling", *IEEE Transactions on Magnetics*, Vol. Mag-21, No 5, Sep 1985, pp1805-1810

[35] P.L. DOWELL, "Effects of eddy currents in transformer windings", *Proceedings of the IEE*, Vol. 113, No 8, 1966, p1387

[36] J. PATRICK JESSE, "A coupled thermal-magnetic Finite Element Model for High-Frequency Transformers", MSc Thesis, Virginia Polytechnic and State University, 1990

[37] H.A. MANTOOTH & E. CHRISTEN, "Modeling and Simulation of Electrical and Thermal interactions", Internal White Paper, Analogy Inc.

[38] R. YACAMINI & H. BRONZEADO, "Inrush currents in large transformers using an electromagnetic model in Saber", Analogy Application Note, Analogy Inc.

[39] L.H. LEWIS, J. GAO, D.C. JILES & D.O. WELCH, "Modeling of permanent magnets: interpretation of parameters obtained from the Jiles-Atherton hysteresis model", *Journal of Applied Physics*, Vol. 79, No 8, 1996, pp6470-6472.

[40] N. SCHMIDT & H GULDNER, "Simple method to determine dynamic hysteresis loops of soft magnetic materials", *IEEE Transactions on Magnetics*, Vol. 32, No 2, Mar 1996, pp489-496

[41] W. ROSHEN, "Ferrite Core Loss for Power Magnetic Component Design", *IEEE Transactions on Magnetics*, Vol. 27, No 6, Nov 1991, pp4407-4415

[42] J.G ZHU, S.Y.R. HUI & V.S. RAMSDEN, "Discrete Modeling of magnetic cores including hysteresis eddy current and anomalous losses", *Proceedings of the IEE*, Vol. 140, No 4, July 1993, pp317-322

[43] E. DE LA TORRE, "Energy considerations in Hysteresis models", *IEEE Transactions on Magnetics*, Vol. 28, No 5, 1992, pp2608-2611

[44] J.G ZHU, S.Y.R. HUI & V.S. RAMSDEN, "A Generalized dynamic circuit model of magnetic cores for low- and high-frequency applications-Part I: Theoretical Calculation of the equivalent core loss resistance", *IEEE Transactions on Power Electronics*, Vol. 11, No 2, 1996, pp246-250

[45] J.G ZHU, S.Y.R. HUI & V.S. RAMSDEN, "A Generalized dynamic circuit model of magnetic cores for low- and high-frequency applications-Part 2: Circuit Model Formulation and Implementation", *IEEE Transactions on Power Electronics*, Vol. 11, No 2, 1996, pp251-259

[46] S MULDER, "Power Ferrite Loss Formulas for transformer design", *PCIM Magazine*, July 1995, pp22-31

[47] D.C. JILES , Introduction to Magnetism and Magnetic Materials, Chapman and Hall, 1st Edition, 1991

[48] P. R. WILSON, J. NEIL ROSS & ANDREW D. BROWN, "Dynamic Electric-Magnetic-Thermal Simulation of Magnetic Components", *IEEE Conference on Computers in Power Electronics (COMPEL 2000),* July 2000

[49] C.D. BOLEY & M.L. HODGDON, "Model and Simulations of hysteresis in magnetic cores", *IEEE Transactions on Magnetics*, Vol. 25, No. 5, Sep 1989, pp3922-3924

[50] S. PRIGOZY, "PSPICE Computer Modeling of hysteresis effects", *IEEE Transactions on Education*, Vol. 36, No. 1, Feb 1993, pp2-5

[51] K.H. CARPENTER, "A differential equation approach to minor loops in the Jiles-Atherton hysteresis model", *IEEE Transactions on Magnetics*, Vol. 27, No. 6, Nov 1991, pp4404-4406

[52] D.C. JILES, "A self consistent generalized model for the calculation of minor loop excursions in the theory of hysteresis", *IEEE Transactions on Magnetics*, Vol. 28, No.5, Sep 1992, pp2602-2604

[53] M.L. HODGDON, "Applications of a theory of ferromagnetic hysteresis", *IEEE Transactions on Magnetics*, Vol. 27, No 6, Nov 1991, pp4404-4406

[54] D. DIEBOLT, "An implementation of a Rate Dependent Magnetics Model suitable for circuit simulation", *APEC Proceedings*, 1992

[55] M.D. TAKACH & P.O. LAURITZEN, "Survey of Magnetic Core Models", *APEC Proceedings*, 1995, pp560-566

[56] D.A. PHILIPS, L.R. DUPRE & J.A. MELKEBEEK, "Comparison of Jiles and Preisach hysteresis models in magnetodynamics", *IEEE Transactions on Magnetics*, Vole 31, No 6, Nov 1995, pp3551-3553

[57] W.A. MANLY, "An appraisal of several non-linear hysteresis loop models", *IEEE Transactions on Magnetics*, Vole 9, No. 3, Sep 1973, pp256-260

[58] D. NITZAN, "MTRAC: Computer Program for transient analysis of circuits including magnetic cores", *IEEE Transactions on Magnetics*, Vol. 5, No 3, Sep 1969, 524-533

[59] M.K. EL-SHARBINY, "Representation of magnetic characteristics by a sum of exponentials", *IEEE Transactions on Magnetics*, Vol. 9, March 1973, pp60-61

[60] P.R. WILSON, "Advanced modeling and simulation techniques for magnetic components", *IEE Power Electronics and Variable Speed Drives Conference Proceedings*, Sep 1998, pp187-193

[61] K.W.E. CHENG & P.D. EVANS, "Calculation of winding losses in high frequency toroidal inductors using single strand conductors", *IEE Proceedings - Electric Power Applications*, Vol. 141, No 2, Mar 1994, pp52-62

[62] K.W.E. CHENG & P.D. EVANS, "Calculation of winding losses in high frequency toroidal inductors using multi-strand conductors", *IEE Proceedings - Electric Power Applications*, Vol. 142, No 5, Sep 1995, pp313-322

[63] J.M. LOPERA, M. PERNIA, J.M. ALONSO & F. NUNO, "A complete transformer electric model including frequency and geometric effects", *PESC '92 Record. 23rd Annual IEEE Power Electronics Specialists Conference (Cat. No.92CH3163-3)*, Vol. 2., pp 1247-52

[64] D.A. PIERRE, Optimization theory with applications, Dover, 2nd Edition, 1986

[65] P.J.M. LAARHOVEN & E.H.L. AARTS, Simulated Annealing: Theory and Applications, Kluwer Academic Publishers, 1989

[66] D.E. GOLDBERG, Genetic Algorithms in search, optimization and machine learning, Addison-Wesley, 1989.

[67] W.T. MCLYMAN, Transformer and Inductor Design Handbook, Marcel Dekker, Inc.,1988

[68] A. MASSARINI & M. KAZIMIERCZUK, "Self Capacitance of inductors", *IEEE Transactions on Power Electronics*, Vol. 12, No. 4, July 1997, pp671-676

[69] S.Y.R. HUI & J. ZHU, "Magnetic hysteresis modeling and simulation using the Preisach theory and TLM technique", *PESC '94*, 1994, pp837-842

[70] P.D. MITCHLER, E.D. DAHLBERG, E.E. WESSELING and R.M. ROSHKO, "Henkel plots in a temperature and time dependent Preisach model", *IEEE Transactions on Magnetics*, Vol. 32, No. 4, Jul 1996, 3185-3193

[71] G.S. PARK, S.Y. HAHN, "Implementation of hysteresis characteristics using the Preisach model with M-B variables", *IEEE Transactions on Magnetics*, Vol. 29, No. 2, March 1993, 1542-1545

[72] P.D. MITCHLER, E.D. DAHLBERG, E.E. WESSELING and R.M. ROSHKO, "Henkel plots in a thermally demagnetized scalar Preisach model", *IEEE Transactions on Magnetics*, Vol. 31, No. 5, Sep 1995, 2499-2503

[73] D.L. ATHERTON, B. SZPUNAR & J.A. SZPUNAR, "A new approach to Preisach diagrams", *IEEE Transactions on Magnetics*, Vole 23, No.3, May 1987, 1856-1865

[74] T. DOONG & I.D. MAYERGOYZ, "On numerical implementation of hysteresis models", *IEEE Transactions on Magnetics*, Vol. 21, No. 5, Sep 1985, 1853-1855

[75] E.D. TORRE, J. OTI & G. KADAR, "Preisach modeling and reversible magnetisation", *IEEE Transactions on Magnetics*, Vol. 26, No. 6, Nov 1990, 3052-3058

[76] I.D. MAYERGOYZ & G. FRIEDMAN, "Generalized Preisach model of hysteresis (invited)", *IEEE Transactions on Magnetics*, Vol. 24, No. 1, Jan 1988,212-217

[77] F. VAJDA & E.D. TORRE, "Efficient numerical implementation of complete moving hysteresis model (invited)", *IEEE Transactions on Magnetics*, Vol. 29, No. 2, Mar 1993, 1532-1537

[78] H.A. MANTOOTH & M. FIEGENBAUM, Modeling with an analog hardware description language, Kluwer Academic Publishers, 1995, 205-222

[79] E.D. TORRE & F. VAJDA, "Physical basis for parameter identification in magnetic materials", *IEEE Transactions on Magnetics*, Vol. 32, No. 5. Sep 1996, 4186

[80] F. HENROTTE, A. NICOLET, F. DELINCE, A. GENON & W. LEGROS," Modeling of ferromagnetic materials in 2D finite element problems using Preisach's model", *IEEE Transactions on Magnetics*, Vol. 28, No. 5, Sep 1992, 2614

[81] A.R. HEFNER & D.L. BLACKBURN, "Simulating the dynamic electro-thermal behaviour of power electronic circuits and systems", *Conf. Rec. IEEE Workshop on Computers in Power Electronics*, p143, 1992

[82] "IEEE 1076.1 (VHDL-AMS) Language Reference Manual (LRM)", IEEE, 1999

[83] W.H. PRESS, S.A. TEUKOLSKY, W.T. VETTERLING & B.P. FLANNERY, "Numerical Recipes in C", Cambridge University Press, 2nd Edition, 1992

[84] ANATOL GLOBUS, PAUL DUPLEX and MARECEL GUYOT, "Determination of Initial Magnetization Curve form Crystallites Sizes and Effective Anisotropy field", *INTERMAG Conference Proceedings,* 1971, pp617-622

[85] J.W. NIMS, R.E. SMITH & A.A. EL-KEIB, "Application of a Genetic Algorithm to Power Transformer Design", *Electric Machines and Power Systems*, Vol. 24, 1995, pp669-680

[86] J.H. HOLLAND, "Adaption in Natural and Artificial Systems", University of Michigan Press, Ann Arbor, Michigan, 1975.

[87] "Genetic Algorithms in Engineering Systems: Innovations and Applications", IEE Conference Publications, Sep. 1997.

[88] D. LEDERER, H. IGARASHI, A. KOST & T. HONMA , "On the Parameter Identification and Application of the Jiles-Atherton Hysteresis Model for Numerical Modeling of Measured Characteristics", *IEEE Transactions on Magnetics*, Vol. 35, No 3, May 1999, pp1211-1214

[89] P.R. WILSON & J.N. ROSS, "Definition and Application of Magnetic Material Metrics in Modeling and Optimization", *Submitted to IEEE Transactions on Magnetics*, Feb 2000, Accepted for Publication

[90] P.R. WILSON, J.N. ROSS & A.D. BROWN, "Optimizing the Jiles-Atherton model of hysteresis using a Genetic Algorithm", *IEEE Transactions on Magnetics*, May 2000 (Accepted for Publication October 2000)

[91] F. LIORZOU, B. PHELPS & D.L. ATHERTON, "Macroscopic models of Magnetization", *IEEE Transactions on Magnetics*, Vol. 36, No. 2, March 2000, pp418-428

[92] C.P. STEINMETZ, "On the Law of Hysteresis", *American Institute of Electrical Engineers Transactions*, Vol. 9, 1892, pp3-64

[93] M. JACKSON, H.U. WORM & S.K. BANERJEE, "Fourier Analysis of digital hysteresis data: rock magnetic applications", *Physics of the Earth and Planetary Interiors*, No. 65, 1990, pp78-87

[94] E.C. STONER & E.P. WOHLFARTH, "A Mechanism of Magnetic Hysteresis in Heterogeneous Alloys", *Phil. Trans. Roy. Soc.*, Vol. 240, May 1948, pp599-642

[95] L.H. DIXON, "Magnetics Design for Switching Power Supplies", Unitrode Magnetics Design Handbook MAG100A, Texas Instruments Corporation

[96] RAYLEIGH, Notes on Electricity and Magnetism, III, Phil. Mag., Vol 23, p225, 1887

[97] D.C. JILES & J.B. THOELKE, "Theory of Ferromagnetic Hysteresis: Determination of model parameters from experimental hysteresis loops", *IEEE Transactions on Magnetics*, Vol. 25, No. 5, Sep. 1989, pp3928-3930

[98] K.H. CARPENTER, "A wide bandwidth, dynamic hysteresis model for magnetization in soft ferrites", *IEEE Transactions on Magnetics*, Vol. 28, No. 5, Sep 1992, pp2037-2040

[99] J.G. ZHU, S.Y.R. HUI & V.S. RAMSDEN, "A dynamic equivalent circuit model for solid magnetic cores for high switching frequency operations", *IEEE Transactions on Power Electronics*, Vol. 10, No. 6, Nov. 1995, pp791-795

[100] D.C. JILES & D.L. ATHERTON, "Ferromagnetic Hysteresis", *IEEE Transactions on Magnetics*, Vol 19, No. 5, Sep 1983, pp2183-2185

[101] A. COURTAY, "The Preisach Model", Analogy Technical Note, Analogy Inc. 1999.

[102] F.LIOURZOU, B. PHELPS & D.L. ATHERTON, "Macroscopic Models of Hysteresis", *IEEE Transactions on Magnetics*, Vol. 36, No. 2, March 2000, pp418-428

[103] J.T. HSU and D.T. NGO, "A Hammerstein-Based Dynamic Model for Hysteresis Phenomenon", *IEEE Transactions on Power Electronics*, Vol 12, No. 3, May 1997, pp406-413.

[104] P. TENANT, J.J. ROUSSEAU, L. ZEGADI, "Hysteresis modeling taking into account the temperature", *European Power Electronics Conference proceedings*, 1995, Volume 1, pp1.001-1.006.

[105] Saber Template Library Reference Manual, Analogy Inc.

[106] D.H. EVERETT, "A general approach to hysteresis -part 4", *Transactions of the Faraday Society*, Vol. 51, 1955, pp1551-1557

[107] A. COURTAY, " The Preisach Model and its characterization", Analogy Internal Report, Analogy Inc.

[108] J. OTI, F. VAJDA & E.De La TORRE, "Identification of parameters in a moving model", *Journal of Applied Physics*, Vol. 69, No. 8, April 1991, pp4826-4828

[109] F. VAJDA & E.De La TORRE, "Parameter Identification of the complete moving hysteresis model using major loop data", *IEEE Transactions on Magnetics*, Vol. 30, No. 6, Nov 1994, pp4987-5000

[110] L.L. ROUVE, T. WAECKERLE & KEDOUS-LEBOUC, "Application of Preisach Model to Grain Oriented Steels - Comparison of different characterizations for the Preisach function p(a,b)", *IEEE Transactions on Magnetics*, Vol 31, No. 6, Nov 1995, 3557-3559

[111] T.J. KAZMIERSKI & J. BARANOWSKI, "A modified Jiles-Atherton model of ferromagnetic hysteresis for behavioural circuit simulation in VHDL-AMS", *IEEE Conference on Behavioural Modeling and Simulation*, 1999.

[112] A. DAUHAJRE, "Modeling and Estimation of Leakage Phenomena in Magnetic Circuits", PhD Thesis, California Institute of Technology, Pasadena, California, 1986.

[113] S. TABAGA, L. PIERRAT & F. BLACHE, "Parameter Computation of a planar transformer by 3D Finite Element Method", *EPE Conference Proceedings*, Seville, 1995, pp1.273-276

[114] G. SKUTT, F.C. LEE, R. RIDLEY & D. NICOL, "Leakage Inductance and Termination Effects in a High Power Planar Magnetic Structure", Application Note, Ansoft Corporation.

[115] E. PIERZCHALA & P.R. WILSON, Internal Technical Communication, Analogy Inc., June 1999.

[116] "Recommended Standard Practice for testing electronic transformers and inductors", IEEE Std 389-1979.

[117] MagNet User's Guide, Infolytica Corporation, Canada, Vn 5.2

[118] R. PRIETO, V. BATALLER, J.A. COBOS & J. UCEDA ,"Influence of the winding strategy in toroidal transformers", *IECON 1998*, Volume 1, pp359-64

[119] R. PRIETO, J.A. COBOS, O. GARCIA, P. ALOU & J. UCEDA, "Taking into account all the parasitic effects in the design of magnetic components", *APEC '98*, Vol. 1, pp400-406

[120] R. PRIETO, J.A. COBOS, O. GARCIA & J. UCEDA, "Interleaving techniques in magnetic components", *APEC '97*, Vol. 2, pp931-936

[121] R. PRIETO, J.A. COBOS, O. GARCIA & J. UCEDA, "Influence of the winding strategy on the parasitics of magnetic components", *EPE '97*, Vol. 2, pp38-43

[122] F. ROBERT, P. MATHYS & J.P. SCHAUWERS, "Ohmic Losses Calculation in SMPS Transformers: numerical study of Dowell's approach accuracy", *IEEE Transactions on Magnetics*, Vol 34, No. 4, July 1998, pp1255-7

[123] DUERDOTH W.T., "Equivalent capacitances of transformer windings", *Wireless Engineer*, Vol 23, 1946, p161

[124] MAURICE & MINNS, "Very wide band radio frequency transformers", *Wireless Engineer*, Vol 24, 1947, p168 (Part 1) and p209 (Part 2)

[125] RICHARDSON I., "The technique of transformer design", *Electro-technology*, January 1961, pp58-67

[126] ZUHRT, "Einfache Näheringsformela für die eigenkapazität Mehrlagiger-Spulen", *Electrotech. Zeitung*, Vol 55, 1934, p662

[127] MEDHURST, "H.F. Resistance & Self Capacitance of single layer solenoids", *Wireless Engineer*, Vol 24, 1947, p35

[128] COLLINS J.A., "An accurate method for modeling transformer winding capacitances", *IECON 1990*, pp1094-1099

[129] BLACHE F., KERADEC J-P.,COGITORE B., "Stray Capacitances of two winding transformers: equivalent circuit, measurements, calculation and lowering", *IAS Proc.*, Vol. 2, 1994, pp1211-1217

[130] LU H.Y., ZHU J.G., V.S. RAMSDEN & HUI S.Y.R., "Measurement and Modeling of Stray Capacitances in High Frequency Transformers", *PESC '99 Record - IEEE Annual Power Electronics Specialists Conference*, Vol. 2, (1999), pp 763-768

[131] PRIETO M.J., FERNANDEZ A., DIAZ J.M., LOPERA J.M., SEBASTIAN J., "Influence of transformer parasitics in low power applications", *APEC '99*, Vol. 2, 1175-1180

[132] PRIETO, R., ASENSI, R., COBOS, J. A., GARCIA, O., UCEDA, J., "Model of the capacitive effects in magnetic components", *PESC '95 Record - IEEE Annual Power Electronics Specialists Conference,* Vol. 2, (1995), p 678-683

[133] MORK B.A., "Five-Legged Wound-Core Transformer Model: Derivation, Parameters, Implementation and Evaluation", *IEEE Transactions on Power Delivery*, Vol. 14, No. 4, October 1999, p1519-1526

[134] CASEY L.F., GOLDBERG A.F., SCHLECHT M.F., "Issues regarding the capacitance of 1-10MHz Transformers", *APEC '88*, pp352-360

[135] MALY D., NOVOTNY D.W., THOMPSON C., "The Influence of Winding Capacitance on High Frequency Time Harmonic Losses in Induction Motors", *Conference Record of the 1992 Industry Applications Society Annual Meeting*, IEEE , 1992, Vol. 1, pp33-39.

[136] LEON F., SEMLEYN A., "Efficient Calculation of Elementary Parameters of Transformers", *IEEE Transactions on Power Delivery*, Vol. 7, No. 1, January 1992, pp376-383

[137] CHENG D.K.W., WONG L.P., LEE Y.S., "Modeling, Analysis and Design of Integrated Magnetics for Modern Power Electronics Circuits", *PEDS '99*, July 1999, p14

[138] OKYERE P.F. & HEINEMANN L., "An Advanced Spice-Compatible Model for High Frequency Multiwinding Transformers", *PESC '99*, pp592-597

[139] POPOVIC L.M., "New Method for Calculation of Series Capacitance for Transient Analysis of Windings", ", *MELECON '98*, Vol. 2, 1042-1046

[140] BARTOLI M., REATTI A., KAZIMIERCZUK M.K., "High Frequency Models of Ferrite Core Inductors", *IECON Proc.*, Vol. 3, 1994, pp1670-1675

[141] MUYSHONDT G.P., PORTNOY W.M., "Development of High Frequency SPICE models for Ferrite core inductors and transformers", *IAS Proc.*, Pt. 2, 1989, pp1328-1333

[142] AHMAD A., AURIOL P., "Dielectric Losses in Power Transformers under High Frequency Transients", *Conference Record of the 1992 IEEE International Symposium on Electrical Insulation*, June 7-10 1992, pp460-463

[143] VERMEULEN H.J., DANN L.R., Van ROOIJEN J., "Equivalent circuit modeling of a capacitive voltage transformer for power system harmonic frequencies", *IEEE Transactions on Power Delivery*, Vol. 10, No. 4, Octopber 1995, pp1743-1749

[144] CHERPENTIER J.F., LEFEVRE Y., LAJOIE-MAZENC M., "A 2D Finite Element Formulation for the study of the high frequency behaviour of wound components", *IEEE Transactions on Magnetics*, Vol. 32, No. 3, May 1996, pp1098-1101

[145] ABE N.M., CARDOSO J.R., "Coupling Electric Circuit and 2D-FEM Model with Dommell's approach for transient analysis", *IEEE Transactions on Magnetics*, Vol. 34, No. 5, September 1998, p3487-3490

[146] DAI N., LEE F.C., "Characterization and Analysis of Parasitic Parameters and their effects in Power Electronics Circuit", *PESC '96*, pp1370-1375

[147] MASSARINI A., KAZIMIERCZUK M.K., GRANDI G., "Lumped Parameter Models for Single- and Multiple-Layer Inductors", *PESC '96*, pp295-301

[148] BACCIGALUPI A., DAPONTE P., GRIMALDI D., "On Circuit Theory Approach to Evaluate the Stray Capacitances of Two Coupled Inductors", *IEEE Instrumentation and Measurement Conference*, 1993, pp549-553

[149] NIEMELA V.A., SKUTT G.R., URLING, A.M., CHANG Y.N., WILSON T.G., OWEN H.A., WONG R.C., "Calculating the short-circuit impedance of a multiwinding transformer from its geometry", *PESC '89*, pp607-617

[150] PRIETO R., COBOS J.A., GARCIA O., ASENSI R., UCEDA J., "Optimizing the winding strategy of the transformer in a flyback converter", *PESC '96*, 1456-1462

[151] HURLEY W.G., WILCOX D.J., "Calculation of Leakage Inductance in Transformer Windings", *IEEE Transactions on Power Electronics*, Vol. 9, No. 1, January 1994, pp121-126

[152] SEVERNS R., "Additional Losses in High Frequency Magnetics due to non-ideal field distributions", *APEC'92*, February 1992

[153] SEMLYEN A., DE LEON F., "Eddy Current add-on for frequency dependent representation of winding losses in transformer models used in computing electromagnetic transients", *IEE Proceedings on Generation, Transmission and Distribution*, Vol. 141, No. 3, 1994, pp209-214

[154] CHEN J.Y., DING S.Q., ZHU G.Y., "Study and design of high voltage flyback transformer for TV and Monitor", *Proc. Asian Symposium on Information Display*, 1997, pp57-60

[155] PRIETO R., OLIVER J.A., COBOS J.A., UCEDA J., CHRISTINI M., "Errors obtained when 1D Magnetic Component Models are not properly applied", *APEC '99*, pp206-212

[156] PLEITE J., PRIETO R., ASENSI R., COBOS J.A., OLIAS E., "Modeling of Magnetic Components based on Finite Element Techniques", *CIEP '96*, October 1996, pp170-175

[157] BECKER B., GROTSTOLLEN H., HEINEMANN L., "Computer Aided Design and Modeling of High Frequency Magnetic Components", *APEC '95*, Vol. 1, pp335-341

[158] PRIETO R., OLIVER J.A., COBOS J.A., UCEDA J., "1D Magnetic component model for planar structures", *PESC '99*, pp574-579

[159] PRIETO R., COBOS J.A., GARCIA O., UCEDA J., "Study of the Sensitivity of the parameters in magnetic components", *APEC '97*, pp355-360

[160] MAXIM A., ANDREU D., BOUCHER J., "A Novel Behavioural method of SPICE Macromodeling of Magnetic Components Including the Temperature and Frequency Dependencies", *Conference Proceedings - IEEE Applied Power Electronics Conference and Exposition - APEC*, Vol. 1, 1998, pp 393-399

[161] ASENSI R., COBOS J.A., ALOU P., PRIETO R., UCEDA J., "Characterization of Winding coupling in multi-winding Magnetic Components", *PESC '99*, pp753-758

[162] ODENDAAL W.G., FERREIRA J.A., "A thermal model for high frequency magnetic components", *IEEE IAS Meeting*, New Orleans, La., October 1997, pp1115-1122

[163] El-HAMAMSY S.A., CHANG E.I., "Magnetics Modeling for Computer-Aided Design of Power Electronics Circuits", *PESC '89*, pp635-645

[164] MAXIM A., ANDREU D., BOUCHER J., "A New Behavioural Macromodeling method of Magnetic Components Including the Self-Heating Process", *PESC '99*, pp735-740

[165] XIN A., HAI B., JIAHUA S., YIHAN Y., "The Hall Current Transformer Modeling and Simulation", *International Conference on Power System Technology Proceedings. POWERCON '98*. Vol. 2 , 1998, pp1015 -1020

[166] PERNIA A.M., NUNO F., LOPERA J.M., "1D/2D Transformer Electric Model for Simulation in Power Converters", *PESC '95*, pp1043-1049

[167] HSU J.T., NGO K.D.T., "Finite-Element Formulation of Field-Based Subcircuits for modeling of magnetic components with hysteresis", *IEEE Transactions on Power Electronics*, Vol. 12, No. 3, May 1997, pp414-421

[168] MAXIM A., ANDREU D., BOUCHER J., "A New Analog Behavioural SPICE Macromodel of Magnetic Components", *ISIE '97*, 1997, pp183-188

[169] HAYDOCK L. , "Interactive distributed magnetic and linked electric circuit models for power electronic controller design", *IEE Colloquium*, n020, 1994, pp6/1-6/5

[170] PRIETO M.J., LOPERA J.M., PERNIA A.M., LINERA F.F., NUNO F., "High Frequency Magnetic Elements Design Tool", *COMPEL '98*, pp127-131

[171] SCHELLMANNS A., BERROUCHE K., KERADEC J.P., "Multiwinding transformers : a successive refinement method to characterize a general equivalent circuit", *IEEE Instrumentation and Measurement Technology Conference,* May 1997, pp717-722

[172] PRIETO R., GARCIA O., ASENSI r., COBOS J.A., UCEDA J., "Optimizing the performance of planar transformers", *APEC '96*, pp427-433

[173] DAI N. & LEE F.C., "Edge Effect Analysis in High-Frequency Transformer", *PESC '94*, pp850-855

[174] HOWARD T.O., CARPENTER K.H., "A numerical study of the coupling coefficient for Pot Core transformers", *IEEE Transactions on Magnetics*, Vol. 31, No. 3, May 1995, pp2249-2253

[175] DAI N., LEE F.C., "High-Frequency Eddy-Current Effects in Low-Profile Transformer Windings", *PESC '97*, pp641-647

[176] CHENG K.W., HU Y.Q., HE D.H., MO W.K., "Effect of Geometrical factors on copper loss in high-frequency low-profile transformers", *IAS '96*, pp1397-1404

[177] SUN C., KUTKUT N.H., NOVOTNY D.W., DIVAN D.M., "General Equivalent circuit of a multi-winding co-axial winding transformer", *IAS '95*, pp859-867

[178] DAI N., LOFTI A.W., SKUTT G., TABISZ W., LEE F.C., "A comparative study of high frequency low-profile planar transformer technologies", *APEC '94*, pp226-232

[179] EVANS P.D., HEFFERNAN W.J.B., "Transformer for multimegahertz power applications", *IEE Proceedings on Electric Power Applications*, Vol. 142, No. 6, November 1995, pp379-389

[180] HUANG Y.T., CHEN C.J., SHU W.B., "Finite Element Analysis on characteristics of rotary transformers", *IEEE Transactions on Magnetics*, Vol. 30, No. 6, November 1994, pp4866-4868

[181] HO W.C., PONG M.H., "Analysis and Design of Printed Windings of Power Transformers using Partial Inductance Method", *IECON '95*, pp376-380

[182] HO W.C., PONG M.H., "Inductance Calculations of Printed Windings of Power Transformers using Partial Inductance Method", *Proc. IEEE Applied Power Electronics Conference (APEC) 96,* 1996, pp333-339

[183] TMS320C3x User's Guide, Texas Instruments Corporation, SPRU031E, July 1997

[184] TMS320C3x DSP Starter Kit User's Guide, Texas Instruments Corporation, SPRU163A, 1996

[185] IEEE Working Group on Composite CAD, Minutes June 1999

[186] A. M. PERNÍA, F. NUÑO AND J. M. LOPERA, "Magnetic Elements Simulation in Power Converters", *Congreso Internacional de Electrónica de Potencia, Puebla (Mexico)*, Aug. 1994, pp74-79

[187] S. CHWIRKA, "Using simulation as an integral part of the power converter design process", *IEEE workshop on Computers in Power Electronics (COMPEL)*, 1994, pp121-126

[188] P.R. WILSON, "Simulation of Modular Power Systems", *IEE Colloquium on CAD in Power Electronics*, 1992

[189] P.R. WILSON, "Modeling and Simulation of Power Factor Correction Circuits including automatic compliance to regulations defining current harmonic limits", *Proceedings of the Power Control and Intelligent Motion Conference (PCIM)*, May 1996, p103

[190] A. HEFNER, "A Dynamic Electro-thermal model for the IGBT", *IEEE IAS Conference Record*, p1094, 1992

[191] A.R. HEFNER AND D.L. BLACKBURN, "Thermal Component Models for electro-thermal network simulation, *Proc. IEEE Semiconductor Thrermal Measurement and Management SEMI-THERM Symposium*, p88, 1993.

[192] C.L. MA, P.O. LAURITZEN, *et al*, "A Systematic approach to modeling power semiconductor devices based on charge control principles", *Proc. PESC*, Taiwan, 1994

[193] P.O. LAURITZEN AND C.L. MA, "A simple diode model with reverse recovery", *IEEE Transactions on Power Electronics*, Vol. 6, No. 2, April 1991, pp188-191

[194] R.P.FEYNMAN, R.B.LEIGHTON & M. SANDS, *Lectures in Physics*, Addison-Wesley Publishing Company, Volume 2, 16th Edition, 1983, Chapter 37

[195] HSU, J.T & VU-QUOC, L., "A rational formulation of thermal circuit models for electro-thermal simulation –Part I: Finite Element Method", *IEEE Transactions on Circuits and Systems*, Vol 43, No. 9, pp 721-732, Sep. 1996

[196] HSU, J.T & VU-QUOC, L., "A rational formulation of thermal circuit models for electro-thermal simulation –Part II: Model Reduction Techniques", *IEEE Transactions on Circuits and Systems*, Vol 43, No. 9, pp 733-744, Sep. 1996

[197] LYRA, RENATO O. C., CARDOSO F., BRAZ J., JOHN, V., LIPO, THOMAS A. "Coaxial current transformer for test and characterization of high-power semiconductor devices under hard and soft switching", *IEEE Transactions on Industry Applications*, Vol. 36, No. 4, Jul 2000, pp 1181-1188

[198] AFFOUR B., NACHTERGAELE P., SPIRKOVITCH S., OSTERGAARD D. AND GYIMESI M., "Efficient reduced order modeling for system simulation of micro electro mechanical systems (MEMS) from FEM models", *Proceedings of SPIE - The International Society for Optical Engineering*, Vol. 4019, 2000, pp 50-54

[199] DYCK D., LOWTHER D.,MALIK Z., SPENCE R., NELDER J., "Response surface models of electromagnetic devices and their application to design", *IEEE Transactions on Magnetics*, Vol. 35, No. 3, May 1999, pp 1821-1824

[200] TEEGARDEN D., LORENZ G. AND NEUL R., "How to model and simulate microgyroscope systems", *IEEE Spectrum*, Vol. 35, No. 7, Jul 1998, pp 66-75

[201] VAANANEN J., "Combination of two-dimensional finite element analysis of electrical machines with circuit simualtion techniques", Ph. D. Thesis, Helsinki University of Technology, Helsinki, Finland, 1995

[202] VAANANEN, J., "Circuit theoretical approach to couple two-dimensional finite element models with external circuit equations", *IEEE Transactions on Magnetics*, Vol. 32, No. 2, Mar 1996, pp400-410

[203] Mast Modeling Reference Manual, Avanti Corporation, California, USA.

[204] NAGEL L.W., "A Computer Program to Simulate Semiconductor Circuits", Memorandum No. ERL-M5520, University of California, Berkeley, Ca., USA., 1975

[205] QUARLES T., NEWTON A.R., PEDERSON D.O. & SANGIOVANNI-VINCENTELLI A., "SPICE3 Version 3F4 User's Manual", University of California, Berkeley, Ca., USA., 1989

[206] COX F.L., KUHN W.B., LI J.P., TYNOR S.D., AND WILLIS M.J., "XSPICE Software User's Manual", Georgia Tech Research Institute, Atlanta, Georgia, USA

[207] PUHAN J., TUMA T, FAJFAR I, "SPICE for Windows 95/98/NT", *Electrotechnical Review*, Ljubljana, Slovenia, Vol. 65, No. 5, 1998, pp267-271

[208] SLIM Version 3.1.3 User's Manual, Alstom Research and Technology, Alstom, Stafford, United Kingdom, 1997

[209] OSTERHOUT J., TCL and the T Toolkit, Addison-Wesley, Reading, Ma., 1994

[210] MUKHOPADHYAY, S. C.; DAWSON, F. P.; IWAHARA, M.; YAMADA, S., "Analysis, design and experimental results for a passive current limiting device*", IEE Proceedings: Electric Power Applications*, Vol. 146, No. 3, (1999), pp309-316

[211] DAWSON FP, YAMADA S, IWAHARA M, "Experimental Results for a 2-Material Passive Di/Dt Limiter", *IEEE Trans. On Magnetics*, Vol. 31, No. 6, pp3734-3736, Nov. 1995

[212] IBRAHIM ES, "Electromagnetic fault current limiter", *Electric Power Systems Research*, Vol. 42, No. 3, pp189-194, Sep. 1997

[213] INABA T , "Performance of a Fault-Current Current Limiter With a New Type of Direct Cooled Tubular Element", *IEEE Transactions on Power Apparatus and Systems*, Vol. 103, No. 7, pp1888-1894, 1984

[214] ISHIGOHKA T, SASAKI N, "Fundamental Test of New DC Superconducting Fault Current Limiter", *IEEE Transactions on Magnetics*, Vol. 27, No. 2, pp2341-2344, Mar. 1991

[215] ITO D, YONEDA ES, TSURUNAGA K, TADA T, HARA T, OHKUMA T, YAMAMOTO T, "6.6 KV/1.5 KA-Class Superconducting Fault Current Limiter Development", *IEEE Transactions on Magnetics*, Vol. 28, No. 1, pp438-441, Jan. 1992

[216] ITO D, TSURUNAGA K, YONEDA ES, SUGIYAMA Y, HARA T, OKANIWA K, HOSHINO H, YAMAMOTO T, "Superconducting Fault Current Limiter Development", *IEEE Transactions on Magnetics*, Vol. 27, No. 2, pp2345-2348, Mar. 1991

[217] IWAHARA M, MIYAZAWA E, "A Numerical Method for calculation of Electromagnetic Circuits using the tableau approach", *IEEE Transactions on Magnetics*, Vol. 19, No. 6, pp2457-2460, 1983

[218] KARADY GG, "Principles of Fault Current Limitation by a resonant LC circuit", *IEE Proceedings-C Generation Transmission and Distribution*, Vol. 139, No. 1, pp1-6, Jan. 1992

[219] KING EF, CHIKHANI AY, HACKAM R, SALAMA MMA, "A Microprocessor-Controlled Variable Impedance Adaptive Fault Current Limiter", *IEEE Transactions on Power Delivery*, Vol. 5, No. 4, pp1830-1838, Oct. 1990

[220] "Fault Current Limiting - present situation and future needs", CIGRE 23-79-(WG-04)-06, 1979

[221] BOYLE G.R., COHN B.M., PEDERSON D.O., SOLOMON J.E., "Macro-Modeling of integrated circuit operational amplifiers", *IEEE Journal Solid-State Circuits*, Vol. SC-9, No. 6, pp.353-363, Dec. 1974

[222] De La TORRE E. & VAJDA F., "Properties of Accommodation Models", *IEEE Transactions on Magnetics*, Vol. 31, No. 3, May 1995, pp1775-1780

[223] IEEE Standard T1.413-1995, "Network and Customer Installation Interfaces - Asymmetric Digital Subscriber Line (ADSL) Metallic Interface", August 1995, American National Standards Institute, Inc.

[224] J.A.C. BINGHAM, "Multicarrier Modulation for Data Transmission; An Idea whose Time Has Come", *IEEE Communications Magazine*, May 1990, pp5-14.

[225] J. M. CIOFFI, "A multicarrier primer", ANSI Document, T1413 Technical Subcommittee, (91-157).

[226] W. GORALSKI, "ADSL and DSL Technologies", McGraw-Hill, 1st Edition, 1998

[227] W.Y. CHEN, "DSL Simulation Techniques and Standards Development for Digital Subscriber Line Systems", Macmillan Technical Publishing, 1998

[228] B.D. DAY, S. WURCER & T. HOFFMAN,"Optimizing Line Driver Designs for Maximum Power; "Bridging" ADSL Line Driver Challenges", Analog Devices Appication Note, Analog Devices, Inc.

[229] J.P. CORNIL, "Building an ADSL Modem, the Basics", Analog Circuit Design - (X)DSL and other Communications Systems;RF MOST Models;Integrated Filters and Oscillators, 1999, Kluwer Academic Publishers, pp3-48

[230] C.D. CABLER, "Survey of the State of the Art Analog Front End Circuit Techniques for ADSL", Analog Circuit Design - (X)DSL and other Communications Systems;RF MOST Models;Integrated Filters and Oscillators, 1999, Kluwer Academic Publishers, pp117-126

[231] J. TELLADO, "Multicarrier Modulation with low PAR", Kluwer Academic Publishers, 2000.

[232] "The use of Ferrite Cores in DSL wideband Transformers", Application Note, Ferroxcube, Inc., 2001

[233] ARSHAK, K. I., AJINA, A. & EGAN, D., "Development of screen-printed polymer thick film planner transformer using Mn-Zn ferrite as core material", *Microelectronics Journal*, Vol. 32, No. 2, Feb 2001, pp113-116

[234] TANG, S. C., HUI, S. Y. (RON) & CHUNG, HENRY SHU-HUNG, "Coreless planar printed-circuit-board (PCB) transformers - a fundamental concept for signal and energy transfer", *IEEE Transactions on Power Electronics*, Vol. 15, No. 5, Sep 2000, pp931-940

[235] VARSHNEY, U., EICHELBERGER, B. DAVIS III, NEAL, J. A. III, CHURCHILL, R. J., NGO, K. D. T., THIBODEAUX, R. J., "Monolithic magnetic modules for DC-DC power converters", *Journal De Physique*. IV, Vol. 7, No. 1, Mar 1997, pp147-148

[236] PARK, JAE Y., LAGORCE, LAURE K. & ALLEN, MARK G., "Ferrite-based integrated planar inductors and transformers fabricated at low temperature", *IEEE Transactions on Magnetics*, Vol. 33, No. 5 Pt. 1, Sep 1997, pp3322-3324

[237] PARK, JAE Y.; ALLEN, MARK G., "Packaging compatible micromagnetic devices using screen printed polymer/ferrite composites", *International Journal of Microcircuits and Electronic Packaging*, Vol. 21, No. 3, 1998, pp 243-252

[238] BARNWELL, P. G.; JACKSON, T. J., "Low profile high frequency power supplies using thick film planar transformers", *IEE Conference Publication (EPE)*, Vol. 3, No. 377, 1993, pp 93-97

[239] SANTI, E; CUK, S, "Comparison and design of three coupled inductor structures", *IECON Proceedings (Industrial Electronics Conference)*, Vol. 1, (1994), p 262-267

[240] CUK, S; MAKSIMOVIC, D, "Quasi-resonant Cuk DC-to-DC converter employs integrated magnetics. Part I", *Powerconversion & Intelligent Motion,* Vol. 14, No. 12, (Dec 1988)

[241] CUK, S; MAKSIMOVIC, D , "Quasi-resonant Cuk DC-to-DC converter employs integrated magnetics. Part II", *Powerconversion & Intelligent Motion*, Vol. 15, No. 1, (Jan 1989), p 14, 16-19

[242] CUK, S; ZHANG, Z "COUPLED-INDUCTOR ANALYSIS AND DESIGN", *PESC Record - IEEE Power Electronics Specialists Conference*, (1986), p 655-665

[243] CUK, S; ZHANG, Z , "NEW MAGNETIC CIRCUITS FOR POWER ELECTRONICS", *Proceedings - IEEE International Symposium on Circuits and Systems*, (1985), p 1011-1014

[244] Ferroxcube Data Sheet, Integrated Inductive Component IIC10P-14/4, 2001

[245] DEAN D., "Gain Confidence in Network Designs By Simulating the LAN Magnetics", Pulse, Inc. Technical Note.

[246] STEFFES M., "Optimizing Performance in an xDSL Line Driver", *Electronic Design*, April 19, 1999, pp44-58

[247]  E., "Line-Driver Design For Broadband Communications Applications", *Electronic Design*, December 1, 1997, pp81-94

# Bibliography

K.J. BINNS, P.J. LAWRENSON AND C.W. TROWBRIDGE, "The Analytical and Numerical Solution of Electric and Magnetic Fields", Wiley, 1995.

R. BOLL, "Soft Magnetic Materials", Heyden, 1978

W.Y. CHEN, "DSL Simulation Techniques and Standards Development for Digital Subscriber Line Systems",

B. D. CULLITY, "Introduction to magnetic materials", Addison-Wesley, 1972

R.P.FEYNMAN, R.B.LEIGHTON & M. SANDS, "Lectures in Physics", Addison-Wesley Publishing Company, Volume 2, 16th Edition, 1983

W. GORALSKI, "ADSL and DSL Technologies", McGraw-Hill, 1st Edition, 1998

P. HAMMOND & J. K. SYKULSKI, "Engineering Electromagnetism - Physical Processes and Computation", Oxford Science Publications, 3rd Edition, 1999.

D.E. GOLDBERG, "Genetic Algorithms in search, optimization and machine learning", Addison-Wesley, 1989.

J.H. HOLLAND, "Adaption in Natural and Artificial Systems", University of Michigan Press, Ann Arbor, Michigan, 1975.

S. R. H. HOOLE & P. R. P. HOOLE, "A modern short course in Engineering Electromagnetics", Oxford University Press, 1996

R. J. HOSKING, S. JOE, D. C. JOYCE & J. C. TURNER, "First steps in numerical analysis", Arnold, 2nd Edition, 1996

D.C. JILES , "Introduction to Magnetism and Magnetic Materials", Chapman and Hall, 1st Edition, 1991

R. KIELKOWSKI, "Inside SPICE, overcoming the obstacles of circuit simulation", McGraw Hill, 1994

J.D. KRAUS, "Electromagnetics", McGraw-Hill, 3rd Edition, 1984

P.J.M. LAARHOVEN & E.H.L. AARTS, "Simulated Annealing: Theory and Applications", Kluwer Academic Publishers, 1989

D.A. LOWTHER & P. P. SILVESTER, "Computer-aided Design in Magnetics", Springer-Verlag, 1985

H.A. MANTOOTH & M. FIEGENBAUM, "Modeling with an analog hardware description language", Kluwer Academic Publishers, 1995

J.C.MAXWELL, "A Treatise on Electricity and Magnetism", Clarendon Press Oxford, 1873, 3rd Edition.

W.T. MCLYMAN, Transformer and Inductor Design Handbook, Marcel Dekker, Inc.,1988

OSTERHOUT J., TCL and the T Toolkit, Addison-Wesley, Reading, Ma., 1994

PHILIPS COMPONENTS, "Soft Ferrites Databook -MA01", 1998

D.A. PIERRE, "Optimization theory with applications", Dover, 2nd Edition, 1986

W.H. PRESS, S.A. TEUKOLSKY, W.T. VETTERLING & B.P. FLANNERY, "Numerical Recipes in C", Cambridge University Press, 2nd Edition, 1992

P.P. SILVESTER AND R.L. FERRARI, "Finite Elements for Electrical Engineers", Cambridge University Press, 3rd Edition, 1996

E.C. SNELLING, "Soft Ferrites", Butterworths, 2nd Edition, pp330-335

R. S. TEBBLE & D. J. CRAIK, "Magnetic Materials", Wiley-Interscience, 1969

J. TELLADO, "Multicarrier Modulation with low PAR", Kluwer Academic Publishers, 2000.

J. VLACH & K. SINGHAL, "Computer methods for circuit analysis and design", Van Nostrand Rheinhold, 2nd Edition, 1994

"Analog Circuit Design - (X)DSL and other Communications Systems;RF MOST Models;Integrated Filters and Oscillators", 1999, Kluwer Academic Publishers

# Publications

The following are papers published or under review during the course of this thesis work.

[1]     P.R. WILSON, J.N. ROSS & A.D. BROWN, "Optimizing the Jiles-Atherton model of hysteresis using a Genetic Algorithm", *IEEE Transactions on Magnetics*, Vol. 37, No. 2, March 2001, pp989-993

[2]     P.R. WILSON & J.N. ROSS, "Definition and Application of Magnetic Material Metrics in Modeling and Optimization", *IEEE Transactions on Magnetics*, Vol. 37, No. 5, Sep 2001, pp3774-3780

[3]     P. R. WILSON, J. N. ROSS & A. D. BROWN,  "Simulation of Magnetic Component Models in Electric Circuits including Dynamic Thermal Effects", *submitted to IEEE Transactions on Power Electronics*, Accepted for publication 2001.

[4]     P.R. WILSON, J.N. ROSS & A.D. BROWN, "Simulation of Magnetic Components in Electric Circuits using a coupled SPICE-Finite Element Analysis approach*", Submitted to IEE Proceedings – Science, Measurement and Technology*, 2001

[5]     P.R. WILSON, J.N. ROSS & A.D. BROWN, "Magnetic Material Model Characterization and Optimization Software", *Submitted to IEEE Transactions on Magnetics*, Accepted for publication 2001

[6]     P.R. WILSON, J.N. ROSS & A.D. BROWN, "A new method for the effective modeling of leakage inductance in circuit simulation", *submitted to IEEE Transactions on Power Electronics*, 2001.

[7]     P.R. WILSON, J.N. ROSS & A.D. BROWN, "Simulation of Magnetic Components in Electric Circuits using a coupled SPICE-Finite Element Analysis approach*", submitted to IEE Conference on Computation of Electromagnetic Fields (CEM), 2002.*

[8]     P.R. WILSON, P. CHAPMAN, J.N. ROSS & A.D. BROWN, "Experience of Behavioural Modeling in the Mixed-Signal ASIC Design Process - a Case Study", *IEEE Workshop on Behavioural Modeling and Simulation (BMAS),* October 2001

[9]     P.R. WILSON, Y. KILIC, J.N. ROSS, M. ZWOLINSKI & A.D. BROWN, "Behavioural Modeling of Operational Amplifier Faults using a Hardware Description Language", *IEEE Workshop on Behavioural Modeling and Simulation (BMAS),* October 2001

[10]    P.R. WILSON, Y. KILIC, J.N. ROSS, M. ZWOLINSKI & A.D. BROWN, "Behavioural Modeling of Operational Amplifier Faults using VHDL-AMS", *DATE 2002,* March 2002, Paper Submitted

[11]     P. R. WILSON, J. N. ROSS, T. J. KAZMIERSKI & A. D. BROWN, "VHDL-AMS Editor and Debugging for Analogue and Mixed Signal Models (VEDAMS)", *Forum on Design Languages FDL 2001*, Lyon, Sep3-7 2001

[12]     P.R. WILSON, J.N. ROSS & A.D. BROWN, "Magnetic material model optimization and characterization software*", IEEE Conference on Computation of Magnetic Fields (COMPUMAG)*, July 2001, Evian, France.

[13]     P. R. WILSON, J. NEIL ROSS & ANDREW D. BROWN, "Dynamic Electric-Magnetic-Thermal Simulation of Magnetic Components", *IEEE Conference on Computers in Power Electronics (COMPEL 2000)*, July 2000, Virginia, USA.

The following are papers published prior to the work in this thesis.

[1]      P.R. WILSON, "Design and Analysis of Phase Locked Loops using behavioral modeling and mixed mode simulation techniques", *DATE 1999*, March 1999

[2]      P.R. WILSON, "Advanced modeling and simulation techniques for magnetic components", *IEE Power Electronics and Variable Speed Drives Conference Proceedings*, Sep 1998, pp187-193

[3]      P.R. WILSON, "Advanced Modeling and simulation techniques for magnetic component optimization", *Analog and Mixed Signal Conference*, San Jose, July 1998

[4]      P.R. WILSON, "Design of Electric Vehicle Systems using simulation", *Power Electronics and Variable Speed Drives Conference (Hong Kong) Proceedings*, 1997

[5]      P.R. WILSON, "Advanced Modeling and Simulation techniques for magnetic components", *Power Electronics and Variable Speed Drives Conference (Hong Kong) Proceedings*, 1997

[6]      P.R. WILSON, "Advanced Mixed Signal Modeling and Simulation Techniques for Telecommunications Design", *Analog and Mixed Signal Conference*, San Jose, July 1997

[7]      P.R. WILSON, "Modeling and Simulation of Power Factor Correction Circuits including automatic compliance to regulations defining current harmonic limits", *Proceedings of the Power Control and Intelligent Motion Conference (PCIM),* May 1996, p103

[8]      P.R. WILSON, "Advanced Simulation and Modeling Techniques for Telecommunications Designers", *Electronic Product Design (EPD),* 1996

[1]      P.R. WILSON & ANDREW G.R. PATTERSON, "Behavioral Modeling Techniques for EMC Compliance testing", *Electronic Engineering*, 1995

[9]     P.R. WILSON, "Sigma Delta Converter Modeling and Simulation", *Silicon Design*, London, 1995

[10]    P.R.WILSON, "Scanner Simulation using Saber", *ICAT '95*, Birmingham 1995

[11]    P.R. WILSON, "Simulation of Modular Power Systems", *IEE Colloquium on CAD in Power Electronics*, 1992

# Appendix A : Spice model Listings

```
.SUBCKT winding    1     2     3     4     PARAMS: N=1 RD=100MEG RW=1M
RP    1     8     {RW}
V1    5     2     0
V2    6     4     0
E1    8     5     VALUE={N*V(7)}
E2    3     6     VALUE={N*I(V1)}
R2    3     6     {RD}
F1    7     0     V2    1
R1    7     0     {RD}
L1    7     0     1
E3    MMF   0     VALUE={V(3,4)}
E5    FLUX  0     VALUE={I(V2)}
.ENDS
```

**Listing A.1: Spice Winding Netlist**

```
.SUBCKT winding_th    1     2     3     4     5     PARAMS: N=1
RD=100MEG RW=1M
RP    1     8     {RW}
V1    9     2     0
V2    6     4     0
E1    8     9     VALUE={N*V(7)}
E2    3     6     VALUE={N*I(V1)}
R2    3     6     {RD}
F1    7     0     V2    1
R1    7     0     {RD}
L1    7     0     1
E3    MMF   0     VALUE={V(3,4)}
E5    FLUX  0     VALUE={I(V2)}
*
* Thermal Circuit
*
ETH   PLOSS 0     VALUE={I(V1)*I(V1)*RW}
GTH   5     0     PLOSS 0     1
.ENDS
```

**Listing A.2: Spice winding_th Netlist**

```
.SUBCKT CORE    1     2 PARAMS: UR=1000 AREA=10e-6 LEN=10e-3
R1    1     2     {LEN/(12.8e-7*UR*AREA)}
E1    B     0     VALUE={(V(1,2)/LEN)/(LEN/(12.8e-7*UR*AREA))}
E2    H     0     VALUE={V(1,2)/LEN}
E3    MMF   0     VALUE={V(1,2)}
E4    FLUX  0     VALUE={V(B)*AREA}
.ENDS
```

**Listing A.3: Spice core Netlist**

```
.SUBCKT CLASSICJA       1     2    PARAMS:     AREA=10E-6 LEN=10E-3
+ MS=400K A=10 K=10 C=0.5 ALPHA=5.0U
* CONVERT MMF TO HE
E1     3     0     VALUE={V(1,2)/LEN+ALPHA*MS*V(12)}
R1     3     0     1MEG
* ANHYSTERETIC MAGNETISATION
E2     4     0     VALUE={IF(ABS(V(3))>1E-3,1/TANH(V(3)/A)-
A/V(3),0.333*V(3)/A)}
R2     4     0     1MEG
* 1DH/DT
E3     5     0     1     2     1
C1     5     6     1M    (IC=0)
RD     6     7     1M
V1     7     0     0V
* DELTA*K
E4     8     0     VALUE={K*SGN(I(V1))}
R3     8     9     1K
C2     9     0     1PF
* INTEGRATE MAGNETISATION
E5     10    0     VALUE={V(4,12)/(V(9)-ALPHA*MS*V(4,12)+1M)/LEN}
D1     10    11    DMOD
R4     11    0     1K
E6     12    0     VALUE={SDT(1000*I(V1)*V(11)/(1+C))+C*V(4)/(1+C)}
R5     12    0     1K
E7     FLUX  0     VALUE={AREA*1.258E-6*(MS*V(12)+V(1,2)/LEN)}
R6     FLUX  0     1MEG
G1     1     2     FLUX  0     1
*
* Calculate B and H for postprocessing
*
E21    B     0     VALUE={V(FLUX)/AREA}
E22    H     0     VALUE={V(1,2)/LEN}
.MODEL      DMOD  D(N=0.01)
.ENDS
```

**Listing A.4: Spice classicja Netlist**

```
.SUBCKT classicja2      1     2     PARAMS:     AREA=10E-6 LEN=10E-3
+ MS=400K A=10 K=10 C=0.5 ALPHA=5.0U
* CONVERT MMF TO HE
E1     3     0     VALUE={V(1,2)/LEN+ALPHA*MS*V(12)}
R1     3     0     1MEG
* ANHYSTERETIC MAGNETISATION
E2     4     0     VALUE={IF(ABS(V(3))>1E-3,1/TANH(V(3)/A)-
A/V(3),0.333*V(3)/A)}
R2     4     0     1MEG
* 1DH/DT
E3     5     0     1     2     1
C1     5     6     1M    (IC=0)
RD     6     7     1M
V1     7     0     0V
* DELTA*K
E4     8     0     VALUE={K*SGN(I(V1))}
R3     8     9     1K
C2     9     0     1PF
* INTEGRATE MAGNETISATION
E5     10    0     VALUE={V(4,12)/(V(9)-ALPHA*MS*(1+c)*V(4,12)+1M)/LEN}
D1     10    11    DMOD
R4     11    0     1K
E6     12    0     VALUE={SDT(1000*I(V1)*V(11))+C*V(4)/(1+C)}
R5     12    0     1K
E7     FLUX  0     VALUE={AREA*1.258E-6*(MS*V(12)+V(1,2)/LEN)}
R6     FLUX  0     1MEG
```

```
G1     1     2     FLUX  0     1
*
* Calculate B and H for postprocessing
*
E21   B     0     VALUE={V(FLUX)/AREA}
E22   H     0     VALUE={V(1,2)/LEN}
.MODEL     DMOD  D(N=0.01)
.ENDS
```

**Listing A.5: Spice classicja2 Netlist**

```
.SUBCKT classicja3      1     2     PARAMS:     AREA=10E-6 LEN=10E-3
+ MS=400K A=10 K=10 C=0.5 ALPHA=5.0U MR=40.0
* CONVERT MMF TO HE
E1     3     0     VALUE={V(1,2)/LEN+ALPHA*MS*V(12)}
R1     3     0     1MEG
* ANHYSTERETIC MAGNETISATION
E2     4     0     VALUE={IF(ABS(V(3))>1E-3,1/TANH(V(3)/A)-
A/V(3),0.333*V(3)/A)}
R2     4     0     1MEG
* 1DH/DT
E3     5     0     1     2     1
C1     5     6     1M    (IC=0)
RD     6     7     1M
V1     7     0     0V
* DELTA*K
E4     8     0     VALUE={K*SGN(I(V1))}
R3     8     9     1K
C2     9     0     1PF
* INTEGRATE MAGNETISATION
E5     10    0     VALUE={V(4,12)/(V(9)-ALPHA*MS*(1+c)*V(4,12)+1M)/LEN}
D1     10    11    DMOD
R4     11    0     1K
E6     12    0     VALUE={SDT(1000*I(V1)*V(11))+C*V(4)/(1+C)}
R5     12    0     1K
E7     FLUX  0     VALUE={AREA*1.258E-6*(MS*V(12)+MR*V(1,2)/LEN)}
R6     FLUX  0     1MEG
G1     1     2     FLUX  0     1
*
* Calculate B and H for postprocessing
*
E21   B     0     VALUE={V(FLUX)/AREA}
E22   H     0     VALUE={V(1,2)/LEN}
.MODEL     DMOD  D(N=0.01)
.ENDS
```

**Listing A.6: Spice classicja4 Netlist**

```
.subckt     xfr3  p1 p2 p3 p4 p5 p6 PARAMS:
+ n1=1 n2=1 n3=1 ur=1 area=100u length=10m
X_U3       p5 p6 $N_0001 $N_0002 WINDING PARAMS:  N={n3}
X_U1       p2 p1 $N_0002 $N_0003 WINDING PARAMS:  N={n1}
X_U4       $N_0003 0 CORE PARAMS: UR={ur} AREA={area} LEN={length}
X_U2       p3 p4 0 $N_0001 WINDING PARAMS:  N={n2}
.ends
```

**Listing A.7: Spice xfr3 Netlist**

```
.subckt     xfr4  p1 p2 p3 p4 p7 p8 p9 p10 PARAMS:
+ n1=1 n2=1 n3=1 n4=1 ur=1 area=100u length=10m gap=0
X_U1        p1 p2 mag1 mag2 WINDING PARAMS:  N={n1}
X_U2        p3 p4 mag2 mag3 WINDING PARAMS:  N={n2}
X_U3        p10 p8 mag3 mag4 WINDING PARAMS:  N={n3}
X_U4        p9 p7 mag4 0 WINDING PARAMS:  N={n4}
X_U5        mag1 maggap CORE PARAMS: UR={ur} AREA={area} LEN={length}
X_U6        maggap 0 CORE PARAMS: UR=1 AREA={area} LEN={gap}
.ends
```

**Listing A.8: Spice xfr4 Netlist**

```
.subckt     xfr3_4a11   p1 p2 p3 p4 p5 p6 PARAMS: n1=1 n2=1 n3=1 ur=1
area=100u length=10m
X_U3        p5 p6 $N_0001 $N_0002 WINDING PARAMS:  N={n3}
X_U1        p2 p1 $N_0002 $N_0003 WINDING PARAMS:  N={n1}
X_U4        $N_0003 0 CLASSICJA PARAMS: AREA={area} LEN={length}
+ A=150 C=0.2 K=3 ALPHA=5.0U MS=350K
X_U2        p3 p4 0 $N_0001 WINDING PARAMS:  N={n2}
.ends
```

**Listing A.9: Spice xfr3_4a11 Netlist**

```
.subckt     vdslxfr3rx  p1 p2 p3 p4 p5 p6 PARAMS:
+ n1=38 n2=16 n3=16 ur=2100 area=1.97u length=15.3m
+ l1=3.0u l2=0.48u l3=0.6u
+ c12=14p c23=12p c13=13.4p
+ r1=0.596 r2=0.368 r3=0.383
* Basic Transformer
X_U3        p5b p6 $N_0001 $N_0002 WINDING PARAMS:  N={n3}
X_U1        p2 p1b $N_0002 $N_0003 WINDING PARAMS:  N={n1}
X_U4        $N_0003 0 CORE PARAMS: UR={ur} AREA={area} LEN={length}
X_U2        p3b p4 0 $N_0001 WINDING PARAMS:  N={n2}
* Leakage Inductances
LL1   p1    p1a    {L1}
LL2   p3    p3a    {L2}
LL3   p5    p5a    {L3}
* Interwinding Capacitances
CC12  p1b   p3b    {C12}
CC13  p1b   p5b    {C13}
CC23  p3b   p5b    {C23}
* Winding Resistances
RR1   p1a   p1b    {R1}
RR2   p3a   p3b    {R2}
RR3   p5a   p5b    {R3}
* Winding Capacitances
C11   p1b   p2     10p
C22   p3b   p4     10p
C33   p5b   p6     10p
.ends
```

**Listing A.10: Spice vdslxfr3rx Netlist**

```
.subckt     vdslxfr3tx  p1 p2 p3 p4 p5 p6 PARAMS:
+ n1=22 n2=25 n3=25 ur=2100 area=1.97u length=15.3m
+ l1=0.45u l2=0.48u l3=0.48u
+ c12=14p c23=12p c13=13.4p
+ r1=0.463 r2=0.463 r3=0.47
* Basic Transformer
X_U3        p5b p6 $N_0001 $N_0002 WINDING PARAMS:  N={n3}
X_U1        p2 p1b $N_0002 $N_0003 WINDING PARAMS:  N={n1}
```

```
X_U4          $N_0003 0 CORE PARAMS: UR={ur} AREA={area} LEN={length}
X_U2          p3b p4 0 $N_0001 WINDING PARAMS:  N={n2}
* Leakage Inductances
LL1   p1    p1a    {L1}
LL2   p3    p3a    {L2}
LL3   p5    p5a    {L3}
* Interwinding Capacitances
CC12  p1b   p3b    {C12}
CC13  p1b   p5b    {C13}
CC23  p3b   p5b    {C23}
* Winding Resistances
RR1   p1a   p1b    {R1}
RR2   p3a   p3b    {R2}
RR3   p5a   p5b    {R3}
* Winding Capacitances
C11   p1b   p2    10p
C22   p3b   p4    10p
C33   p5b   p6    10p
.ends
```

**Listing A.11: Spice vdslxfr3rx Netlist**

```
.SUBCKT EXPKJA   1    2    PARAMS:    AREA=10E-6 LEN=10E-3
+ MS=400K A=10 K=10 C=0.5 ALPHA=5.0U ECRATE=100
* CONVERT MMF TO HE
E1    HE    0    VALUE={V(H)+ALPHA*MS*V(M)}
R1    HE    0    1MEG
* ANHYSTERETIC MAGNETISATION
E2    MAN   0    VALUE={IF(ABS(V(HE))>1E-3,1/TANH(V(HE)/A)-
A/V(HE),0.333*V(HE)/A)}
R2    MAN   0    1MEG
* 1DH/DT
E3    5     0    1    2    1
C1    5     6    1M    (IC=0)
RD    6     7    1M
V1    7     0    0V
* DELTA*K
E4    8     0    VALUE={K*EXP(-
(V(H)*V(H)/(2*ECRATE*ECRATE)))*SGN(I(V1))}
R3    8     DELTAK    1K
C2    DELTAK    0    1PF
* INTEGRATE MAGNETISATION
E5    10    0    VALUE={V(MAN,M)/(V(DELTAK)-ALPHA*MS*V(MAN,M)+1M)/LEN}
D1    10    DMDH  DMOD
R4    DMDH  0    1K
* E24 DMDH  0    VALUE={IF(V(10)>0,V(10),0)}
E6    M     0    VALUE={SDT(1000*I(V1)*V(DMDH)/(1+C))+C*V(MAN)/(1+C)}
R5    M     0    1K
E7    FLUX  0    VALUE={AREA*1.258E-6*(MS*V(M)+V(H))}
R6    FLUX  0    1MEG
G1    1     2    FLUX  0    1
*
* Calculate B and H for postprocessing
*
E21   B     0    VALUE={V(FLUX)/AREA}
E22   H     0    VALUE={V(1,2)/LEN}
E23   REL   0    VALUE={V(1,2)*SGN(V(FLUX))/(ABS(V(FLUX))+1p)}
.MODEL    DMOD  D(N=0.01)
.ENDS
```

**Listing A.12: Spice expja Netlist**

```
.SUBCKT expkja2   1    2    PARAMS:    AREA=10E-6 LEN=10E-3
```

```
+ MS=400K A=10 K=10 C=0.5 ALPHA=5.0U ECRATE=100 A2=0.1
* CONVERT MMF TO HE
E1     HE     0      VALUE={V(H)+ALPHA*MS*V(M)}
R1     HE     0      1MEG
* ANHYSTERETIC MAGNETISATION
E2     MAN    0      VALUE={IF(ABS(V(HE))>1E-3,1/TANH(V(HE)/A)-
A/V(HE),0.333*V(HE)/A)}
R2     MAN    0      1MEG
* 1DH/DT
E3     5      0      1      2      1
C1     5      6      1M     (IC=0)
RD     6      7      1M
V1     7      0      0V
E23    IV1    0      VALUE={I(V1)}
E24    SI     0      VALUE={IF(ABS(V(IV1))>1E-3,1/TANH(V(IV1)/A2)-
A2/V(IV1),0.333*V(IV1)/A2)}
* DELTA*K
E4     8      0      VALUE={K*EXP(-
(V(H)*V(H)/(2*ECRATE*ECRATE)))*V(SI)/(ABS(V(SI))+1u)}
R3     8      DELTAK    1K
C2     DELTAK    0      1PF
* INTEGRATE MAGNETISATION
E5     10     0      VALUE={V(MAN,M)/(V(DELTAK)-ALPHA*MS*V(MAN,M)+1M)/LEN}
D1     10     DMDH   DMOD
R4     DMDH   0      1K
E6     M      0      VALUE={SDT(1000*I(V1)*V(DMDH)/(1+C))+C*V(MAN)/(1+C)}
R5     M      0      1K
E7     FLUX   0      VALUE={AREA*1.258E-6*(MS*V(M)+V(H))}
R6     FLUX   0      1MEG
G1     1      2      FLUX   0      1
RG1    1      0      1Meg
*
* Calculate B and H for postprocessing
*
E21    B      0      VALUE={V(FLUX)/AREA}
E22    H      0      VALUE={V(1,2)/LEN}
.MODEL      DMOD   D(N=0.01)
.ENDS
```

**Listing A.13: Spice expja2 Netlist**

```
.SUBCKT thermalja 1   2   3   4   5   6   7      8      PARAMS: AREA=10E-6
LEN=10E-3
*                    p   m   a   c   k   ms  alpha  th
+ MS=400K A=10 K=10 C=0.5 ALPHA=5.0U ECRATE=1
* CONVERT MMF TO HE
E1     HE     0      VALUE={V(1,2)/LEN+ALPHA*MS*V(M)}
R1     HE     0      1MEG
* ANHYSTERETIC MAGNETISATION
E2     MAN    0      VALUE={IF(ABS(V(HE))>1E-3,1/TANH(V(HE)/V(3))-
V(3)/V(HE),0.333*V(HE)/V(3))}
R2     MAN    0      1MEG
* 1DH/DT
E3     HIN    0      VALUE={V(1,2)}
C1     HIN    CR     1M     (IC=0)
RD     CR     21     1M
V1     21     0      0V
* DELTA*K
E4     DK     0      VALUE={V(5)*EXP(-
(V(HIN)*V(HIN)/(2*ECRATE*ECRATE)))*SGN(I(V1))}
R3     DK     DELTAK    1K
C2     DELTAK    0      1PF
```

248

```
* INTEGRATE MAGNETISATION
E5    DMDH  0      VALUE={V(MAN,M)/(V(DELTAK)-ALPHA*MS*V(MAN,M)+1M)/LEN}
D1    DMDH  MIRR   DMOD
R4    MIRR  0      1K
E6    M     0
      VALUE={SDT(1000*I(V1)*V(MIRR)/(1+V(4)))+V(4)*V(MAN)/(1+V(4)))}
R5    M     0      1K
E7    FLUX  0      VALUE={AREA*1.258E-6*(MS*V(M)+V(HIN)/LEN)}
R6    FLUX  0      1MEG
G1    1     2      FLUX  0      1
* Thermal Variable Input
RVA   3     0      1k
RVC   4     0      1k
RVK   5     0      1k
RVRMS 6     0      1K
RVALPHA     7      0      1k
* Thermal Output
RTH   8     0      1G
*
* Calculate B and H for postprocessing
*
E21   B     0      VALUE={V(FLUX)/AREA}
E22   H     0      VALUE={V(1,2)/LEN}
.MODEL      DMOD  D(N=0.01)
.ENDS
```

**Listing A.14: Spice thermalja Netlist**

```
.SUBCKT expja_th7      1     2     3     PARAMS:      AREA=10E-6
LEN=10E-3
+ MS=430K A=33.5 K=27.98 C=0.406 ALPHA=3.28U ECRATE=54.1
+ MSTC=-1138.2 KTC=-0.073 CTC=1.63m ATC=-1.11e-3 ALPHATC=5.28e-9
+ ECRATEATC=0
* CONVERT MMF TO HE
E1    HE    0      VALUE={V(H)+ALPHA*V(TALPHA)*MS*V(TMS)*V(M)}
R1    HE    0      1MEG
* ANHYSTERETIC MAGNETISATION
E2    MAN   0      VALUE={IF(ABS(V(HE))>1E-3,1/TANH(V(HE)/(A*V(TA)+1u))-
(A*V(TA))/V(HE),0.333*V(HE)/(A*V(TA)+1u))}
R2    MAN   0      1MEG
* 1DH/DT
E3    5     0      1     2     1
C1    5     6      1M    (IC=0)
RD    6     7      1M
V1    7     0      0V
* DELTA*K
E4    8     0      VALUE={K*V(TK)*EXP(-
(V(H)*V(H)/(2*ECRATE*ECRATE*V(TEC)*V(TEC))))*SGN(I(V1))}
R3    8     DELTAK      1K
C2    DELTAK      0      1PF
* INTEGRATE MAGNETISATION
E5    10    0      VALUE={V(MAN,M)/(V(DELTAK)-
ALPHA*V(TALPHA)*MS*V(TMS)*V(MAN,M)+1M)/LEN}
D1    10    DMDH  DMOD
R4    DMDH  0      1K
E6    M     0
      VALUE={SDT(1000*I(V1)*V(DMDH)/(1+C*V(TC)))+C*V(TC)*V(MAN)/(1+C*V(T
C))}
R5    M     0      1K
E7    FLUX  0      VALUE={AREA*1.258E-6*(MS*V(TMS)*V(M)+V(H))}
R6    FLUX  0      1MEG
```

249

```
G1      1       2       FLUX    0       1
*
* Calculate thermal Output
*
E8      MIRR    0       VALUE={V(M)-V(MAN)}
E9      PLOSS   0       VALUE={V(1,2)*1.258E-6*(MS*V(TMS)*V(MIRR) + V(H))}
G10     3       0       PLOSS   0       1
E10     T       0       3       0       1
*
* Thermal Variables
*
* MS
EMS     TMS     0       VALUE={(MS+(V(T)*MSTC))/MS}
RMS     TMS     0       1000
* K
EK      TK      0       value={(k+(v(t)*ktc))/K}
RK      TK      0       1000
* C
EC      TC      0       value={(c+(v(t)*ctc))/c}
RC      TC      0       1000
* A
EA      TA      0       value={(A+(v(t)*ATC))/A}
RA      TA      0       1000
* ECRATE
EEC     TEC     0       value={(ECRATE+(v(t)*ECRATEATC))/ECRATE}
REC     TEC     0       1000
* ALPHA
EALPHA          TALPHA          0       value={(ALPHA+(v(t)*ALPHATC))/ALPHA}
RALPHA          TALPHA          0       1000
*
* Calculate B and H for postprocessing
*
E21     B       0       VALUE={V(FLUX)/AREA}
E22     H       0       VALUE={V(1,2)/LEN}
.MODEL          DMOD    D(N=0.01)
.ENDS
```

**Listing A.15: Spice Expja_th7 Netlist**

```
.SUBCKT emission 1      2 PARAMS: AREA=1.0 E=1.0
*
G1      1       3       VALUE={5.67e-8*E*(V(THETAS)**4-V(THETAA)**4)*AREA}
V1      3       2       0
E2      POWER 0         VALUE={I(V1)}
E3      THETAS          0       VALUE={V(1)+273.0}
E4      THETAA          0       VALUE={V(2)+273.0}
.ENDS
```

**Listing A.16: Spice Emission Netlist**

```
.SUBCKT rconv    1      2 PARAMS: AREA=1.0 D=10.0e-3 K=6.3
G1      1       3       VALUE={K*(V(1,2)**1.25)/(D**0.25)*AREA}
V1      3       2       0
E2      POWER 0         VALUE={I(V1)}
E3      DELTAT          0       VALUE={V(1,2)}
.ENDS
```

**Listing A.17: Spice Rconv Netlist**

```
.SUBCKT ctherm   1      2 PARAMS: CTH=1.0
C1      1       3       {CTH}
V1      3       2       0
E3      POWER 0         VALUE={I(V1)}
```

```
E4     DELTAT      0      VALUE={V(1,2)}
.ENDS
```

**Listing A.18: Spice ctherm Netlist**

```
.SUBCKT rtherm     1     2 PARAMS: RTH=1.0
R1     1     2      {RTH}
E3     POWER 0      VALUE={V(1,2)/RTH}
E4     DELTAT      0      VALUE={V(1,2)}
.ENDS
```

**Listing A.19: Spice rtherm Netlist**

```
.SUBCKT pmlang     1     2 PARAMS: UR=40 HC=300k BR=1.1 A=10 AREA=10e-6
LEN=10e-3
E1     B     0      VALUE={(1+V(BEFF))*(IF(ABS(V(HE))>1e-
3,1/TANH(V(HE)/A)-A/V(HE),0.333*V(HE)/A))}
E2     MMF   0      VALUE={V(1,2)}
E3     H     0      VALUE={V(MMF)/LEN}
E4     FLUX  0      VALUE={V(B)*AREA}
E5     HE    0      VALUE={V(H)-HC}
E6     BEFF  0      VALUE={ABS(V(HE))*UR*12.58E-6}
G1     1     2      FLUX  0     1
.ENDS
```

**Listing A.20: Spice pmlang Netlist**

```
.SUBCKT pmagnet    1     2 PARAMS: UR=1000 HC=-100 AREA=10e-6 LEN=10e-3
E1     B     0      VALUE={V(HE)*(12.8e-7*UR)}
E2     MMF   0      VALUE={V(1,2)}
E3     H     0      VALUE={V(MMF)/LEN}
E4     FLUX  0      VALUE={V(B)*AREA}
E5     HE    0      VALUE={V(H)-HC}
G1     1     2      FLUX  0     1
.ENDS
```

**Listing A.21: Spice pmagnet Netlist**

```
.SUBCKT pmagnet2 1     2 PARAMS: UR=1000 HC=-100 AREA=10e-6 LEN=10e-3
BR=1.0
I1     1     2      {BR*AREA}
.ENDS
```

**Listing A.22: Spice pmagnet2 Netlist**

## Appendix B : Saber (MAST) model listings

```
template coreja p m=a,c,k,ms,alpha,ecrate,len,area
magnetic p,m
number a=20
number c=0.5
number k=20
number ms=480k
number alpha=5.0u
number ecrate=100
number len=10m
number area=100u
{
<consts.sin
var f f
var hm dhdt
var nu mirr
val mmf mmf
val hm h,absh,han,he
val bsi b
val nu man,sign,deltak,dmdh,dmdt,mtotal,dm
number mu0

parameters{
    mu0 = 4*math_pi*1e-7
    }

values {
    #...Get the mmf across the core
    mmf = mmf(p) - mmf(m)
    #...Calculate the Applied Magnetic Field Strength and Flux Density
    h = mmf/len
    #...Calculate the Effective Magnetic Field Strength
    he = h + (alpha * ms * mtotal)
    absh = abs(he)
    #...Anhysteretic Magnetization
    if (absh>1m) {
        han = (1/tanh(he/a)) - a/he
    }
    else {
        han = 0.333*he/a
    }
    man = han
    #...deltak
    if (dhdt>0) {
      sign=1
    }
    else {
      sign=-1
    }
    deltak = sign*k*exp(-h*h/(2*ecrate*ecrate))
    #deltak = sign*k
    mtotal = man*c/(1+c) + mirr
    dm = man-mtotal
    dmdh = dm/((deltak*area/mu0)-(alpha*(1+c)*ms*dm))/len
    if (dmdh>0) {
        dmdt = dmdh*dhdt
    }
    else {
        dmdt=0
    }
```

252

```
    b = mu0*(ms*mtotal + h)
    }
equations{
    f(p->m)-=f
    f: f = b*area
    dhdt = d_by_dt(h)
    mirr: d_by_dt(mirr) + dc_domain*0.0 = dmdt + dc_domain*mirr
    }
}
```

**Listing B.1 Saber Mast Jiles-Atherton (Gaussian k) coreja Model Listing**

```
template coreja2 p m=a,c,k,ms,alpha,ecrate,len,area
magnetic p,m
number a=20
number c=0.5
number k=20
number ms=480k
number alpha=5.0u
number ecrate=100
number len=10m
number area=100u
{
<consts.sin
var f f
var hm dhdt
var nu mirr, man
val mmf mmf
val hm h,absh,han,he
val bsi b
val nu man_calc,sign,deltak,dm,dmdt
number mu0
var nu mtotal, dmdh

parameters{
    mu0 = 4*math_pi*1e-7
    }

values {
    # Get the mmf across the core
    mmf = mmf(p) - mmf(m)

    # Calculate the Applied Magnetic Field Strength and Flux Density
    h = mmf/len

    # Calculate the Effective Magnetic Field Strength
    he = h + (alpha * ms * mtotal)
    absh = abs(he)

    # Anhysteretic Magnetization
    if (absh>1m) {
        han = (1/tanh(he/a)) - a/he
    }
    else {
        han = 0.333*he/a
    }

    # deltak
    if (dhdt>0) {
      sign=1
    }
```

```
    else {
      sign=-1
    }
    #deltak = sign*k*exp(-h*h/(2*ecrate*ecrate))
    deltak = sign*k

    # dmdh
    dm = man-mtotal
    if (dmdh>0) {
        dmdt = dmdh*dhdt
    }
    else {
        dmdt=0
    }

    b = mu0*(ms*mtotal + h)
    }


equations{
    f(p->m)-=f
    f: f = b*area
    man: man = han
    mtotal : mtotal = man*c/(1+c) + mirr
    dmdh: dmdh = dm/((deltak*area/mu0)-(alpha*(1+c)*ms*dm))/len
    dhdt = d_by_dt(h)
    mirr: d_by_dt(mirr) + dc_domain*0.0 = dmdt + dc_domain*mirr
    }
}
```

**Listing B.2 : Saber MAST Original Jiles-Atherton Model coreja2 Listing**

```
template coreja3 p m=a,c,k,ms,alpha,ecrate,len,area,vfext
magnetic p,m
number a=20
number c=0.5
number k=20
number ms=480k
number alpha=5.0u
number ecrate=100
number len=10m
number area=100u
number vfext=1.0
{
<consts.sin
var f f
var hm dhdt
var nu mirr, man
val mmf mmf
val hm h,absh,han,he
val bsi b
val nu man_calc,sign,deltak,dm,dmdt,vf
number mu0
var nu mtotal, dmdh
state nu last,next,dir=-1
state nu hpos=100,hneg=100,hdiff=200

parameters{
    mu0 = 4*math_pi*1e-7
    }
```

```
when(threshold(dhdt,0,last,next)) {
    if (last<next) {
        schedule_event(time,dir,1)
    }
    else {
        schedule_event(time,dir,-1)
    }
    }

when(event_on(dir)) {
    if(dir<0) {
        hpos=h
    }
    else {
        hneg=h
    }
    schedule_event(time,hdiff,hpos-hneg)
    }

values {
    # Get the mmf across the core
    mmf = mmf(p) - mmf(m)

    # Calculate the Applied Magnetic Field Strength and Flux Density
    h = mmf/len

    # Calculate the Effective Magnetic Field Strength
    he = h + (alpha * ms * mtotal)
    absh = abs(he)

    # Anhysteretic Magnetization
    if (absh>1m) {
        han = (1/tanh(he/a)) - a/he
    }
    else {
        han = 0.333*he/a
    }

    # deltak
    if (dhdt>0) {
      sign=1
    }
    else {
      sign=-1
    }
    #deltak = sign*k*exp(-h*h/(2*ecrate*ecrate))
    deltak = sign*k

    # dmdh
    dm = man-mtotal
    if (dmdh>0) {
        dmdt = dmdh*dhdt
    }
    else {
        dmdt=0
    }

    #...Calculate the volume fraction change in dmdt
    #...assuming ecrate is the largest full loop size
    vf = hdiff/(ecrate*2)
    #dmdt = dmdt*vfext
    dmdt = dmdt*vf
```

```
    b = mu0*(ms*mtotal + h)
    }


equations{
    f(p->m)-=f
    f: f = b*area
    man: man = han
    mtotal : mtotal = man*c/(1+c) + mirr
    dmdh: dmdh = dm/((deltak*area/mu0)-(alpha*(1+c)*ms*dm))/len
    dhdt = d_by_dt(h)
    mirr: d_by_dt(mirr) + dc_domain*0.0 = dmdt + dc_domain*mirr
    }
}
```

**Listing B.3: Saber MAST Jiles-Atherton with minor loop extensions coreja3 Model Listing**

```
template coreja_th p m th=a,c,k,ms,alpha,ecrate,len,area
magnetic p,m
thermal_c th
number a=20
number c=0.5
number k=20
number ms=480k
number alpha=5.0u
number ecrate=80
number len=10m
number area=100u
{
<consts.sin
var f f
var hm dhdt
var nu mirr
val p pwrd
val mmf mmf
val hm h,absh,han,he
val bsi b
val nu man,sign,deltak,dmdh,dmdt,mtotal,dm
val tc tempc
number mu0

parameters{
    mu0 = 4*math_pi*1e-7
    }

values {
    #...Get the mmf across the core
    mmf = mmf(p) - mmf(m)
    #...Calculate the Applied Magnetic Field Strength and Flux Density
    h = mmf/len
    #...Calculate the Effective Magnetic Field Strength
    he = h + (alpha * ms * mtotal)
    absh = abs(he)
    #...Anhysteretic Magnetization
    if (absh>1m) {
        han = (1/tanh(he/a)) - a/he
    }
    else {
        han = 0.333*he/a
    }
    man = han
    #...deltak
    if (dhdt>0) {
```

256

```
      sign=1
    }
    else {
      sign=-1
    }
    deltak = sign*k*exp(-h*h/(2*ecrate*ecrate))
    #deltak = sign*k
    mtotal = man*c/(1+c) + mirr
    dm = man-mtotal
    dmdh = dm/((deltak*area/mu0)-(alpha*(1+c)*ms*dm))/len
    if (dmdh>0) {
        dmdt = dmdh*dhdt
    }
    else {
        dmdt=0
    }
    b = mu0*(ms*mtotal + h)
    pwrd = mmf*dmdt*mu0*ms*area
    tempc = tc(th)
    }
equations{
    p(th)-=pwrd
    f(p->m)-=f
    f: f = b*area
    dhdt = d_by_dt(h)
    mirr: d_by_dt(mirr) + dc_domain*0.0 = dmdt + dc_domain*mirr
    }
}
```

**Listing B.4: Saber MAST Jiles-Atherton with thermal extensions coreja_th Model Listing**

# Appendix C : VHDL-AMS model Listings

```
USE work.electrical_systems.ALL;

ENTITY core IS

  GENERIC (
    ur,                                   -- Relative permeability.
    len,                                  -- Core length [m].
    area  : real);                        -- Core area [m**2].

  PORT (
    TERMINAL p,
            m : magnetic);

END ENTITY core;
```

**Listing C.1 : VHDL-AMS Core Entity Model Listing**

```
USE work.electrical_systems.ALL;
USE work.energy_systems.ALL;

ARCHITECTURE core_linear OF core IS

  CONSTANT mg      : real := MU0*ur*area/len;
  QUANTITY mmf across flux through p TO m;
  QUANTITY h : real;
  QUANTITY b : real;

BEGIN  -- architecture core_linear

  ASSERT len /= 0.0
    REPORT "len should not be set to 0!"
    SEVERITY error;

  ASSERT k /= 0.0
    REPORT "k should not be set to 0!"
    SEVERITY error;

  flux == mg * mmf;
  h == mmf/len;
  b == flux/area;

END ARCHITECTURE core_linear;
```

**Listing C.2 : VHDL-AMS Linear Core Architecture Model Listing**

```
LIBRARY ieee;
USE ieee.math_real.ALL;
USE work.electrical_systems.ALL;
USE work.energy_systems.ALL;

ARCHITECTURE core_langevin OF corenl IS

    CONSTANT mg      : real := MU0*ur*area;
    QUANTITY mmf across flux through p TO m;
    QUANTITY lang_h,h : field_strength;
```

```
        QUANTITY b : flux_density;
        CONSTANT minh : real := 1.0e-3;

        FUNCTION lang(x : real) RETURN real IS
              VARIABLE lang_x : real := 0.0;
        BEGIN
              IF abs(x) < 1.0e-3 THEN
                    lang_x := 0.333 * x;
              ELSE
                    lang_x := 1.0/tanh(x) - 1.0/x;
              END IF;

              RETURN lang_x;
        END FUNCTION;

BEGIN  -- architecture core_langevin

        ASSERT len /= 0.0
              REPORT "len should not be set to 0!"
              SEVERITY error;

        ASSERT k /= 0.0
              REPORT "k should not be set to 0!"
              SEVERITY error;

        h == mmf/len;
        lang_h == lang(h);
        flux == mg * lang_h;
        b == flux/area;

END ARCHITECTURE core_langevin;
```

**Listing C.3 : VHDL-AMS Non-Linear Langevin Core Architecture Model Listing**

```
USE work.electrical_systems.ALL;

ENTITY corenl IS

  GENERIC (
      k,                    -- Energy Loss Parameter
      c,                    -- Ratio of Mirr to Mrev
      ms,                   -- Saturation Magnetization
      alpha,                -- Proportion of fed back flux to effective H
      a,                    -- Langevin Function Parameter
      ur,                   -- relative permeability.
      len,                  -- Core length [m].
      area     : real);  -- Core area [m**2].


  PORT (
    TERMINAL p,
             m : magnetic);

END ENTITY corenl;
```

**Listing C.4 : VHDL-AMS Jiles-Atherton Core Entity Model Listing**

```
LIBRARY ieee;
USE ieee.math_real.ALL;
```

259

```
USE work.electrical_systems.ALL;
USE work.energy_systems.ALL;

ARCHITECTURE corenl_ja OF corenl IS

        CONSTANT mg      : real := MU0*area;
        QUANTITY mmf across flux through p TO m;
        QUANTITY h,he : field_strength;
        QUANTITY dhdt,mtotal,delta,mrev,man,mirr,dmdh1,dmdh,dmirrdt,dm :
real;
        QUANTITY b : flux_density;
        QUANTITY test : real;
        CONSTANT minh : real := 1.0e-3;
        SIGNAL dir : real;
        TERMINAL vin : electrical;
        QUANTITY v across i through vin to ground;

        FUNCTION calc_delta(x : real) RETURN real IS
            VARIABLE delta_x : real := 0.0;
        BEGIN
            IF abs(x) < 1.0e-3 THEN
                    delta_x := x*1000.0;
            ELSIF x > 0.0 THEN
                    delta_x := 1.0 + x*1.0e-6;
            ELSE
                    delta_x := -1.0 - x*1.0e-6;
            END IF;

            RETURN delta_x;
        END FUNCTION;

        FUNCTION lang(x : real) RETURN real IS
            VARIABLE lang_x : real := 0.0;
        BEGIN
            IF abs(x) < 1.0e-3 THEN
                    lang_x := 0.333 * x;
            ELSE
                    lang_x := 1.0/tanh(x) - 1.0/x;
            END IF;

            RETURN lang_x;
        END FUNCTION;

BEGIN  -- architecture core_ja

        ASSERT len /= 0.0
            REPORT "len should not be set to 0!"
            SEVERITY error;

        -- Not Supported by Analogy/Avant!
        PROCESS
        BEGIN
            IF dhdt > 0.0  THEN
                    dir <= 1.0;
            ELSE
                    dir <= -1.0;
            END IF;
            WAIT ON dhdt'above(0.0)  ;
        END PROCESS;

        -- Calculate h, effective h and dhdt
        h == mmf/len;
        he == h + (alpha * ms * mtotal);
```

```
        dhdt == he'DOT;

        -- I am using this to replace the unsupported PROCESS above

        IF dhdt > 0.0 USE
                delta == 1.0;
        ELSE
                delta == -1.0;
        END USE;

        --delta == calc_delta(dhdt);
        --delta == dhdt/(abs(dhdt)+1.0e-9);

        -- Anhysteretic Magnetization
        man == lang(h);
        mrev == c * man / ( 1.0 + c );

        -- Calculate magnetization
        dm == man - mtotal;

        -- Calculate dM/dH, (limiting to > 0.0;)
        dmdh1 == dm / ( delta * k - alpha * ms * dm ) / len;

        --IF dmdh1 > 0.0 USE
        --    dmdh == 1.0;
        --ELSE
        --    dmdh == 0.0;
        --END USE;

        -- Calculate dM/dT and then integrate to get Mirr
        dmirrdt == dhdt * dmdh1;

        mirr == 0.0;

        test == 1.0 * dmdh1;
        v == dm / ( k - alpha * ms * dm ) / len;

        --mirr == (1.0 / (1.0 + c)) * dmirrdt'INTEG;

        mtotal == mrev + mirr/(1.0 + c);

        flux == mg * (ms * mtotal + h);
        b == flux/area;

        --cin : ENTITY WORK.c
        --    GENERIC MAP (cnom => 1.0)
        --    PORT MAP (  p       => vin,
        --                m       => ground);

        rin : ENTITY WORK.r
              GENERIC MAP (rnom => 1.0)
              PORT MAP ( p       => vin,
                         m       => ground);


END ARCHITECTURE corenl_ja;
```

**Listing C.5 : VHDL-AMS Jiles-Atherton Architecture Model Listing**

```
USE work.electrical_systems.ALL;
```

```
ENTITY wind IS

   GENERIC (
      r,
      n : real := 0.0);

   PORT (
     TERMINAL ep,
               em    : electrical;
     TERMINAL mp,
               mm    : magnetic);

END ENTITY wind;


-------------------------------------------------------
-- Simple Architecture
-------------------------------------------------------

ARCHITECTURE simple OF wind IS
   QUANTITY h across f through mp TO mm;
   QUANTITY v across i through ep TO em;

BEGIN  -- architecture simple

   h == i*n;
   v == - n*f'dot + i*r;

END ARCHITECTURE simple;
```

**Listing C.6 : VHDL-AMS Winding Model Listing**

# Appendix D : SPICE-FEA Code Listings

```
Port_Name:     in                        out
Description:   "input current"      "output flux"
Direction:     in                        out
Default_Type:  v               v
Allowed_Types:[v,vd,i,id,vnam] [v,vd,i,id]
Vector:        yes             yes
Vector_Bounds:[2 -]             [2 -]
Null_Allowed:  no              no


Parameter_Name:                      n
Description:          "winding turns"
Data_Type:           real
Default_Value:       1.0
Limits:              -
Vector:              no
Vector_Bounds:       -
Null_Allowed:        yes
```

**Figure D.1: Excerpt from ifspec.ifs file for FEA Inductor**

```c
#include <windows.h>
#include <stdlib.h>
#define BUFSIZE 1024

void cm_slim1(ARGS)   /* structure holding parms, inputs, outputs, etc.      */
{
  Mif_Complex_t ac_gain;
  FILE *fptr;
      int i;
      typedef char string[BUFSIZE];
      string cmds[10],msg,stopstr,rn;
      double fout[10];
  PROCESS_INFORMATION pi={0};
  STARTUPINFO si={0};
      si.dwFlags = STARTF_USESHOWWINDOW;
      si.wShowWindow = SW_HIDE;
      strcpy(cmds[0],"wish80.exe run.tcl");
      strcpy(cmds[1],"slim-ma -f basic.cntl");
      strcpy(cmds[2],"slim-sp -f basic.sp");
      strcpy(cmds[3],"wish80.exe postprocess.tcl");

  if(ANALYSIS != MIF_AC) {
            fptr = fopen("sliminfobasic.txt","w");
            for(i=0;i<2;i++) {
              fprintf(fptr,"%f\n",INPUT(in[i]));
            }
            fprintf(fptr,"%f\n",PARAM(n));
            fclose(fptr);
            for(i=0;i<4;i++) {
                    if( CreateProcess(NULL,cmds[i],NULL,NULL,FALSE,0,NULL,NULL,&si,&pi)
) {
                          CloseHandle(pi.hThread);
      WaitForSingleObject(pi.hProcess,INFINITE);
                          CloseHandle(pi.hProcess
            }
            }

            fptr = fopen("slimresultsbasic.txt","r");
            for(i=0;i<2;i++) {
                    fscanf(fptr,"%s\n",rn);
                    fout[i] = strtod(rn,stopstr);
            }
            fclose(fptr);

            for(i=0;i<2;i++) {
      OUTPUT(out[i]) = fout[i];
    }
      cm_analog_auto_partial();
}
}
```

**Figure D.2: cfunc.mod XSPICE FEA Inductor Code Model**

```
begin
 mesh 'basic.m2d'
 beginrun 'study_1'
  beginin
   material permeability air linear 1.0
   material permeability core non-linear 'C:\SLIM\bh\coeff\unisil_30m5_coeff'
   material permeability window linear 1.0
   material winding left    0.0 10.000000
   material winding right -0.0 10.000000
   fixed_potential Z 0
   cg_iterations 1000
   cg_tolerance 1e-009
   cg_drop_tol 0.01
   iterations 20
   error 0.001
  endin

  beginout
   begin_nodal 'basic.nodal'
    begin_data_set 'Potential'
     material air potential
     material core potential
     material window potential
     material right potential
     material left potential
    end_data_set
   end_nodal
   begin_elemental 'basic.elem'
    begin_data_set 'Flux Density'
     material air flux_density
     material core flux_density
     material window flux_density
     material right flux_density
     material left flux_density
    end_data_set
   end_elemental
  endout
 endrun
end
```

**Figure D.3: SLIM FEA Control File – basic.cntl**

```
input -slice 'basic.m2d'
window -vwin 0  0  1  1
input -nodal 'basic.nodal' 'Potential'
input -elem 'basic.elem' 'Flux Density'
label -all
integrate -area -nodal -average -label left
integrate -area -nodal -average -label right
stop
```

**Figure D.4: Example SLIM post-processing control file**

## Appendix E : Planar Magnetic Implementation

To make the task of prototyping as simple and flexible as possible a number of PCBs were designed and constructed for the ER9.5, ER11, E14 and E18 core types with single (straight return track) and double-sided spirals with the maximum track density for a double-sided 1.6mm PCB (based on a track width of 0.15mm and the same track spacing). To construct a 2 winding transformer is then a simple matter of stacking the required number of PCBs to obtain the necessary winding configuration. This will obviously not be as good as a dedicated 4,6 or 8 layer PCB, especially with regard to leakage inductance, but it is an effective approach for prototyping. Each layer is made using an L shape, so that the external connections in a stacked PCB can be easily accessed by 'flipping' subsequent layers. This approach allows up to 4 double sided boards to be stacked if necessary (if space permits).

To automate the generation of the PCB designs, software has been written (using TCL/TK), which automatically calculates the PCB layout based on the core dimensions and track specifications. The simple Graphical User Interface (GUI) uses the geometry of the planar core to estimate the required number of turns and create a command script file for the EAGLE 4.0 layout software. The GUI is shown in figure E.1 and the resulting command script showing all the vias, board outline and connections is given in E.2. The PCB design can then be read directly into the EAGLE 4.0 layout program, with an example shown in figure E.3.
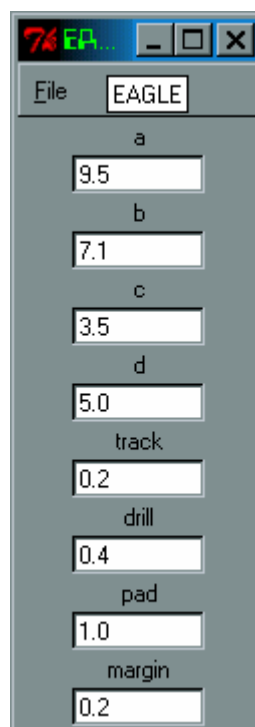


**Figure E.1 : Planar Winding TCL/TK Gui**

```
GRID MM 0.05;
CHANGE LAYER DIMENSION;
```

265

```
WIRE 0 (0 0) (44.0 0) (44.0 18.6) (33.0 18.6) (33.0 13.6) (0 13.6) (0
0);
CHANGE LAYER DIMENSION;
WIRE 0 (11.0 8.9) (22.0 8.9) (22.0 4.7) (11.0 4.7) (11.0 8.9);
WINDOW FIT;
CHANGE DRILL 0.4;
VIA 'via1' 1.0 round (39.2 17.9);
VIA 'via2' 1.0 round (37.8 17.9);
VIA 'via3' 1.0 round (22.7 6.1);
VIA 'via4' 1.0 round (22.7 7.5);
CHANGE LAYER TOP;
WIRE 0.2 (23.6 9.1) (10.8 9.1);
WIRE 0.2 (10.8 9.1) (10.8 4.5);
WIRE 0.2 (10.8 4.5) (24.0 4.5);
WIRE 0.2 (24.0 4.5) (24.0 9.5);
WIRE 0.2 (24.0 9.5) (10.4 9.5);
WIRE 0.2 (10.4 9.5) (10.4 4.1);
WIRE 0.2 (10.4 4.1) (24.4 4.1);
WIRE 0.2 (24.4 4.1) (24.4 9.9);
WIRE 0.2 (24.4 9.9) (10.0 9.9);
WIRE 0.2 (10.0 9.9) (10.0 3.7);
WIRE 0.2 (10.0 3.7) (24.8 3.7);
WIRE 0.2 (24.8 3.7) (24.8 10.3);
WIRE 0.2 (24.8 10.3) (9.6 10.3);
WIRE 0.2 (9.6 10.3) (9.6 3.3);
WIRE 0.2 (9.6 3.3) (25.2 3.3);
WIRE 0.2 (25.2 3.3) (25.2 10.7);
WIRE 0.2 (25.2 10.7) (9.2 10.7);
WIRE 0.2 (9.2 10.7) (9.2 2.9);
WIRE 0.2 (9.2 2.9) (25.6 2.9);
WIRE 0.2 (25.6 2.9) (25.6 11.1);
WIRE 0.2 (25.6 11.1) (8.8 11.1);
WIRE 0.2 (8.8 11.1) (8.8 2.5);
WIRE 0.2 (8.8 2.5) (26.0 2.5);
WIRE 0.2 (26.0 2.5) (26.0 11.5);
WIRE 0.2 (26.0 11.5) (8.4 11.5);
WIRE 0.2 (8.4 11.5) (8.4 2.1);
WIRE 0.2 (8.4 2.1) (26.4 2.1);
WIRE 0.2 (26.4 2.1) (26.4 11.9);
WIRE 0.2 (26.4 11.9) (8.0 11.9);
WIRE 0.2 (8.0 11.9) (8.0 1.7);
WIRE 0.2 (8.0 1.7) (26.8 1.7);
WIRE 0.2 (26.8 1.7) (26.8 12.3);
WIRE 0.2 (26.8 12.3) (7.6 12.3);
WIRE 0.2 (7.6 12.3) (7.6 1.3);
WIRE 0.2 (7.6 1.3) (27.2 1.3);
WIRE 0.2 (27.2 1.3) (27.2 12.7);
WIRE 0.2 (27.2 12.7) (7.2 12.7);
WIRE 0.2 (7.2 12.7) (7.2 0.9);
WIRE 0.2 (7.2 0.9) (27.6 0.9);
WIRE 0.2 (27.6 0.9) (27.6 13.1);
WIRE 0.2 (27.6 13.1) (6.8 13.1);
WIRE 0.2 (6.8 13.1) (6.8 0.5);
WIRE 0.2 (6.8 0.5) (28.0 0.5);
WIRE 0.2 (28.0 0.5) (28.0 13.1);
WIRE 0.2 (23.6 9.1) (23.6 7.5) (22.7 7.5);
WIRE 0.2 (28.0 13.1) (37.8 13.1) (37.8 17.9);
CHANGE LAYER BOTTOM;
WIRE 0.2 (39.2 17.9) (39.2 6.1) (22.7 6.1);
```

**Figure E.2 EAGLE script (automatically generated)**
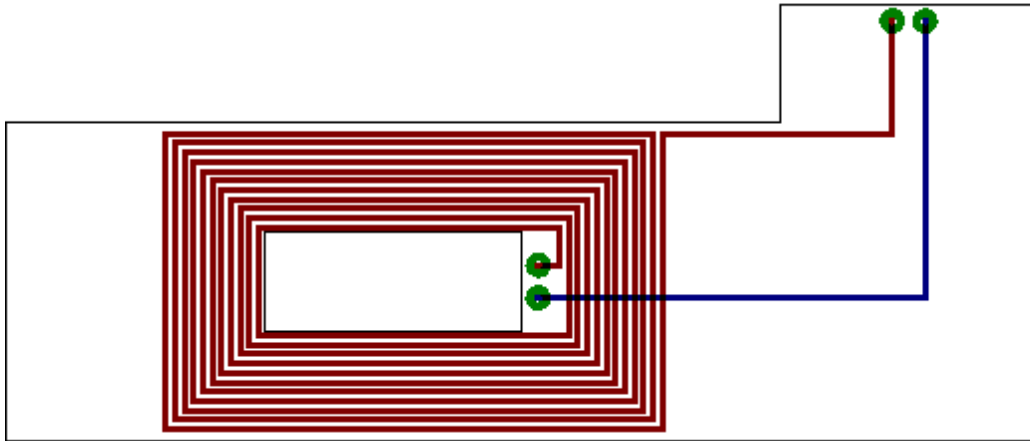
**Figure E.3: Automatically generated PCB design for E18 planar winding**

The software has been configured to create the board outline and cut-out, tracks and vias automatically based on the user specifications. In this case the return track is a straight track to the PCB edge, but the spiral return path has also been implemented. The resulting PCB designs were constructed using 2 layer FR4 PCBs, 1.6mm thick with solder masks on each side. This alternative implementation is shown in Figure E.4.
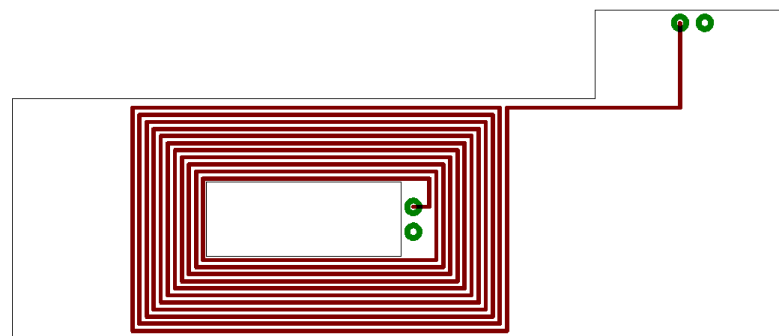


(a) Top Layer
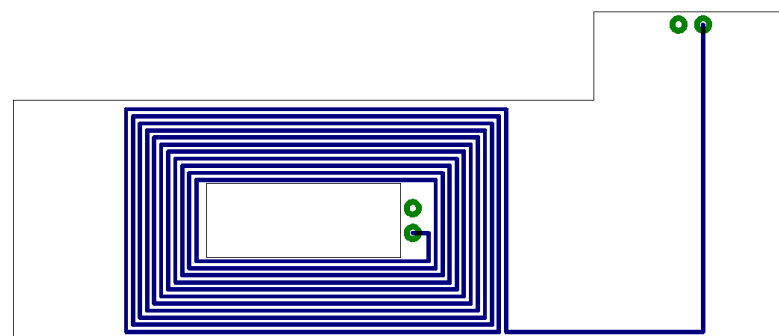


(b) Bottom Layer

**Figure E.4: Double Sided 2-Spiral PCB design for E18 planar winding**

Using this implementation for an E18 planar core, 11 turns will fit in the winding width on each layer. If the inner vias are connected together, then a total number of turns possible is 22. Using an un-gapped E18 core and Plate (made with the 3E6 material), for n=11 the inductance measured was 530uH and for n=22 the inductance was measured as 3.2mH.

To create a 2 winding transformer using these PCB windings can be done using a single PCB, with a turns ratio of 11:11, or by stacking 2 PCBs to give a turns ratio of 22:22. When this was carried out using the stacking method, a magnetizing inductance of 2.99mH, leakage inductance of 44uH and winding resistance of 2.21Ω were measured. The leakage inductance is much higher than the wire wound equivalent primarily due to the inefficient use of the winding space and the thickness of the PCBs. If a thinner PCB was used and all 4 layers integrated in a single PCB, then this would be much reduced.

This device was tested in the same fashion as the IIC previously in this section and compared with the benchmark APC41199 EP13 based component. The E18 planar component was tested with no gap (Inductance = 2.99mH), and gapped (Inductance = 140uH). The resulting comparison of THD measured at 10kHz is given in figure E.5.
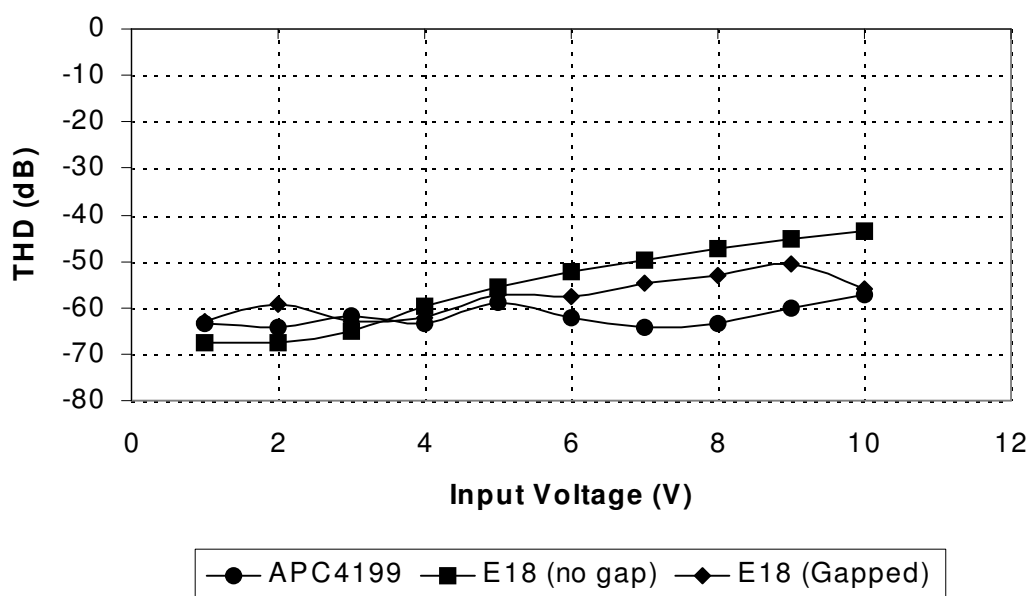


**Figure E.5: E18 and APC41199 THD versus Input Voltage @ 10kHz**

It is clear from these results that the performance of the Planar transformer using the E18 core is substantially improved from the IIC. The tests were again repeated for 100kHz, with the results given in figure E.6.
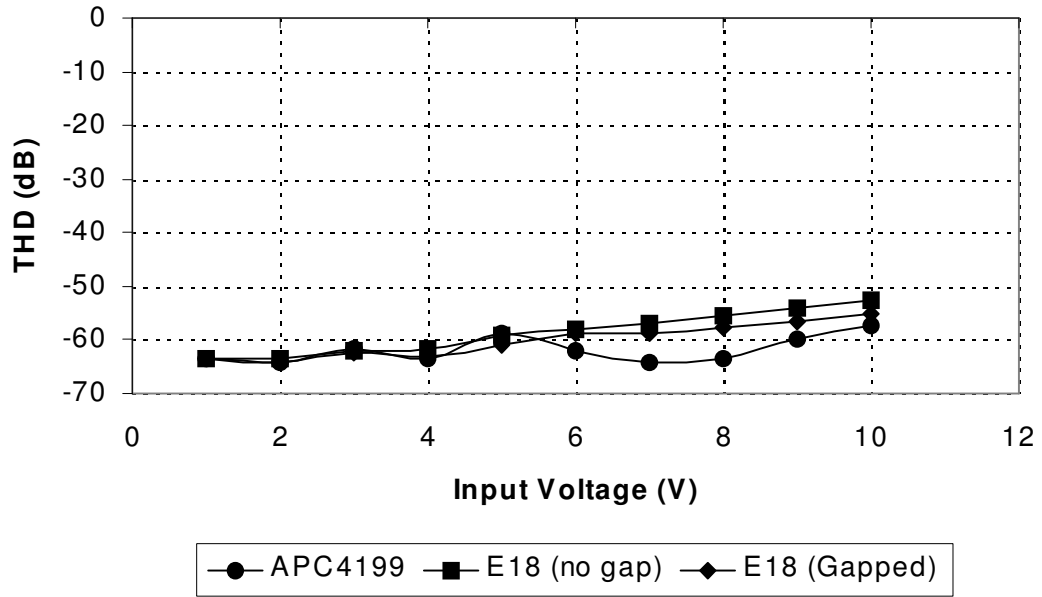
**Figure E.6: E18 and APC41199 THD versus Input Voltage @ 100kHz**

These results indicate a level of performance that is getting close to the benchmark case, with a non-optimal physical construction (i.e. two separate stacked 1.6mm FR4 PCBs). The E18 core size is relatively large in terms of its PCB footprint, and an alternative option is to use an ER11 core. Unfortunately the number of turns possible with this core size is much reduced compared to the E18 core, especially when using a double sided prototype PCB.

Using the same approach as for the E18 core, a 4T:4T transformer implementation was constructed using a double-sided FR4 (1.6mm thick) PCB and the resulting inductance measured with an ER11-3E6 core. The resulting inductance at 1kHz was measured as 11.5uH with a leakage inductance of 2.5uH. This is much lower than the benchmark value of ~200uH (Minimum) and even if the layers were doubled up by connecting the inner vias, the inductance only increased to ~35uH. It was therefore clear that with this implementation, a practically useful ADSL line transformer was not realistically possible.

The initial double sided PCB planar magnetic components indicated that comparable results in terms of the THD performance could be obtained when compared to an existing wire wound component on an EP13 core. It is also clear that by using a stacked double sided PCB implementation excessive leakage inductance would result. In order to combat this, a 4 layer implementation was then constructed for the previously used E18 core and also the E14 core size.

When the transformer was implemented using a 4 layer approach, the number of tracks that could be obtained in the E18 case was 13 per layer, as the track width is slightly reduced from the double sided case (0.2mm to 0.15mm). A slightly increased margin around the winding window edges was also allowed to reduce the risk of the board outline conflicting with the track area. For the E14

core size the number of turns was 11 per layer. The layout approach was to wind from outside to an inside via and out again on the next layer. This provided a simple way of achieving double the number of turns in the available space compared to the conventional approach of a spiral track in and straight track out. A further layout option was tested at this point by implementing a form of bifilar winding on each layer. The layout implementation is shown in figure E.7 with two spirals on each layer.
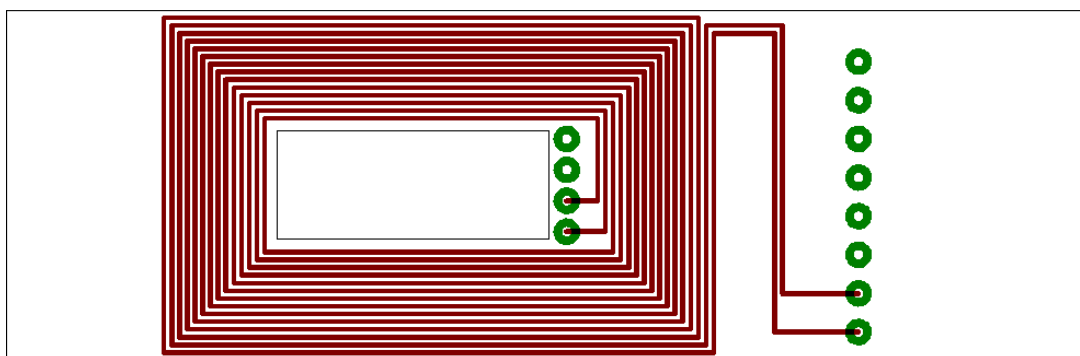


**Figure E.7: Bifilar Layout Implementation**

Tests were carried out to evaluate the THD in the E14 core size and to compare the insertion loss for the APC41199 benchmark transformer with those of the E14 and E18 implementations. The resulting measured E14 THD compared with the benchmark APC41199 THD is given in figure E.8. Again, the performance is comparable with the benchmark APC41199 device, but in this case it is clear that the un-gapped core introduces significant levels of distortion as the voltage level increases. The gapped core (gap ≈100um) shows a level of performance that is comparable with the benchmark APC41199.
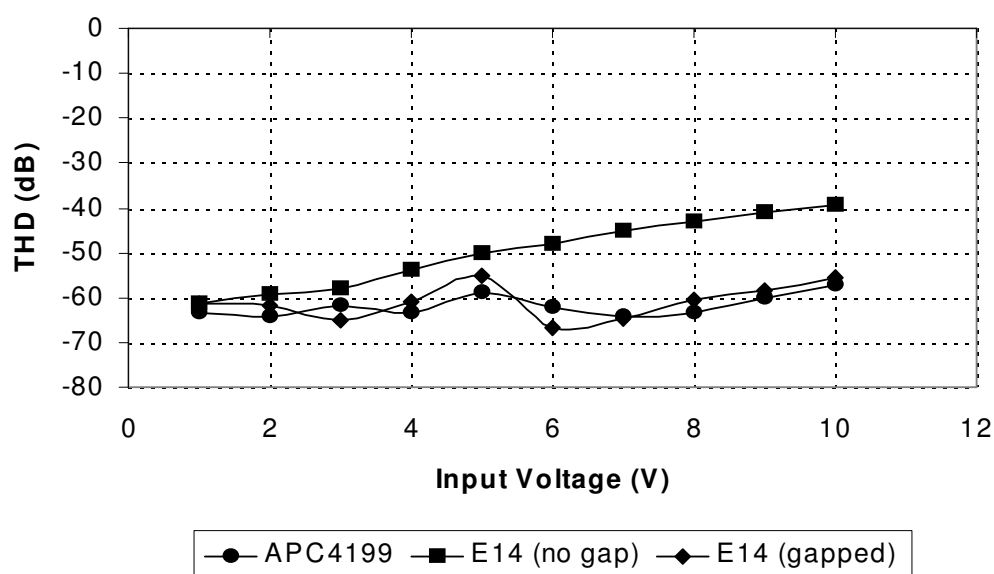


**Figure E.8: E14 and APC41199 THD versus Input Voltage @ 10kHz**

270